Modelling glacial erosional landform development

R.C.A. Hindmarsh

MODELLING GLACIAL EROSIONAL LANDFORM DEVELOPMENT

VOLUME 2

BY

R. C. A. HINDMARSH

A thesis presented for the degree of
Doctor of Philosophy in the
University of Durham

Graduate Society

January 1985

LIST OF FIGURES

Figure 5.7 v_τ against $\sin\gamma$ for an incompressible linear rheology with v_d = 10 alu/a (Case 1).

Figure 5.8 v_τ against $\sin\gamma$ for an incompressible linear rheology with a cavity and v_d = 400 alu/a (Case 7).

Fiugre 5.9 v_τ against $\sin\gamma$ for an incompressible linear rheology with a cavity and v_d = 10 alu/a (Case 6).

Figure 5.10 v_τ against $\sin\gamma$ for a compressible linear rheology with χ = 1 alu^2/bar.a and v_d = 10 alu/a (Case 8).

Figure 5.11 Velocity vector plot for a compressible linear rheology with χ = 10 alu^2/bar.a and v_d = 200 alu/a (Case 16).

Figure 5.12 v_τ against $\sin\gamma$ for a compressible linear rheology with χ = 10 alu^2/bar.a and v_d = 200 alu/a (Case 16).

Figure 5.13 Velocity vector plot for an incompressible linear rheology with bed of S = 100 alu/bar.a and v_d = 100 alu/a (Case 20).

Figure 5.14 v_τ against $\sin\gamma$ for an incompressible linear rheology with bed of S = 10 alu/bar.a, v_d = 10 alu/a (Case 18)

Figure 5.15 v_τ against $\sin\gamma$ for an incompressible linear rheology with bed of S = 400 alu/bar.a, v_d = 400 alu/a (Case 22).

Figure 5.16 Velocity vector plot for an incompressible Glen rheology with v_d = 100 alu/a (Case 25).

Figure 5.28 p' against cosγ for an incompressible linear rheology with v_d = 400 alu/a (Case 1).

Figure 5.29 p' against cosγ for an incompressible linear rheology with a cavity and v_d = 400 alu/a (Case 5).

Figure 5.30 p' against cosγ for a compressible linear rheology with χ = 1 alu²/bar.a and v_d = 400 alu/a (Case 12).

Figure 5.31 Pressure contours in bar for a compressible linear rheology with χ = 10 alu²/bar.a and v_d = 400 alu/a (Case 17)

Figure 5.32 p' against cosγ for a compressible linear rheology with χ = 10 alu²/bar.a and v_d = 200 alu/a (Case 16).

Figure 5.33 Pressure contours in bar for an incompressible linear rheology with bed of S = 100 alu/bar.a and v_d = 100 alu/a (Case 20).

Figure 5.34 p' against cosγ for an incompressible linear rheology with bed of S = 10 alu/bar.a and v_d = 10 alu/a (Case 18).

Figure 5.35 p' against cosγ for an incompressible linear rheology with bed of S = 400 alu/bar.a and v_d = 400 alu/a (Case 22).

Figure 5.36 Pressure contours in bar for an incompressible Glen rheology with v_d = 200 alu/a (Case 25).

Figure 5.37 p' against cosγ for an incompressible Glen rheology with v_d = 10 alu/a (Case 23).

Figure 5.38 p' against $\cos\gamma$ for an incompressible Glen rheology with v_d = 400 alu/a (Case 27).

Figure 5.39 Pressure contours in bar for an incompressible Glen rheology with a cavity and v_d = 10 alu/a (Case 27).

Figure 5.40 p' against $\cos\gamma$ for an incompressible Glen rheology with a cavity and v_d = 10 alu/a (Case 27).

Figure 5.41 Pressure contours in bar for a compressible Glen rheology with χ = 1 alu^2/bar.a and v_d = 100 alu/a (Case 29).

Figure 5.42 p' against $\cos\gamma$ for a compressible Glen rheology with χ = 1 alu^2/bar.a and v_d = 200 alu/a (Case 30).

Figure 5.43 p' against $\cos\gamma$ for an incompressible Glen rheology with bed of S = 10 alu/bar.a and v_d = 10 alu/a (Case 34)

Figure 5.44 p' against position for flow over a truncated sine ridge (Cases 40 - 49).

Figure 5.45 Pressure contours in bar for an incompressible Glen rheology with v_d = 100 alu/a for flow over a truncated sine ridge (Case 47).

Figure 5.46 $\dot{\varepsilon}_v$ in a^{-1} for a compressible linear rheology with χ = 1 alu^2/bar.a and v_d = 400 alu/a (Case 12).

Figure 5.47 $\dot{\varepsilon}_v$ in a^{-1} for a compressible linear rheology with χ = 10 alu^2/bar.a and v_d = 200 alu/a (Case 16).

Figure 5.48 $\dot{\varepsilon}_v$ in a^{-1} for a compressible Glen rheology with χ = 1 alu^2/bar.a and v_d = 10 alu/a (Case 29).

Figure 5.49 $\dot{\varepsilon}_v$ in a^{-1} for a compressible Glen rheology with χ = 1 alu^2/bar.a and v_d = 400 alu/a (Case 33).

Figure 5.50 Regression exponent for $\dot{\varepsilon}_v$ against v_d for a compressible Glen rheology with χ = 1 alu^2/bar.a (Cases 29 - 33).

Figure 5.51 μ in bar.a for an incompressible Glen rheology with v_d = 10 alu/a (Case 23).

Figure 5.52 μ in bar.a for an incompressible Glen rheology with v_d = 400 alu/a (Case 26).

Figure 5.53 μ in bar.a for an incompressible Glen rheology with a cavity and v_d = 10 alu/a (Case 27).

Figure 5.54 μ in bar.a for a compressible Glen rheology with χ = 1 alu^2/bar.a and v_d = 10 alu/a (Case 29).

Figure 5.55 μ in bar.a for a compressible Glen rheology with χ = 1 alu^2/bar.a with v_d = 400 alu/a (Case 33).

Figure 5.56 μ in bar.a for an incompressible Glen rheology with S = 10 alu/bar.a and v_d = 10 alu/a (Case 34).

Figure 5.57 μ in bar.a for an incompressible Glen rheology with v_d = 10 alu/a for flow over a truncated sine ridge (Case 45).

Figure 5.68 Velocity contours in alu/a for v_d = 10 alu/a and a bed of S = 0·02 alu/bar.a, wide-hummocked case.

Figure 5.69 Velocity contours in alu/a for v_d = 10 alu/a and a bed of S = 0·1 alu/bar.a, wide-hummocked case.

Figure 5.70 Velocity contours in alu/a for v_d = 10 alu/a and a bed of S = 0·2 alu/bar.a, wide-hummocked case.

Figure 5.71 Velocity contours in alu/a for v_d = 10 alu/a, and a bed of S = 1 alu/bar.a, wide-hummocked case.

Figure 5.72 Velocity contours in alu/a for v_d = 10 alu/a and a bed of S = 2 alu/bar.a, wide-hummocked case.

Figure 5.73 Velocity contours in alu/a for v_d = 50 alu/a and a bed of S = 0·01 alu/bar.a, wide-hummocked case.

Figure 5.74 Velocity contours in alu/a for v_d = 100 alu/a and a bed of S = 0·01 alu/bar.a, wide-hummocked case.

Figure 5.75 Velocity contours in alu/a for v_d = 200 alu/a and a bed of S = 0·01 alu/bar.a, wide-hummocked case.

Figure 5.76 Velocity contours in alu/a for v_d = 10 alu/a and a bed of S = 0·02 alu/bar.a, narrow-hummocked case.

LIST OF OVERLAYS

Overlay 1 Scaling lines for uniaxial flow.

FIGURE 2.1 DEVELOPMENT OF GLACIALLY ERODED SURFACES BY SCRATCHING AND POLISHING

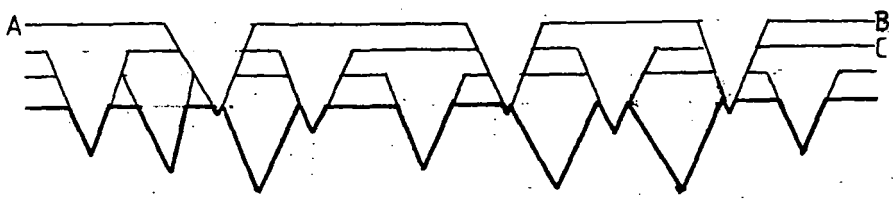

(a) 3 scratches/unit area/unit time

KEY

AB = UNIT WIDTH

BC = POLISHING EFFECTED IN UNIT TIME

UNIT SCRATCH

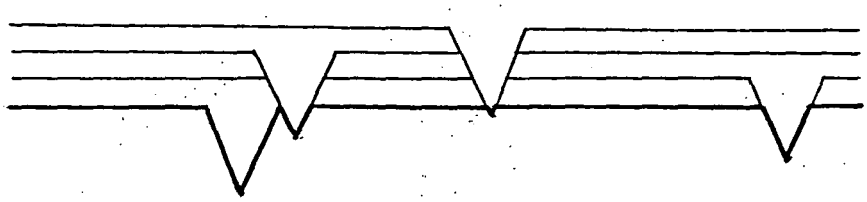

(b) 1 scratch/unit area/unit time

FIGURE 2.2 DERIVATION OF THE ABRASION EQUATION

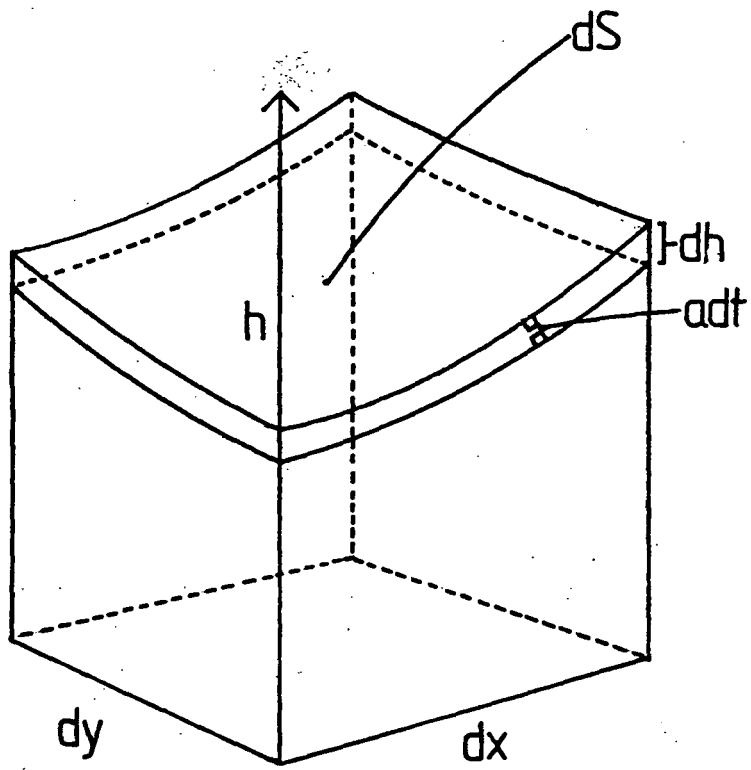

Figure 2.3 Contour plot of surface persistent under constant abrasion: $a = 1$, $\ell = 2$, $m_x = m_y = 0$.

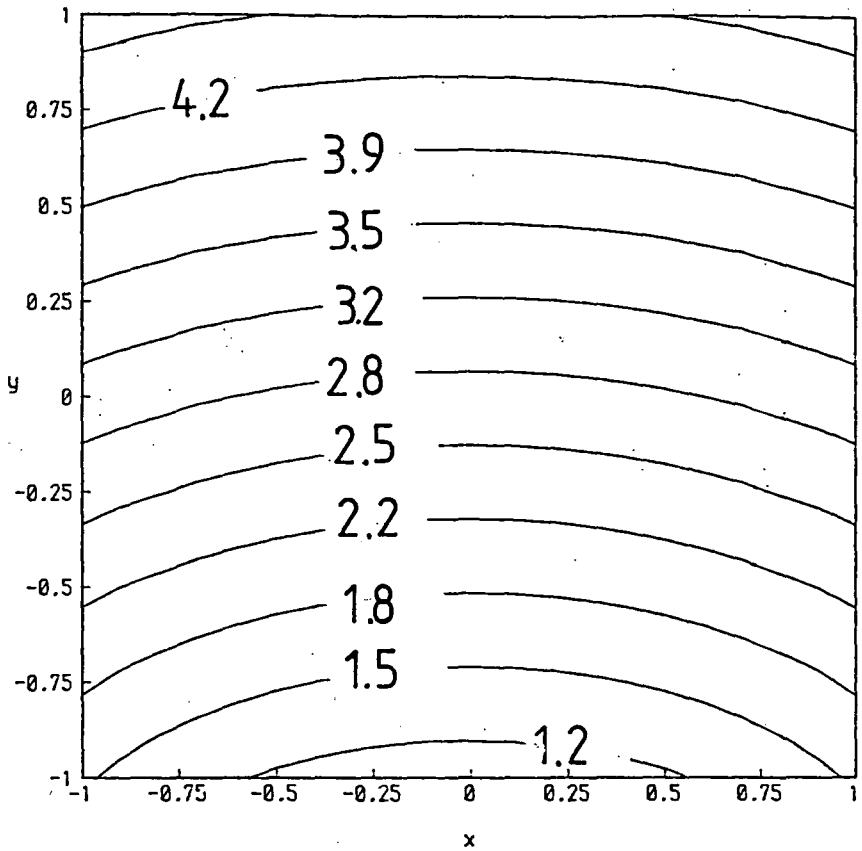

Figure 2.4 Contour plot of surface persistent under constant abrasion: $a = 1$, $\ell = 2$, $m_x = 0{\cdot}0$, $m_y = -0{\cdot}5$.

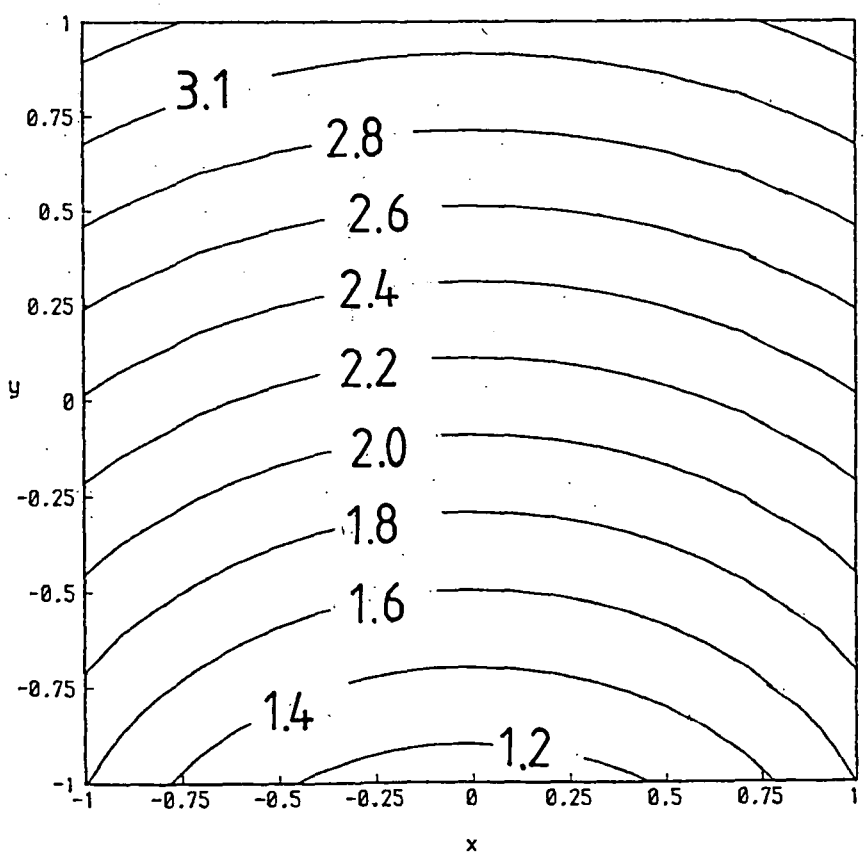

Figure 2.5 Contour plot of surface persistent under constant abrasion: a = 1, ℓ = 2, $m_x = m_y = -0{\cdot}5$.

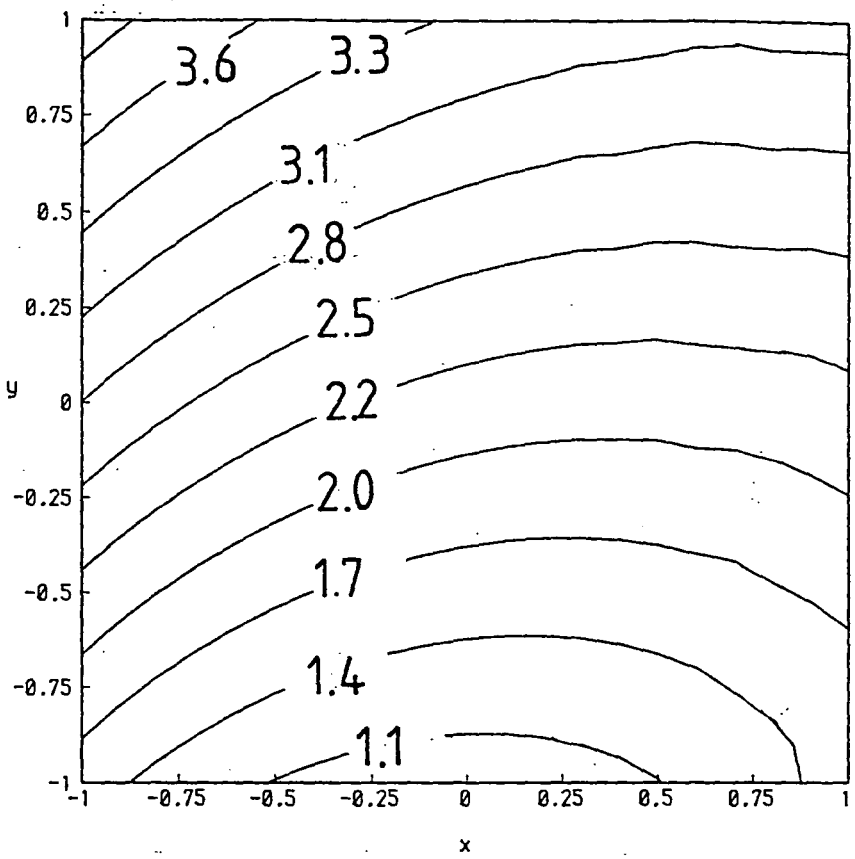

Figure 2.6 Contour plot of surface persistent under constant abrasion: a = 1, ℓ = 2, $m_x = m_y = -0{\cdot}9$.

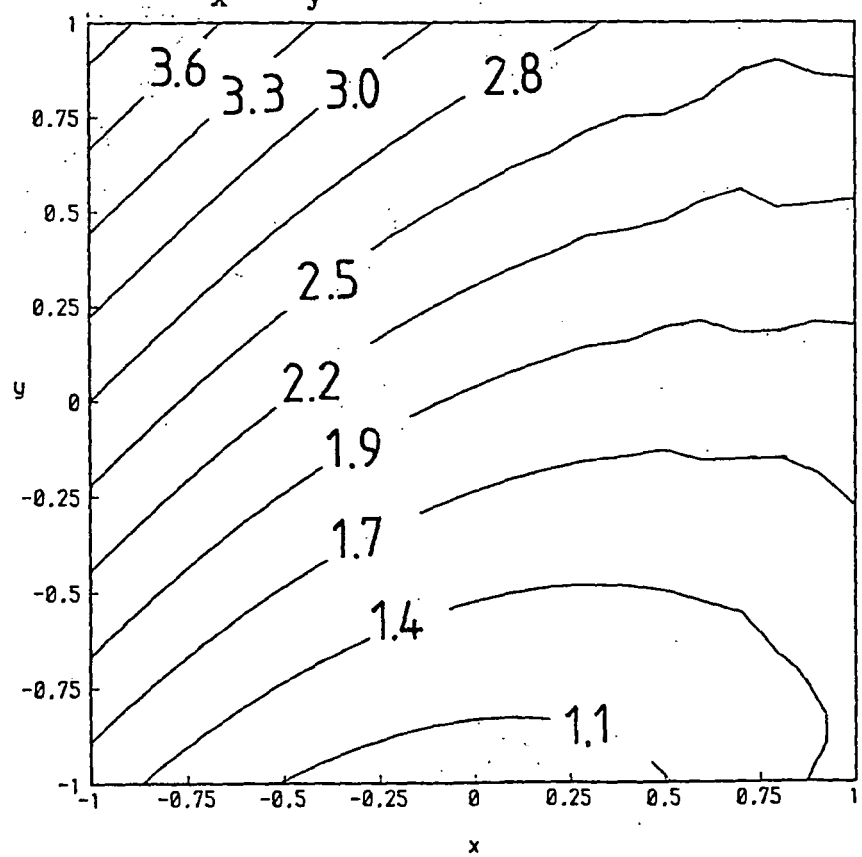

Figure 2.7 Dependence of abrasion on position for persistence of a sine-wave under lowering.

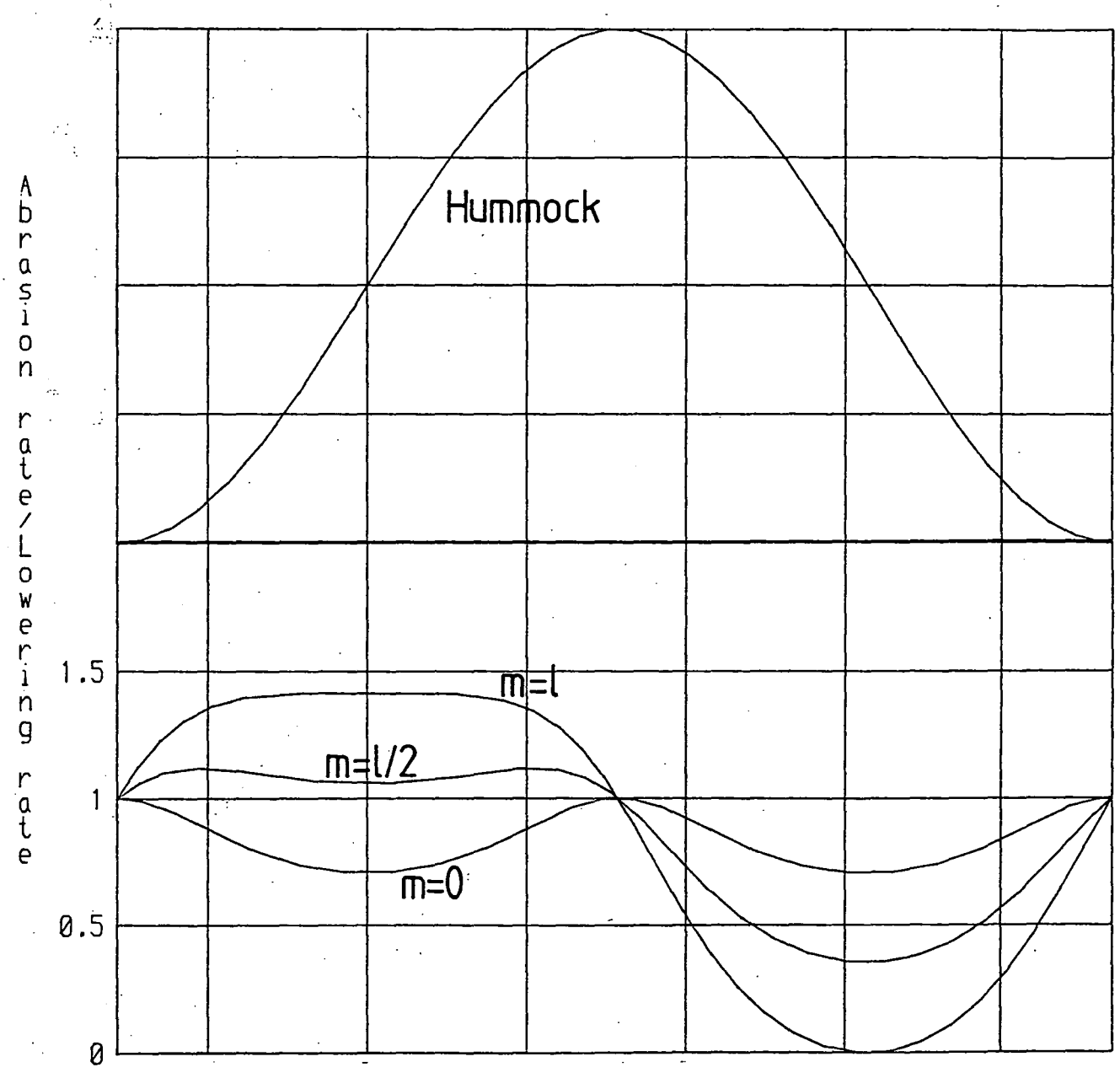

Figure 2.8 Evolution of a slope and plateau under constant abrasion using the method of characteristics.

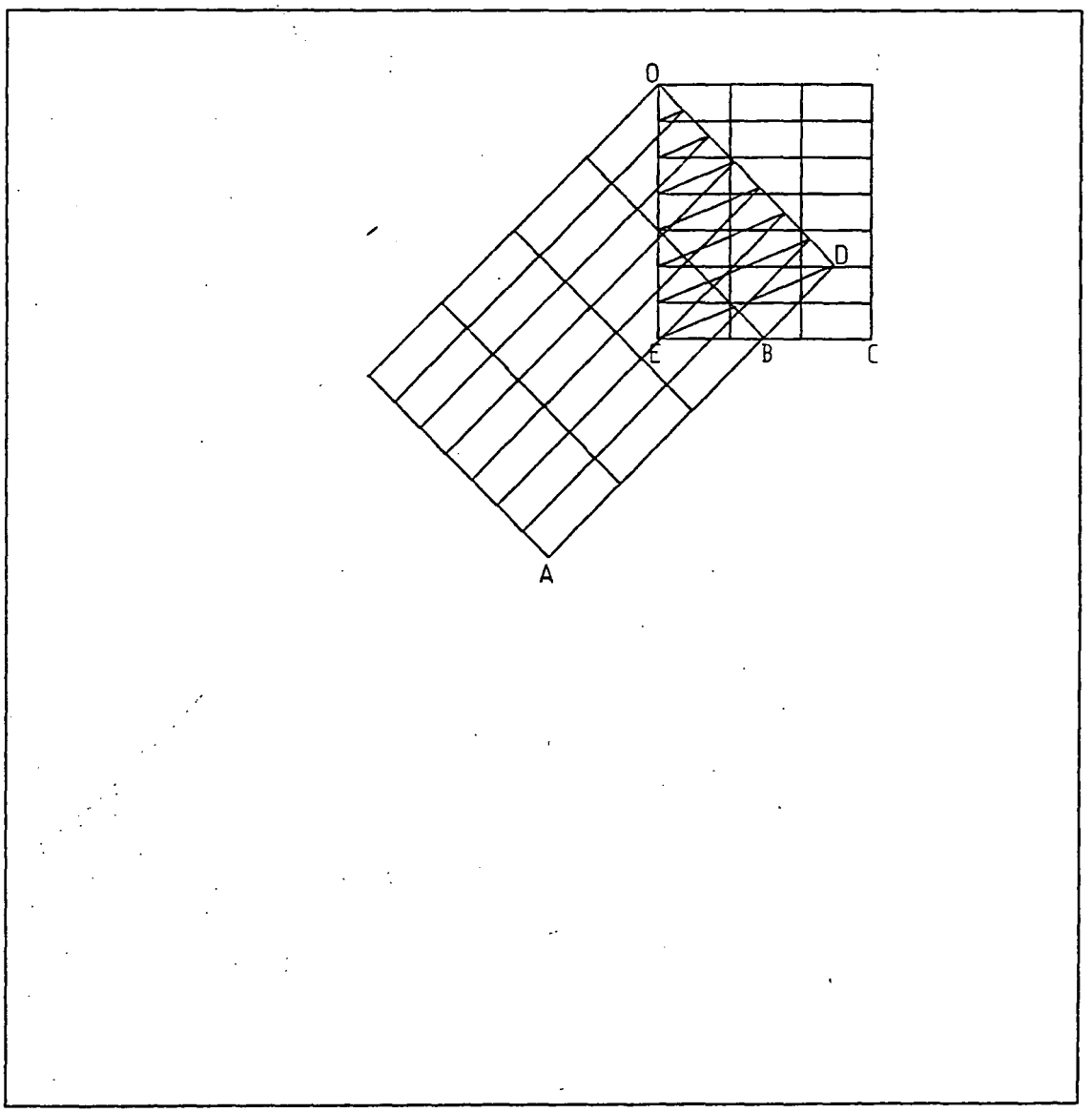

Figure 2.9 Evolution of a bell-shape under constant abrasion using the method of characteristics.

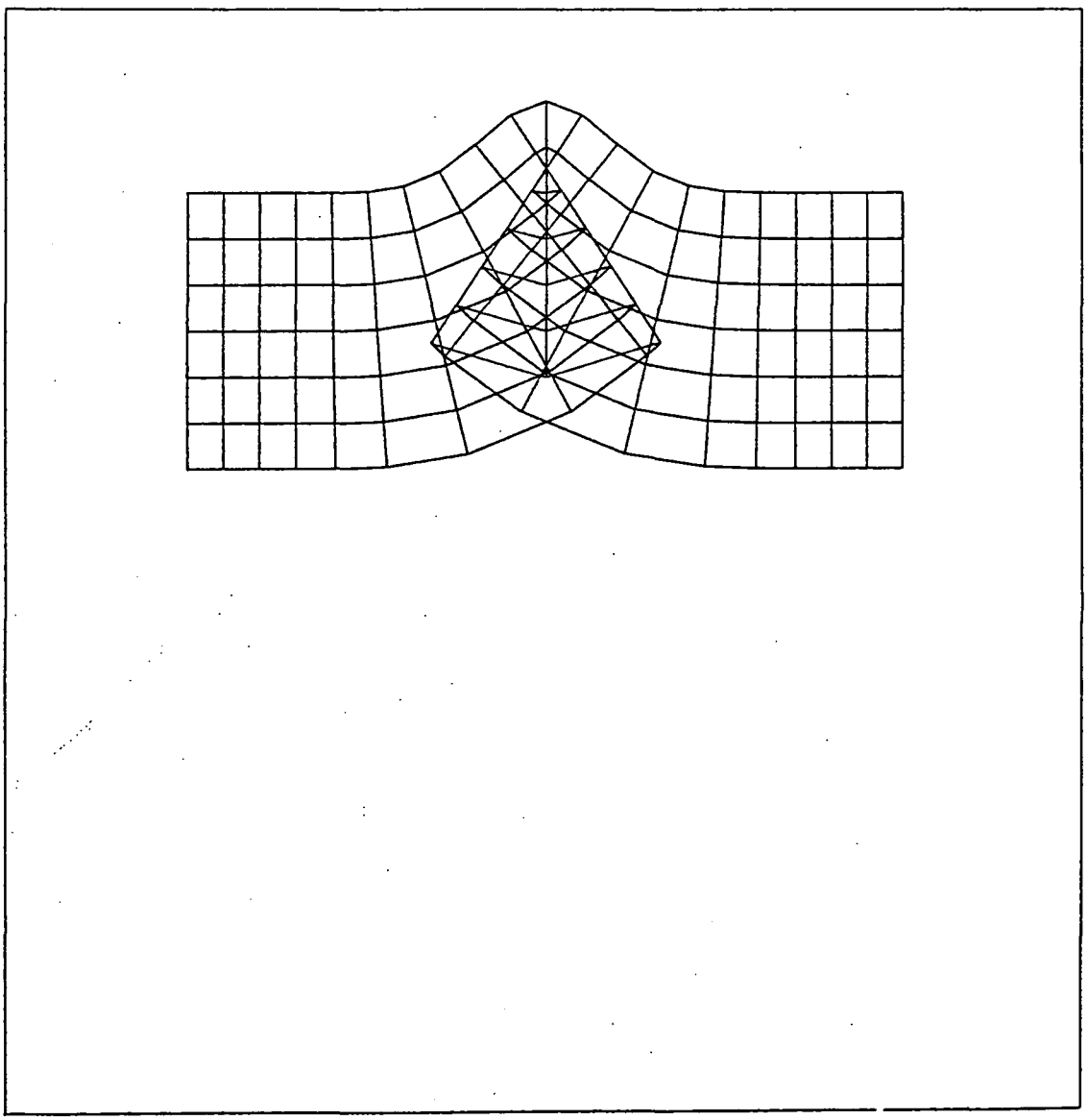

Figure 2.10 Evolution of a V-shaped valley under constant abrasion using a direct finite-difference formulation of the abrasion equation.

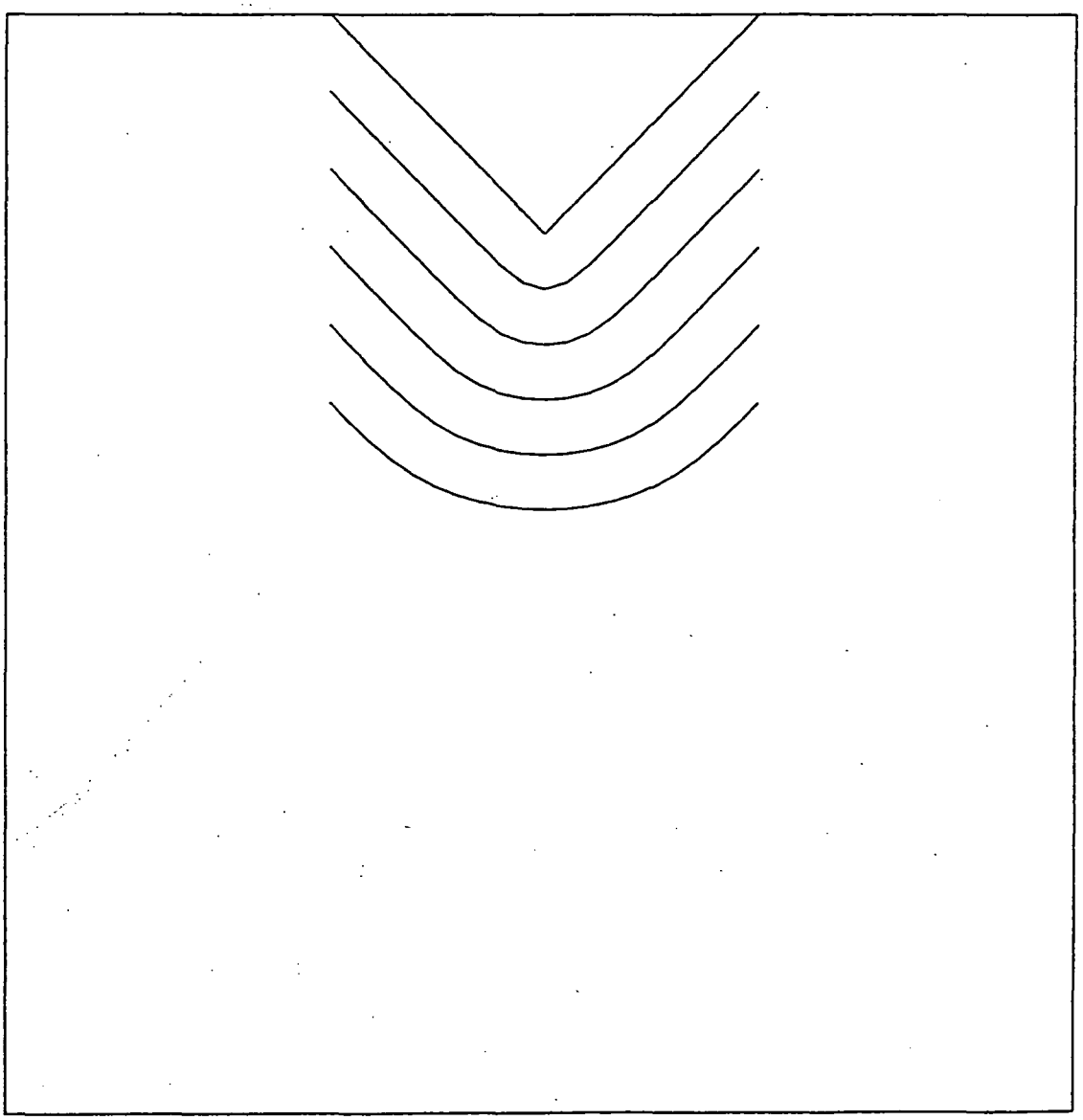

Figure 2.11 Evolution of a bell-shape under constant abrasion using a direct finite-difference formulation of the abrasion equation.

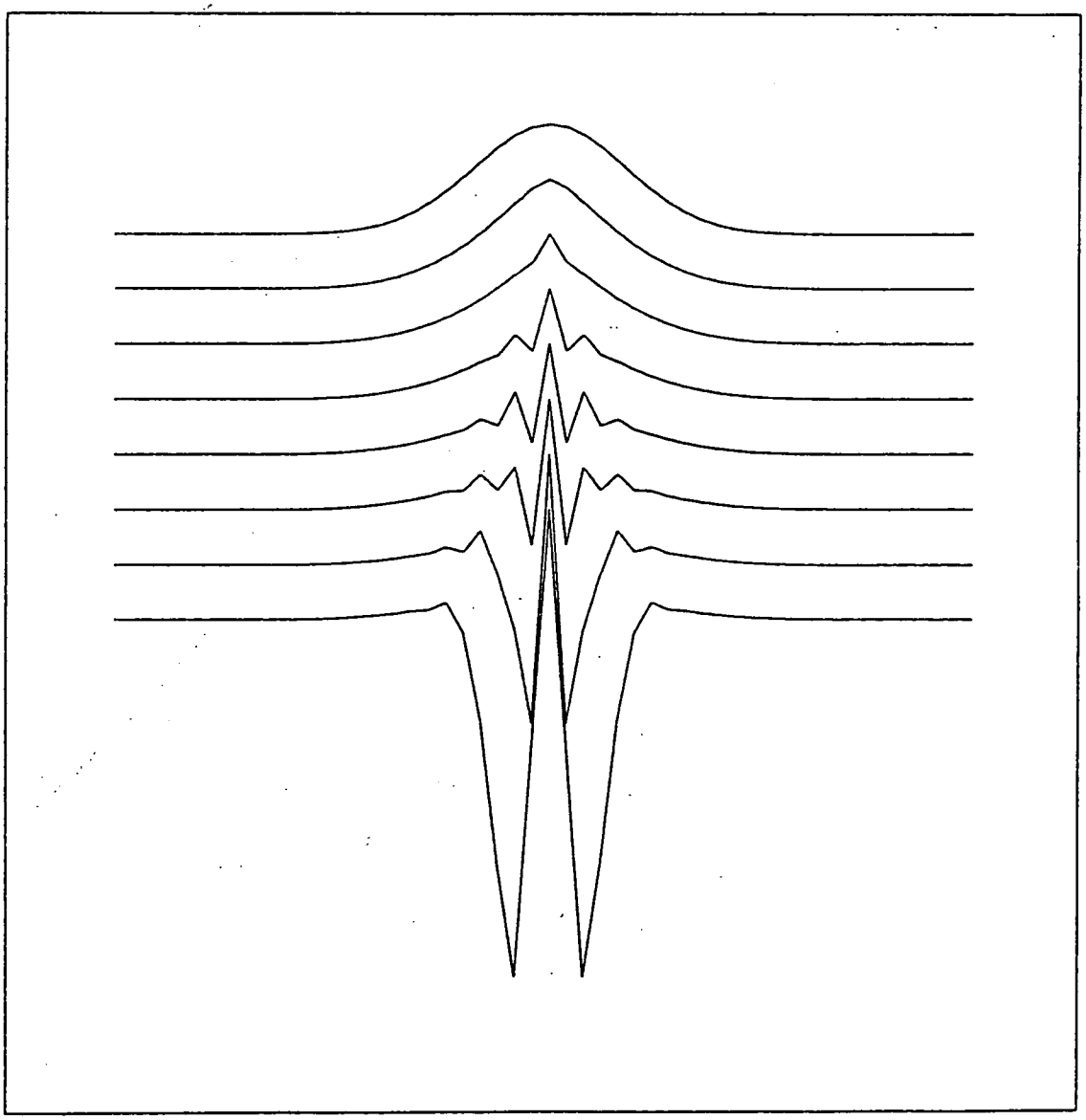

Figure 2.12 Evolution of a V-shaped valley under constant abrasion using the Farmer formulation with a coarse mesh.

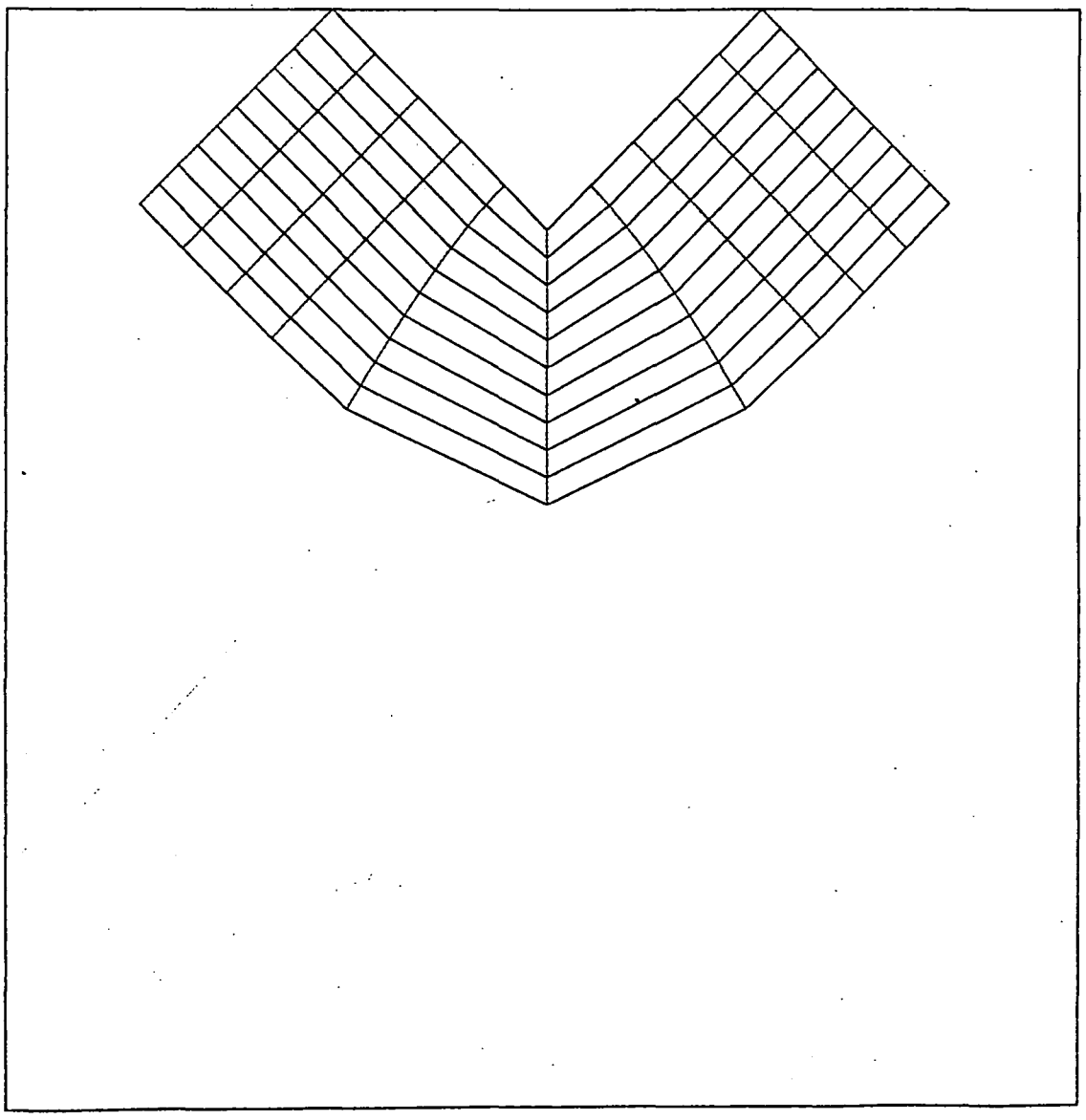

Figure 2.13 Evolution of a V-shaped valley under constant abrasion using the Farmer formulation with a fine mesh.

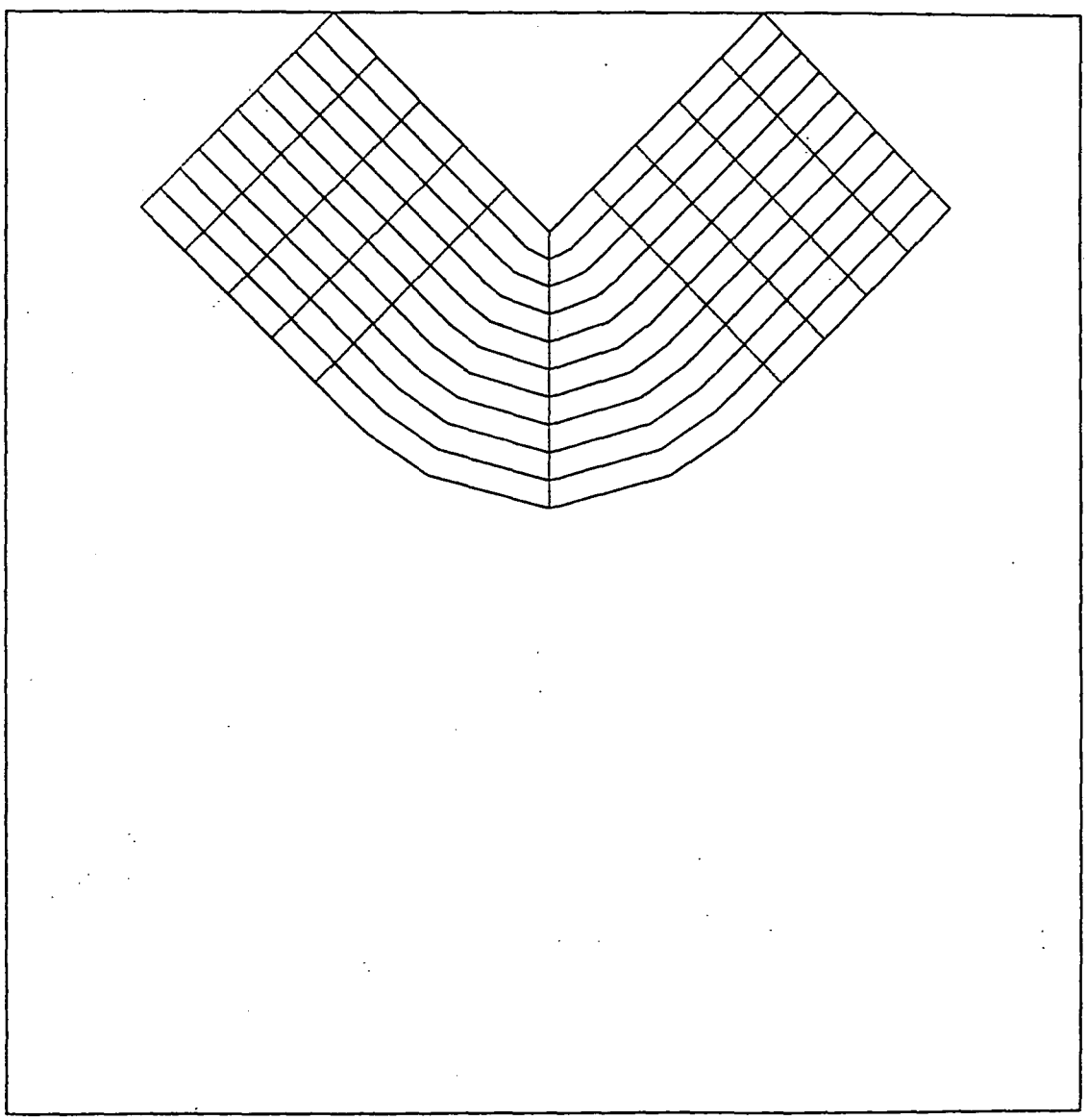

Figure 2.14 Evolution of a bell-shape under constant abrasion using the Farmer formulation.

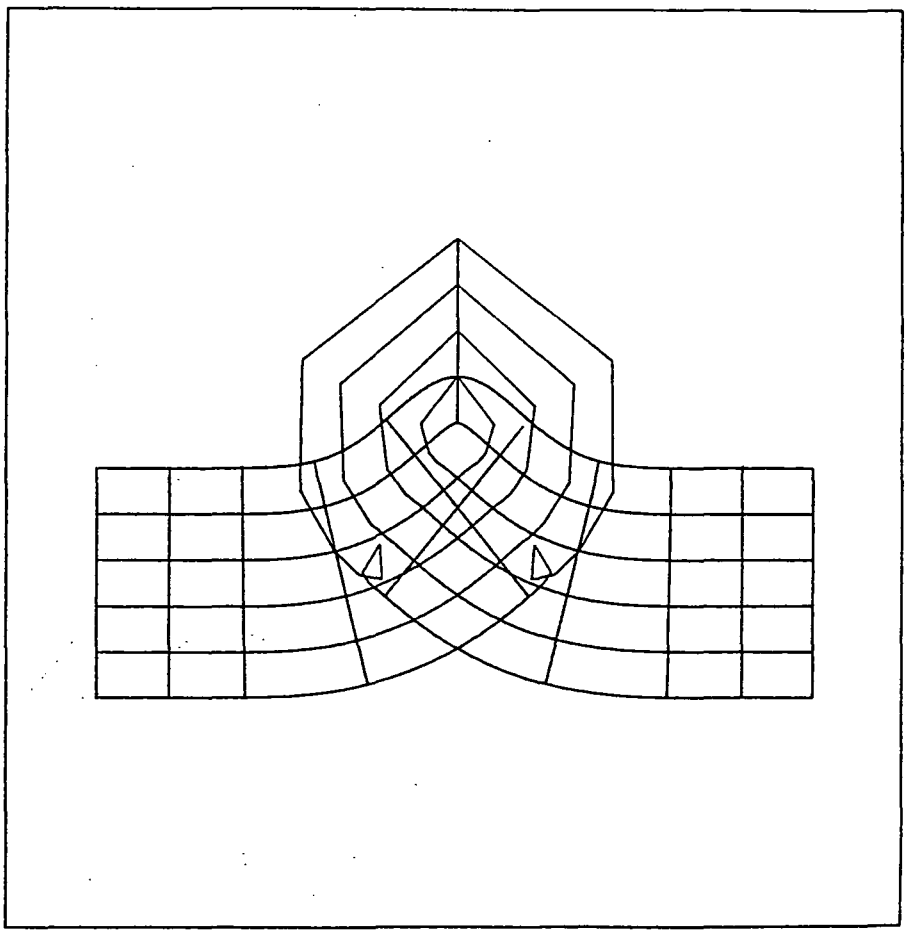

Figure 2.15 Persistence without migration of a bell-shape with lowering.

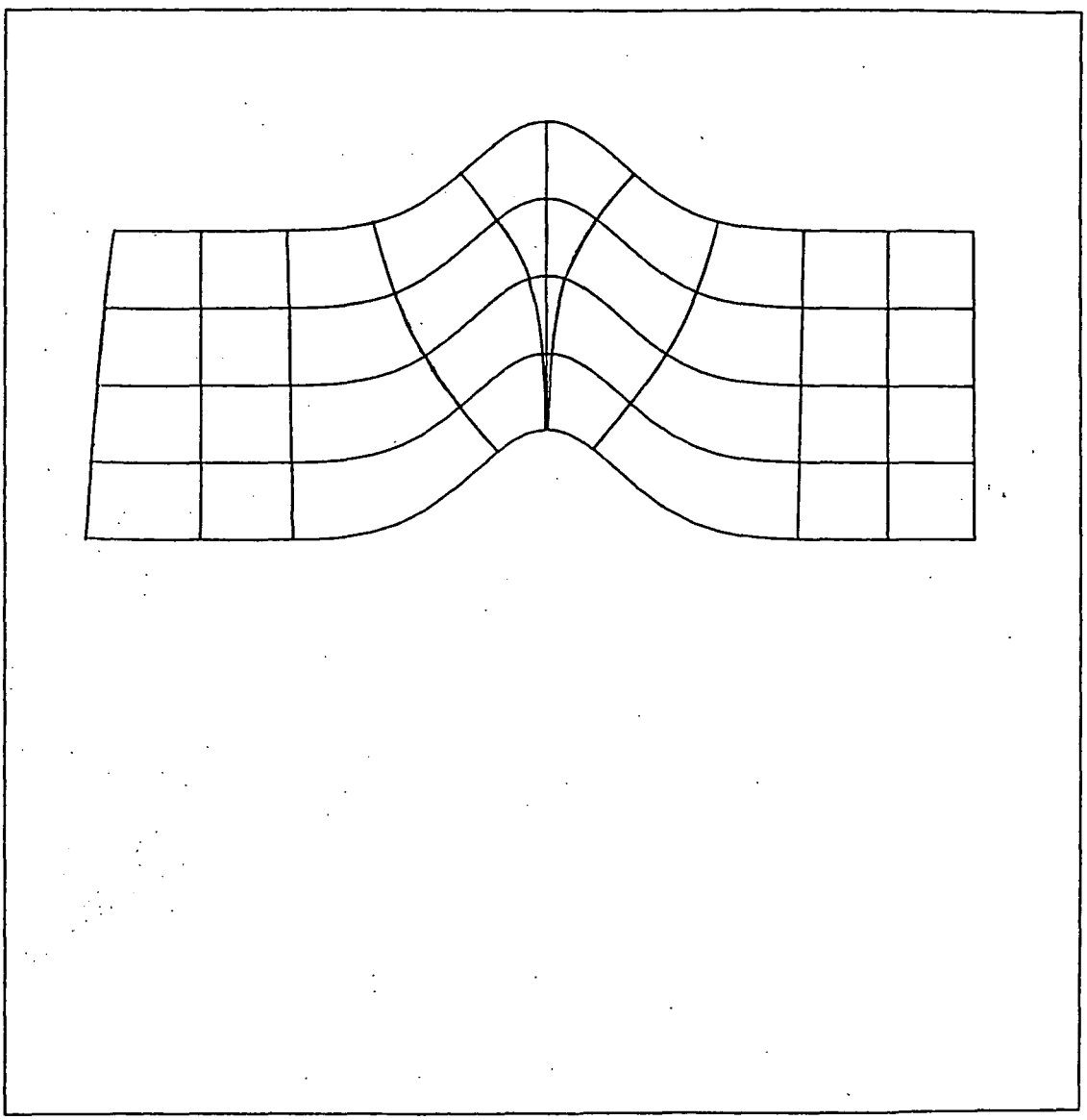

Figure 2.16 Persistence with migration of a bell-shape with lowering.

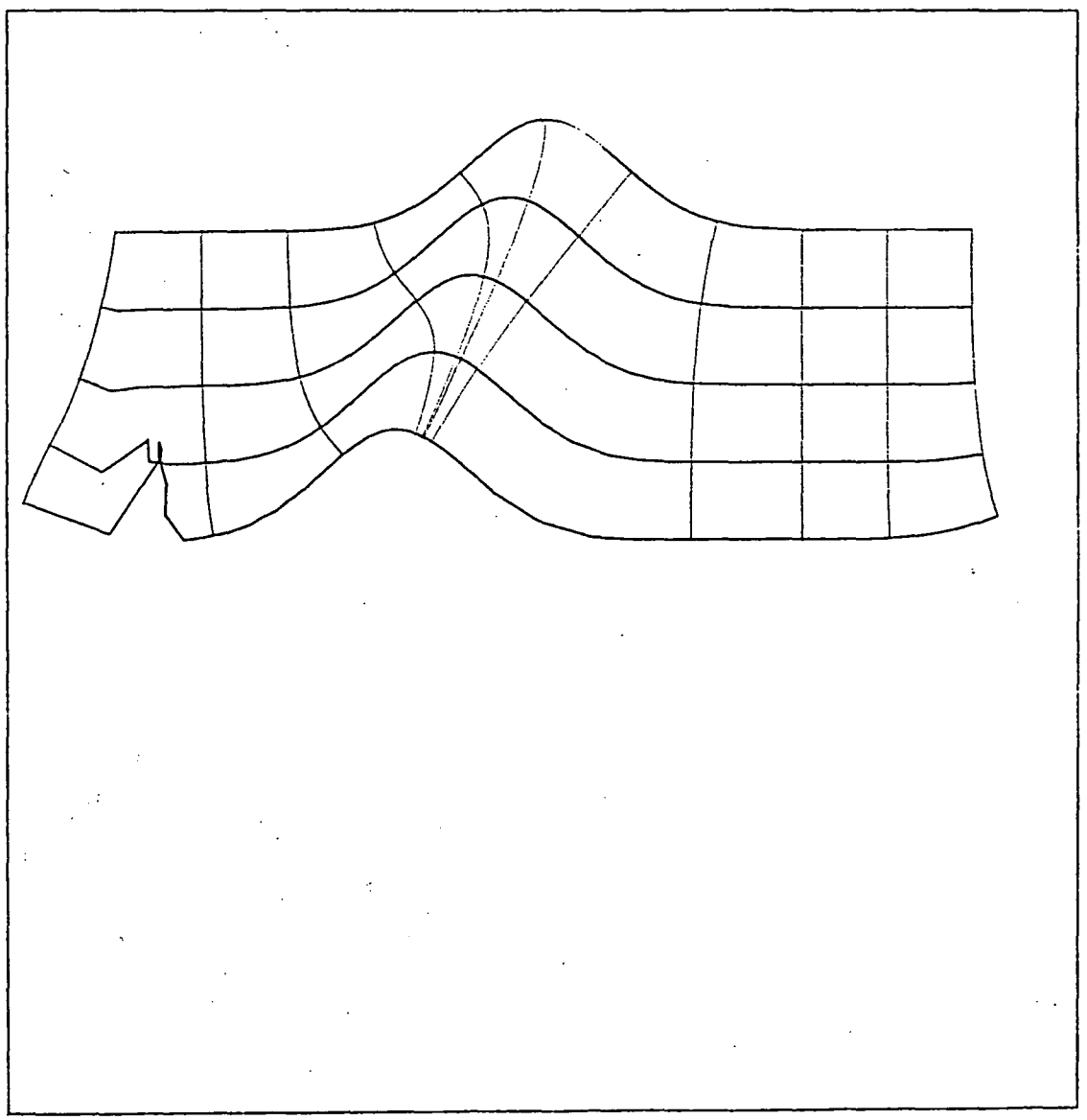

Figure 2.17 Evolution of a V-shaped valley under constant abrasion using the method of characteristics: no definition of point.

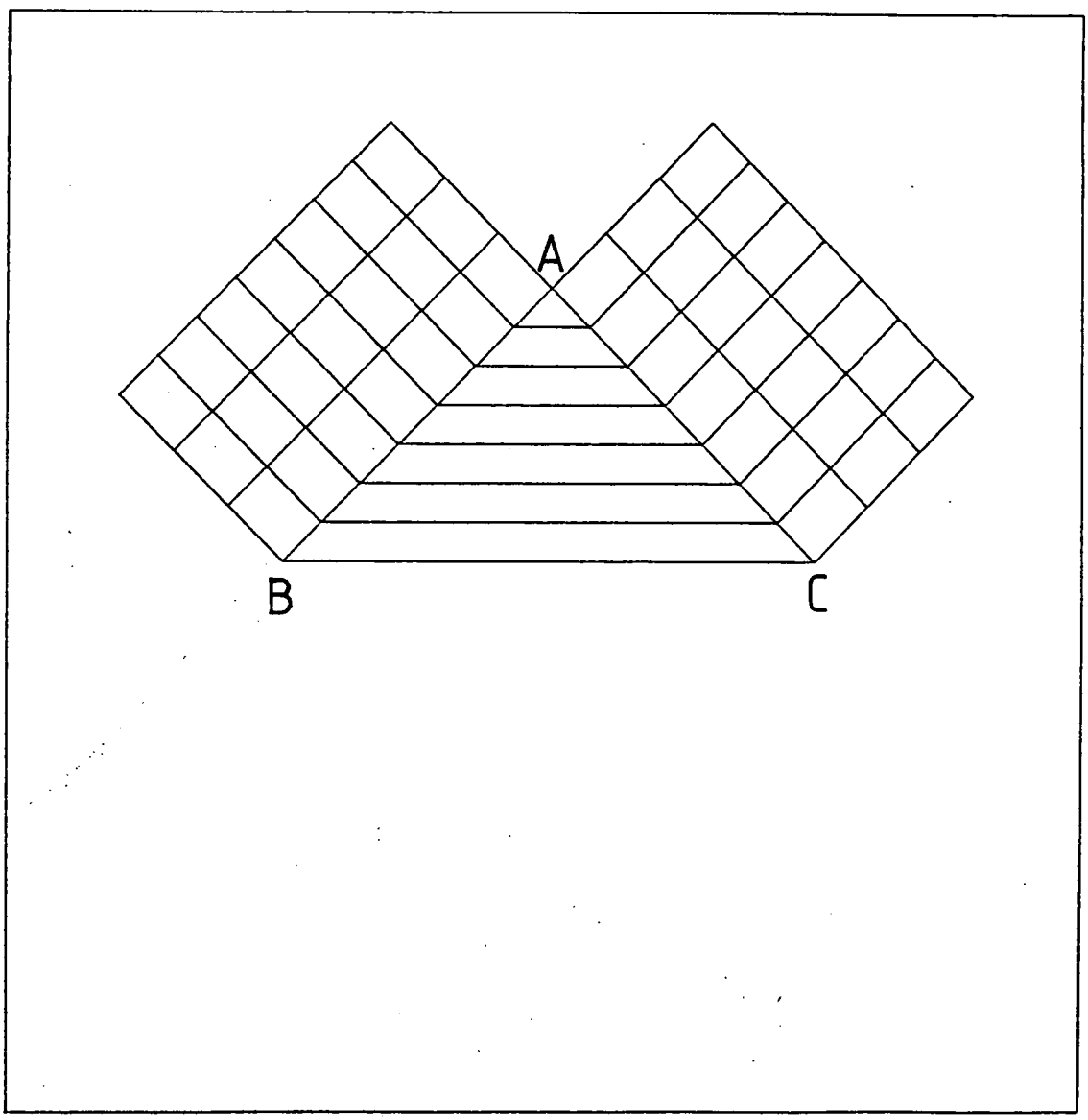

Figure 2.18 Evolution of a V-shaped valley under constant abrasion using the method of characteristics: smooth definition of point.

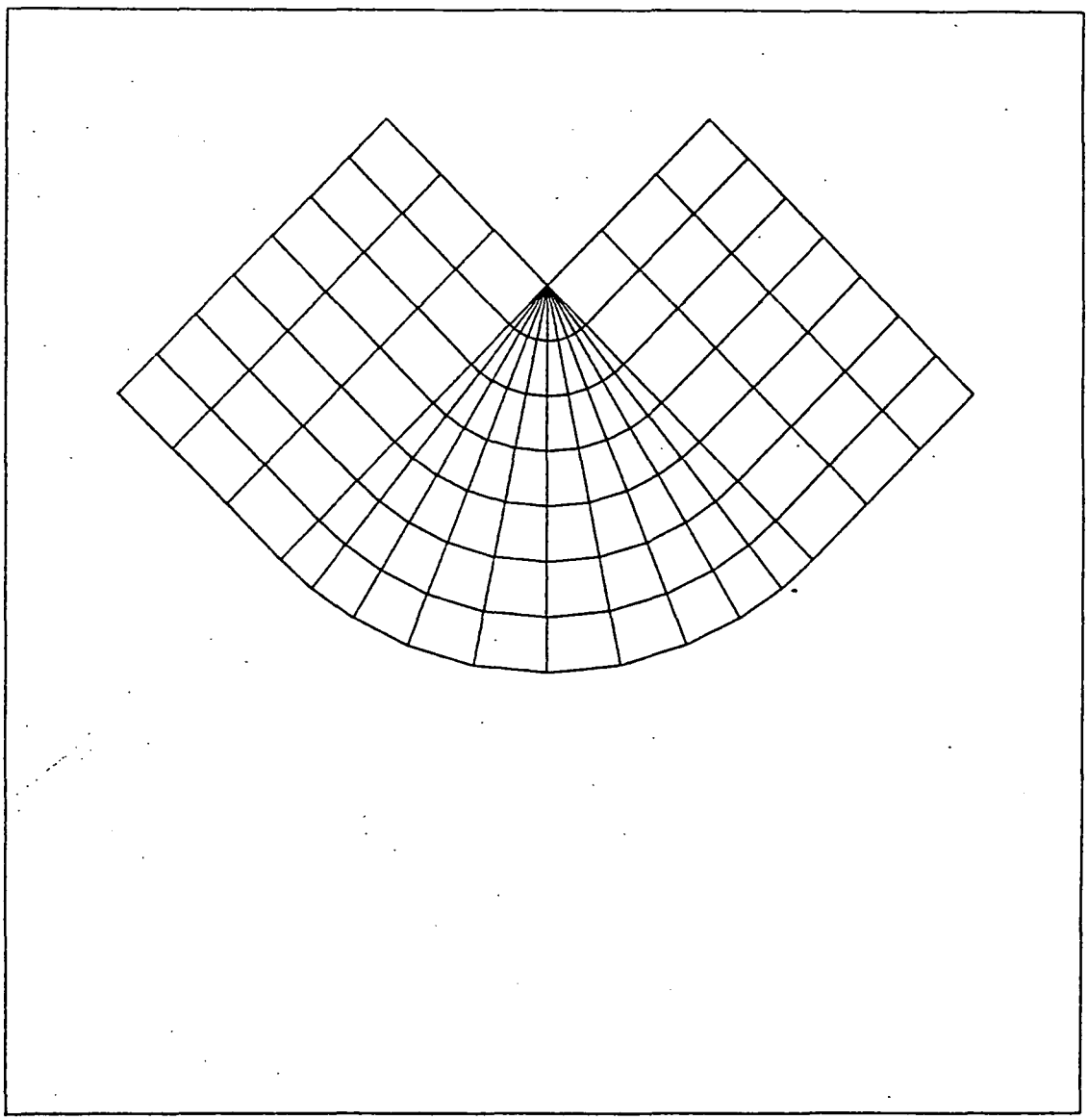

Figure 2.19 Evolution of a V-shaped valley under constant abrasion using the method of characteristics: random definition of point.

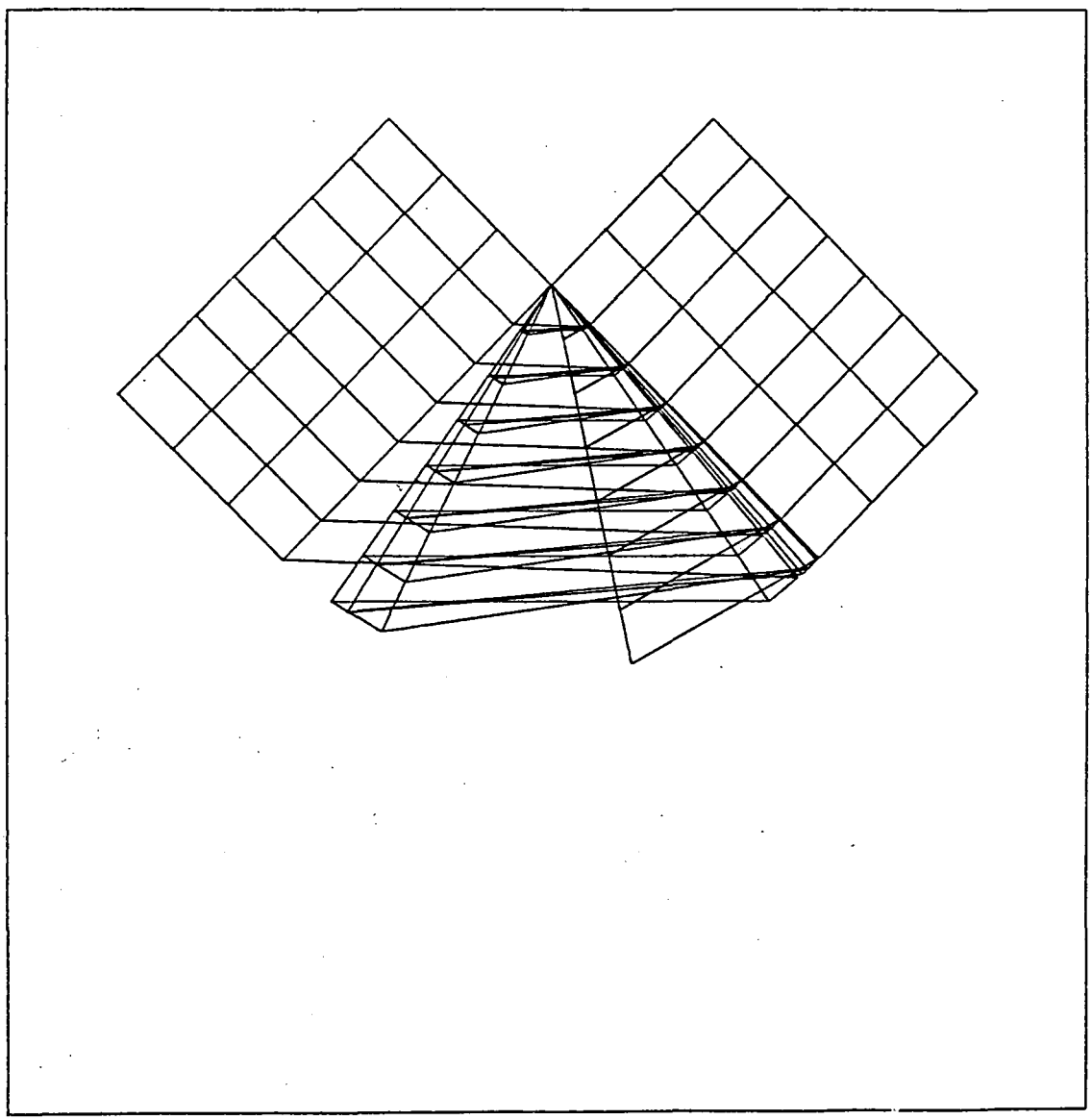

Figure 2.20 Evolution of slope and plateau with curvature dependent abrasion rate using the Farmer formulation.

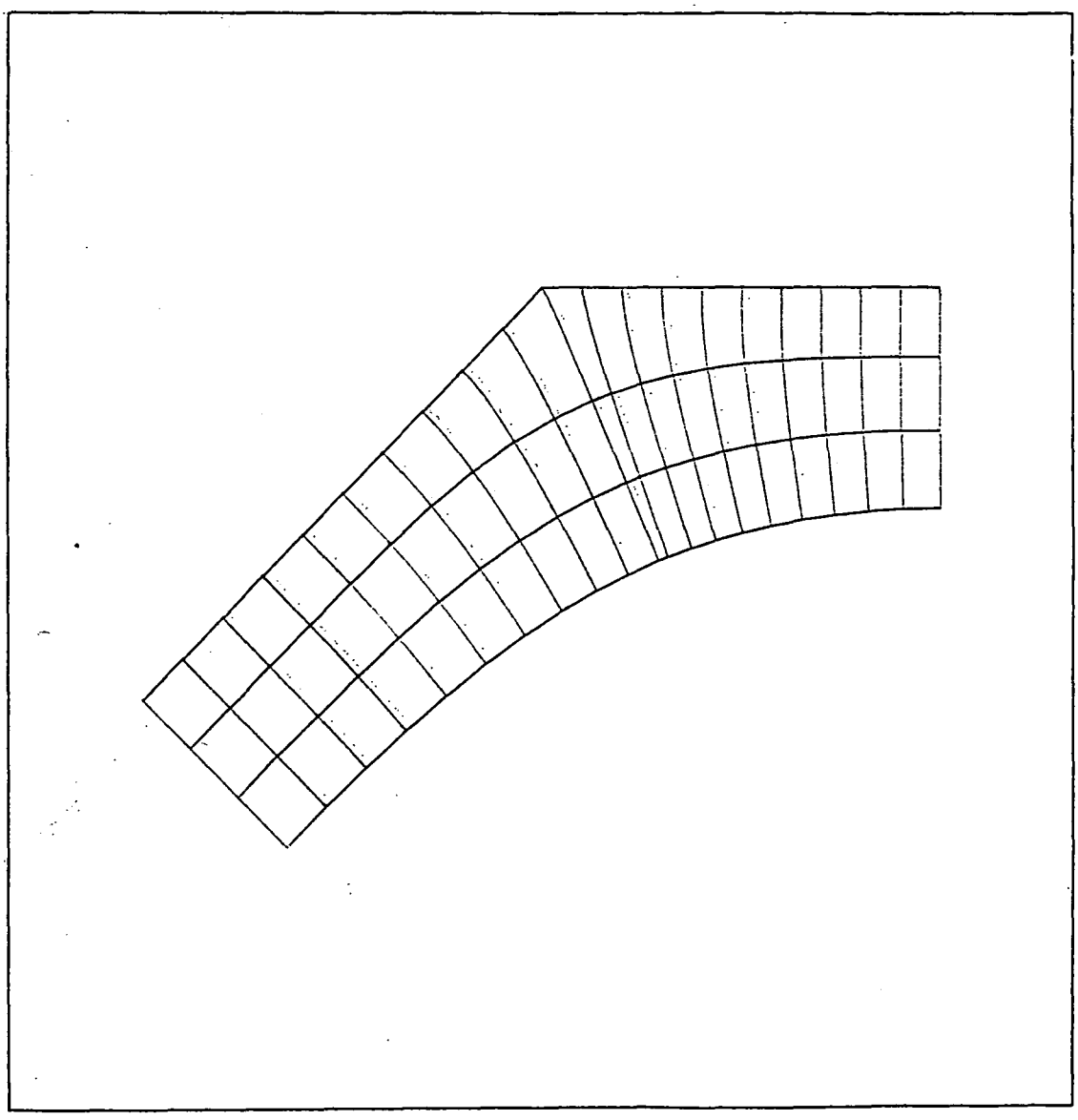

Figure 2.21 Evolution of V-shaped valley with abrasion inhibited by concavity using the Farmer formulation.

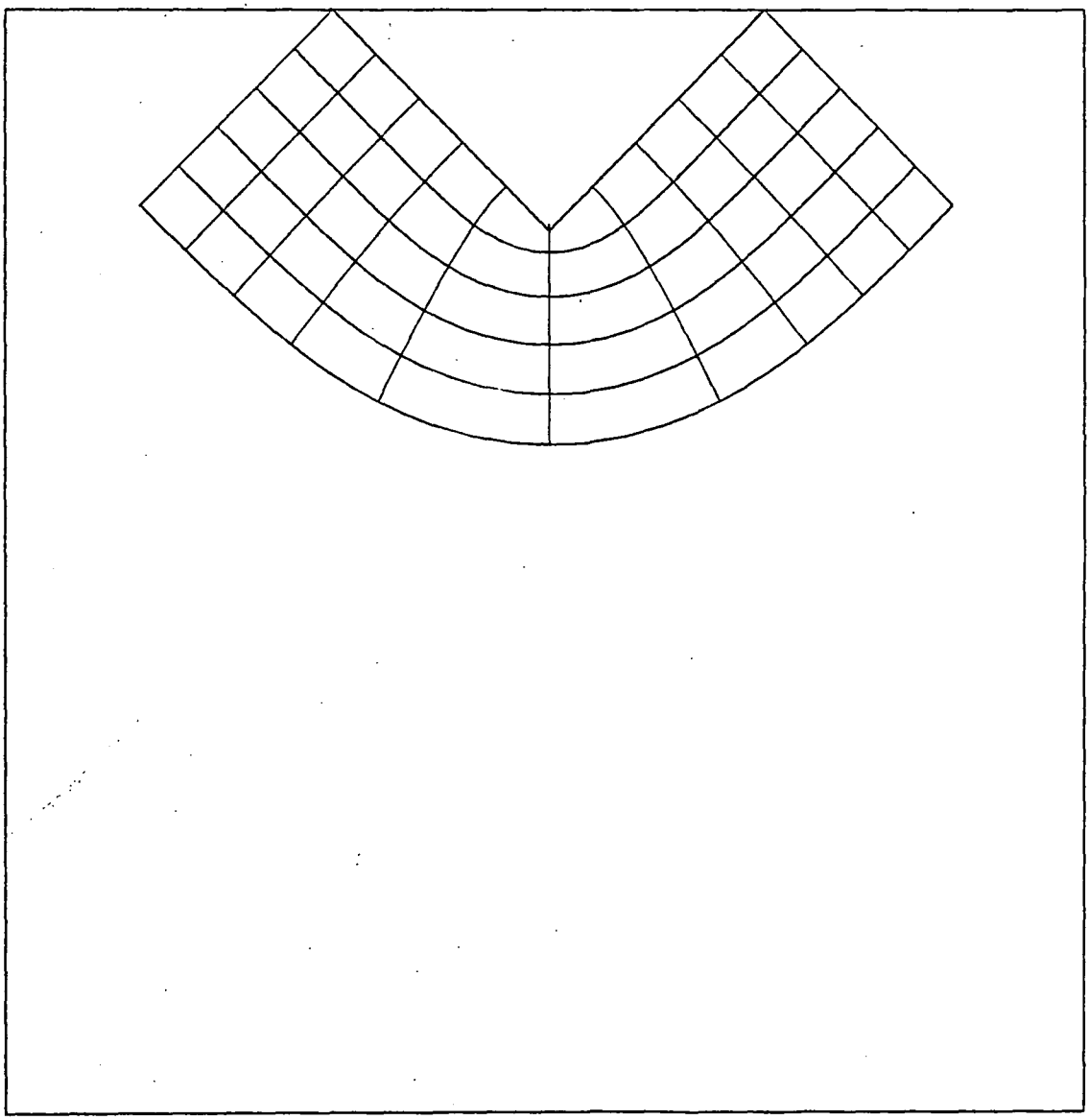

Figure 2.22 Evolution of V-shaped valley with abrasion enhanced by concavity using the Farmer formulation.

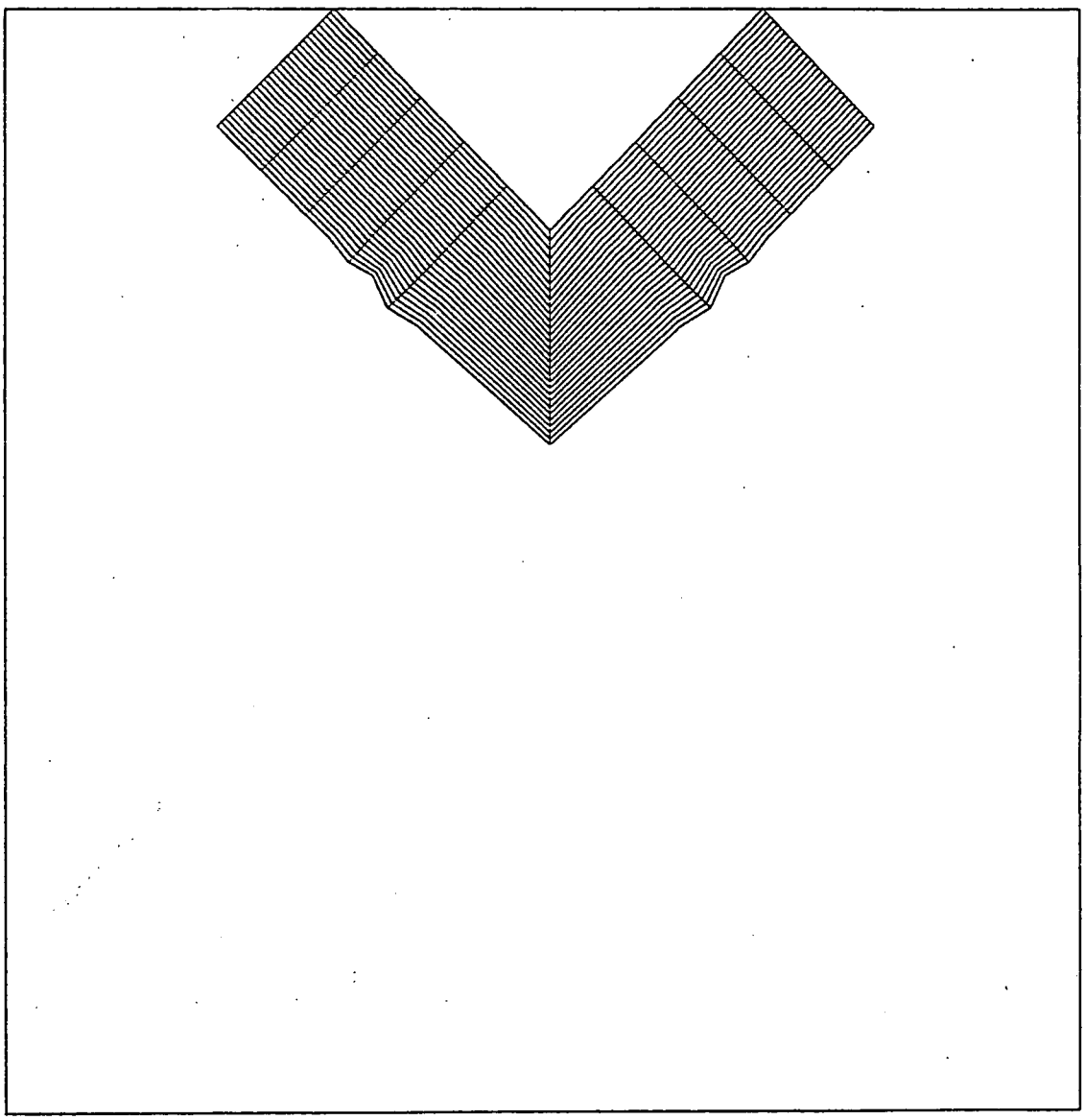

Figure 2.23 Evolution of a V-shaped valley with a Gaussian abrasion function.

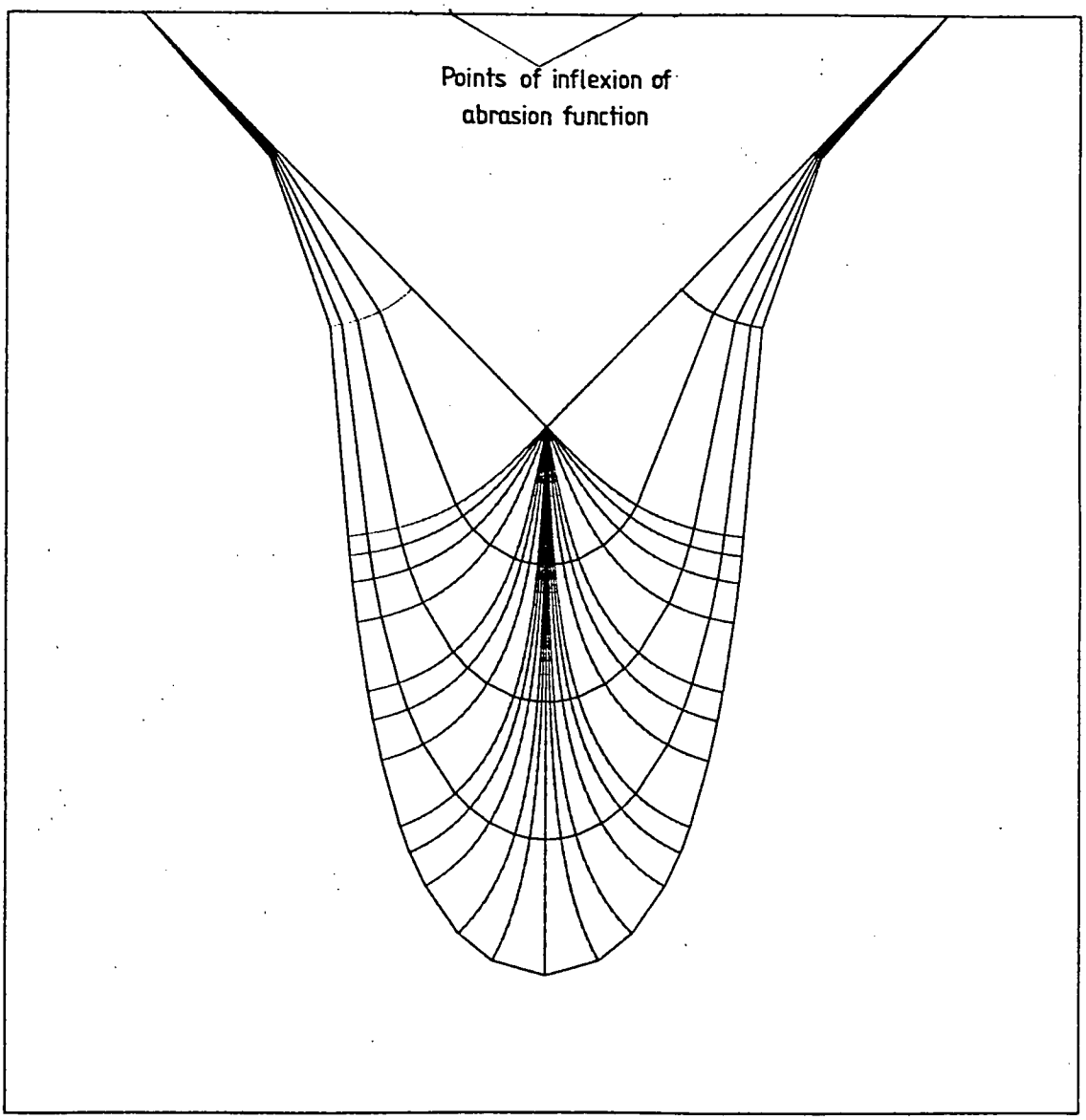

Figure 2.24 Evolution of a V-shaped valley with rocks of different hardness.

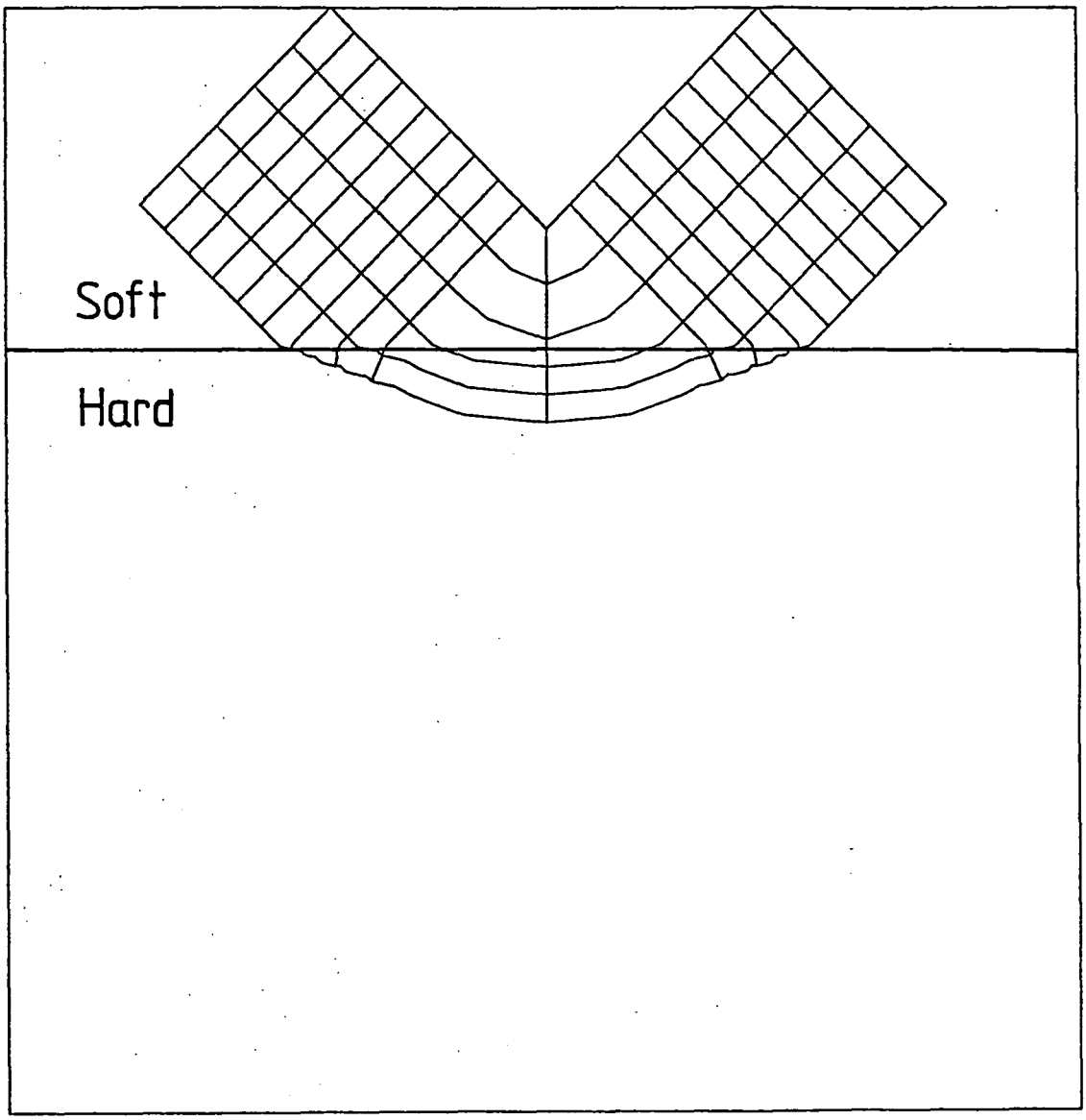

Figure 2.25 Trough persistent under lowering with a α 1/h: hyberbolic cosine.

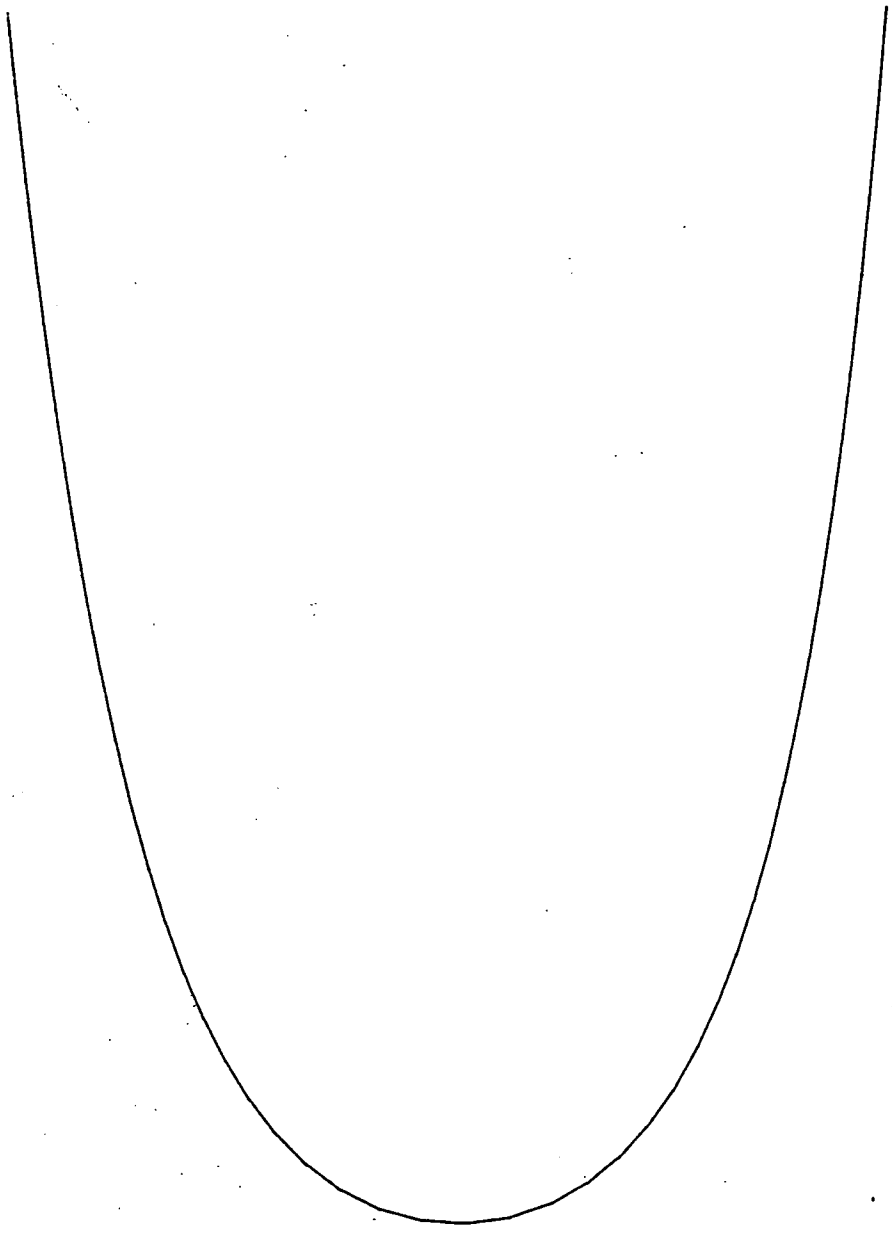

Figure 2.26 Troughs persistent under lowering with abrasion a function of a curvature.

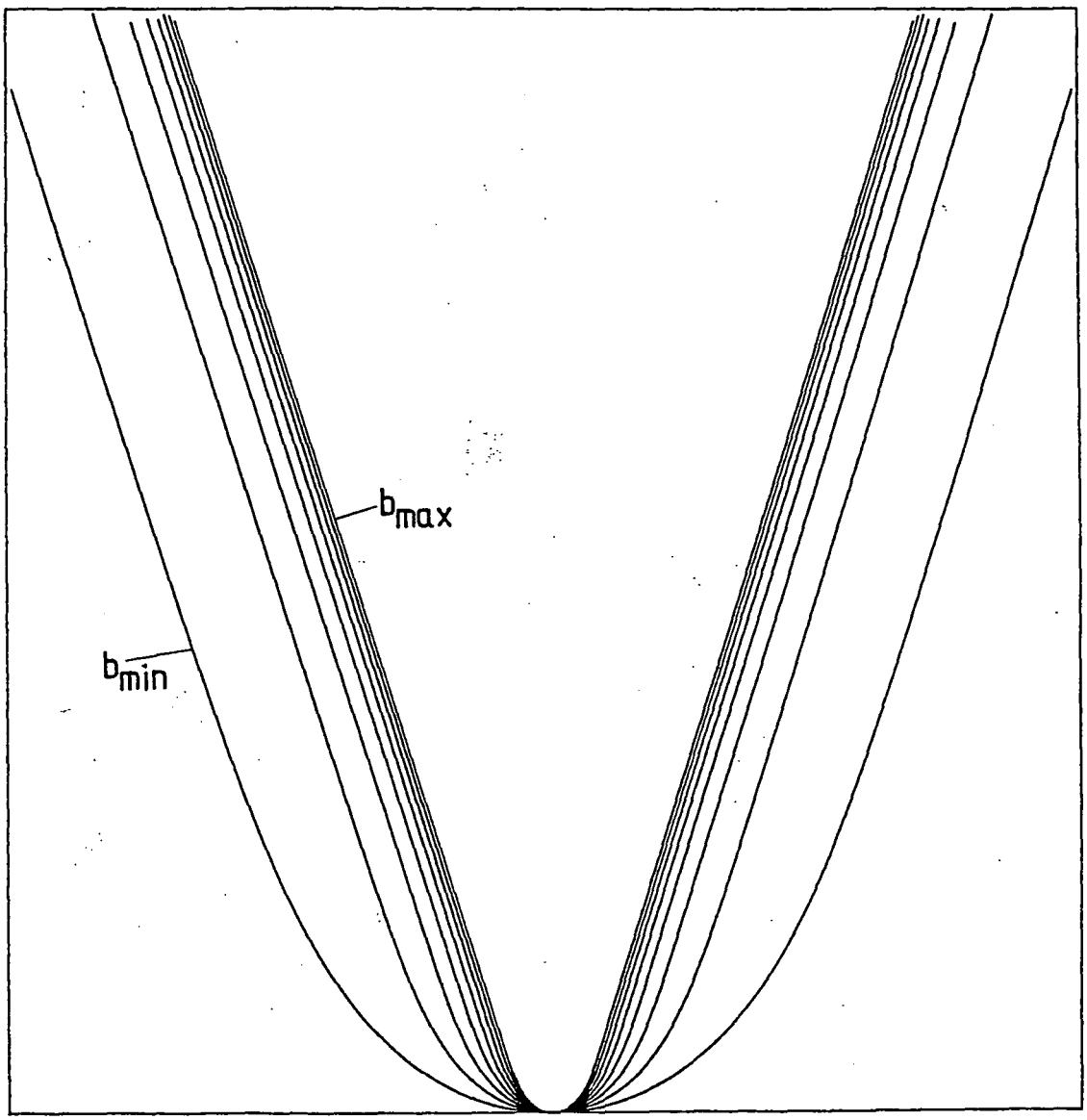

Figure 2.27 Abrasion of a weak zone.

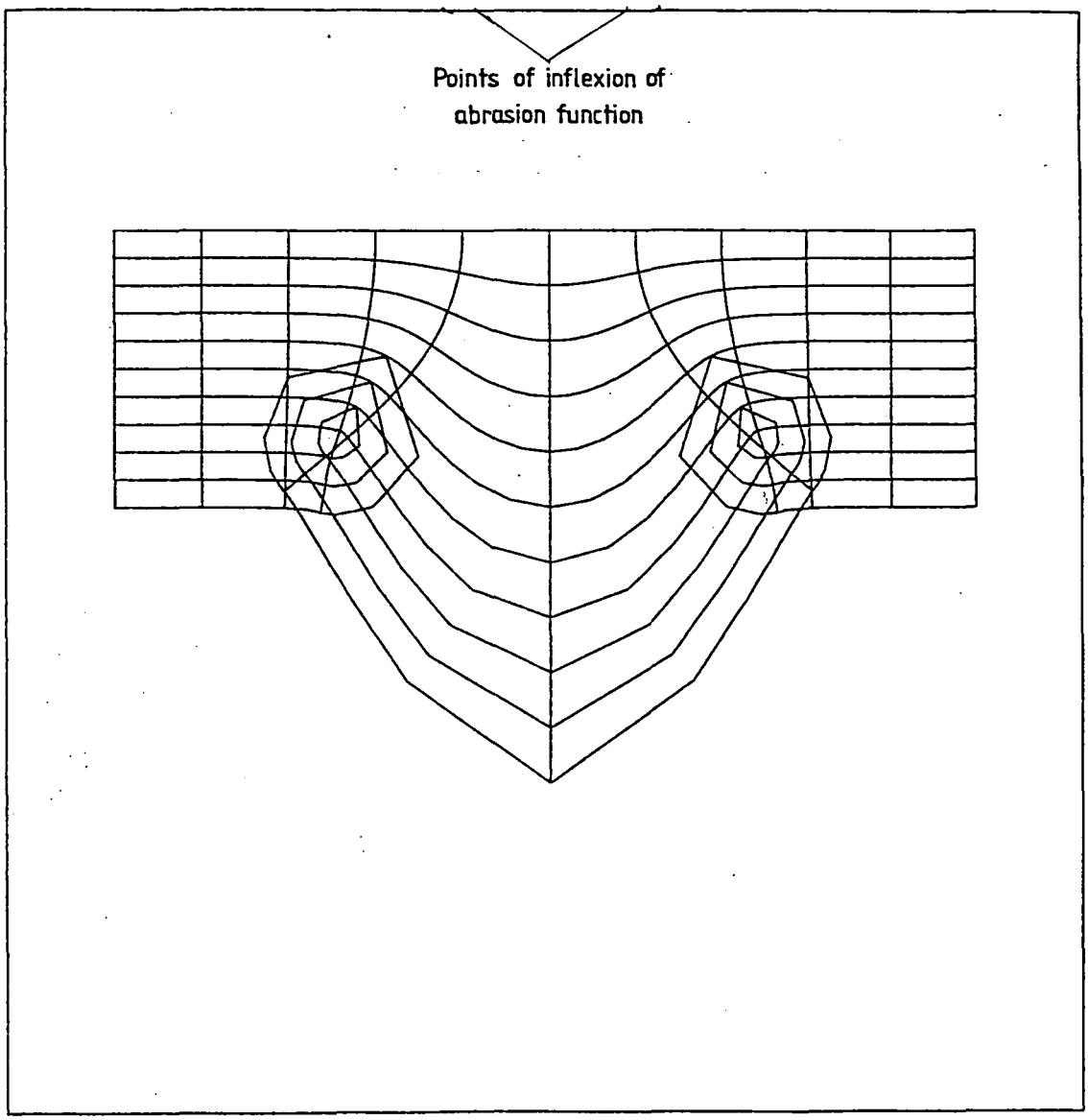

FIGURE 4.1 TWO ELEMENT TEST MODEL

o-Node at which velocity and pressure are solved for

x-Node at which velocity only is solved for

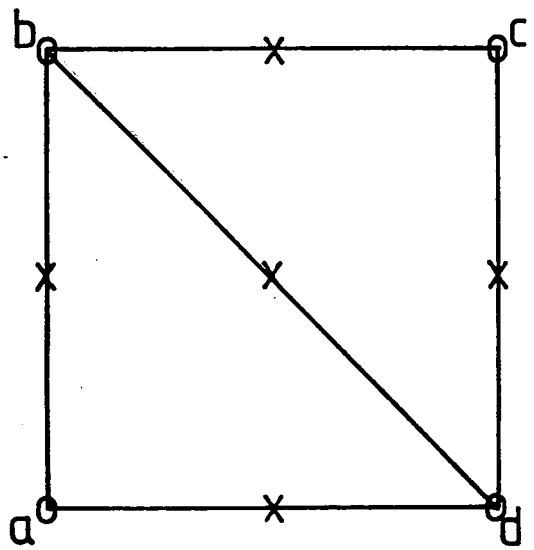

Boundary Conditions

ad - Fixed bed or Weertman

abcd-Prescribed velocity or traction

abd, bcd are the finite elements

Figure 4.2 Inclined plane problem-nine nodes.

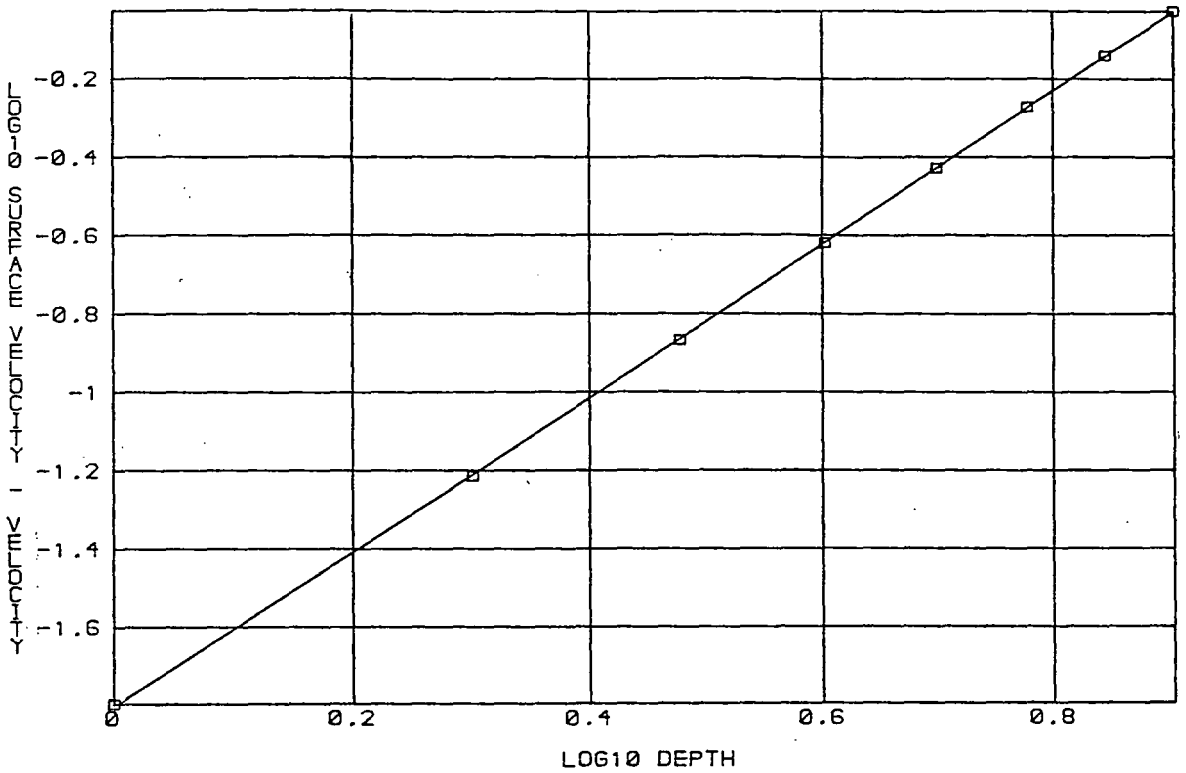

Figure 4.3 Inclined plane problem-seventeen nodes.

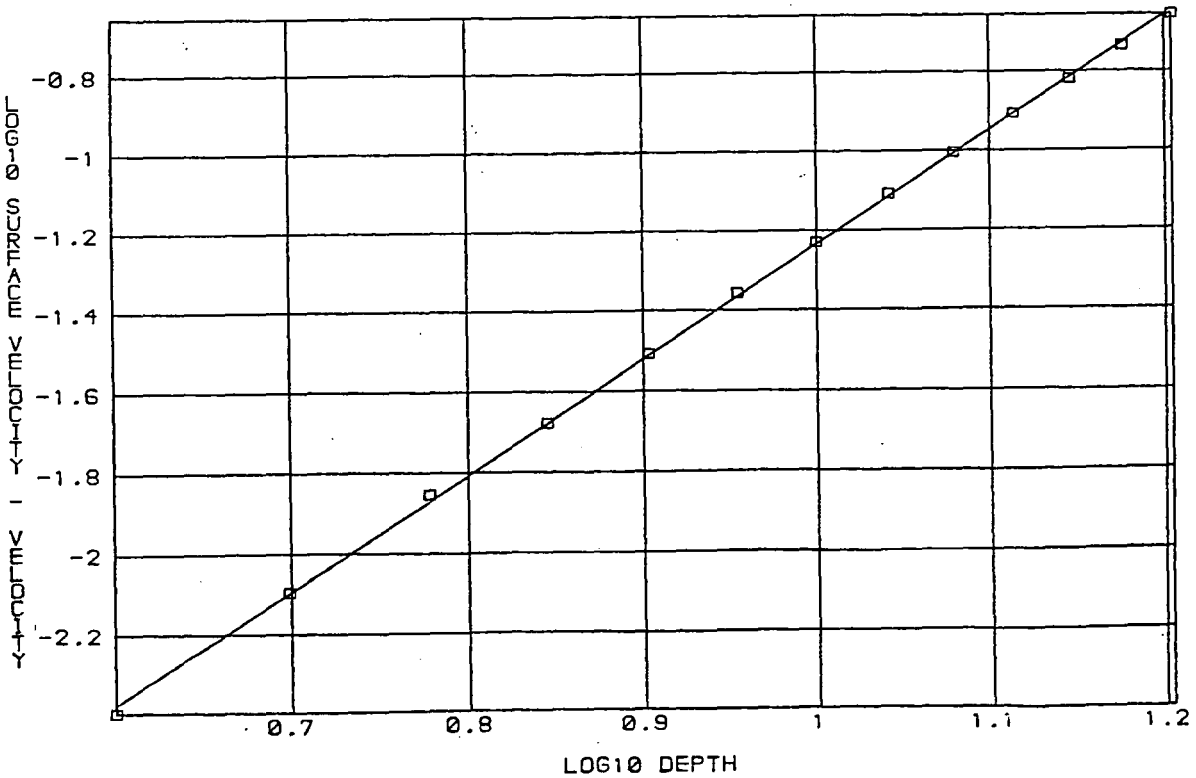

Figure 4.4 Rotating Couette flow.

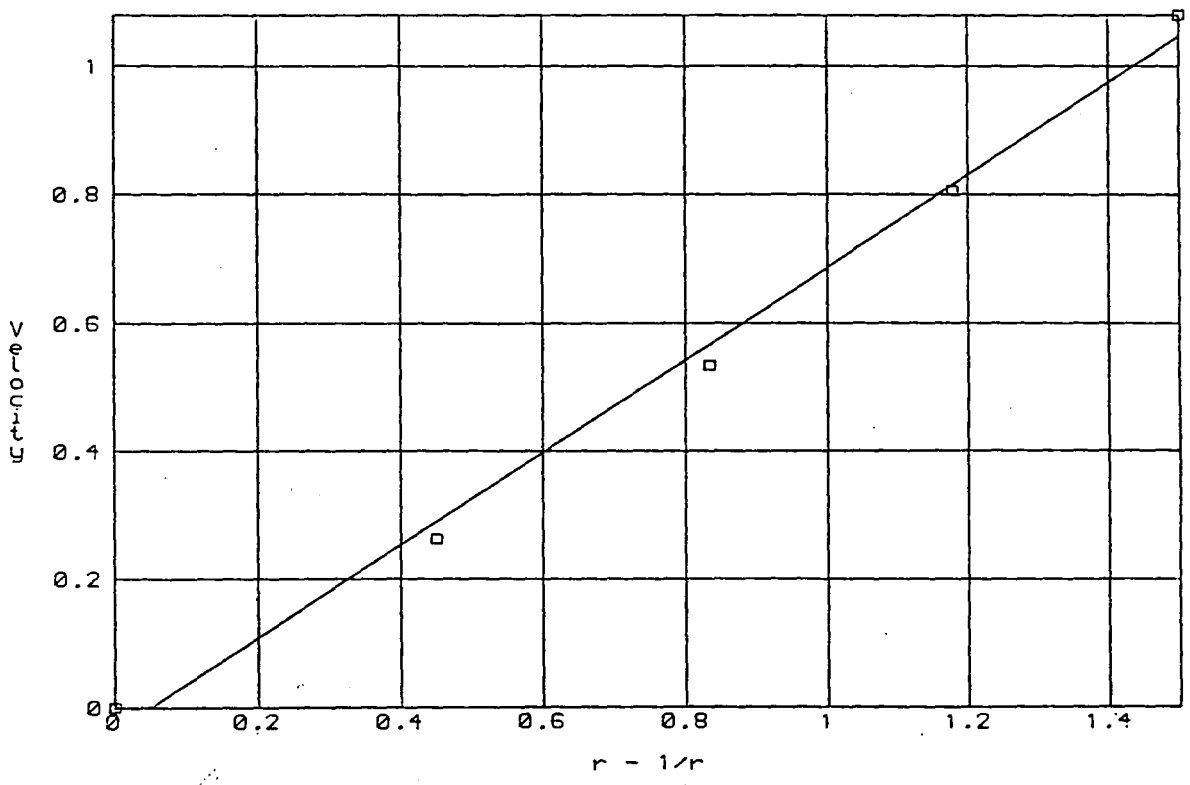

Figure 5.1 View of finite element mesh showing the nesting scheme.

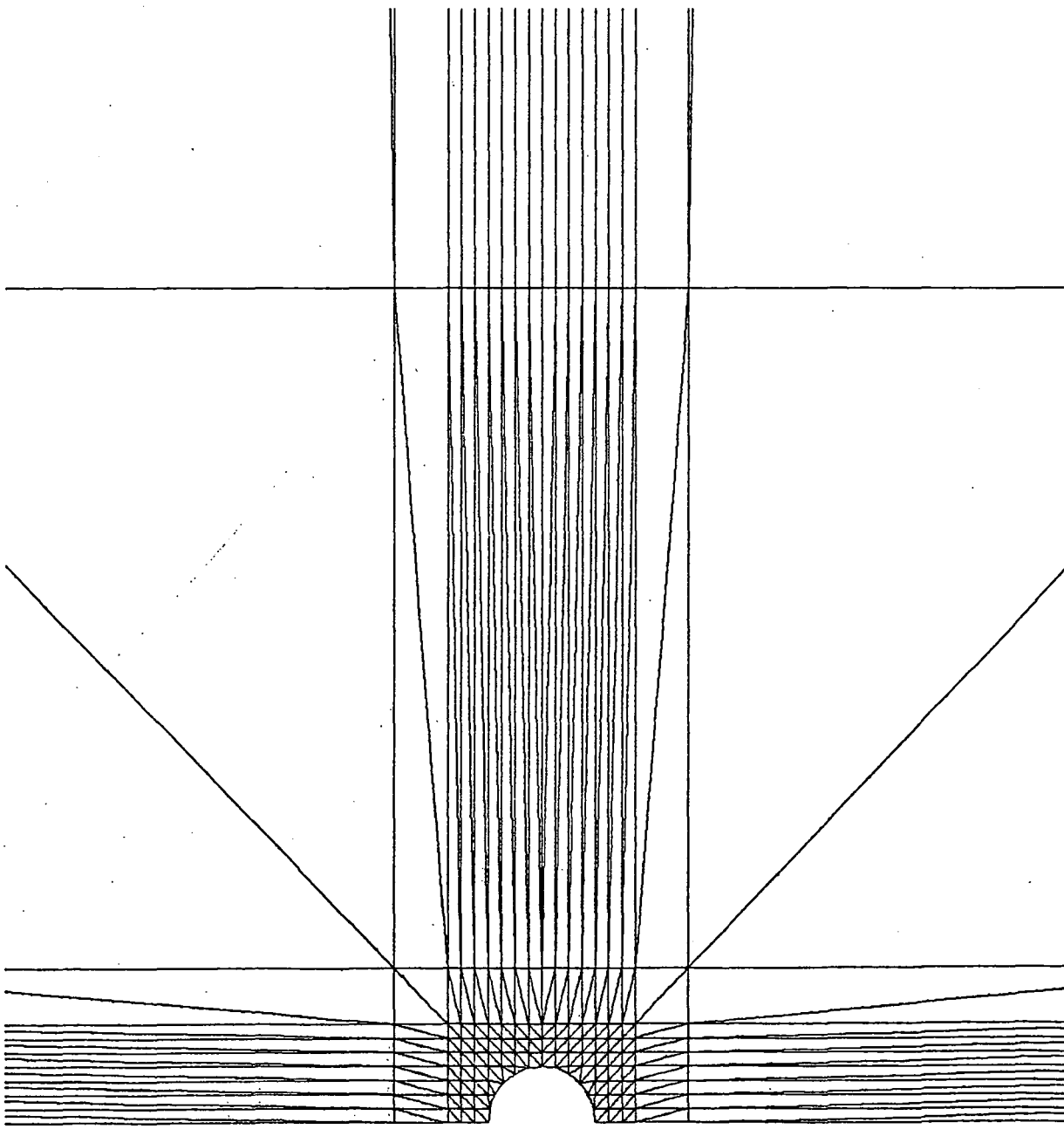

Figure 5.2 Detail from finite element mesh for modelling flow over a semi-cylindrical ridge.

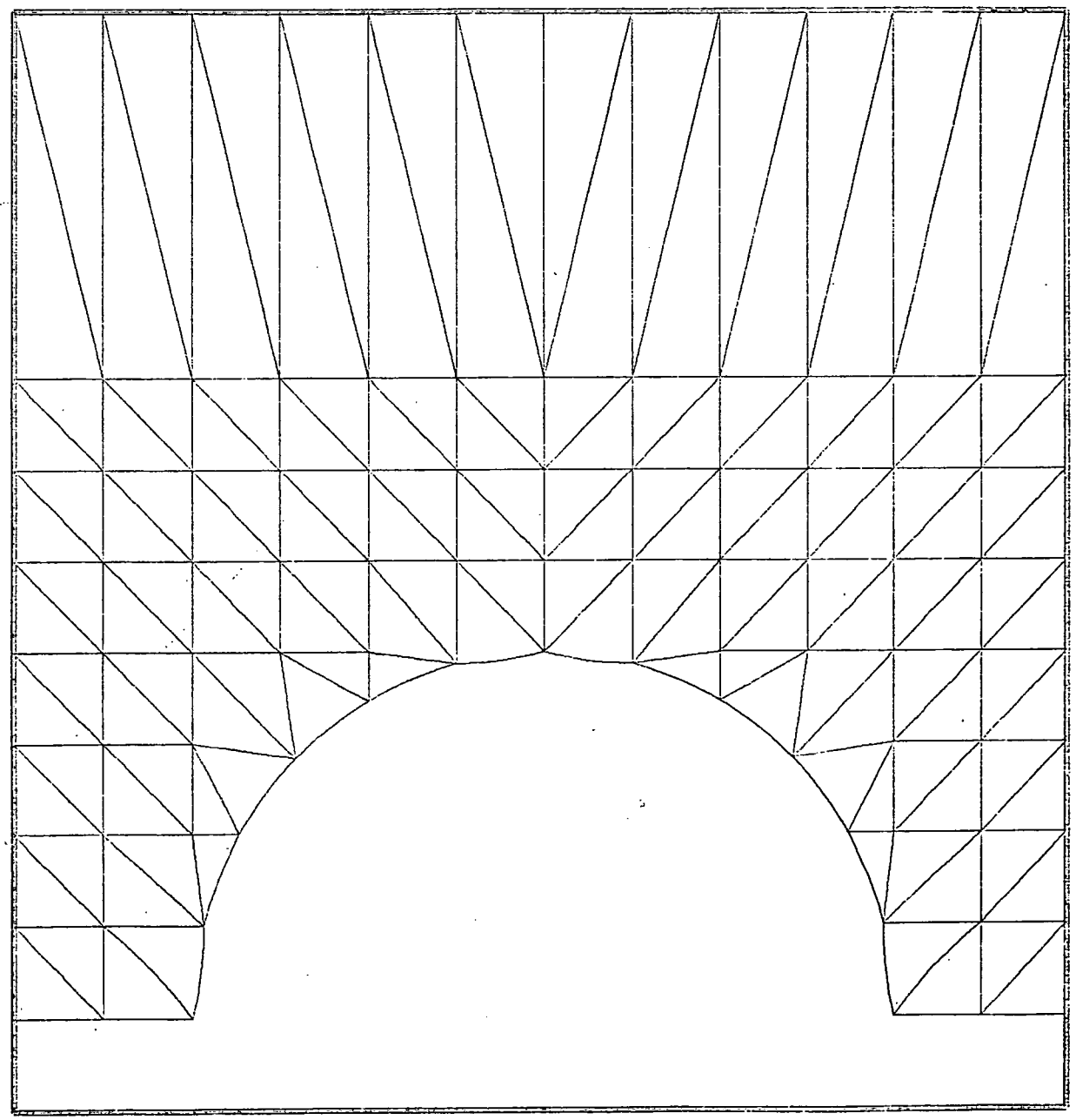

Figure 5.3 Detail from finite element mesh for modelling flow over a truncated sine ridge.

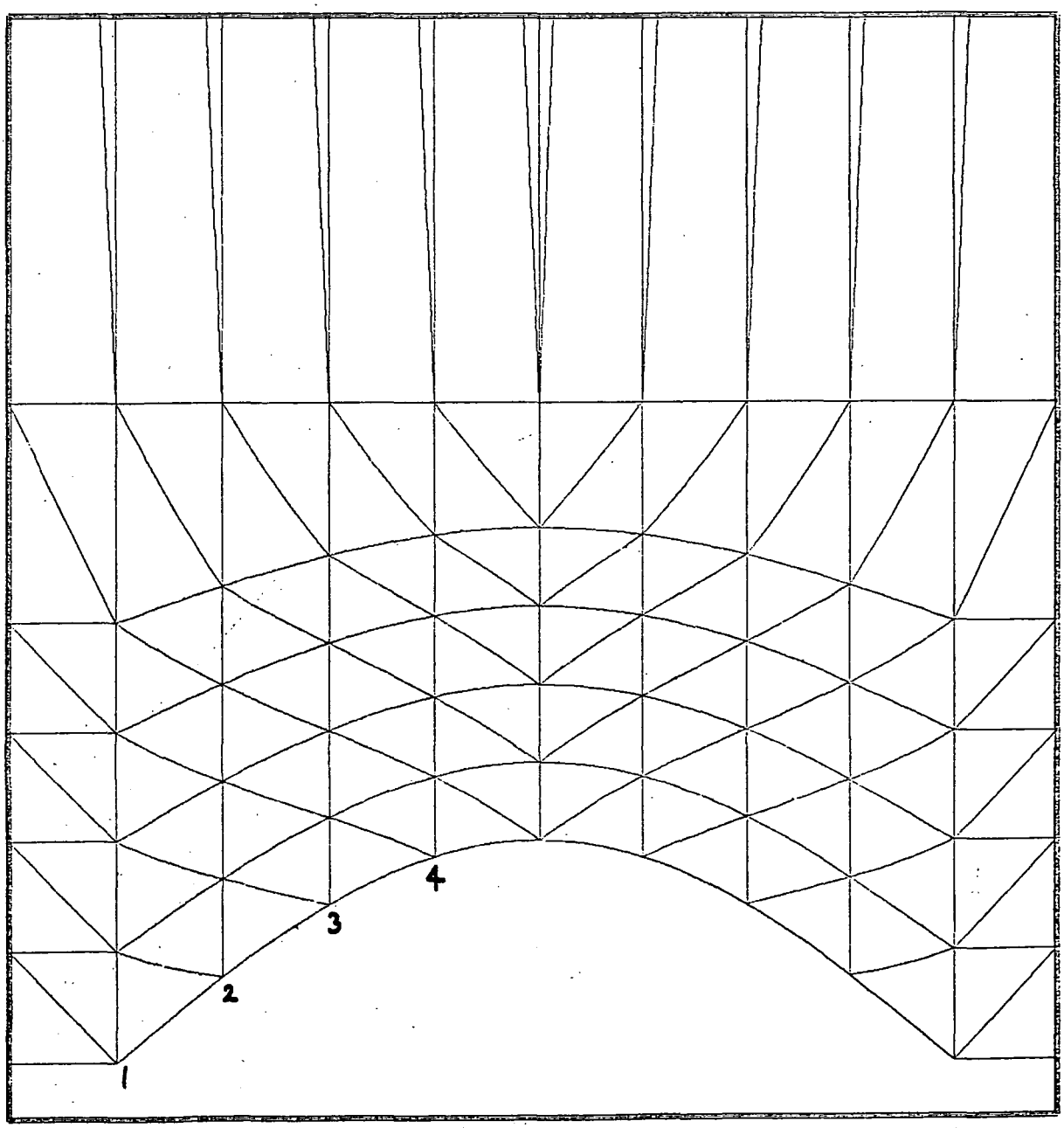

FIGURE 5.4 SCHEMATIC DIAGRAM OF BOUNDARY CONDITIONS FOR PLANE-STRAIN

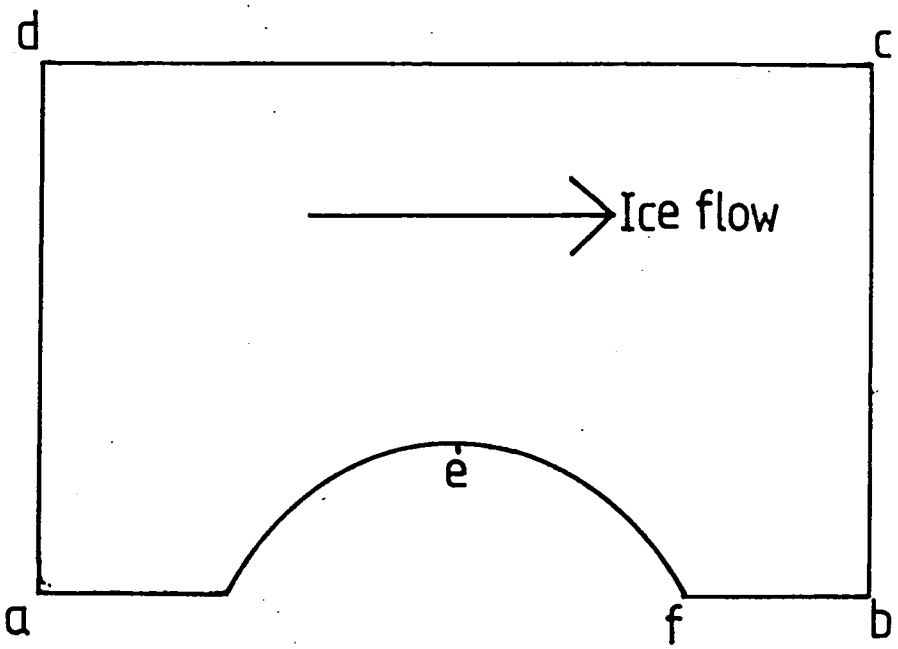

adcb - Tractions at infinity

ab - Zero normal velocity, perfect slip or Weertman; if cavity exists, then tractions along ef

a,b - Slip velocity at infinity

Figure 5.5 Velocity vector plot for an incompressible linear rheology with v_d = 100 alu/a (Case 3).

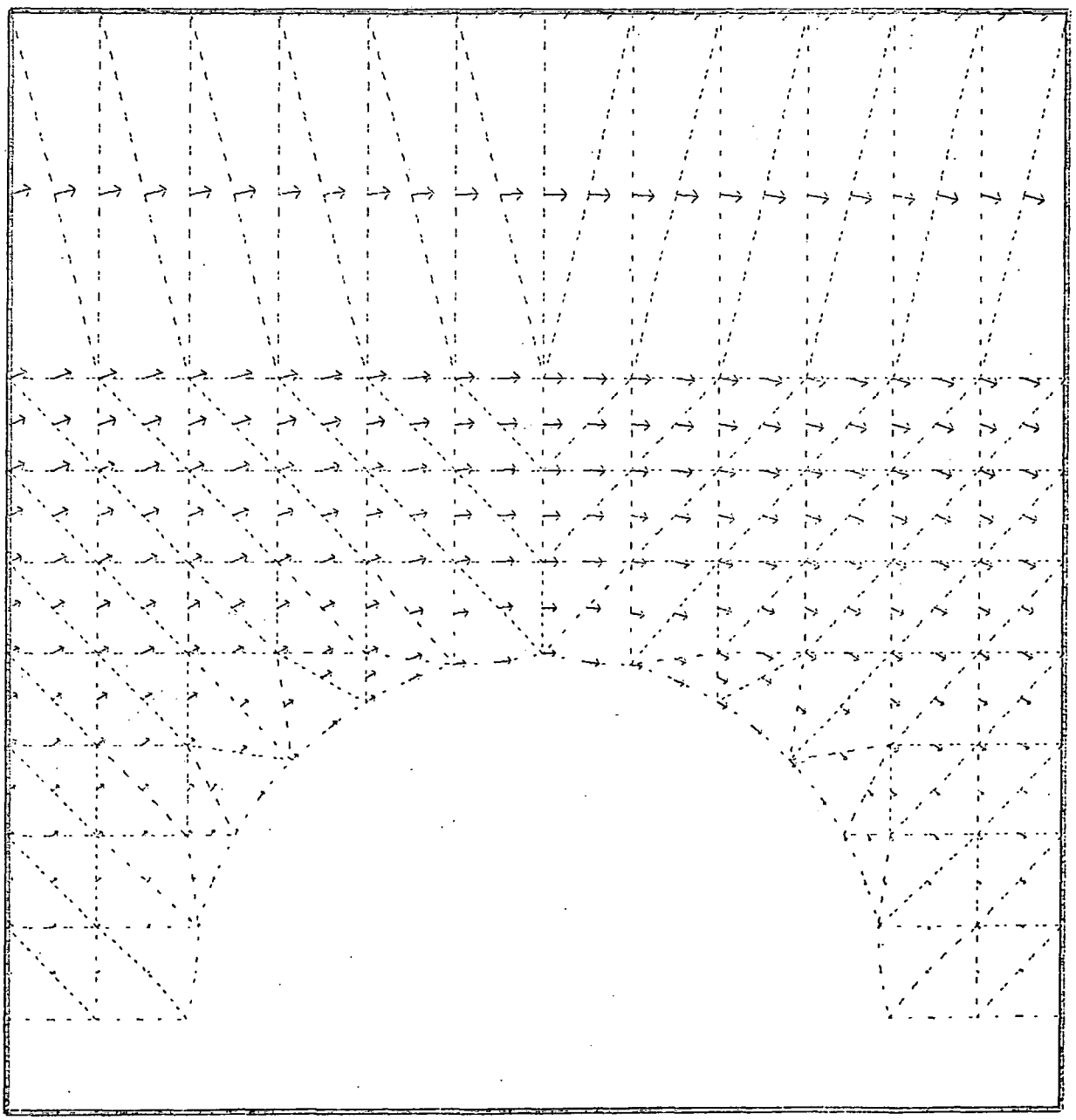

Figure 5.6 Larger view of velocity vector plot for an incompressible linear rheology with v_d = 100 alu/a (Case 3).

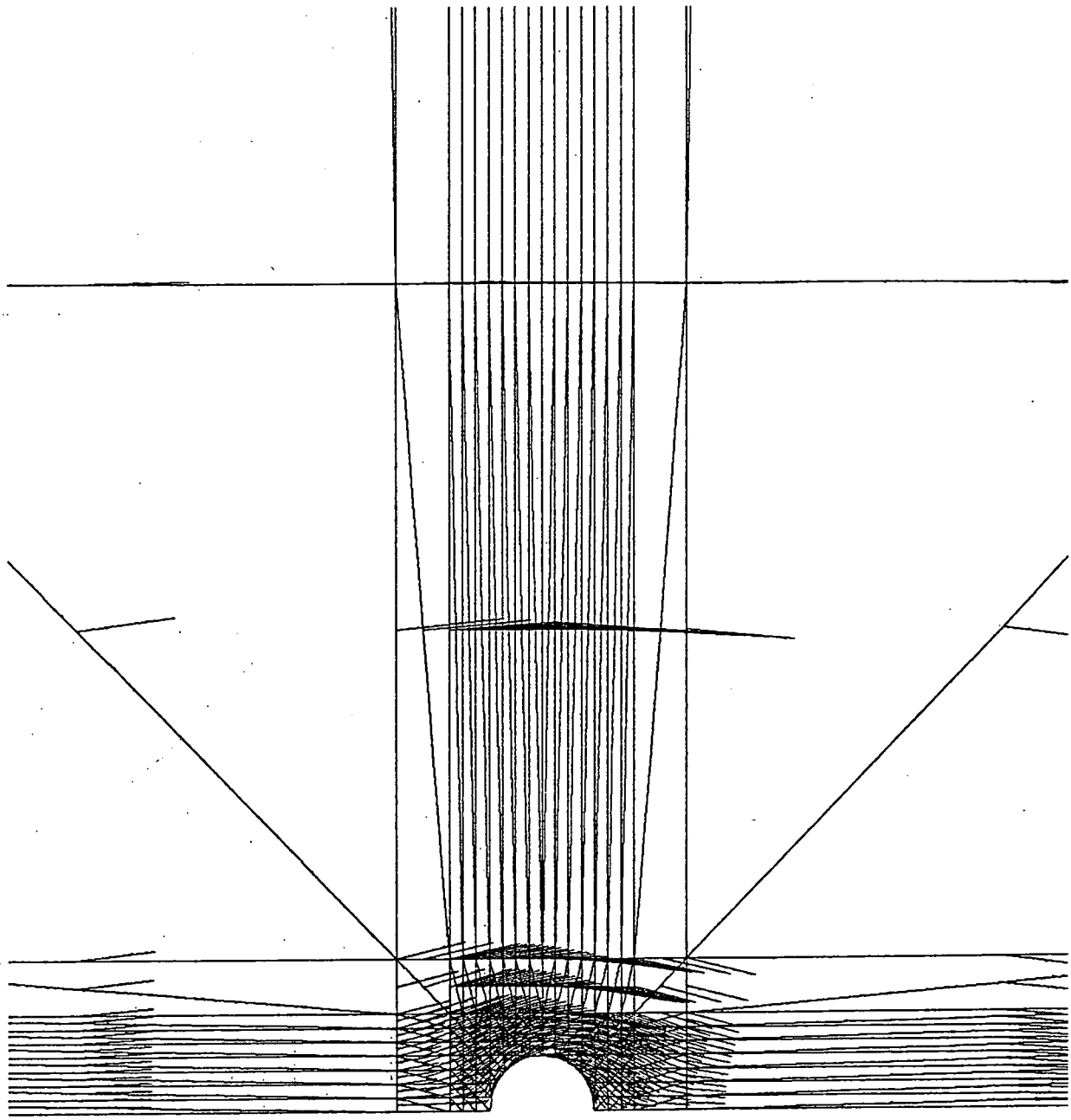

Figure 5.7 v_τ against $\sin\gamma$ for an incompressible linear rheology with v_d = 10 alu/a (Case 1).

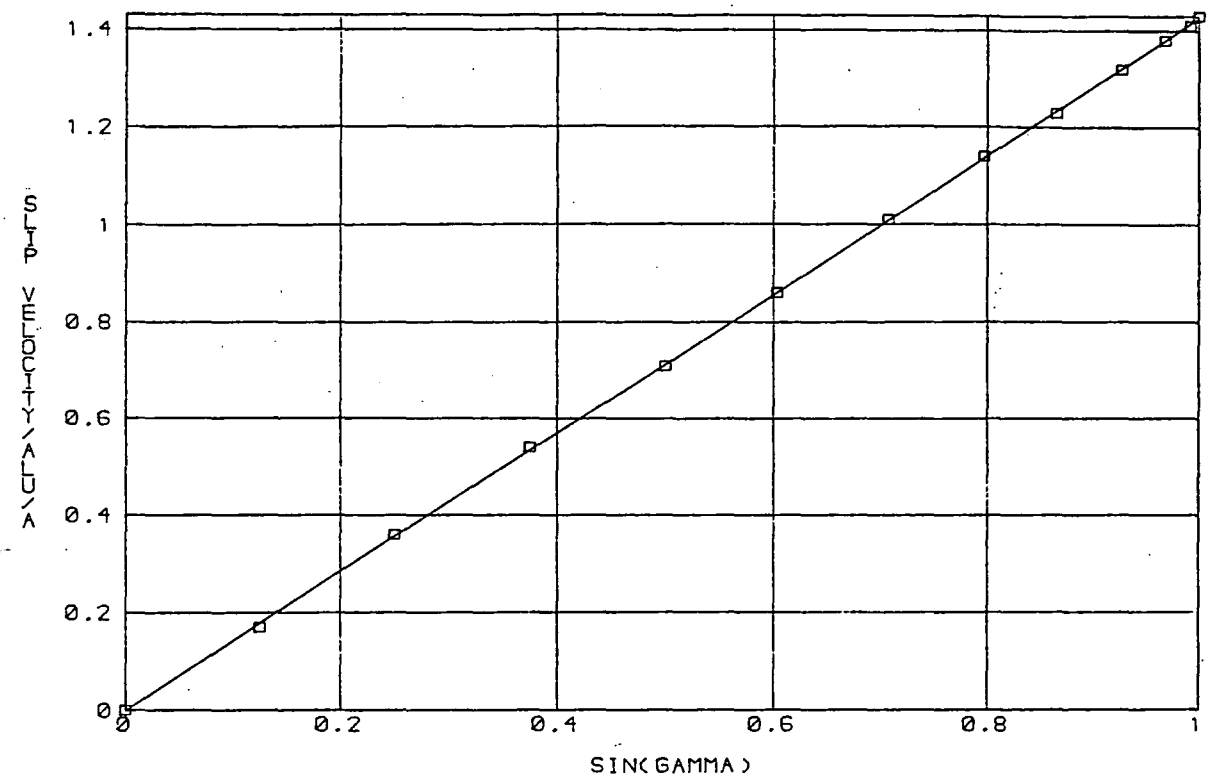

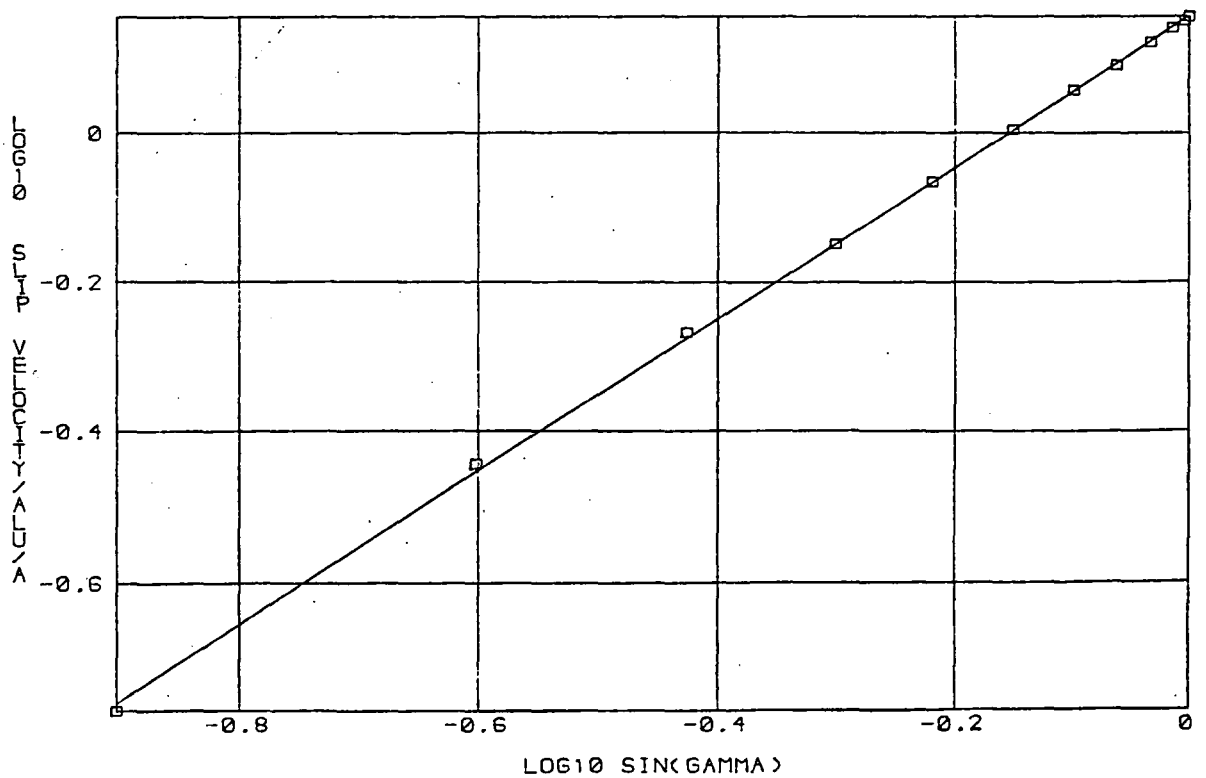

Figure 5.8 v_τ against $\sin\gamma$ for an incompressible linear rheology with a cavity and v_d = 400 alu/a (Case 7).

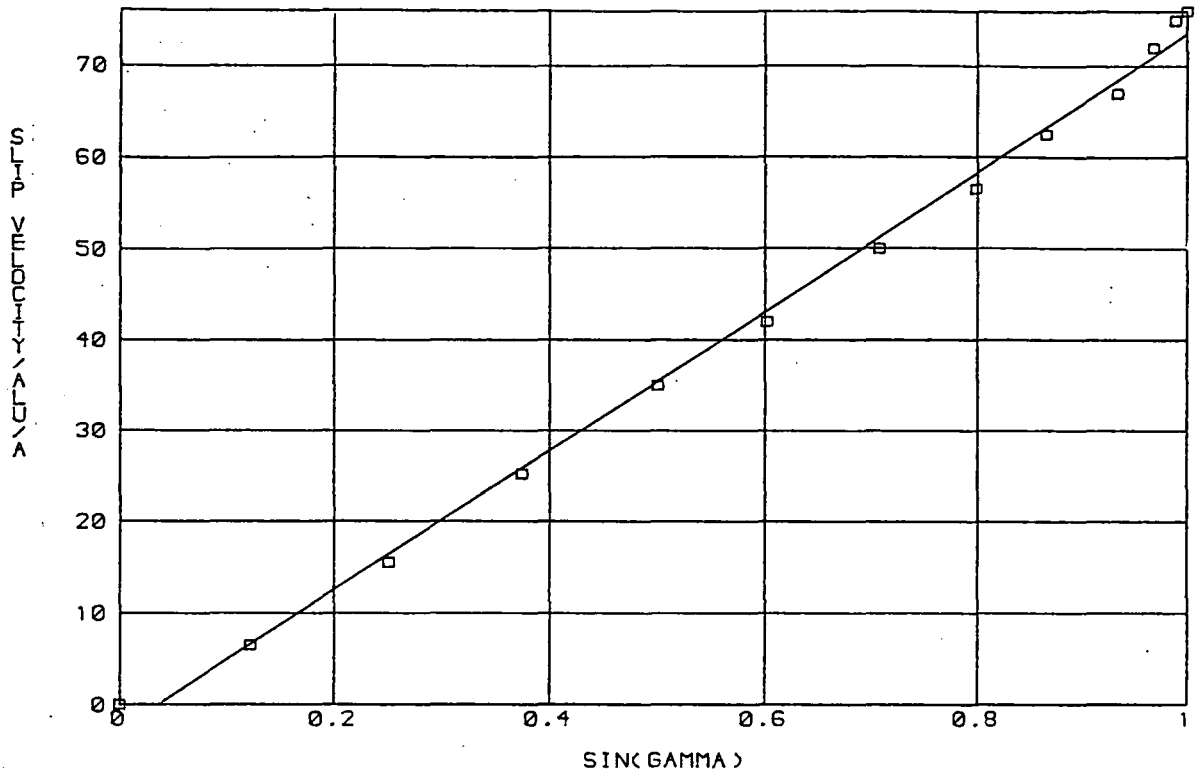

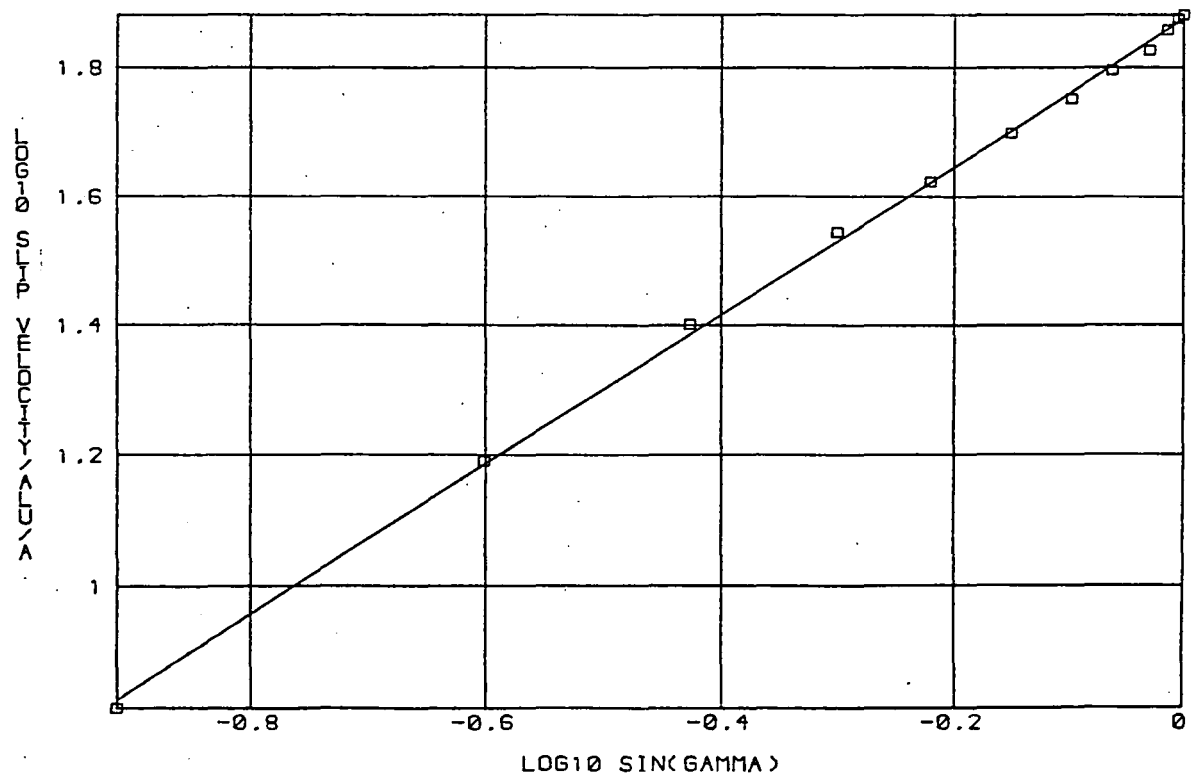

Figure 5.9 v_τ against $\sin\gamma$ for an incompressible linear rheology with a cavity and v_d = 10 alu/a (Case 6).

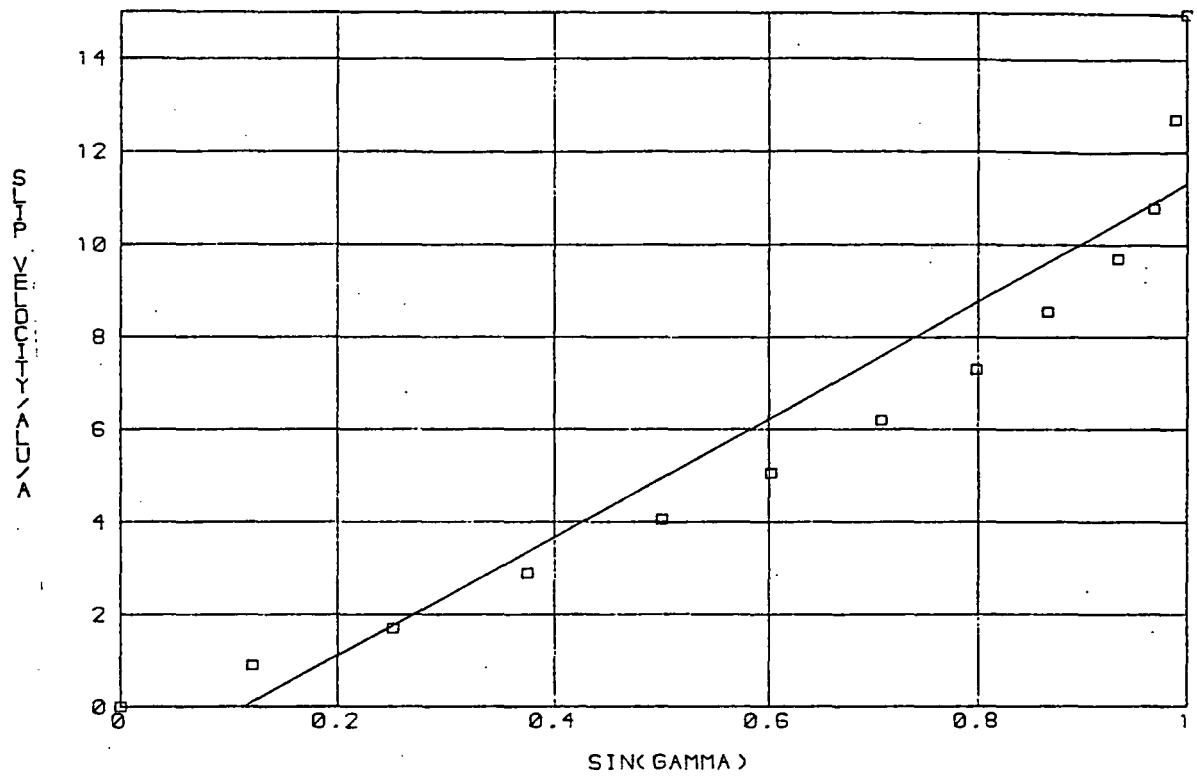

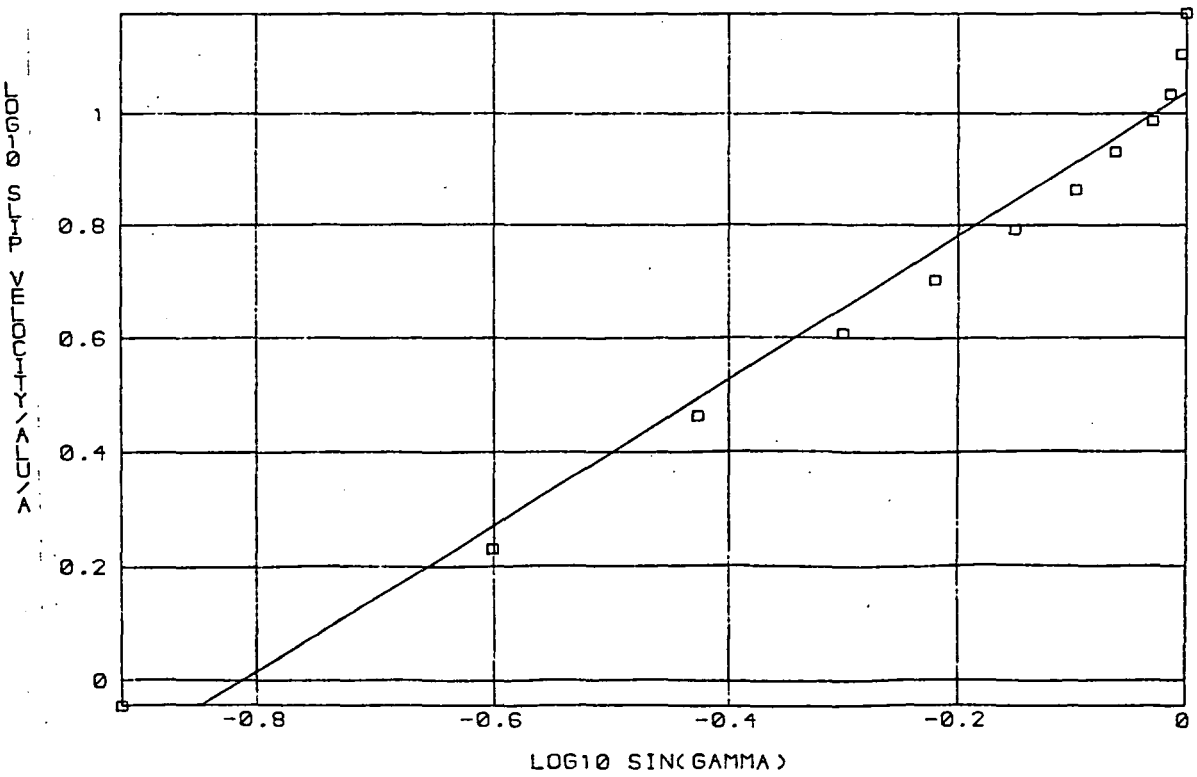

Figure 5.10 v_τ against $\sin\gamma$ for a compressible linear rheology with χ = 1 alu²/bar.a and v_d = 10 alu/a (Case 8).

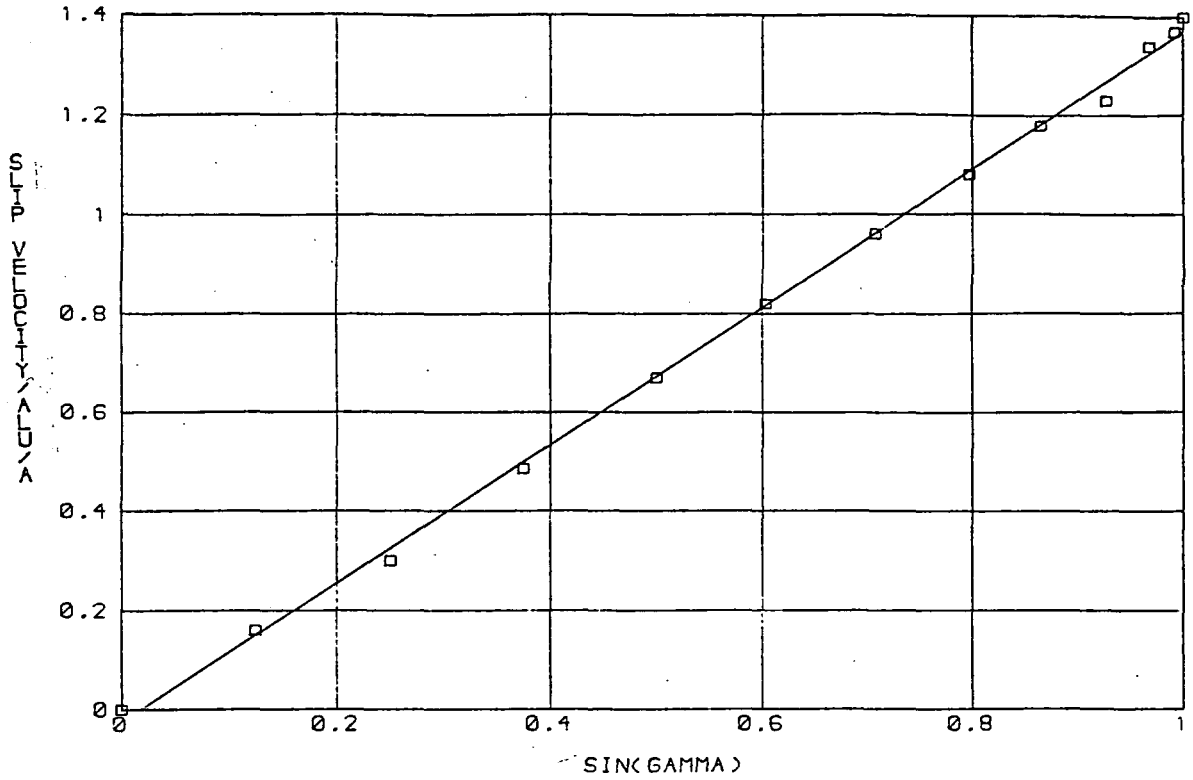

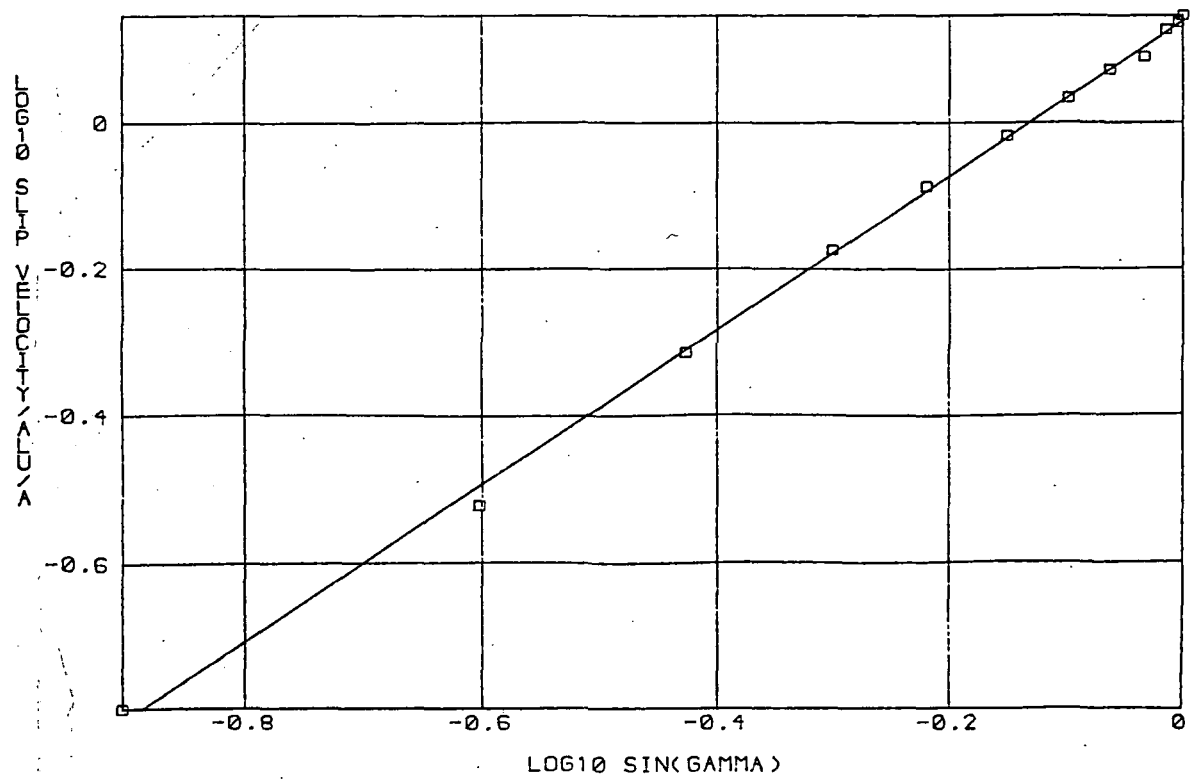

Figure 5.11 Velocity vector plot for a compressible linear rheology with χ = 10 alu^2/bar.a and v_d = 200 alu/a (Case 16).

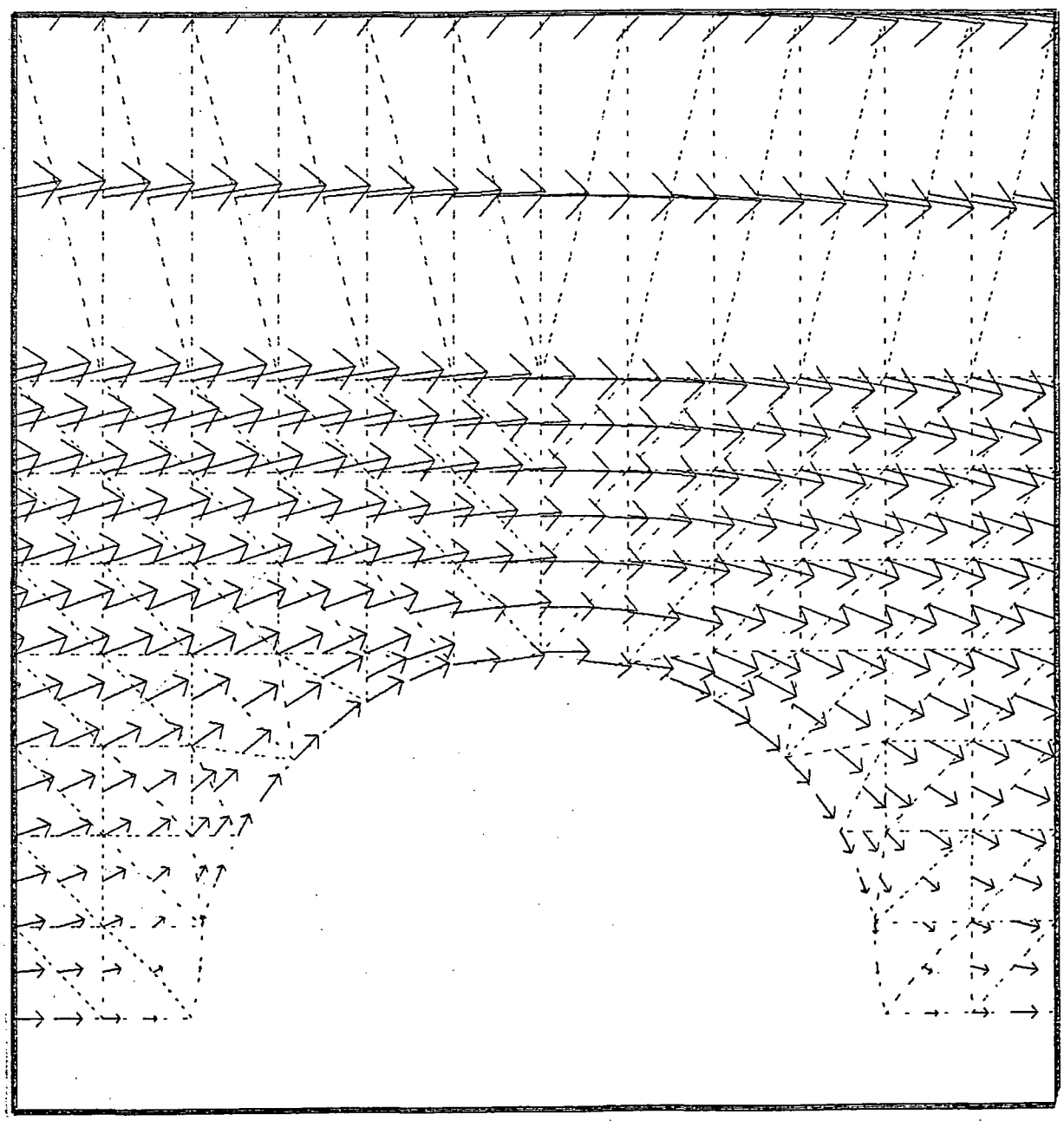

Figure 5.12 v_τ against $\sin\gamma$ for a compressible linear rheology with χ = 10 alu² /bar.a and v_d = 200 alu/a (Case 16).

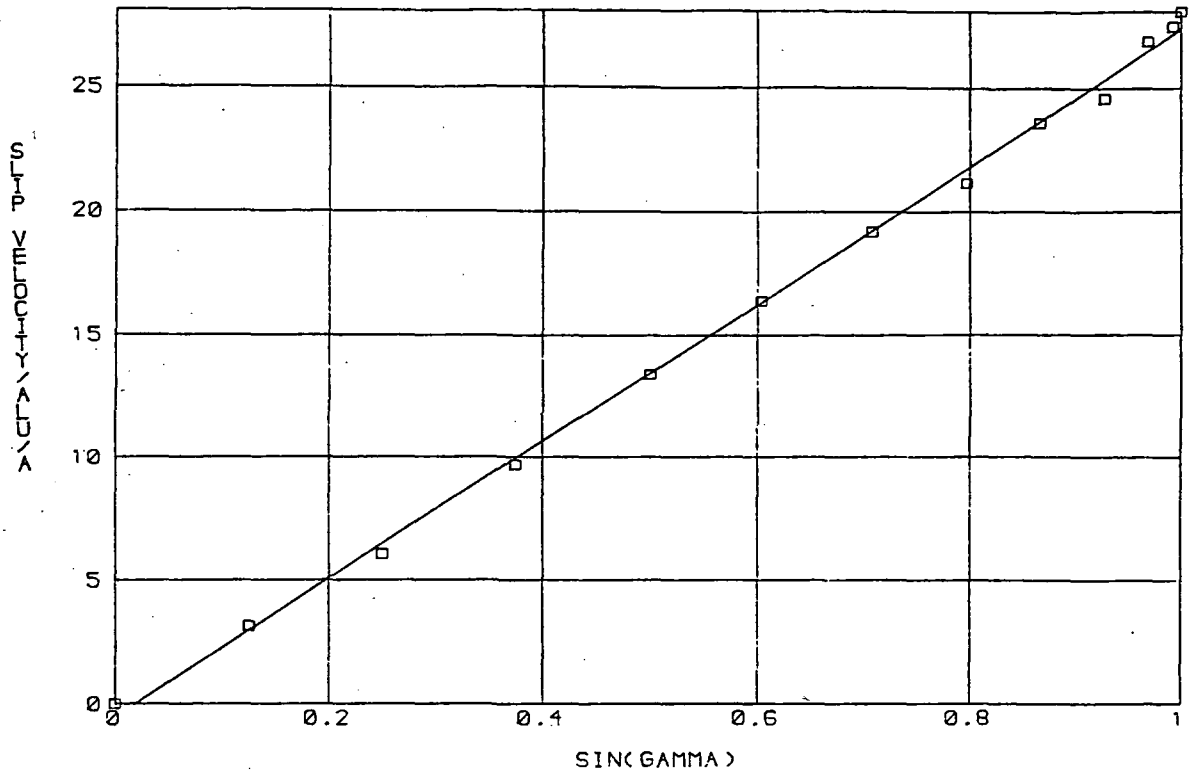

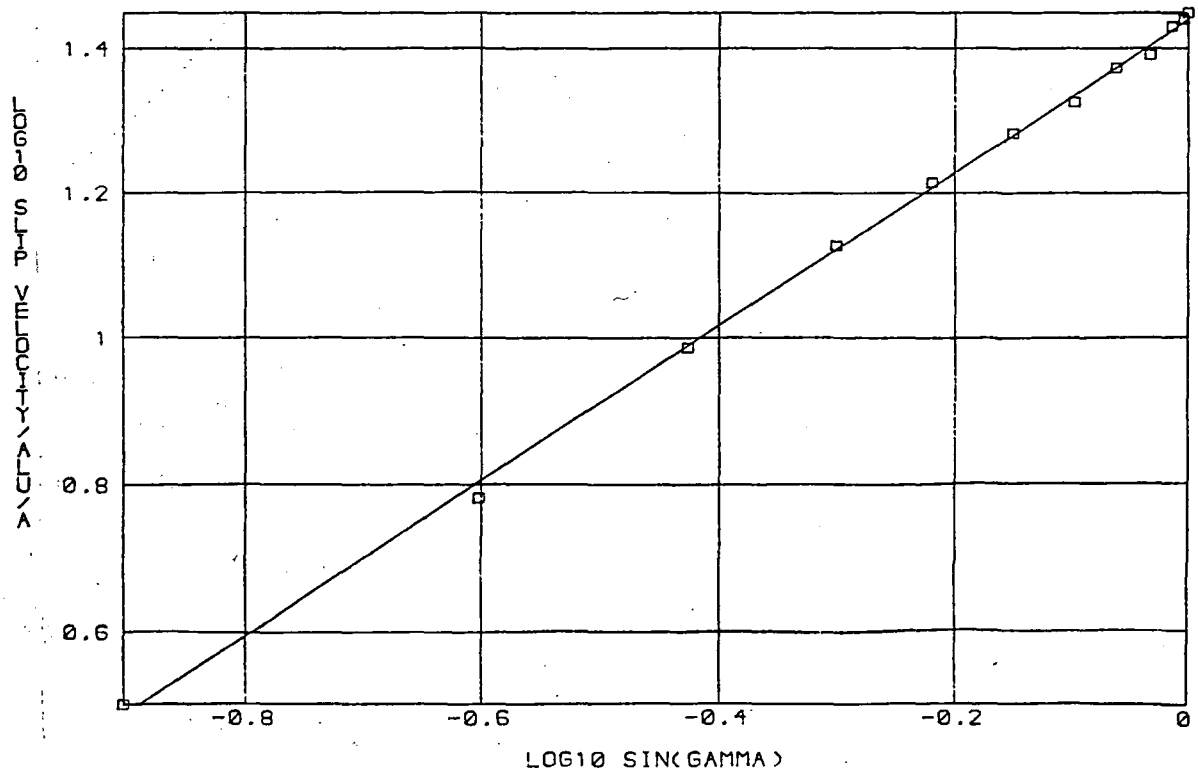

Figure 5.13 Velocity vector plot for an incompressible linear rheology with bed of S = 100 alu/bar.a and v_d = 100 alu/a (Case 20).

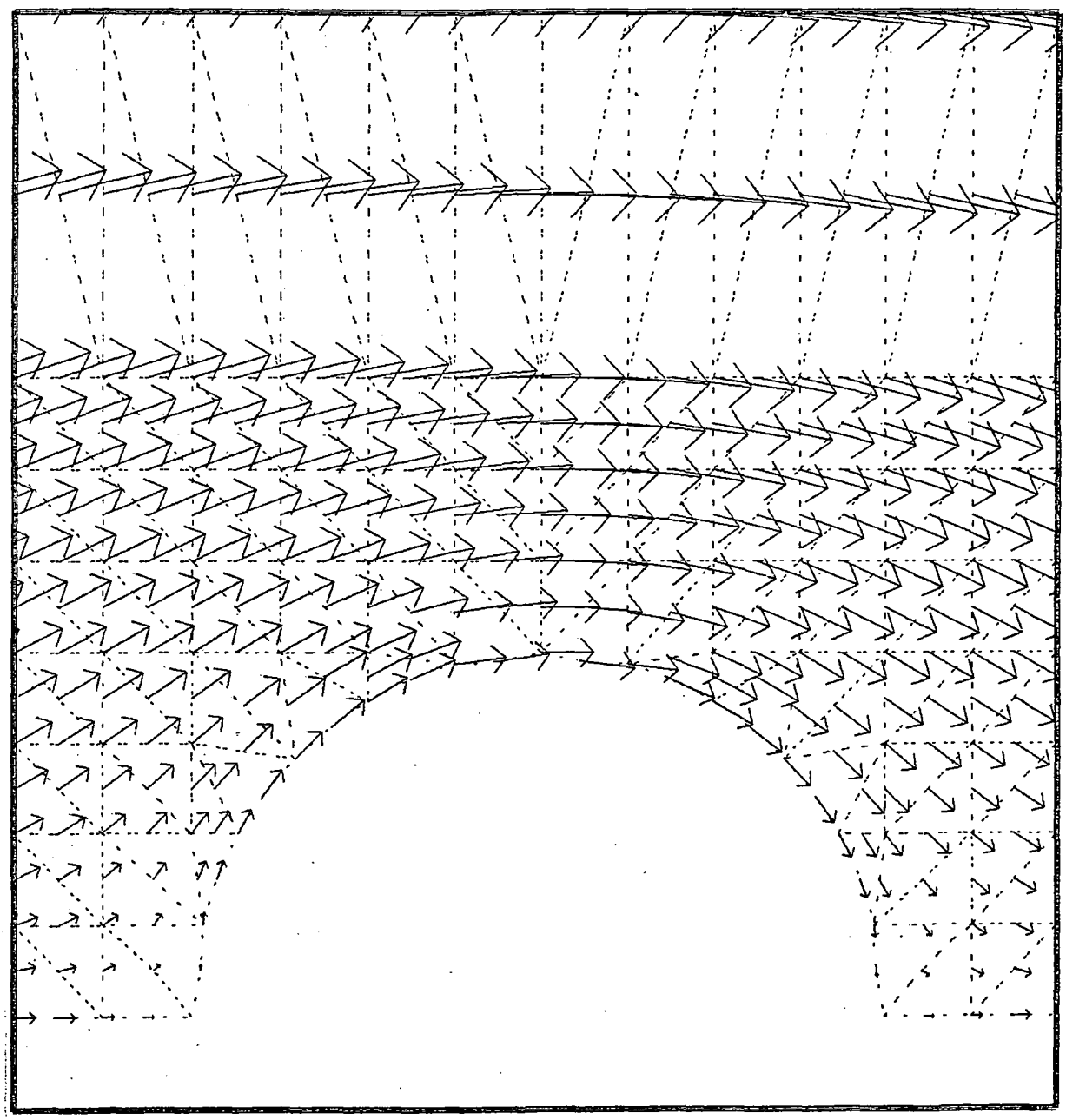

Figure 5.14 v_τ against $\sin\gamma$ for an incompressible linear rheology with bed of S = 10 alu/bar.a, v_d = 10 alu/a (Case 18)

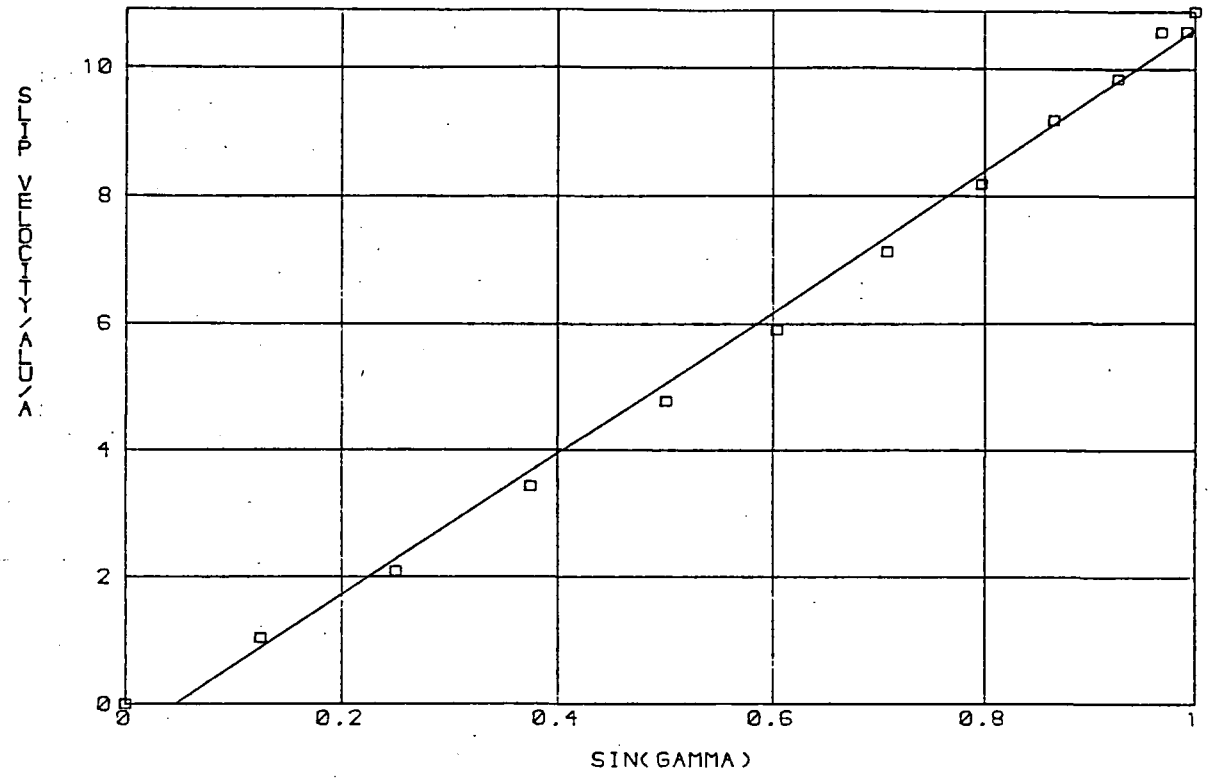

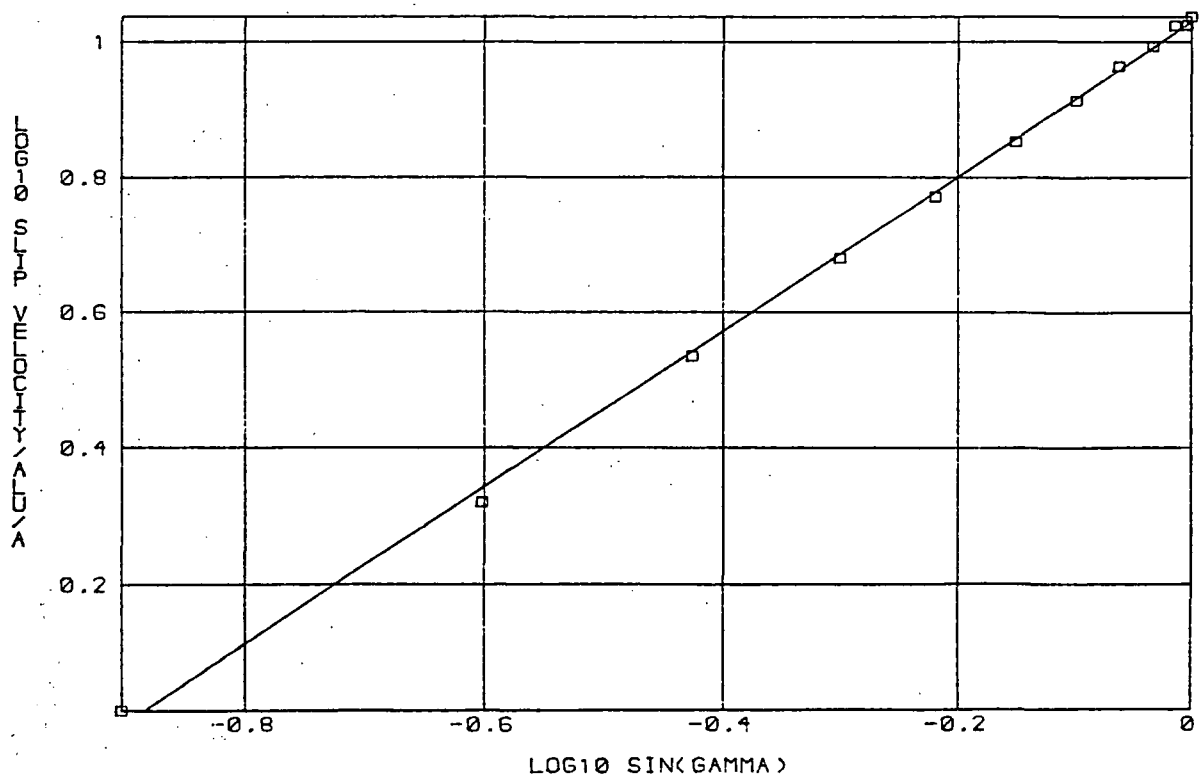

Figure 5.15 v_τ against $\sin\gamma$ for an incompressible linear rheology with bed of S = 400 alu/bar.a, v_d = 400 alu/a (Case 22).

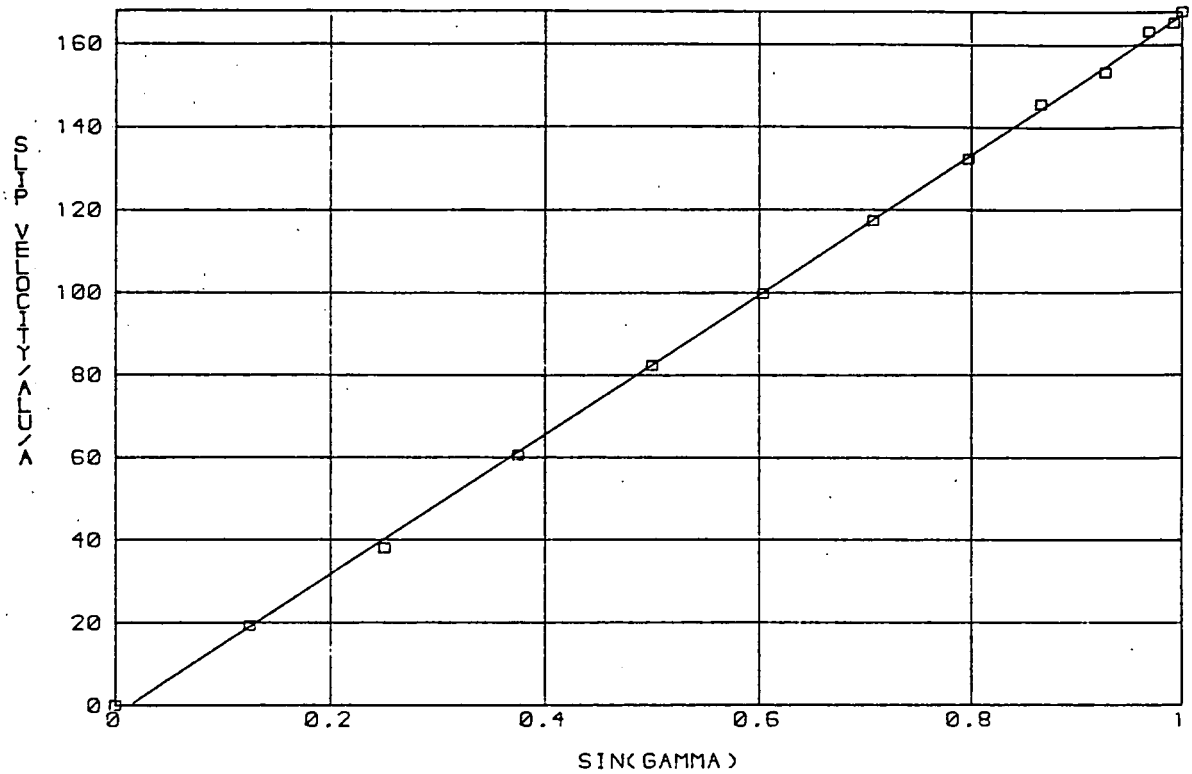

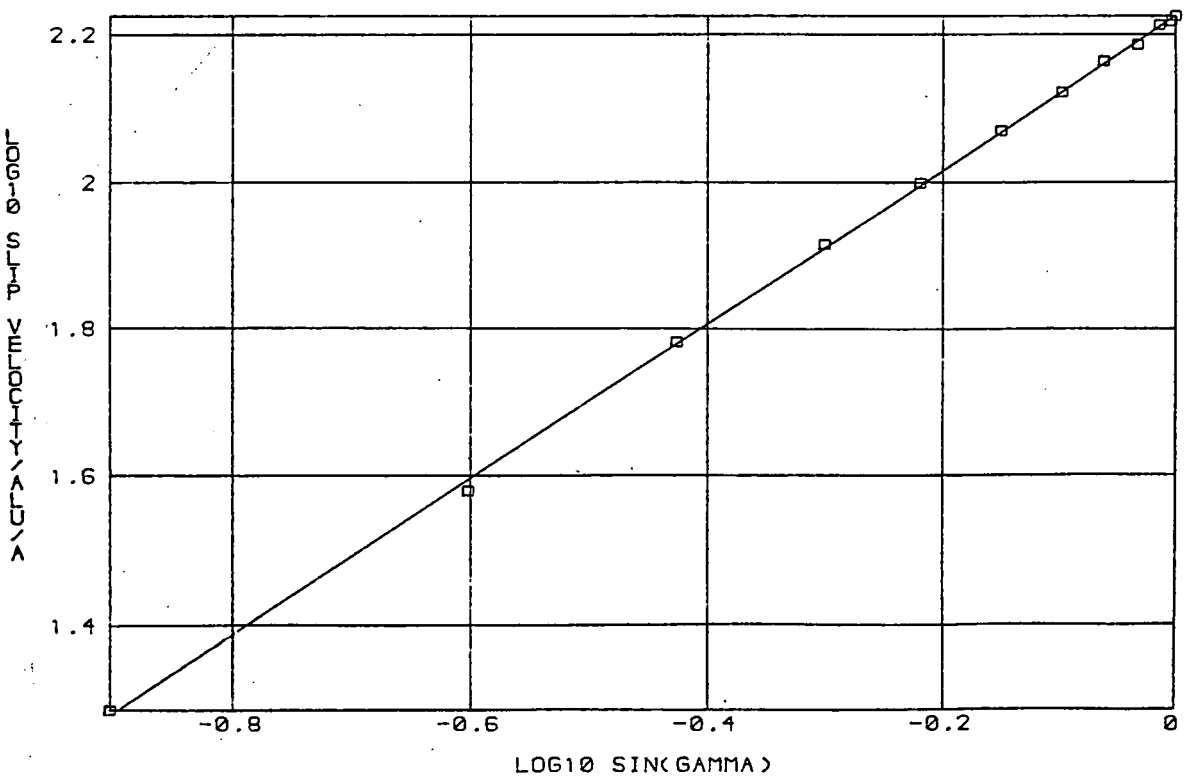

Figure 5.16 Velocity vector plot for an incompressible Glen rheology with v_d = 100 alu/a (Case 25).

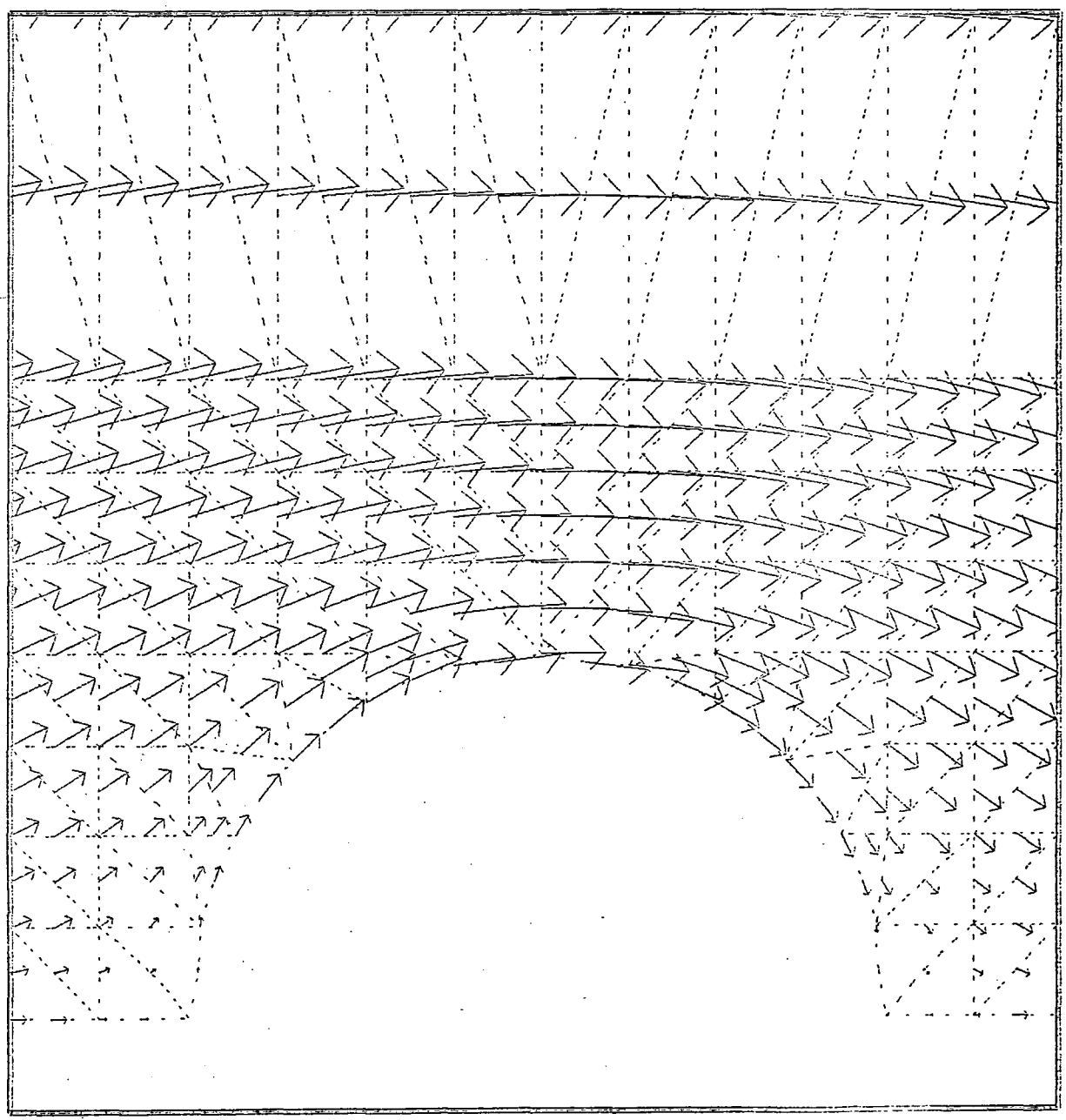

Figure 5.17 v_τ against $\sin\gamma$ for an incompressible Glen rheology with v_d = 10 alu/a (Case 23).

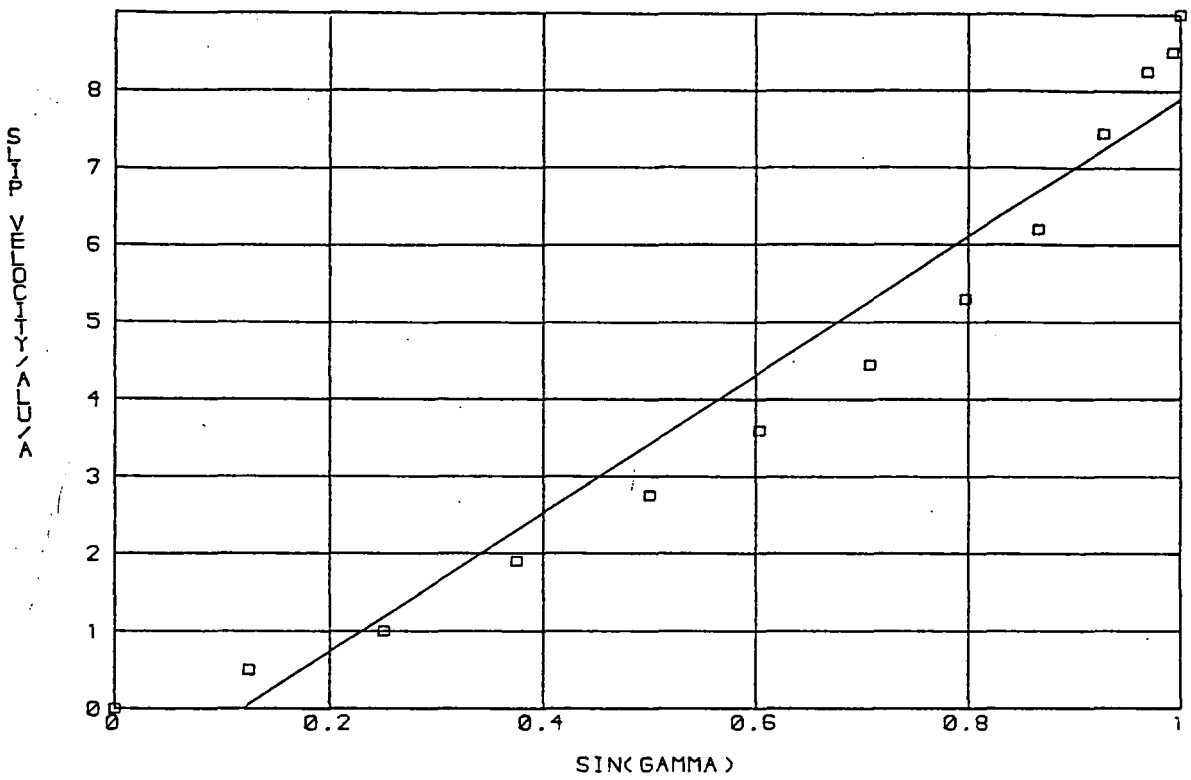

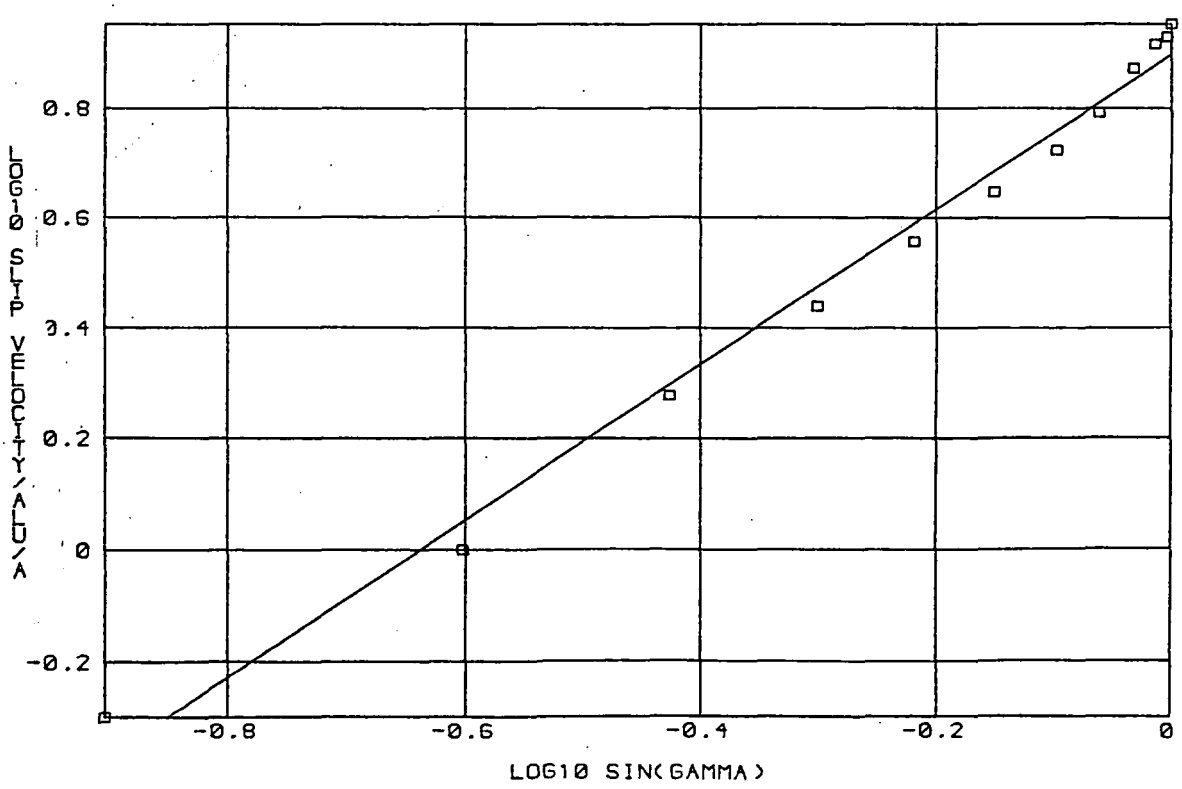

Figure 5.18 v_τ against $\sin\gamma$ for an incompressible Glen rheology with v_d = 400 alu/a (Case 25).

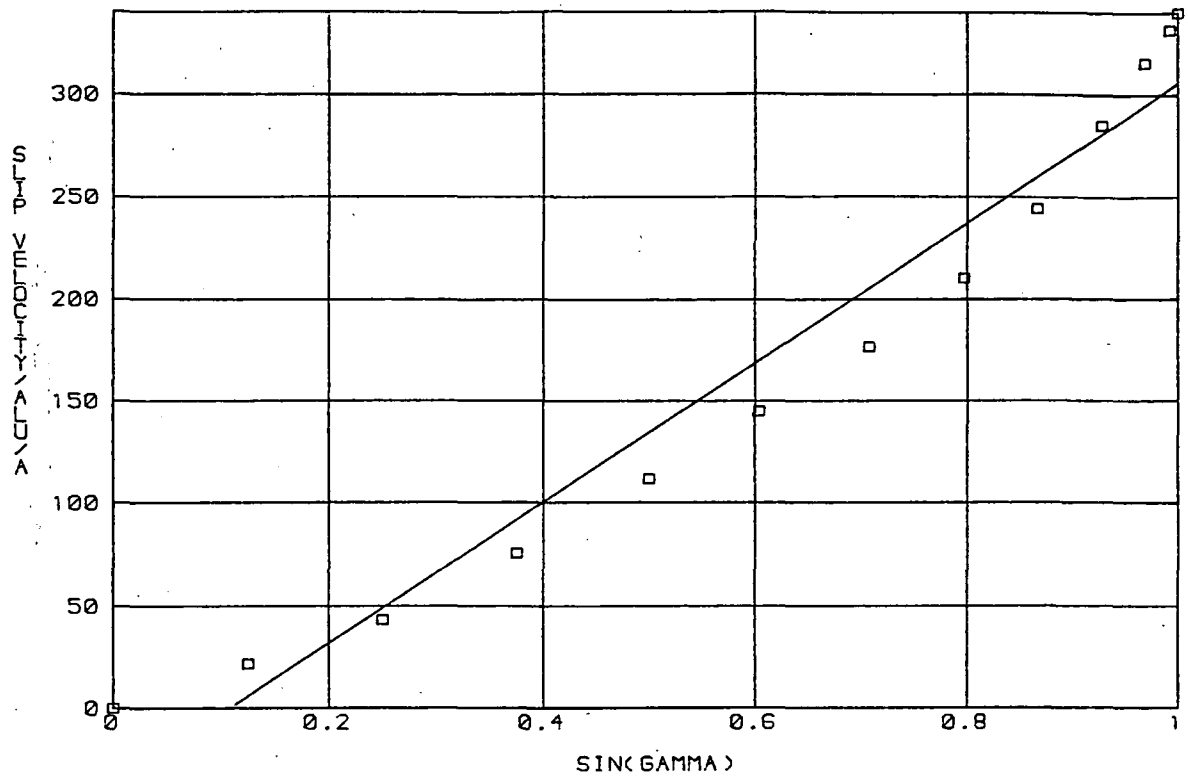

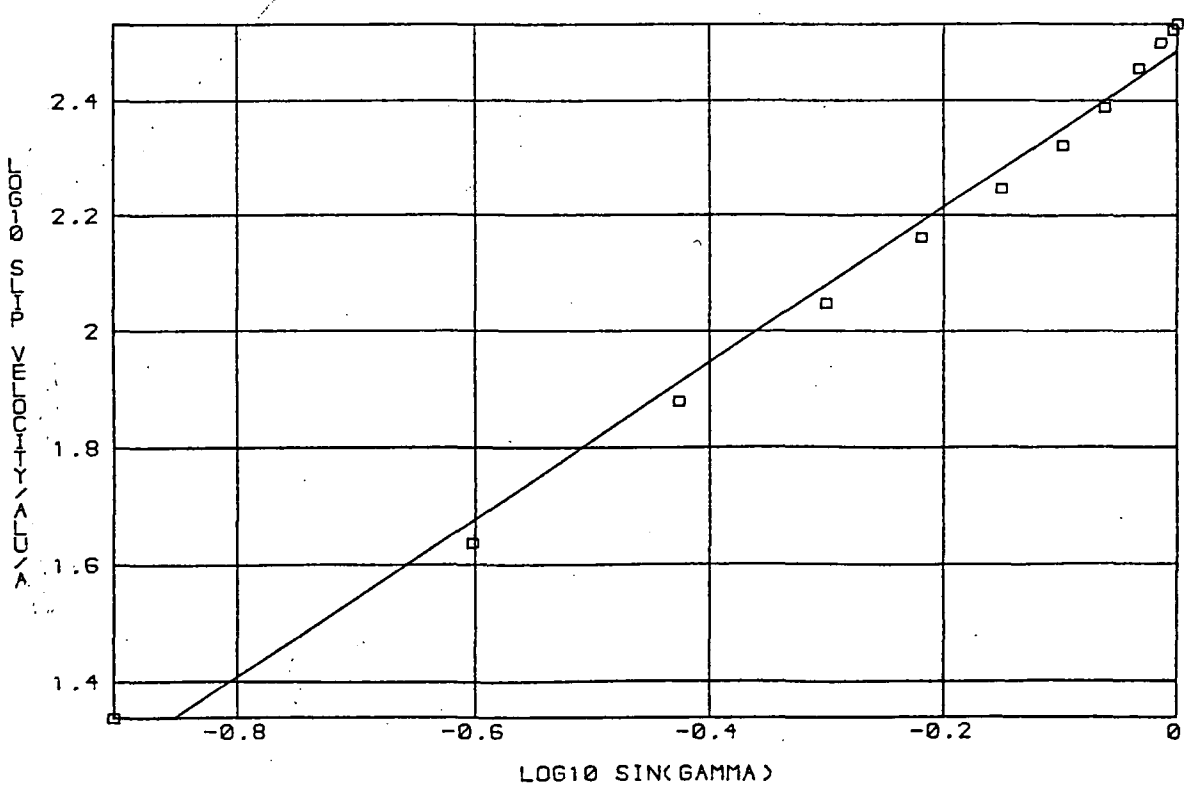

Figure 5.19 Velocity vector plot for an incompressible Glen rheology with a cavity and v_d = 400 alu/a (Case 28).

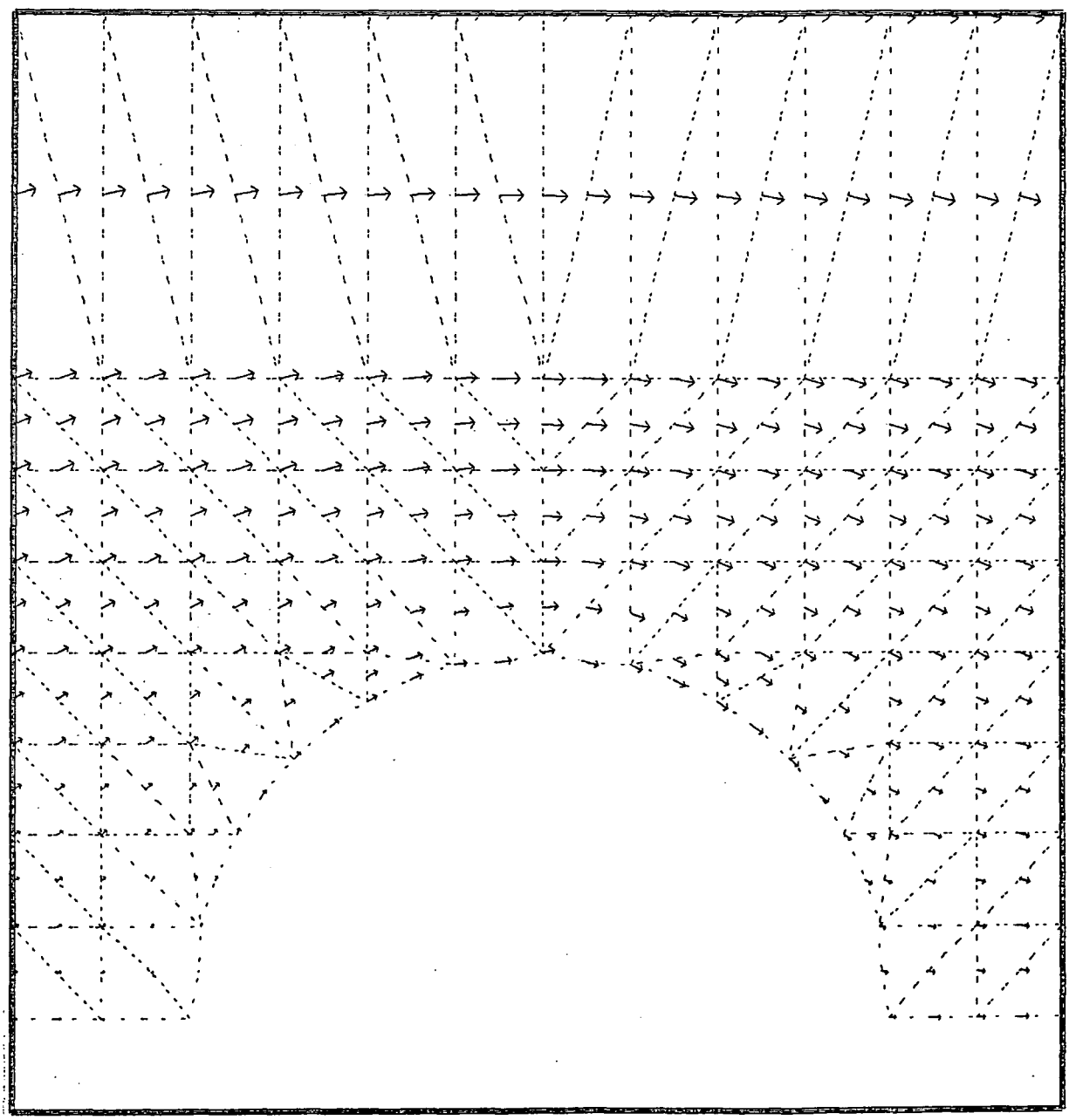

Figure 5.20 v_τ against $\sin\gamma$ for an incompressible Glen rheology with a cavity and v_d = 400 alu/a (Case 28).

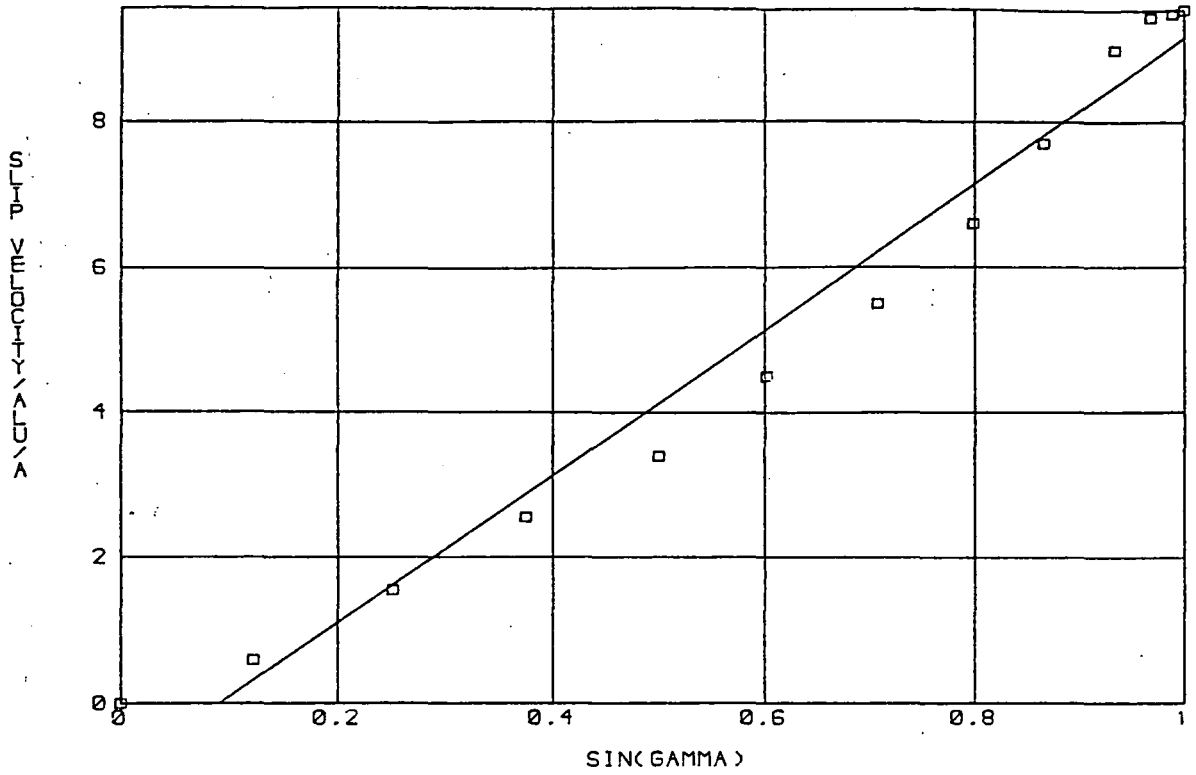

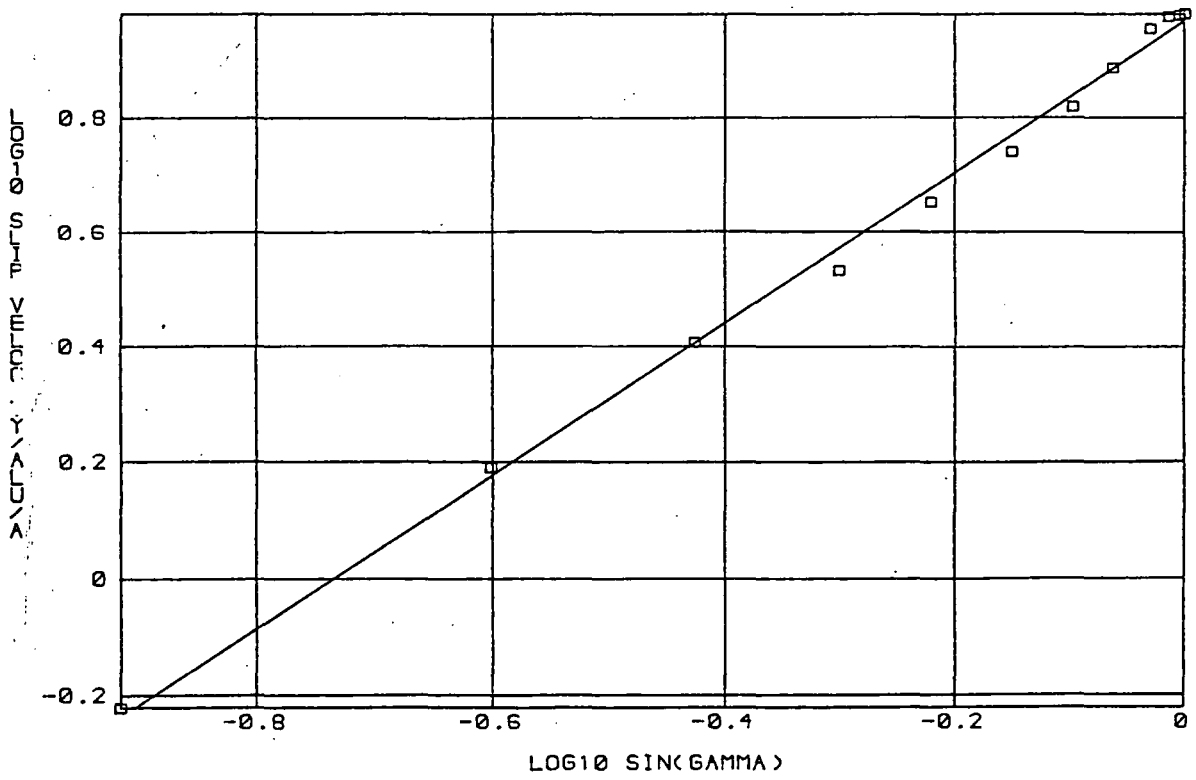

Figure 5.21 Velocity vector plot for a compressible Glen rheology with $\chi = 1$ alu^2/bar.a and $v_d = 100$ alu/a (Case 31).

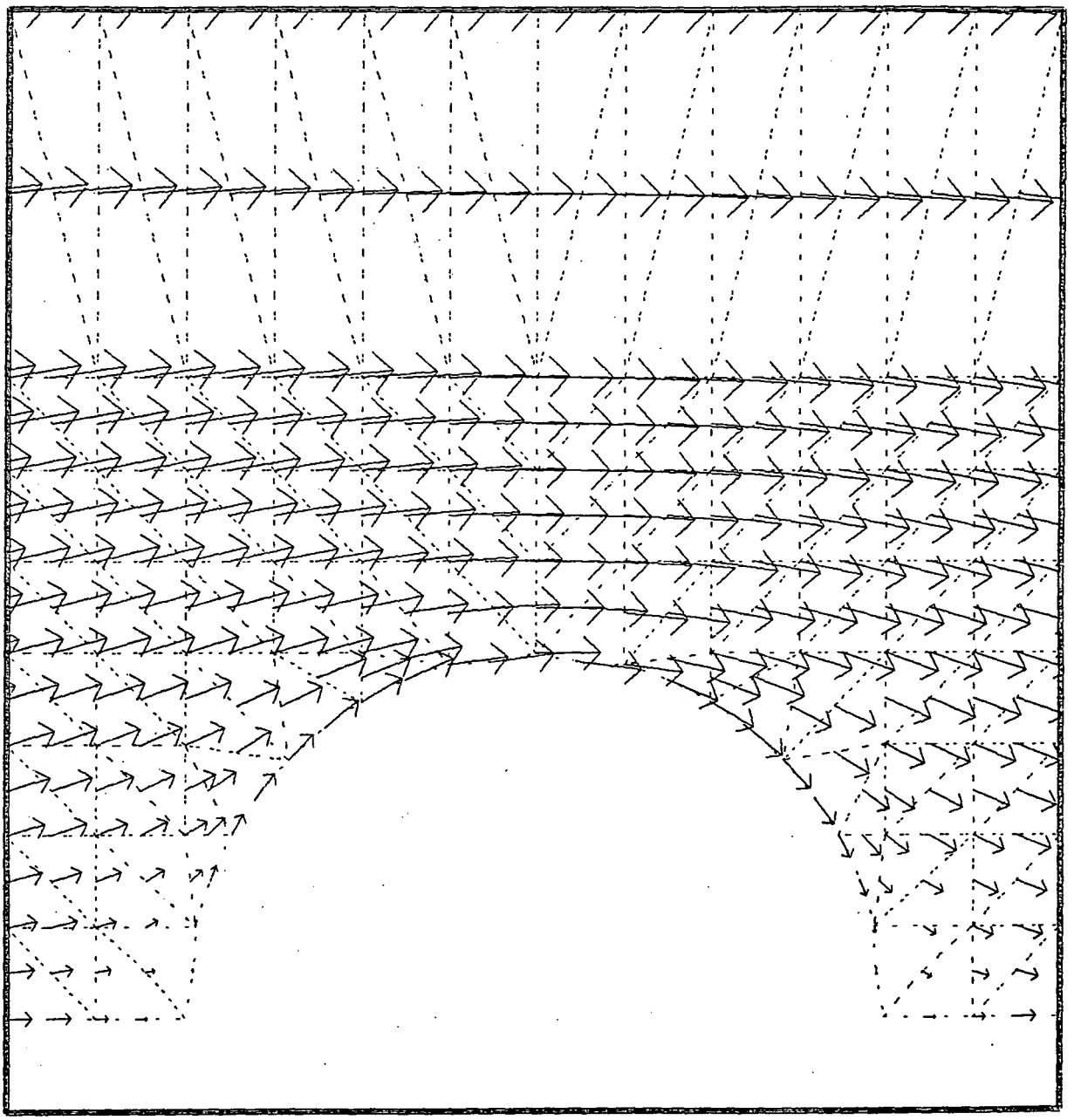

Figure 5.22 v_τ against $\sin\gamma$ for a compressible Glen rheology with χ = 1 alu^2/bar.a and v_d = 200 alu/a (Case 32).

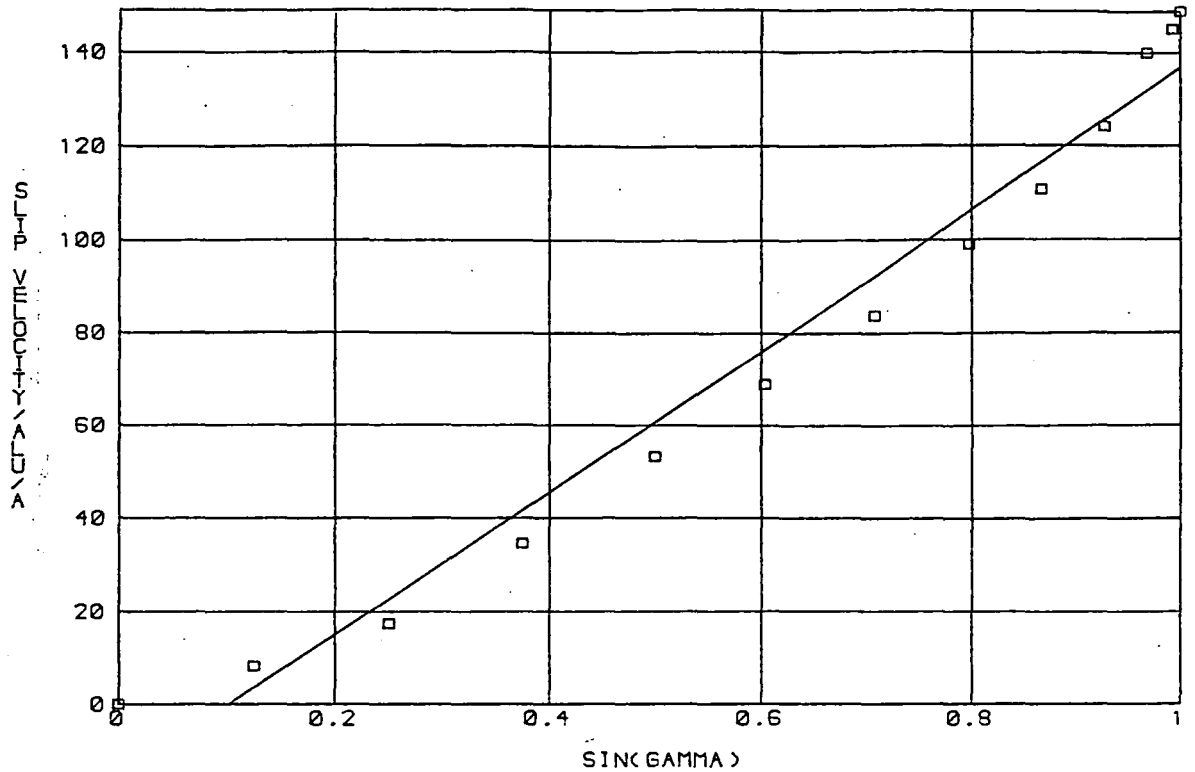

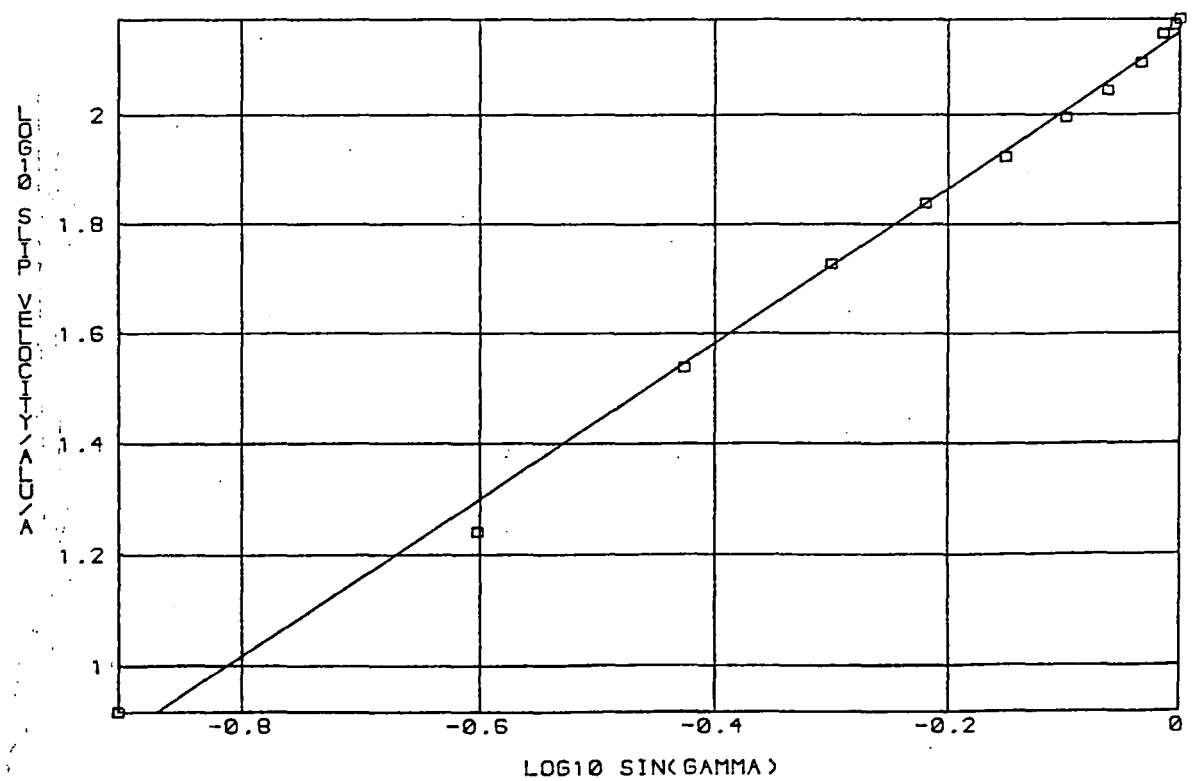

Figure 5.23 v_τ against $\sin\gamma$ for an incompressible Glen rheology with bed S = 10 alu/bar.a and v_d = 10 alu/a (Case 34).

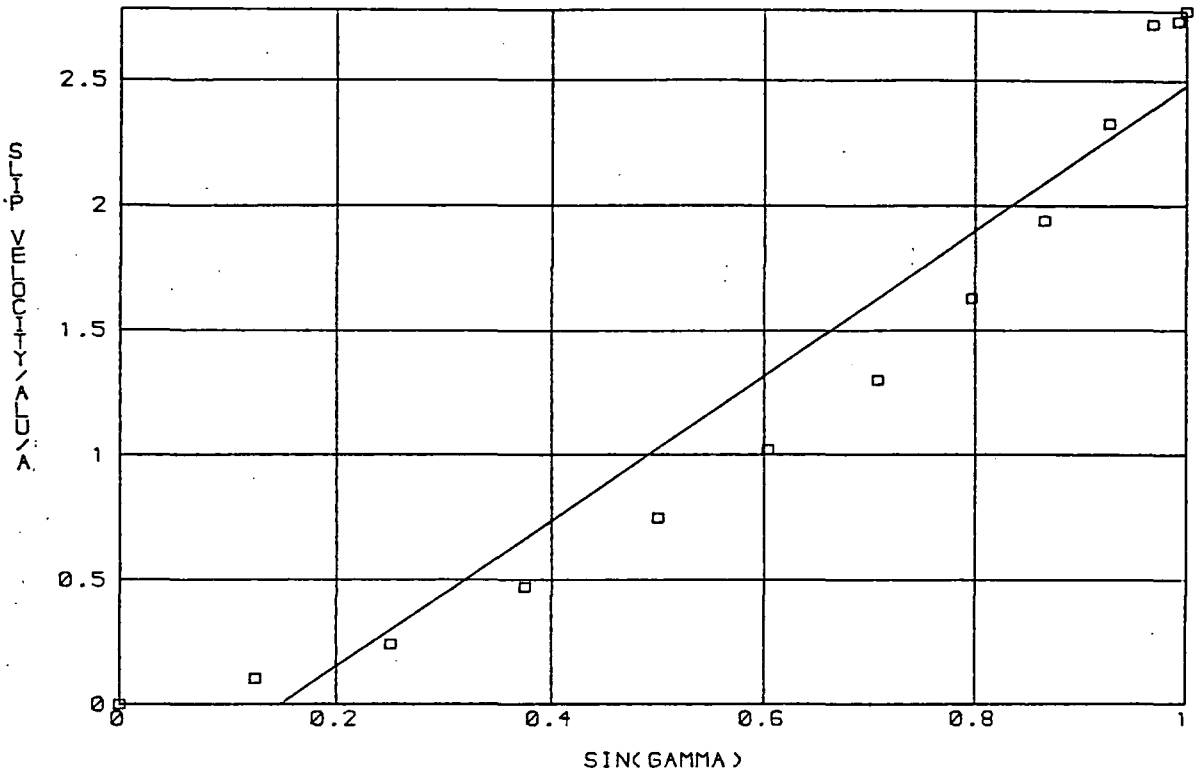

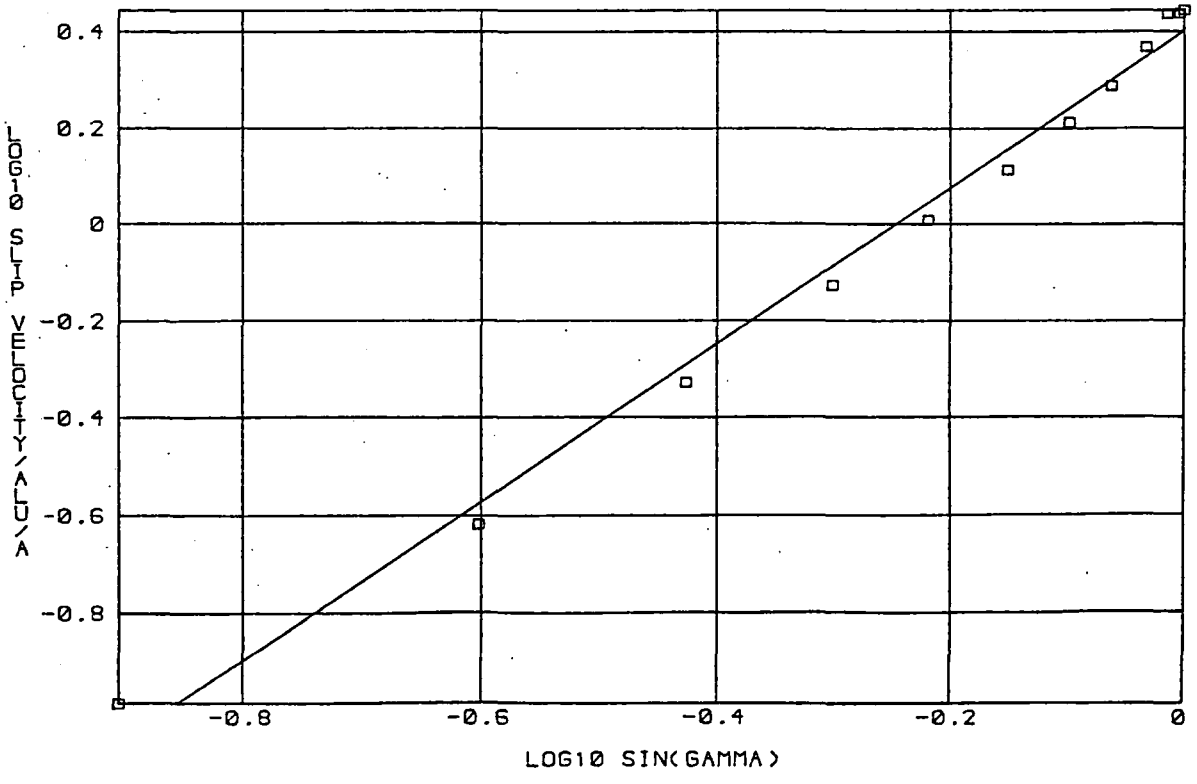

Figure 5.24 Velocity vector plot for an incompressible Glen rheology over a truncated sine ridge with v_d = 100 alu/a (Case 47).

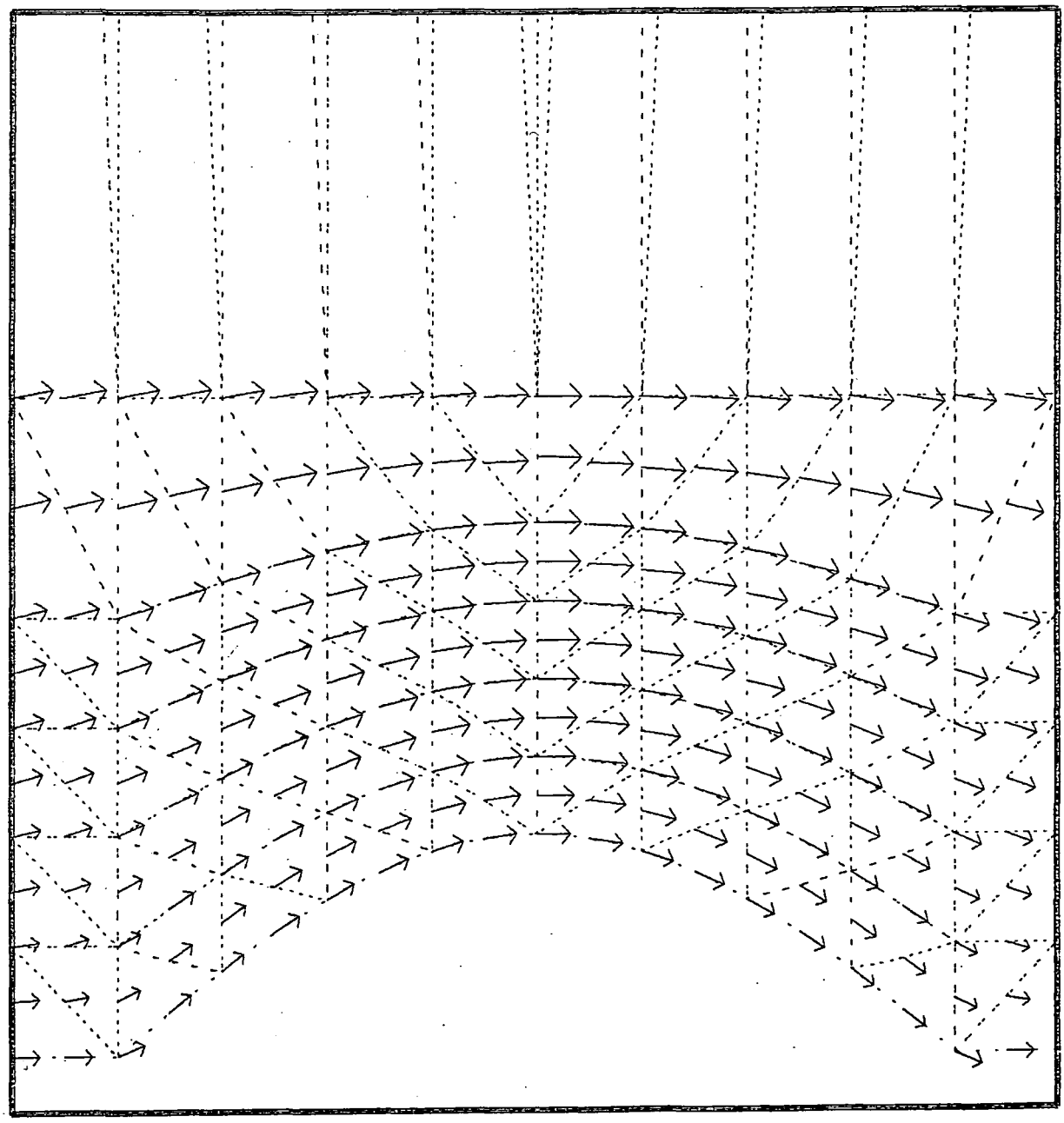

Figure 5.25 v_τ against position for flow over a truncated sine ridge (Cases 40 - 49): Glen rheology

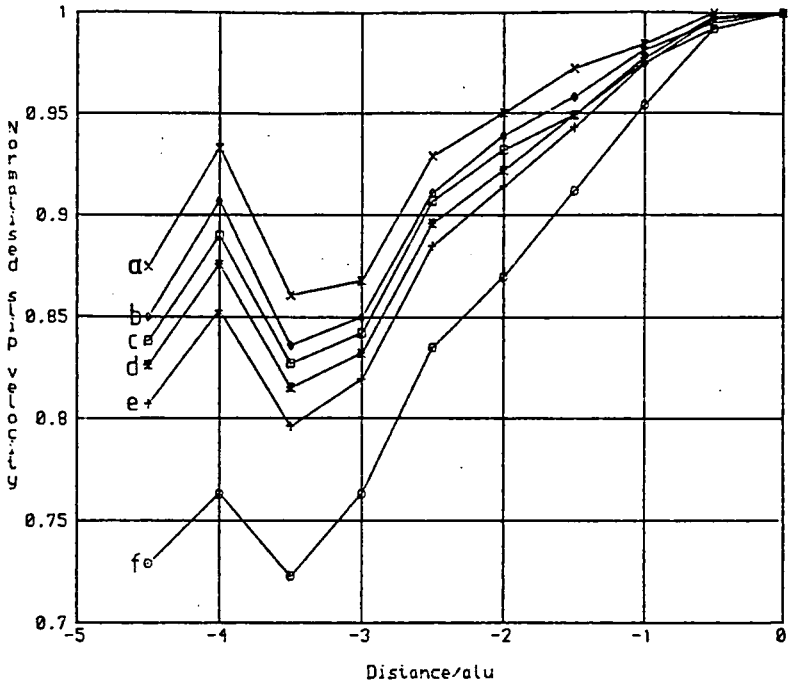

a-Linear
b-Glen, v_a=400alu/a
c-Glen, v_a= 200alu/a
d-Glen, v_a= 100alu/a
e-Glen, v_a= 50alu/a
f-Glen, v_a= 10alu/a

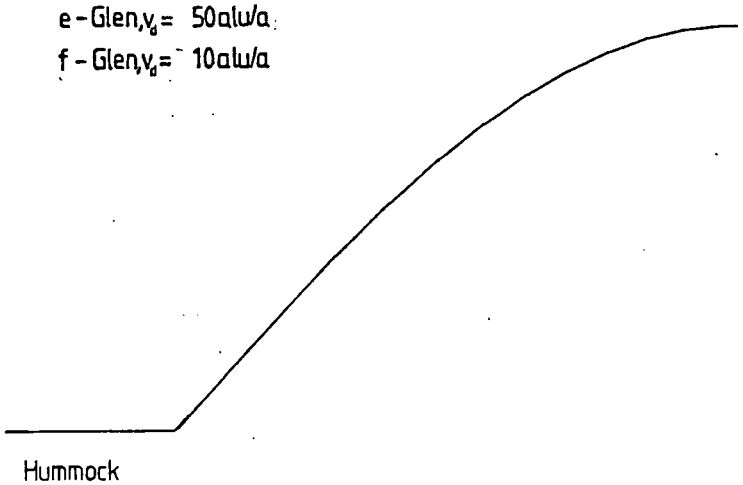

Figure 5.26 Regression coefficients from v_τ against v_d against position for flow over a truncated sine ridge (Cases 45 - 49).

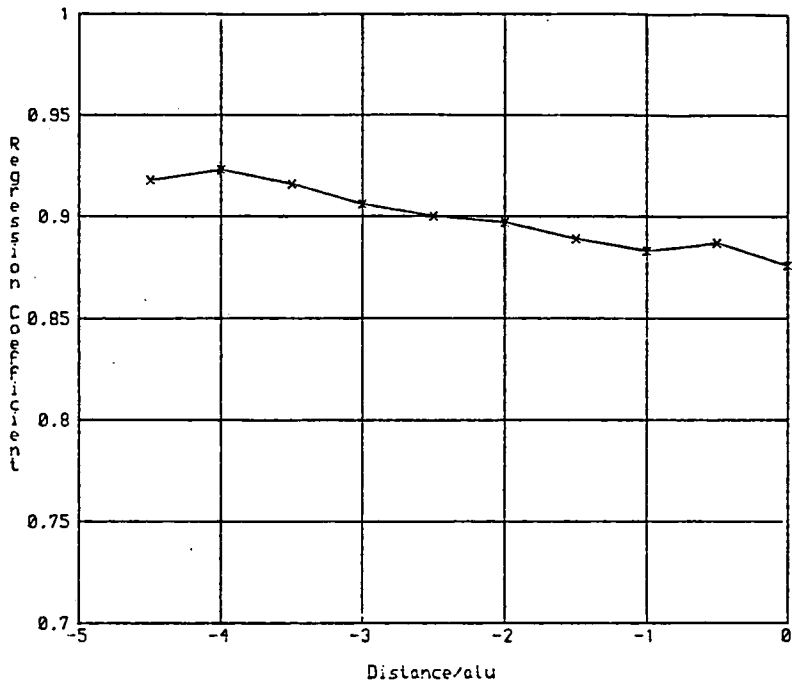

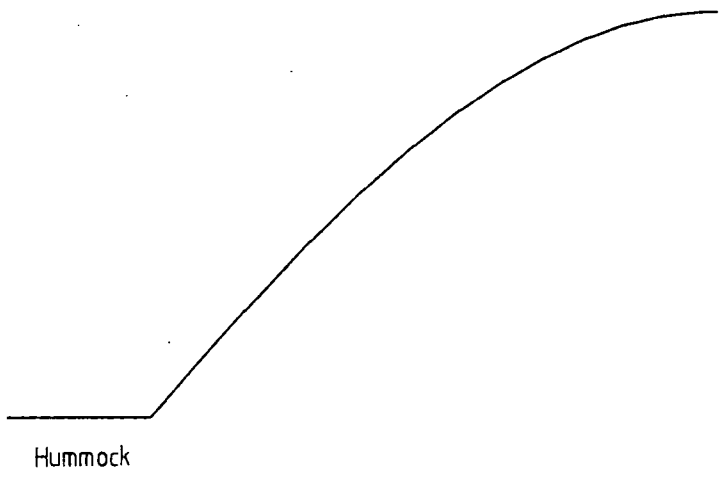

Figure 5.27 Pressure contours in bar for an incompressible linear rheology with v_d = 100 alu/a (Case 3).

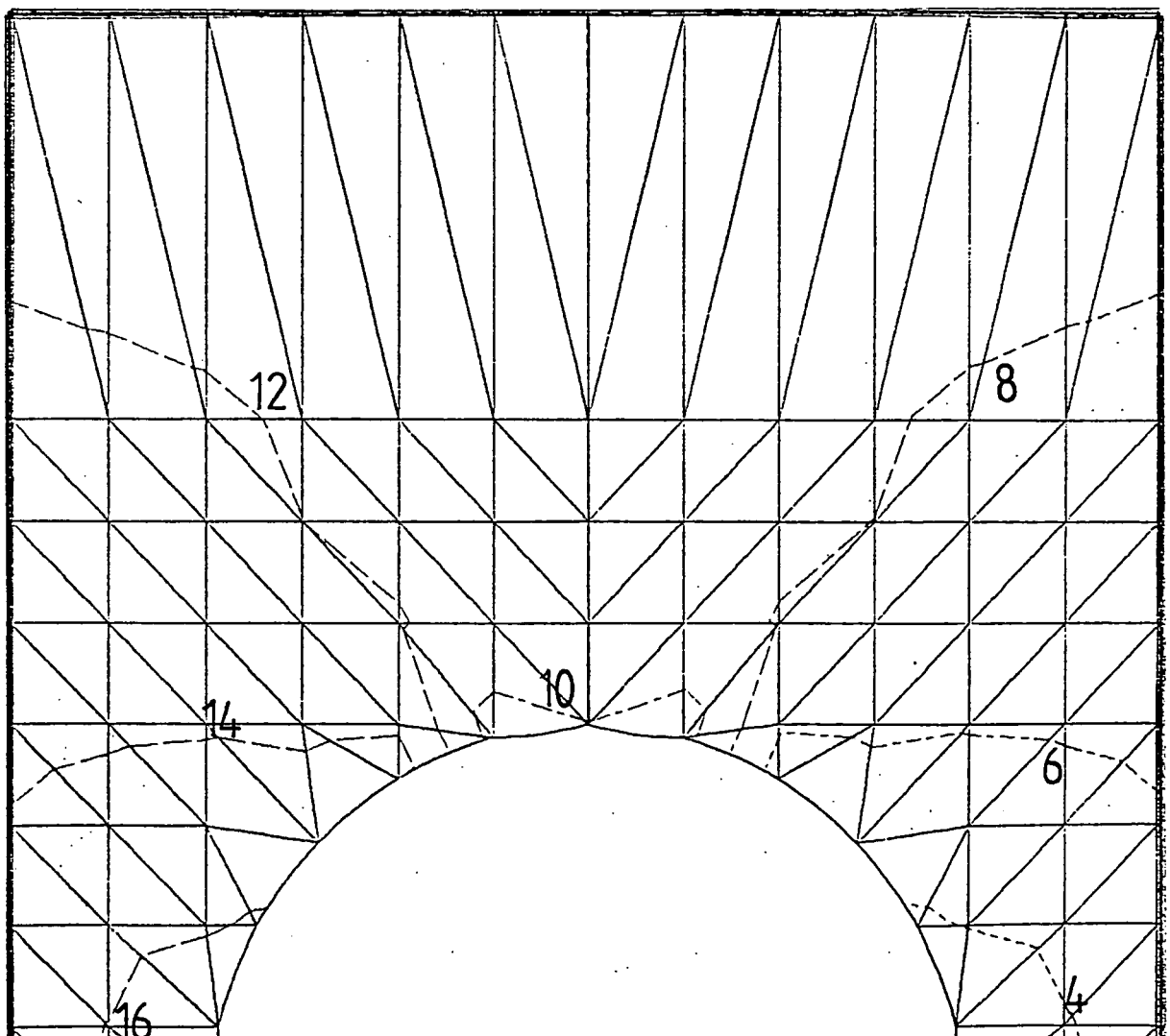

Figure 5.28 p' against cosγ for an incompressible linear rheology with v_d = 400 alu/a (Case 1).

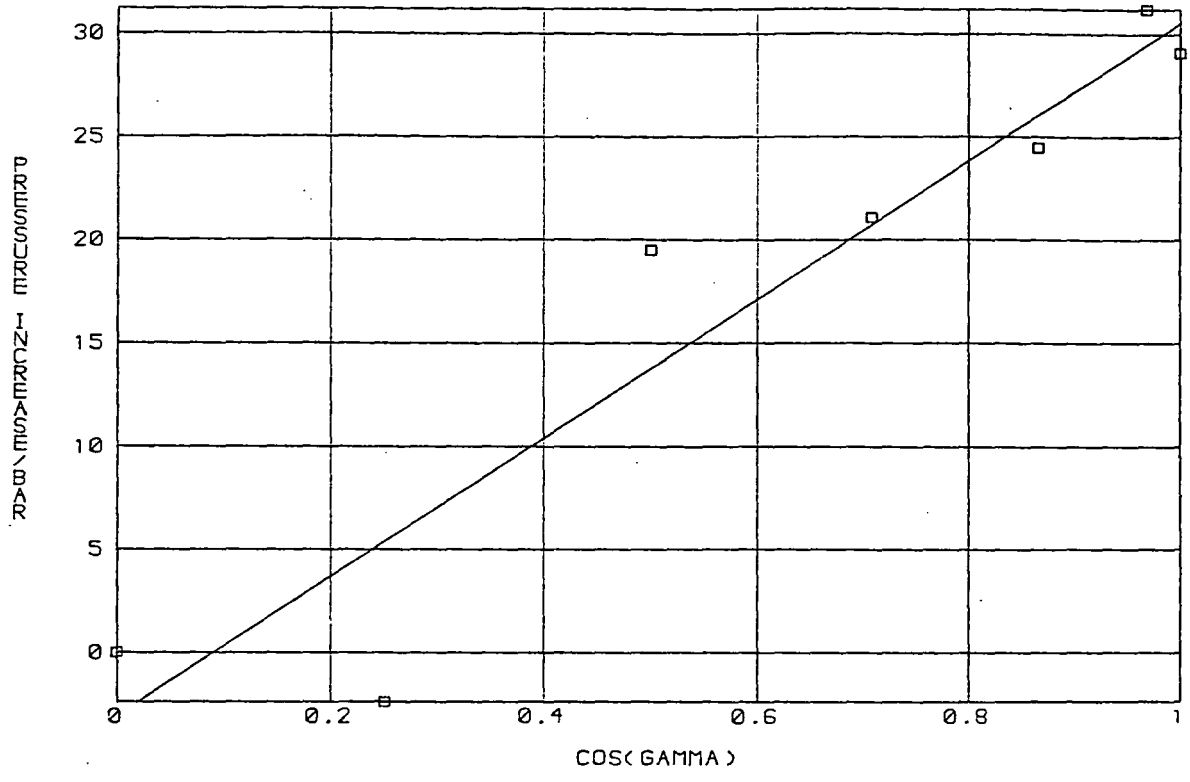

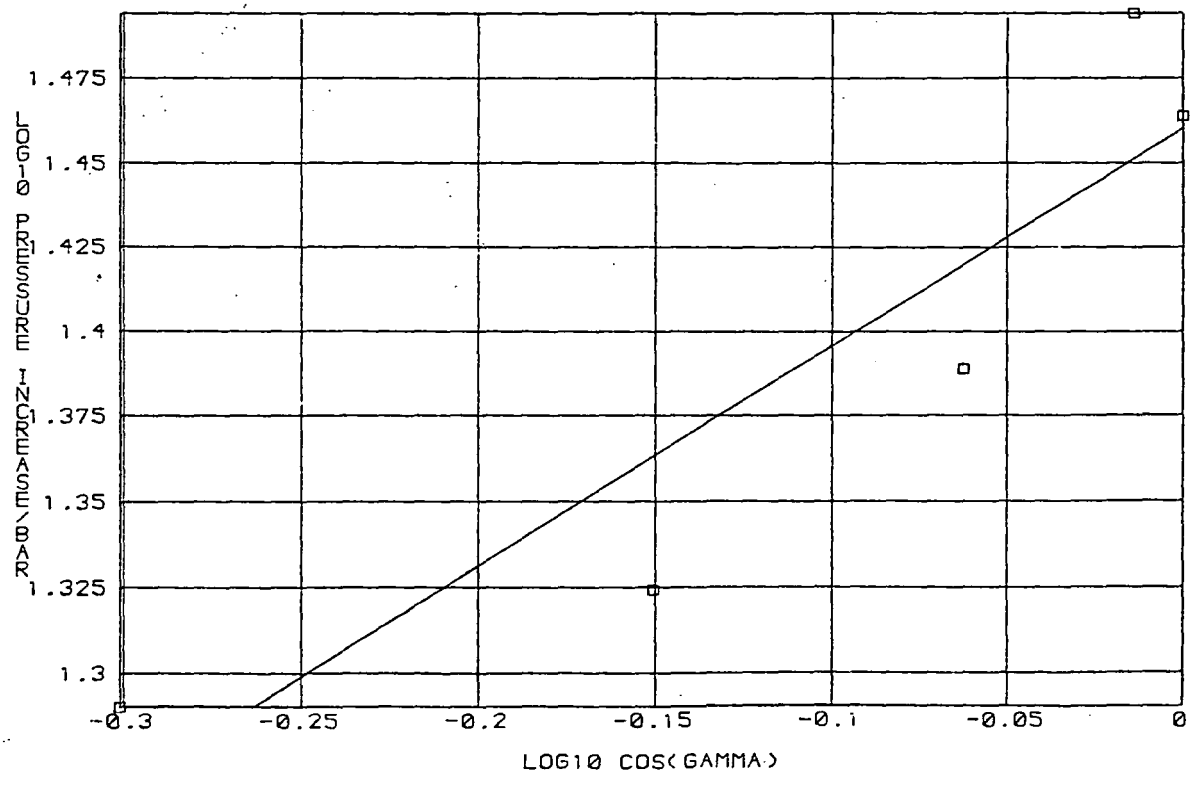

Figure 5.29 p' against $\cos\gamma$ for an incompressible linear rheology with a cavity and v_d = 400 alu/a (Case 5).

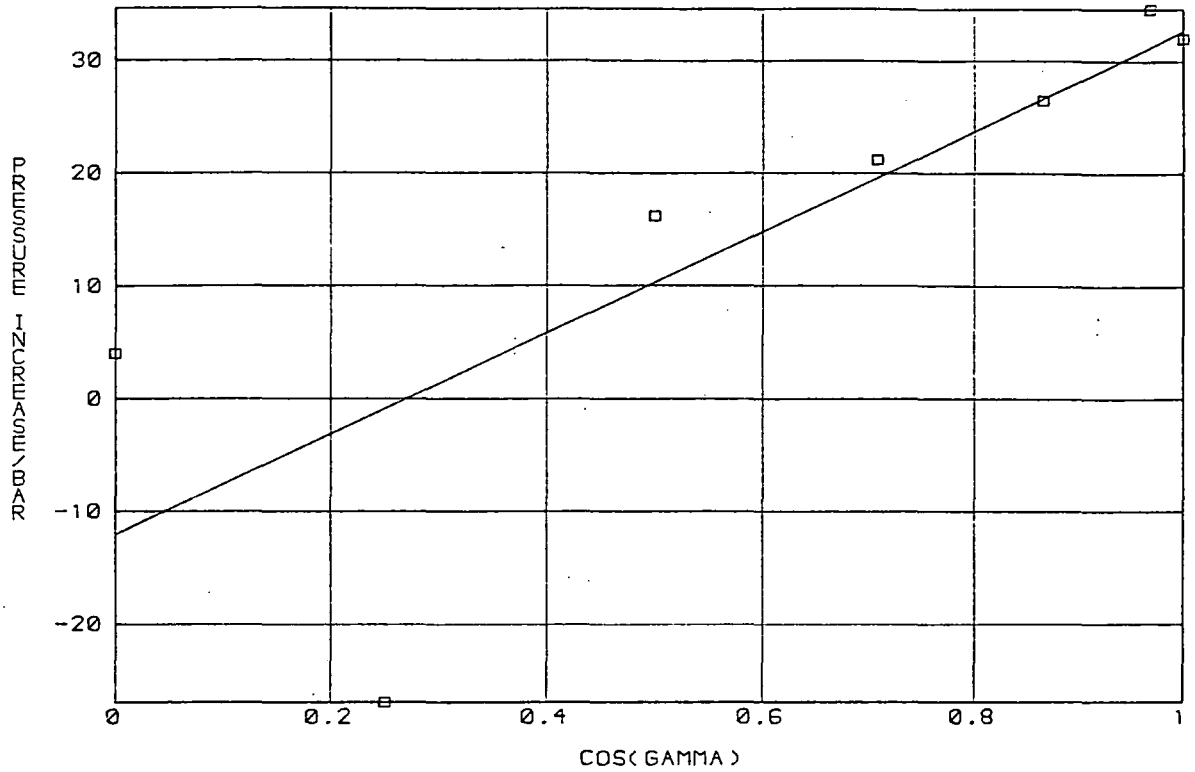

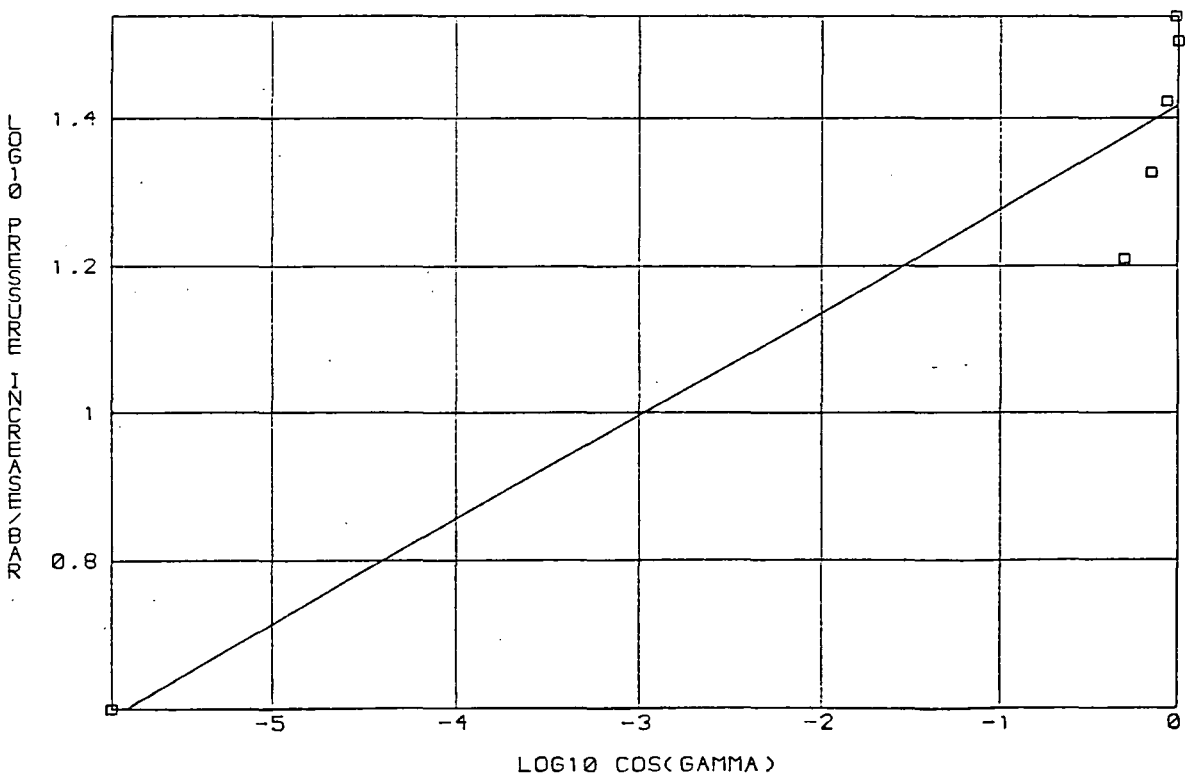

Figure 5.30 p' against cosγ for a compressible linear rheology with χ = 1 alu²/bar.a and v_d = 400 alu/a (Case 12).

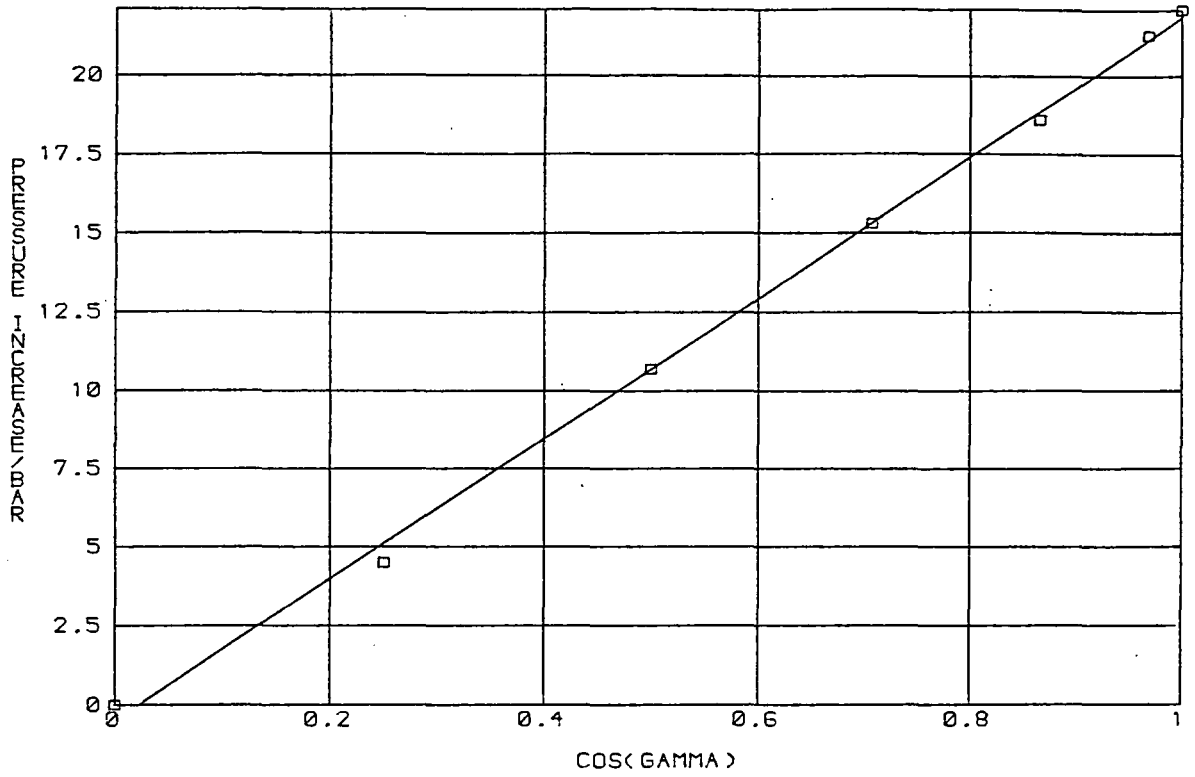

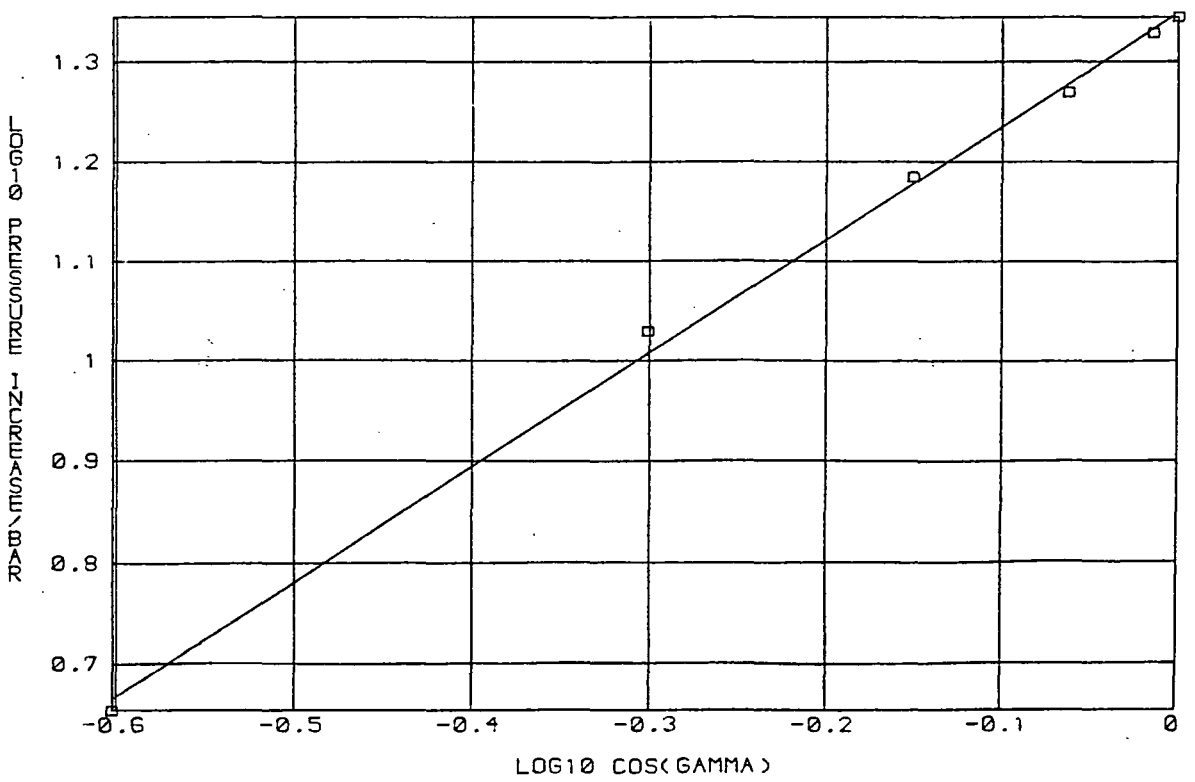

Figure 5.31 Pressure contours in bar for a compressible linear rheology with χ = 10 alu²/bar.a and v_d = 400 alu/a (Case 17).

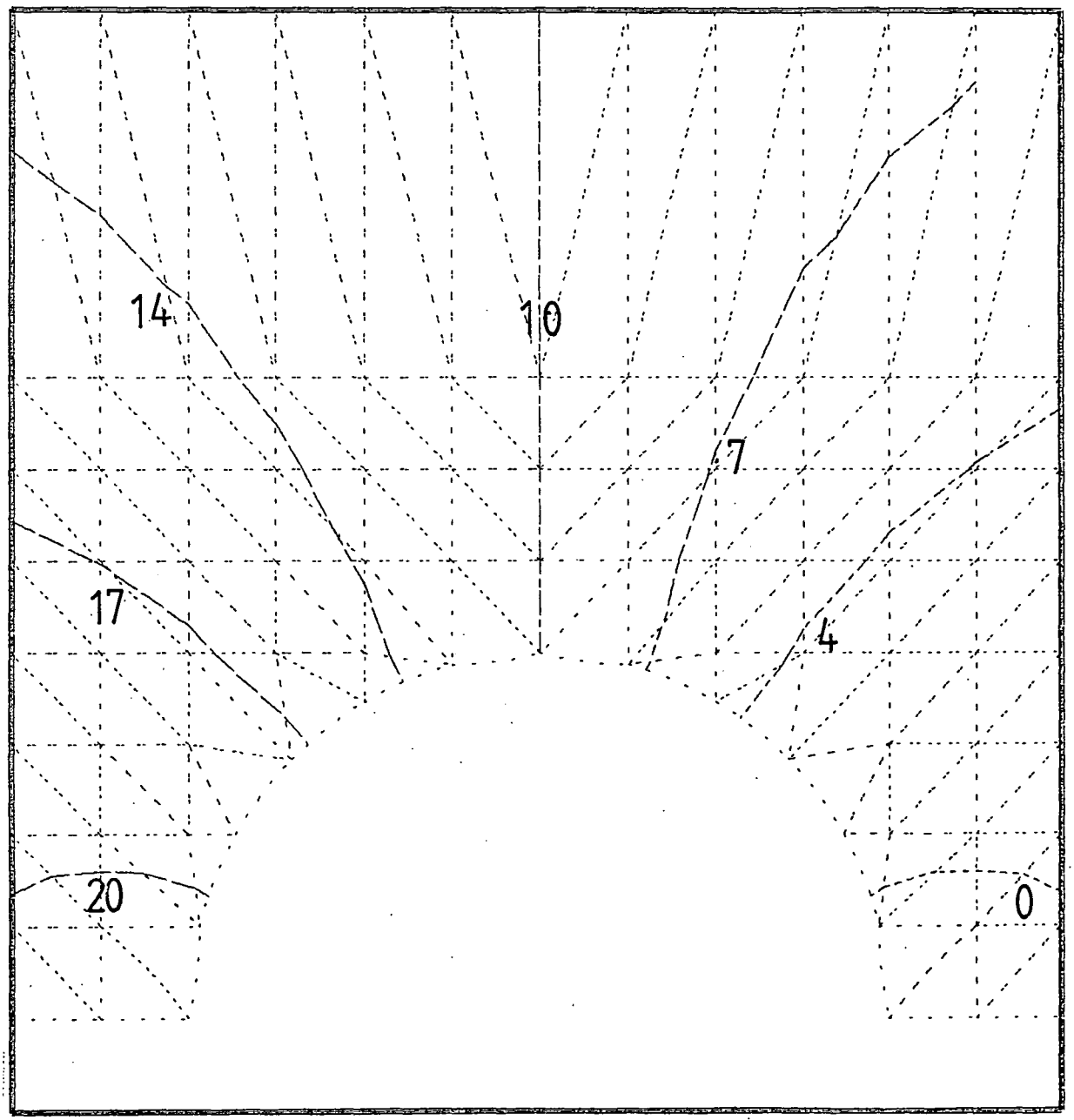

Figure 5.32 p' against cosγ for a compressible linear rheology with χ = 10 alu²/bar.a and v_d = 200 alu / a (Case 16).

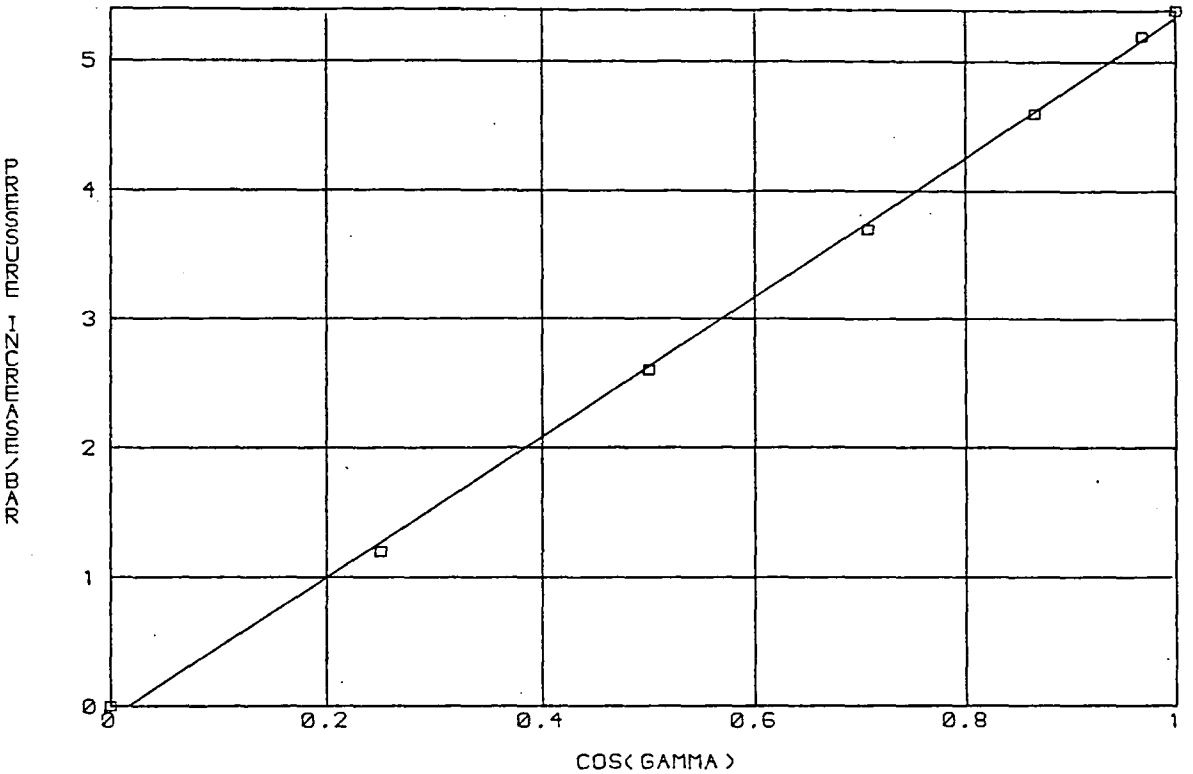

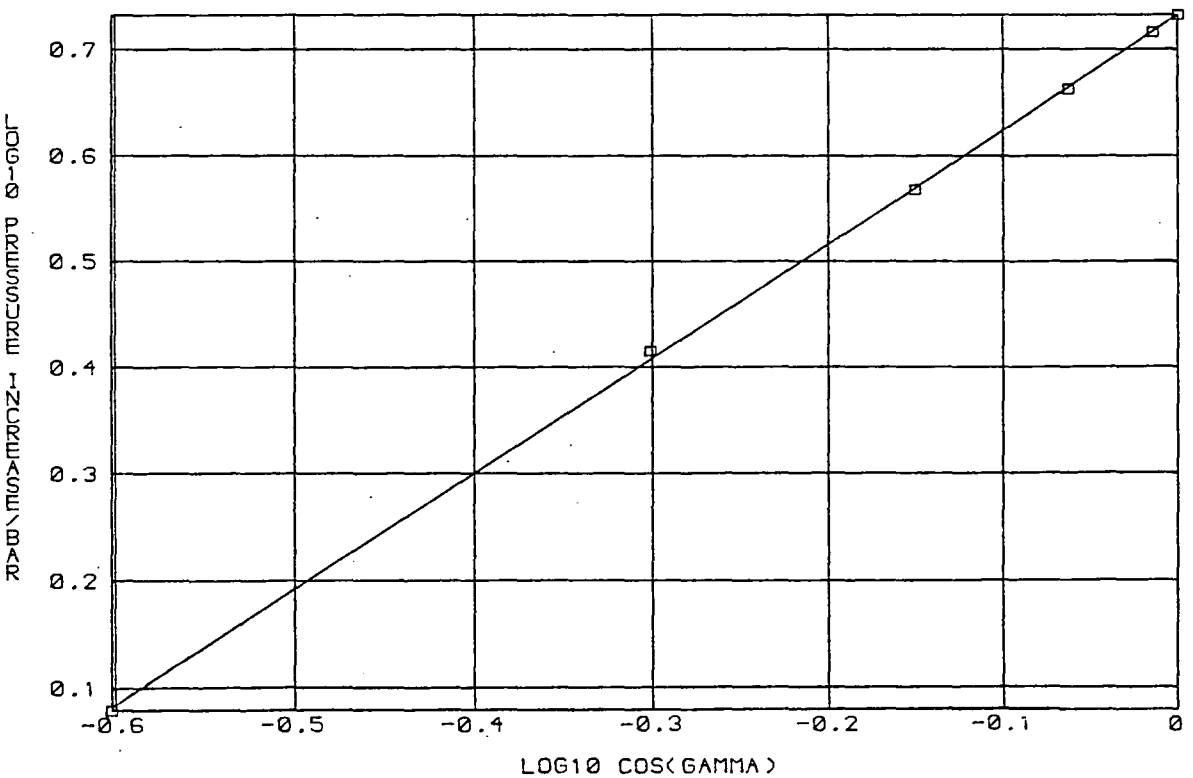

Figure 5.33 Pressure contours in bar for an incompressible linear rheology with bed of S = 100 alu /bar.a and v_d = 100 alu / a . (Case 20).

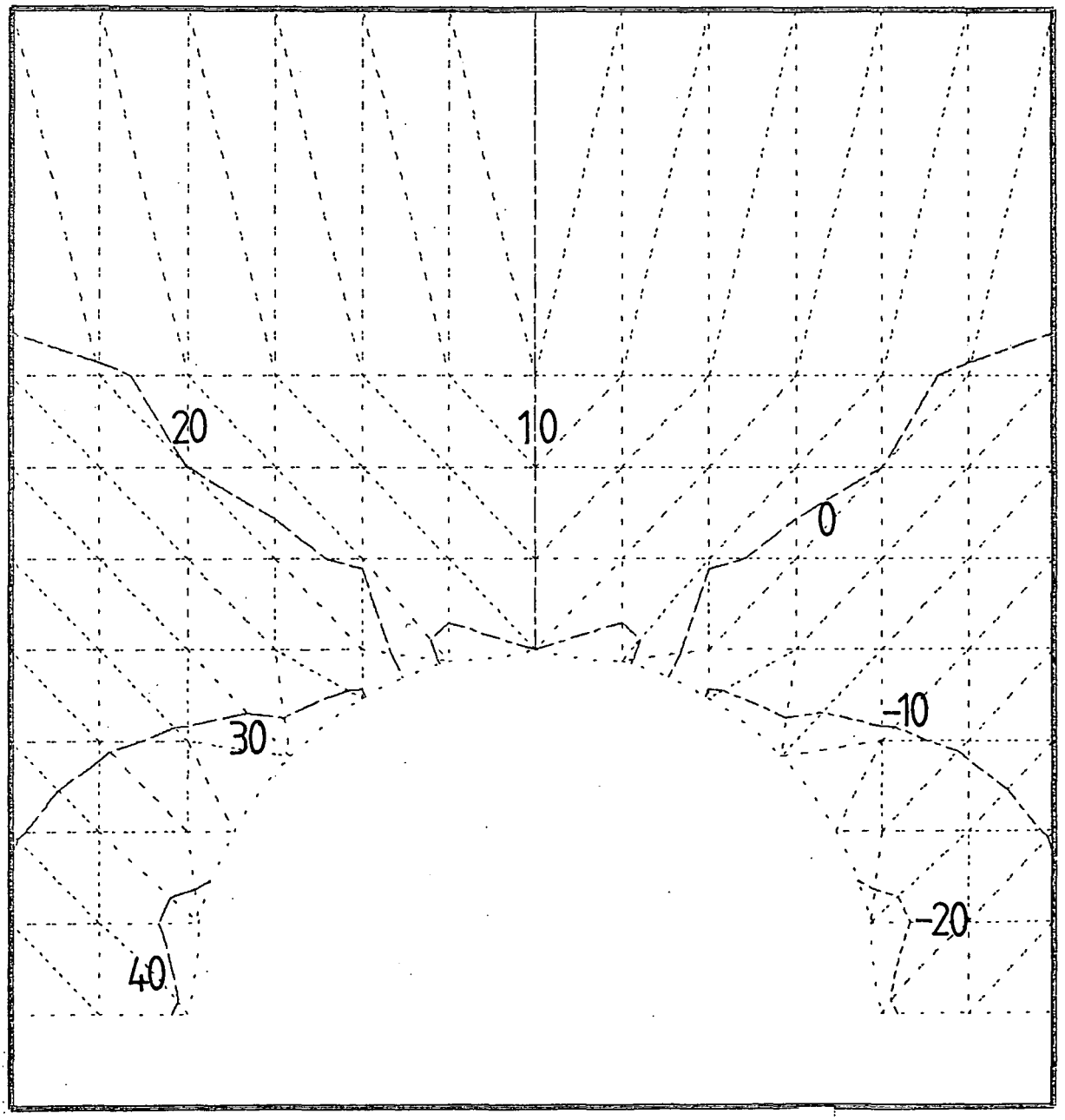

Figure 5.34 p' against cosγ for an incompressible linear rheology with bed of S = 10 alu /bar.a and v_d = 10 alu / a: (Case 18).

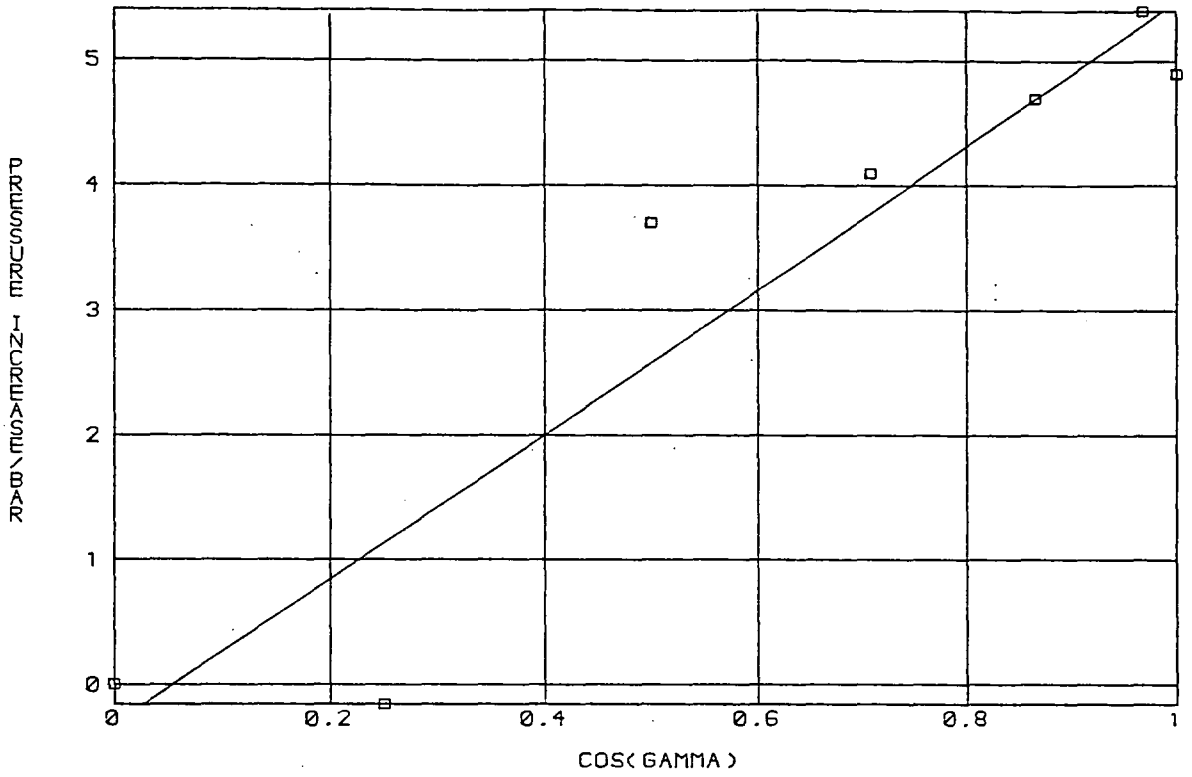

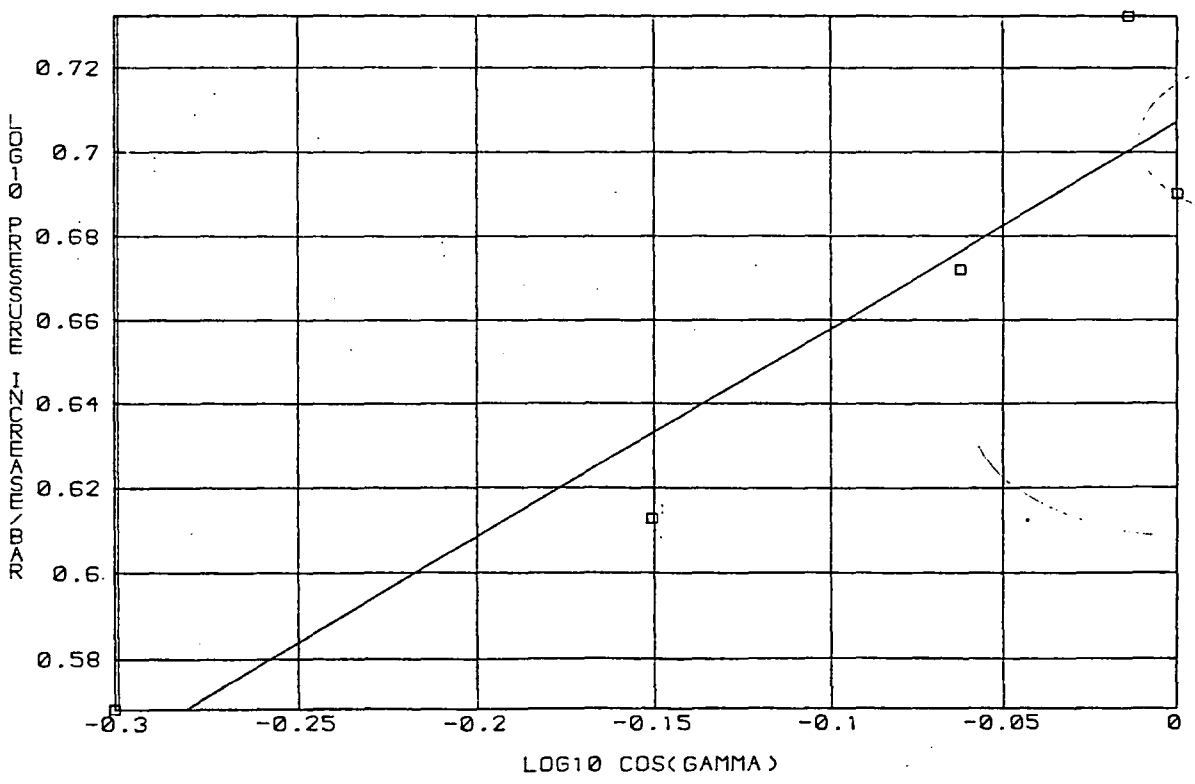

Figure 5.35 p' against cosγ for an incompressible linear rheology with bed of S = 400 alu /bar.a and v_d = 400 alu / a. (Case 22).

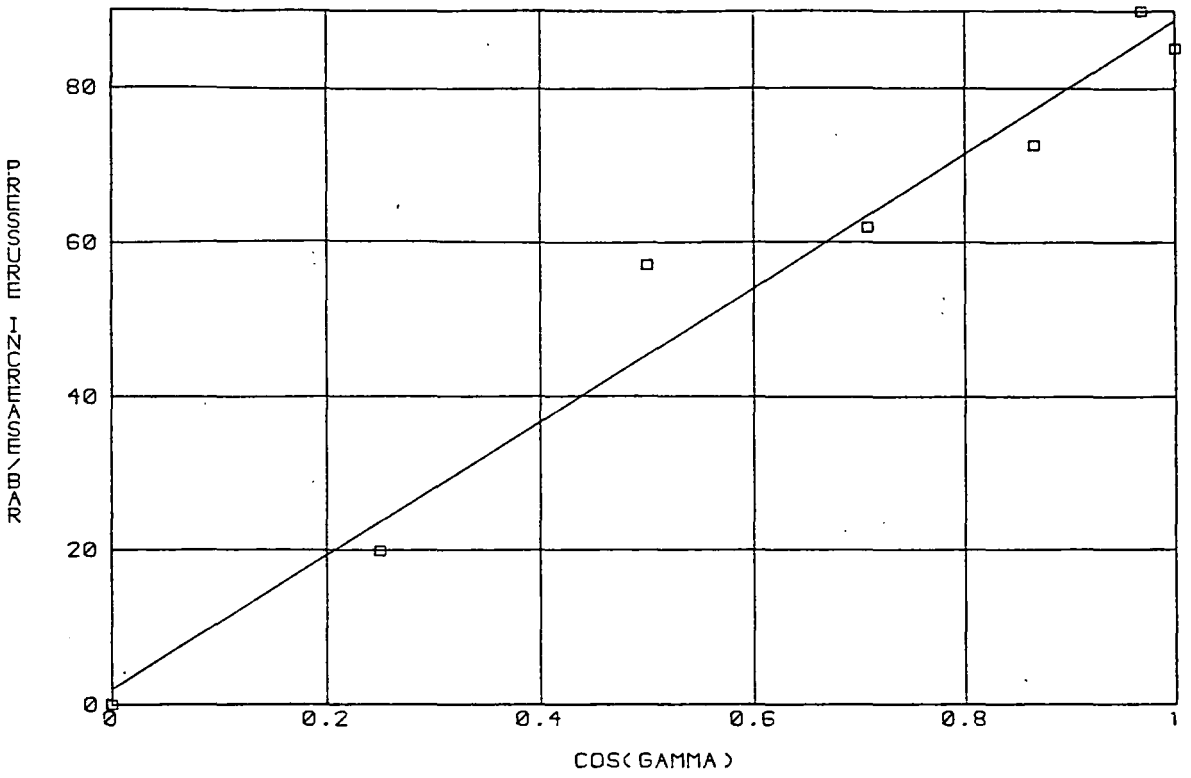

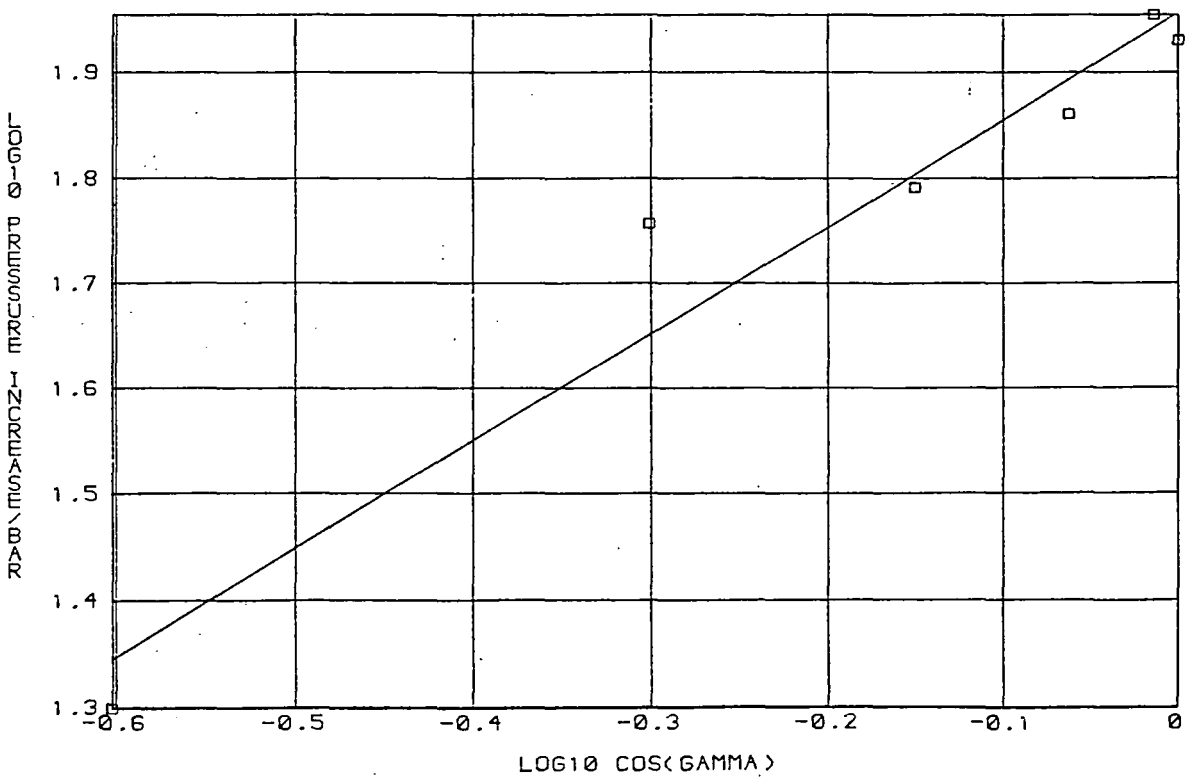

Figure 5.36 Pressure contours in bar for an incompressible Glen rheology with v_d = 200 alu/a (Case 25).

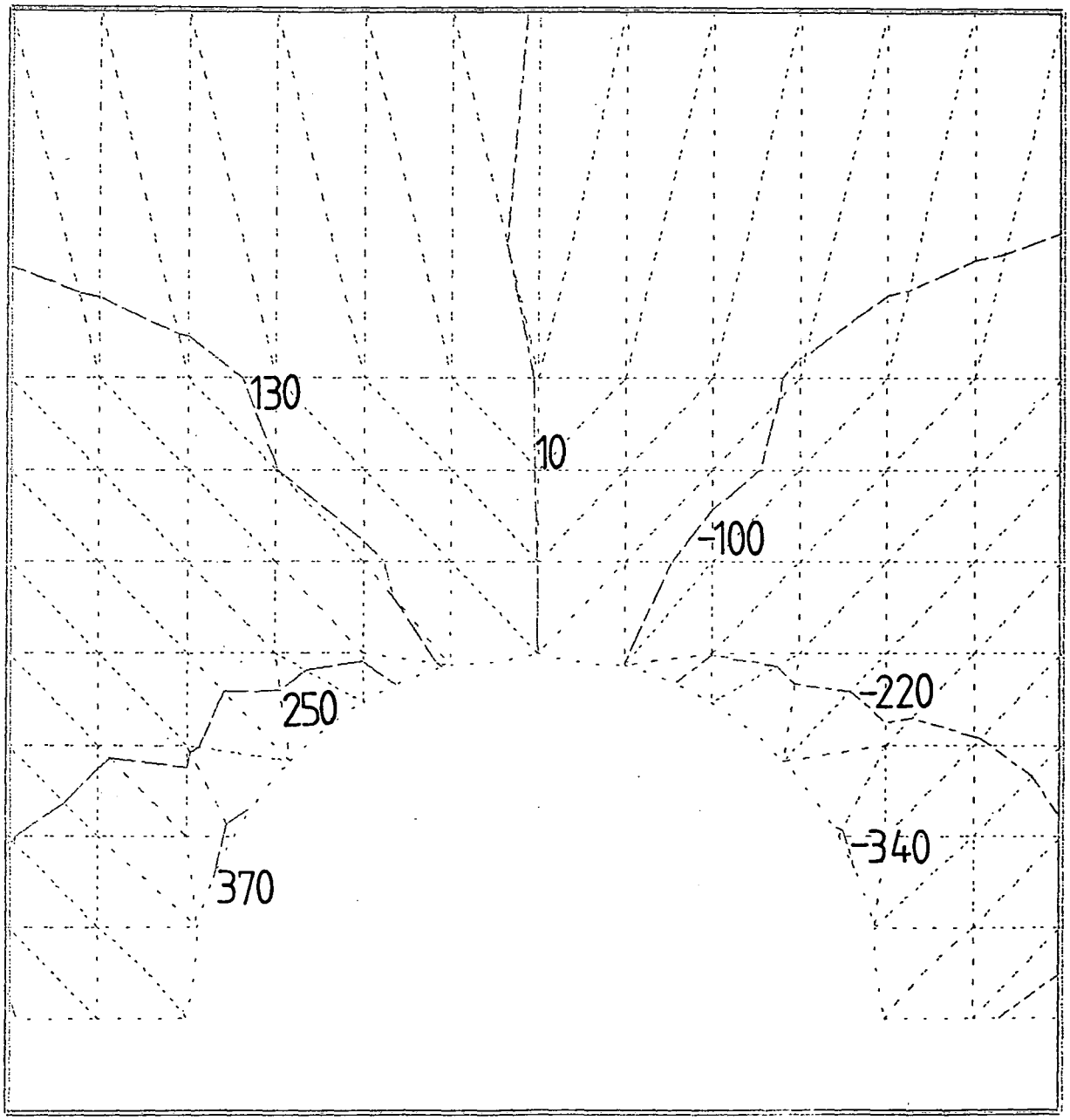

Figure 5.37 p' against cosγ for an incompressible Glen rheology with v_d = 10 alu/a (Case 23).

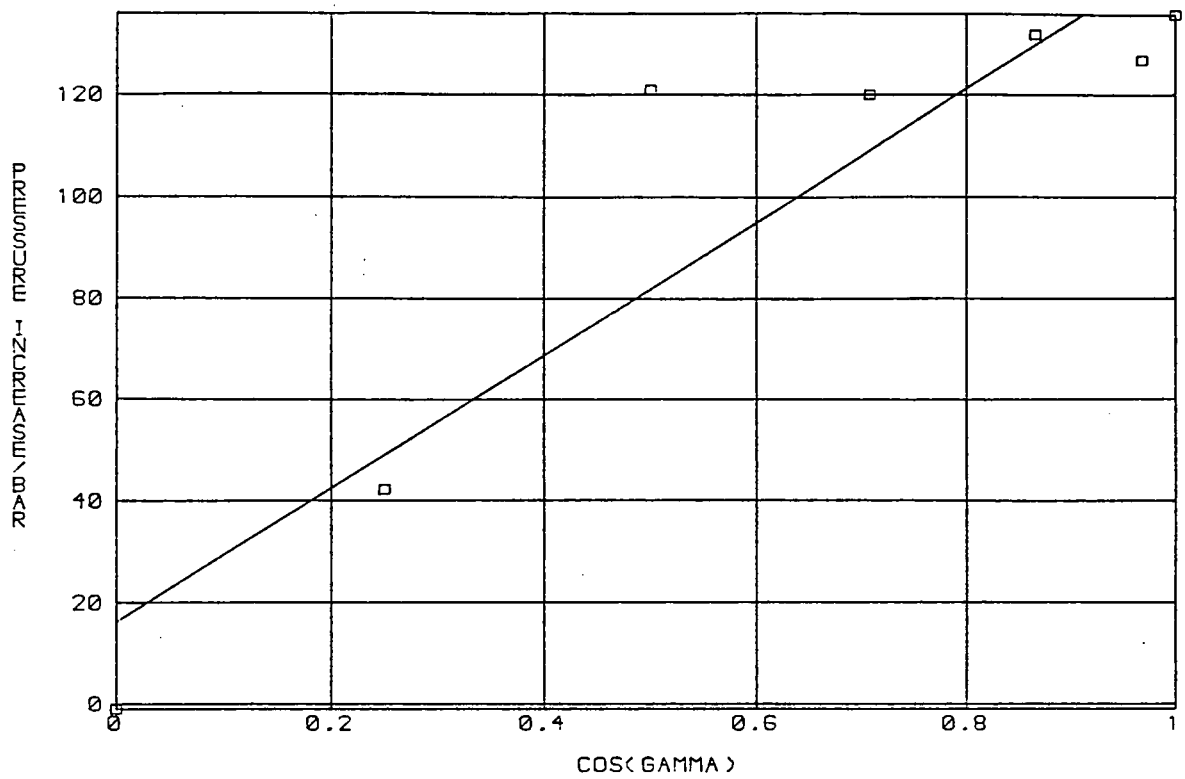

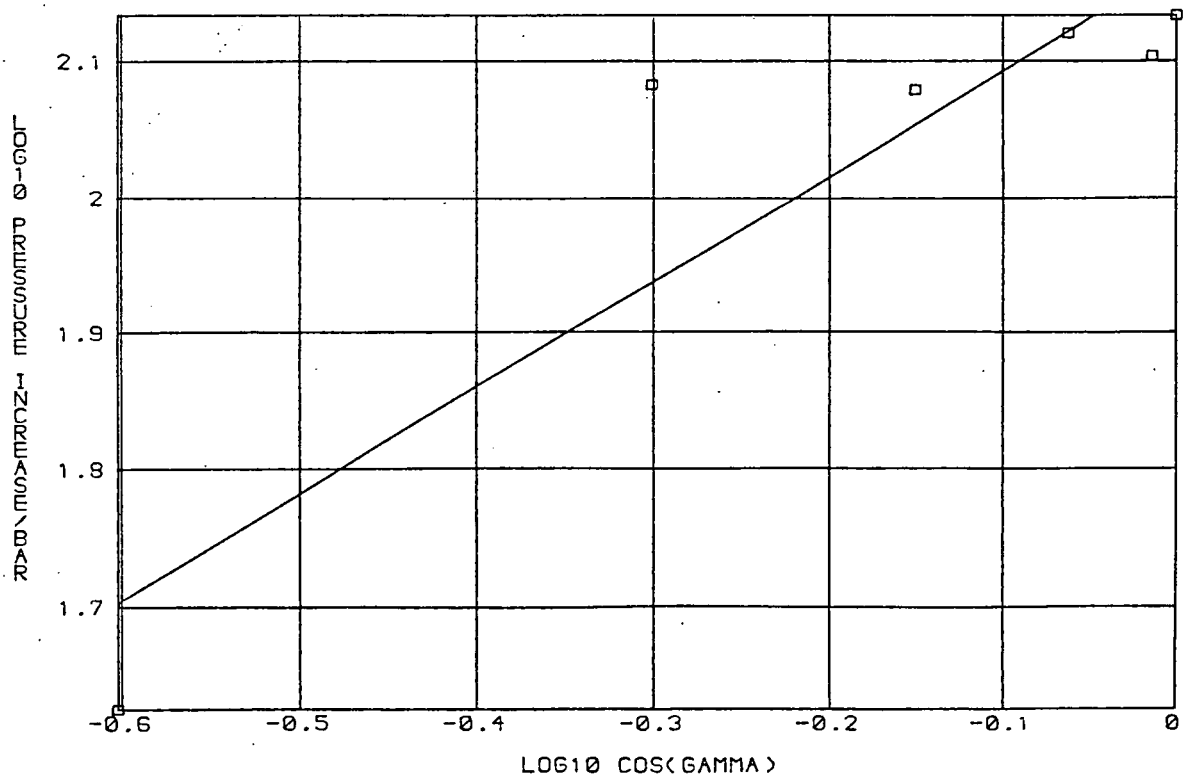

Figure 5.38 p' against $\cos\gamma$ for an incompressible Glen rheology with v_d = 400 alu/a (Case 27).

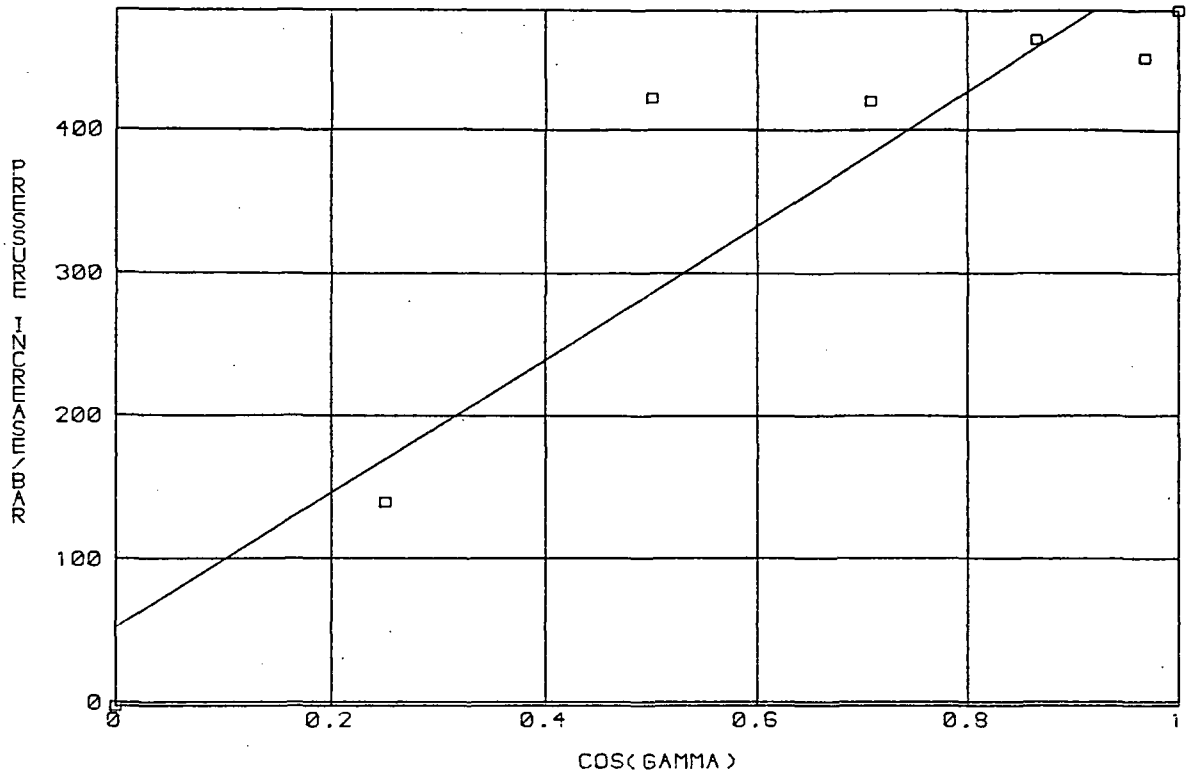

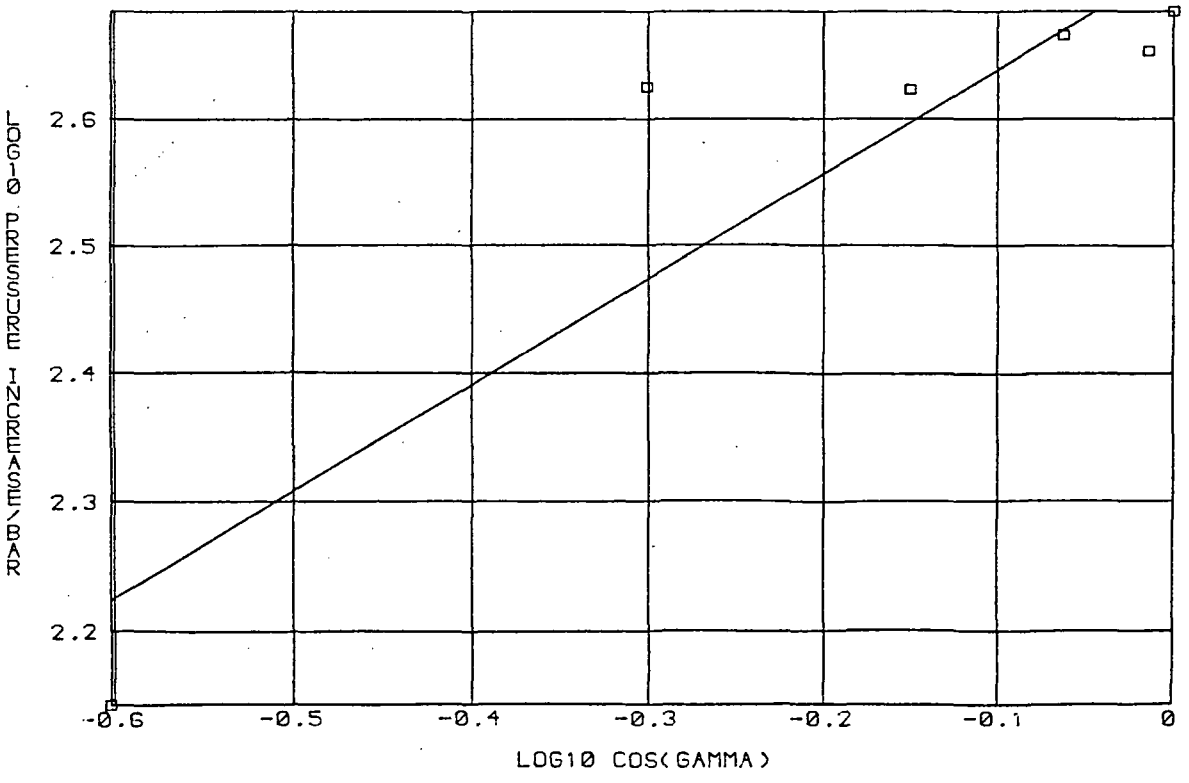

Figure 5.39 Pressure contours in bar for an incompressible Glen rheology with a cavity and v_d = 10 alu/a (Case 27).

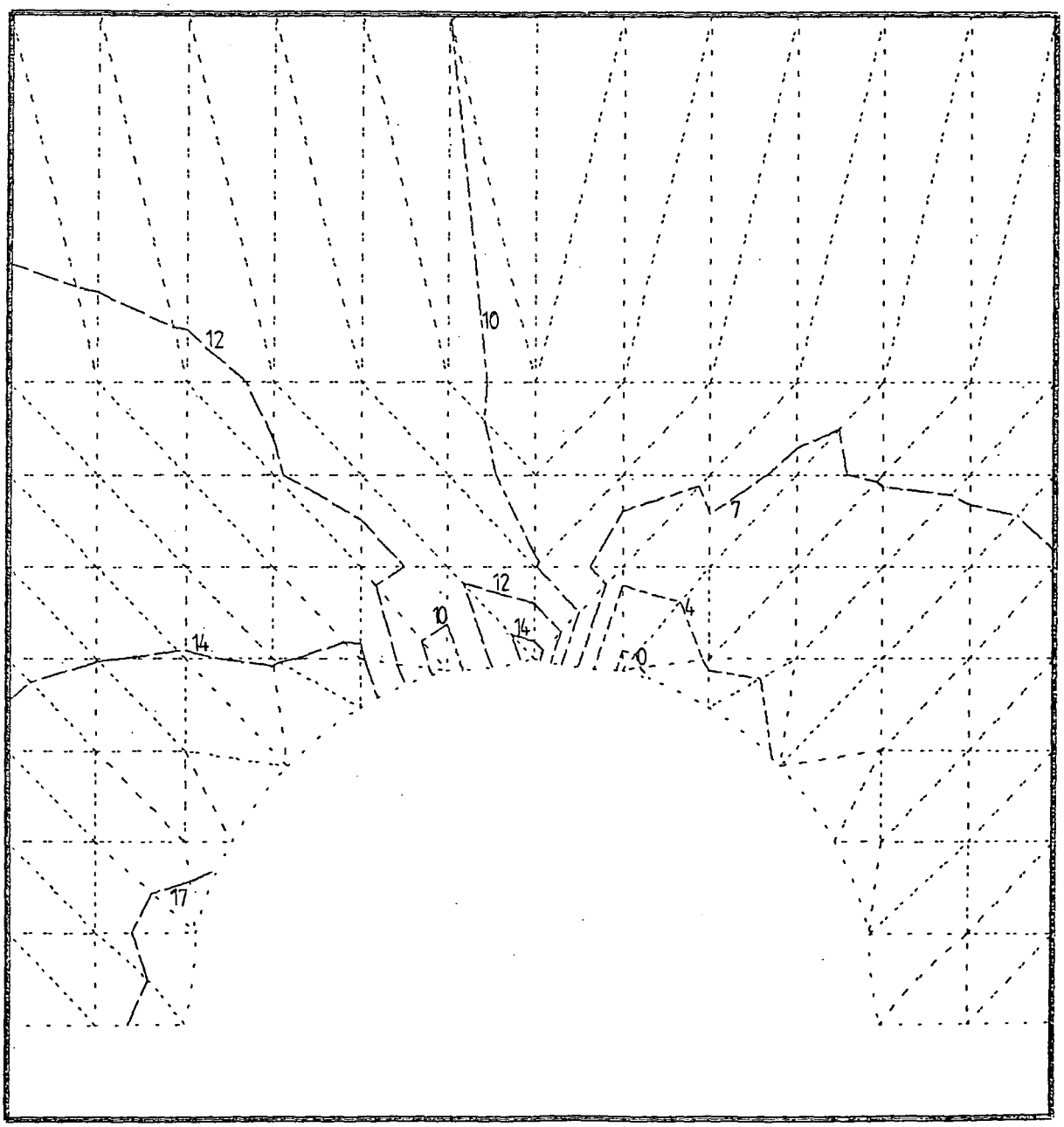

Figure 5.40 p' against cosγ for an incompressible Glen rheology with a cavity and v_d = 10 alu/a (Case 27).

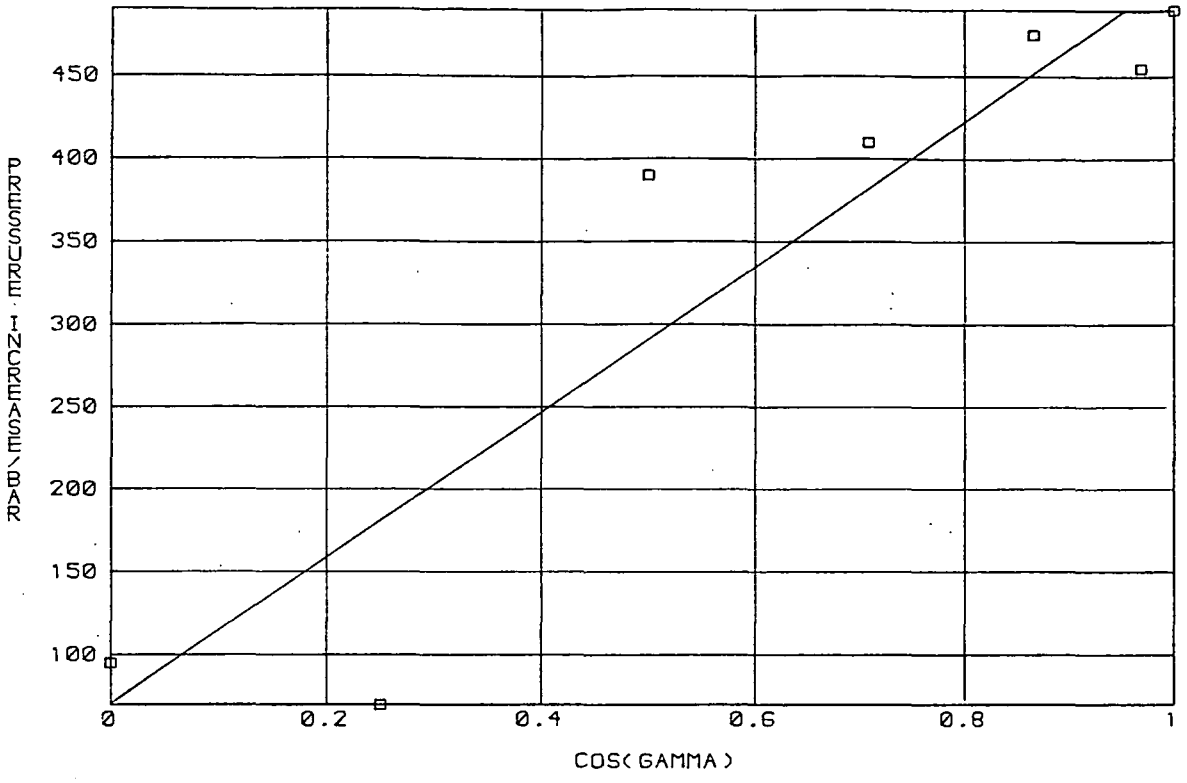

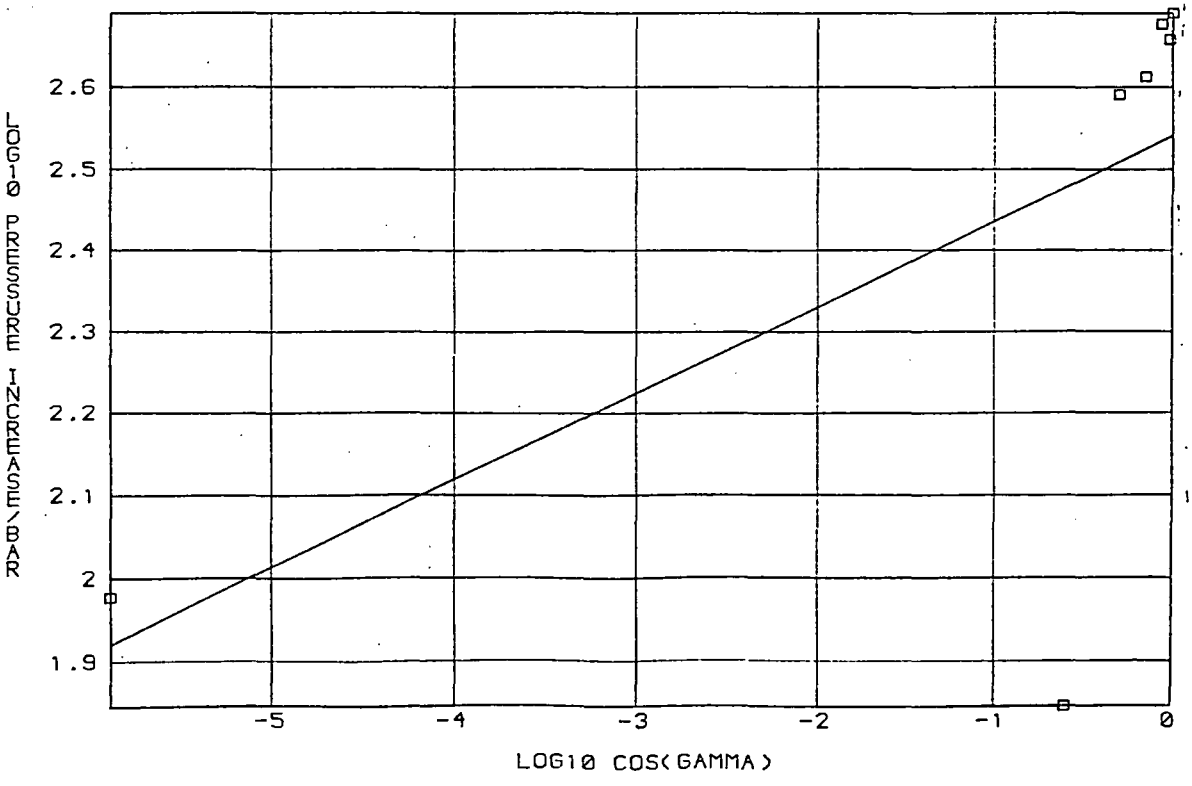

Figure 5.41 Pressure contours in bar for a compressible, Glen rheology with χ = 1 alu^2/bar.a and v_d = 100 alu/a (Case 29).

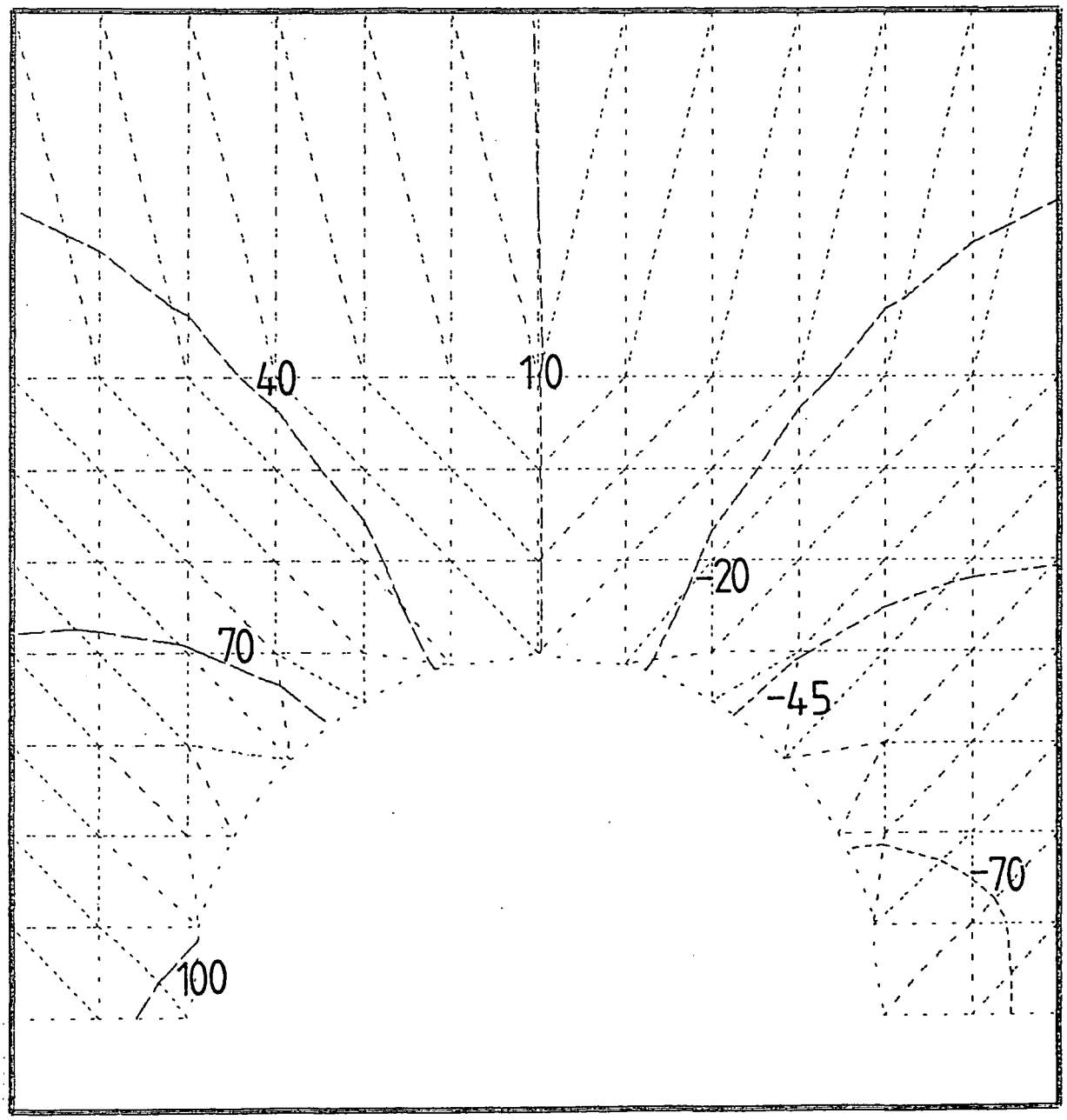

Figure 5.42 p' against $\cos\gamma$ for a compressible Glen rheology with χ = 1 alu²/bar.a and v_d = 200 alu/a (Case 30).

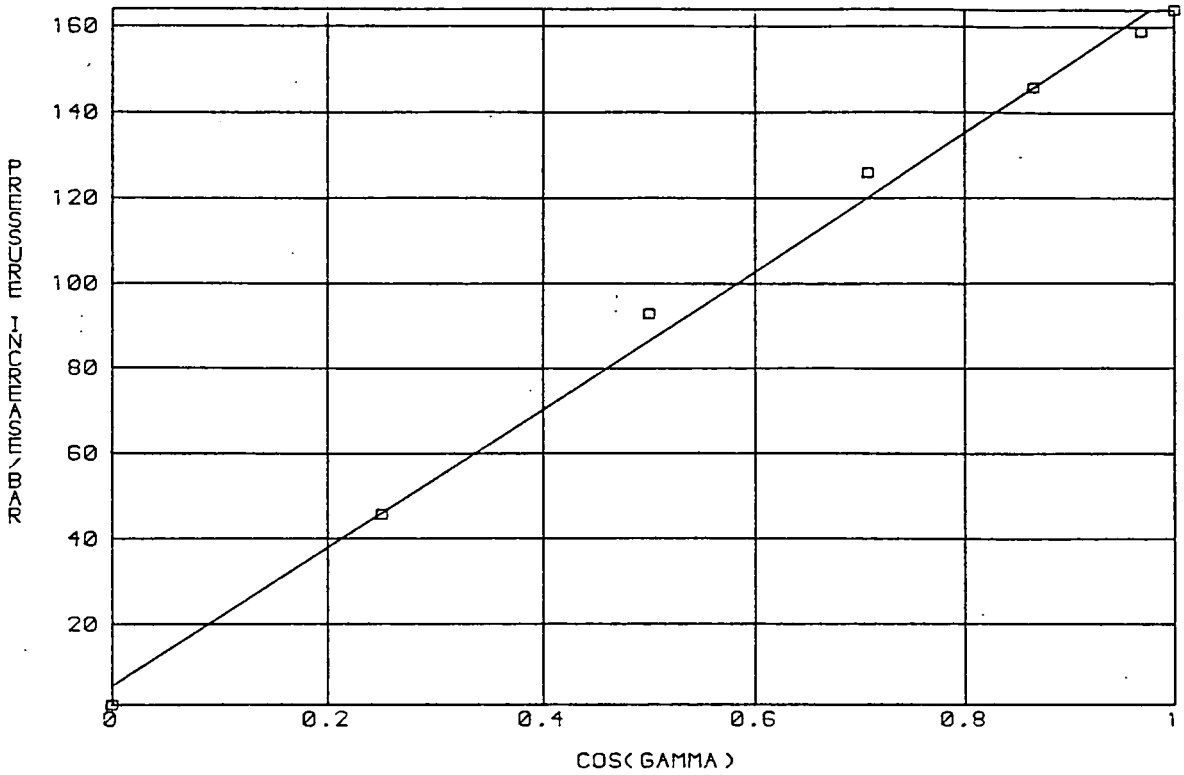

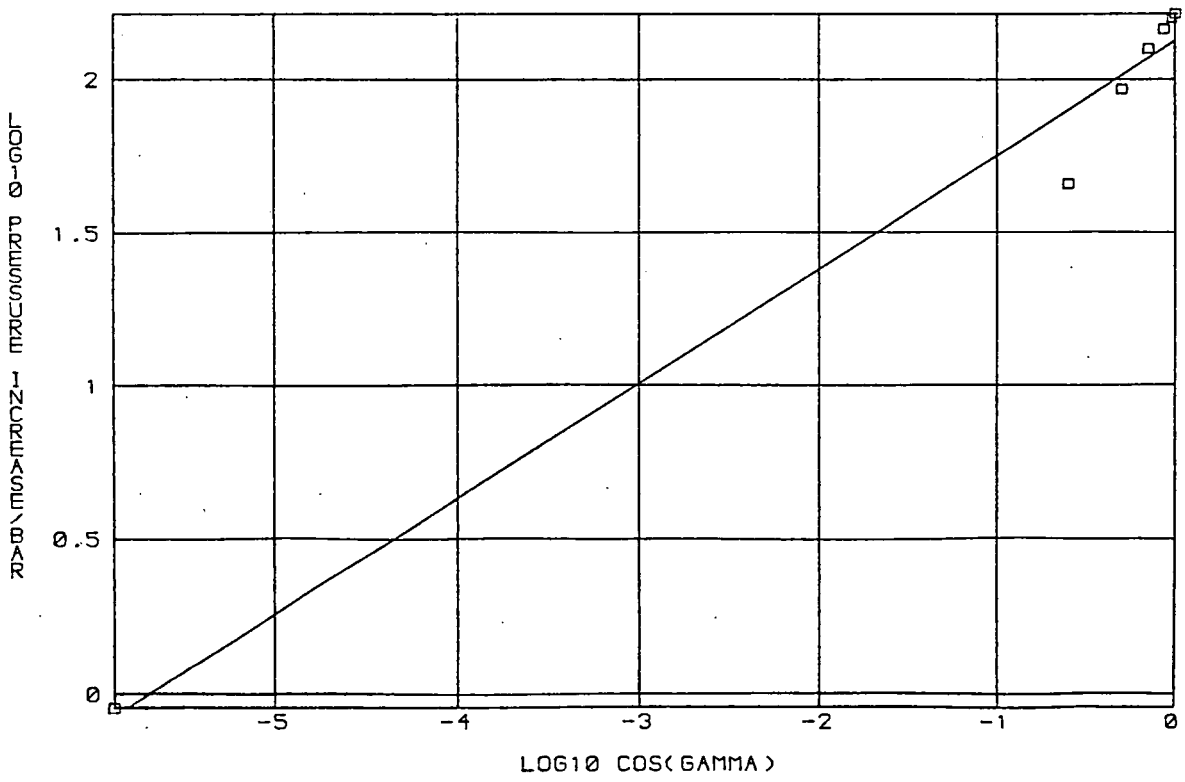

Figure 5.43 p' against $\cos\gamma$ for an incompressible Glen rheology with bed of S = 10 alu/bar.a and v_d = 10 alu/a (Case 34)

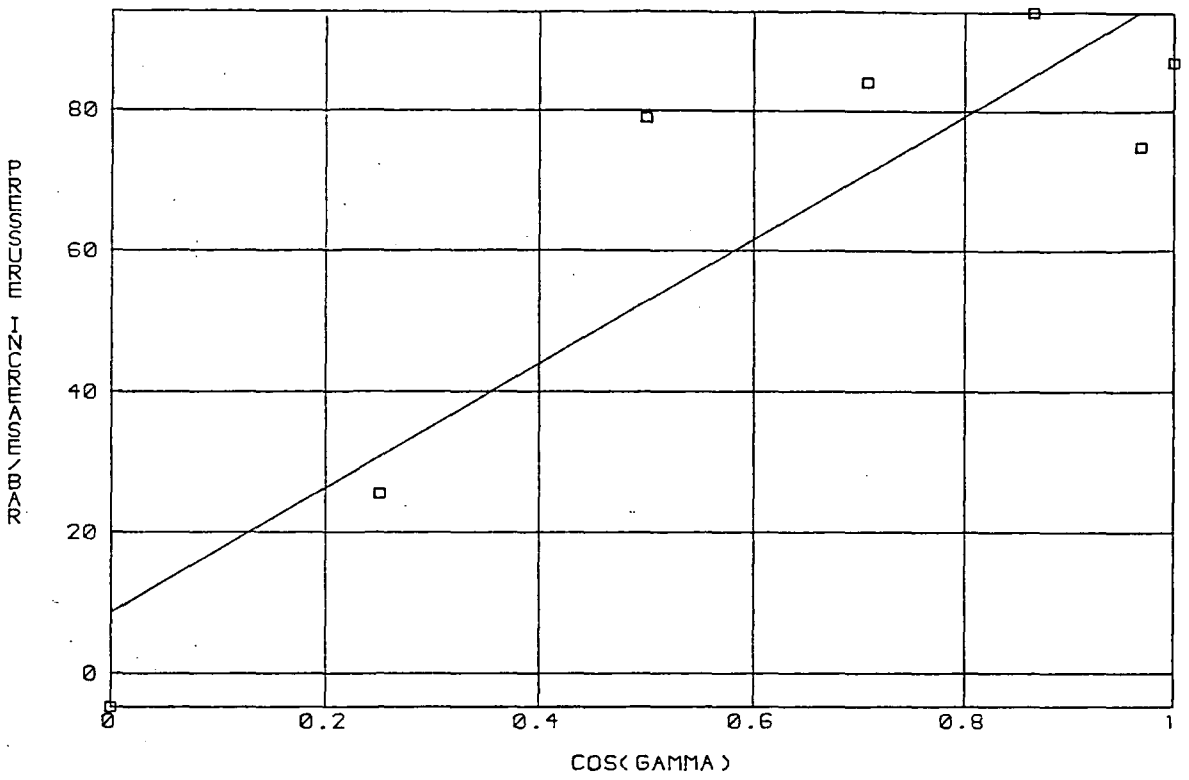

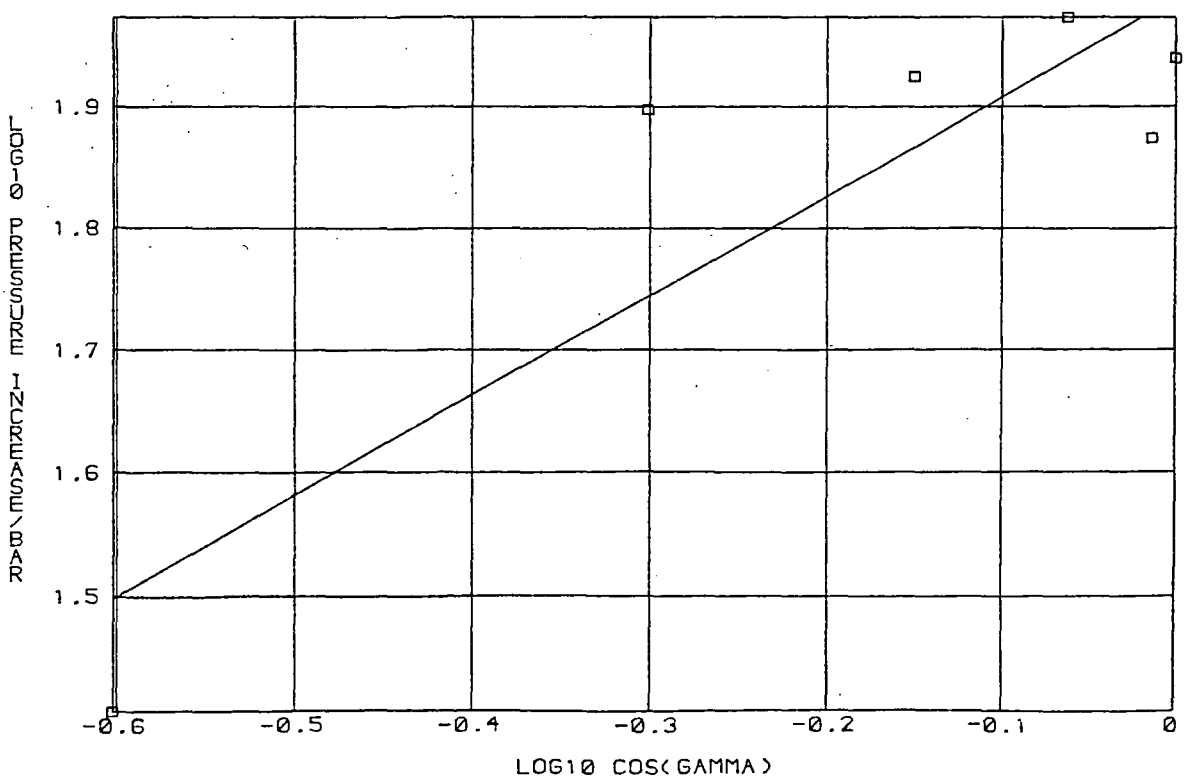

Figure 5.44 p' against position for flow over a truncated sine ridge (Cases 40 - 49).

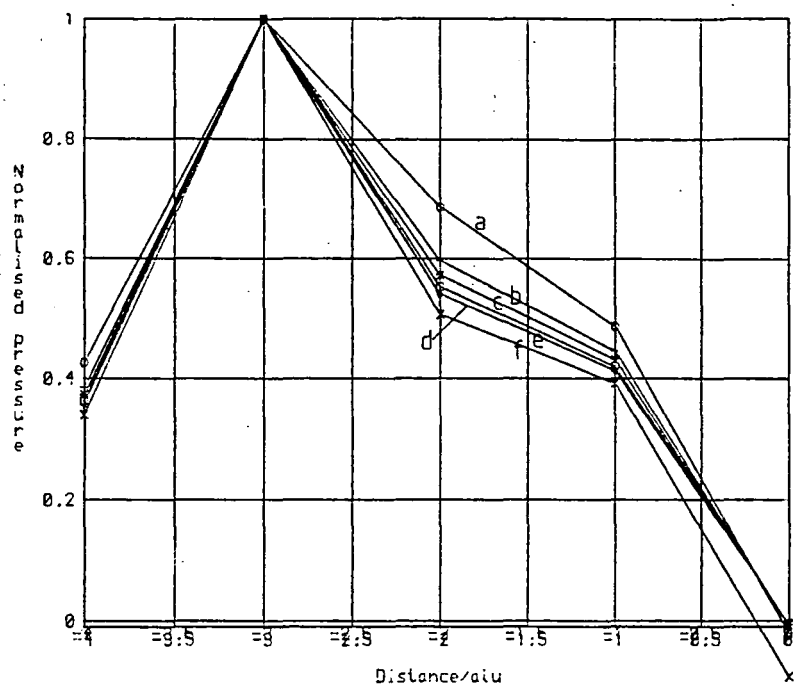

a-Linear
b-Glen, v_g = 400alu/a
c-Glen, v_g = 200alu/a
d-Glen, v_g = 100alu/a
e-Glen, v_g = 50alu/a
f-Glen, v_g = 10alu/a

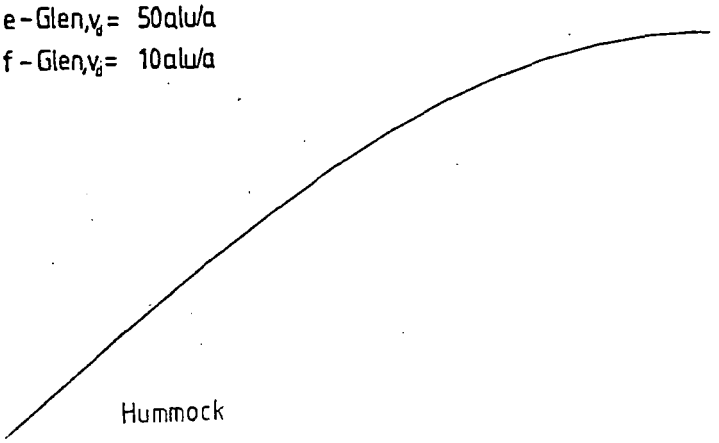

Figure 5.45 Pressure contours in bar for an incompressible Glen rheology with v_d = 100 alu/a for flow over a truncated sine ridge (Case 47).

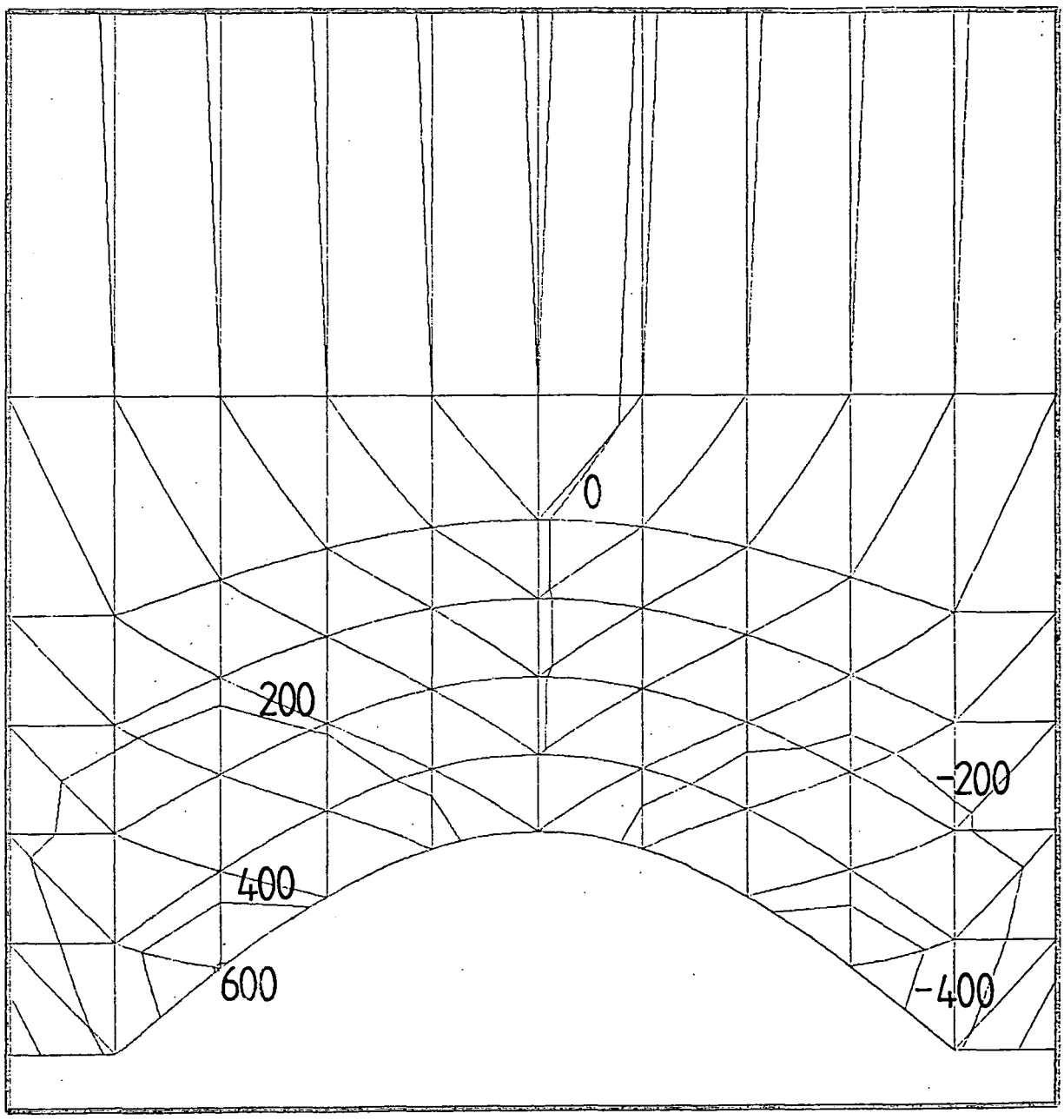

Figure 5.46 $\dot{\varepsilon}_v$ in a^{-1} for a compressible linear rheology with χ = 1 alu²/bar.a and v_d = 400 alu/a (Case 12).

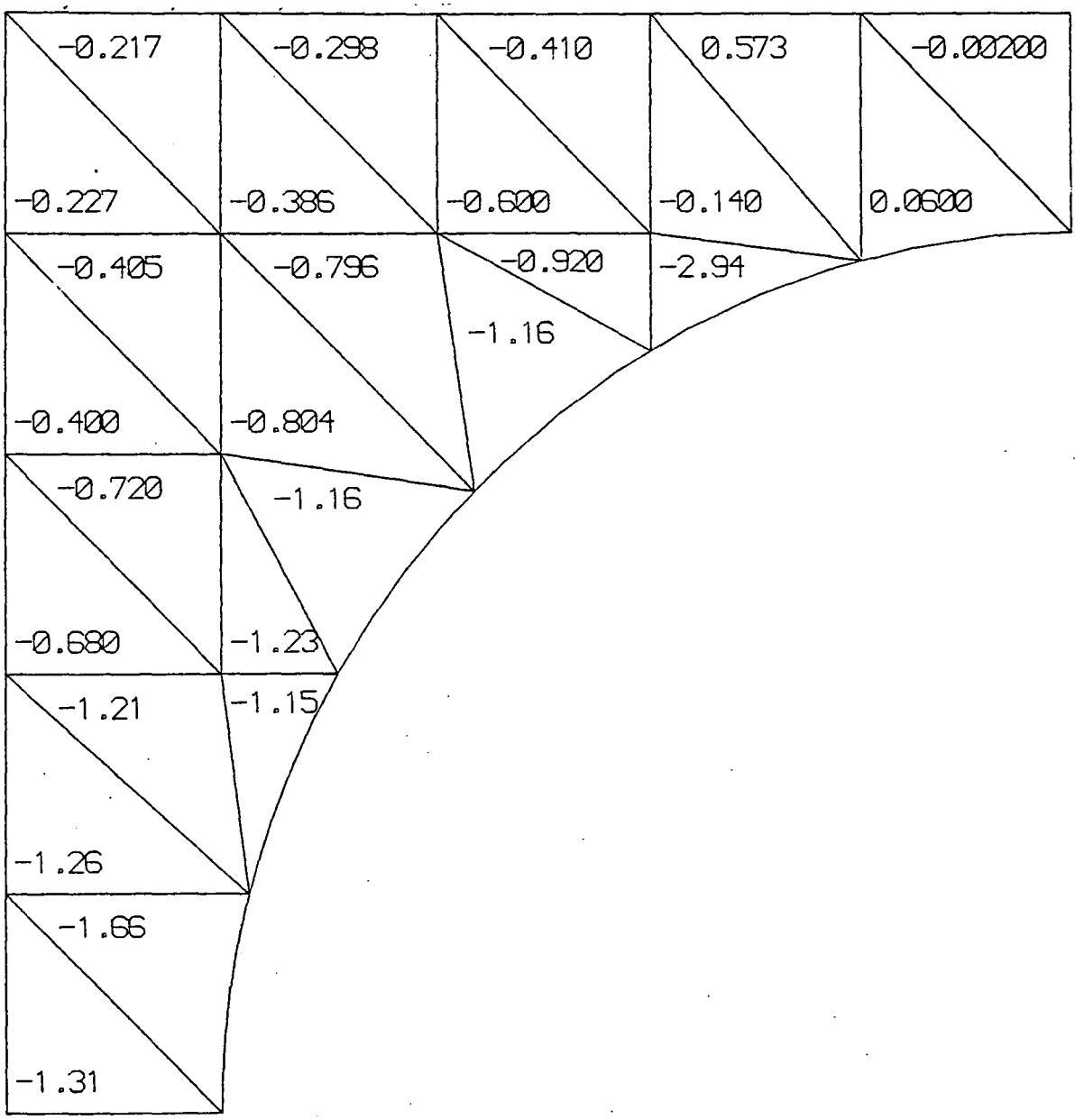

Figure 5.47 $\dot{\varepsilon}_v$ in a^{-1} for a compressible linear rheology with χ = 10 alu²/bar.a and v_d = 200 alu/a (Case 16).

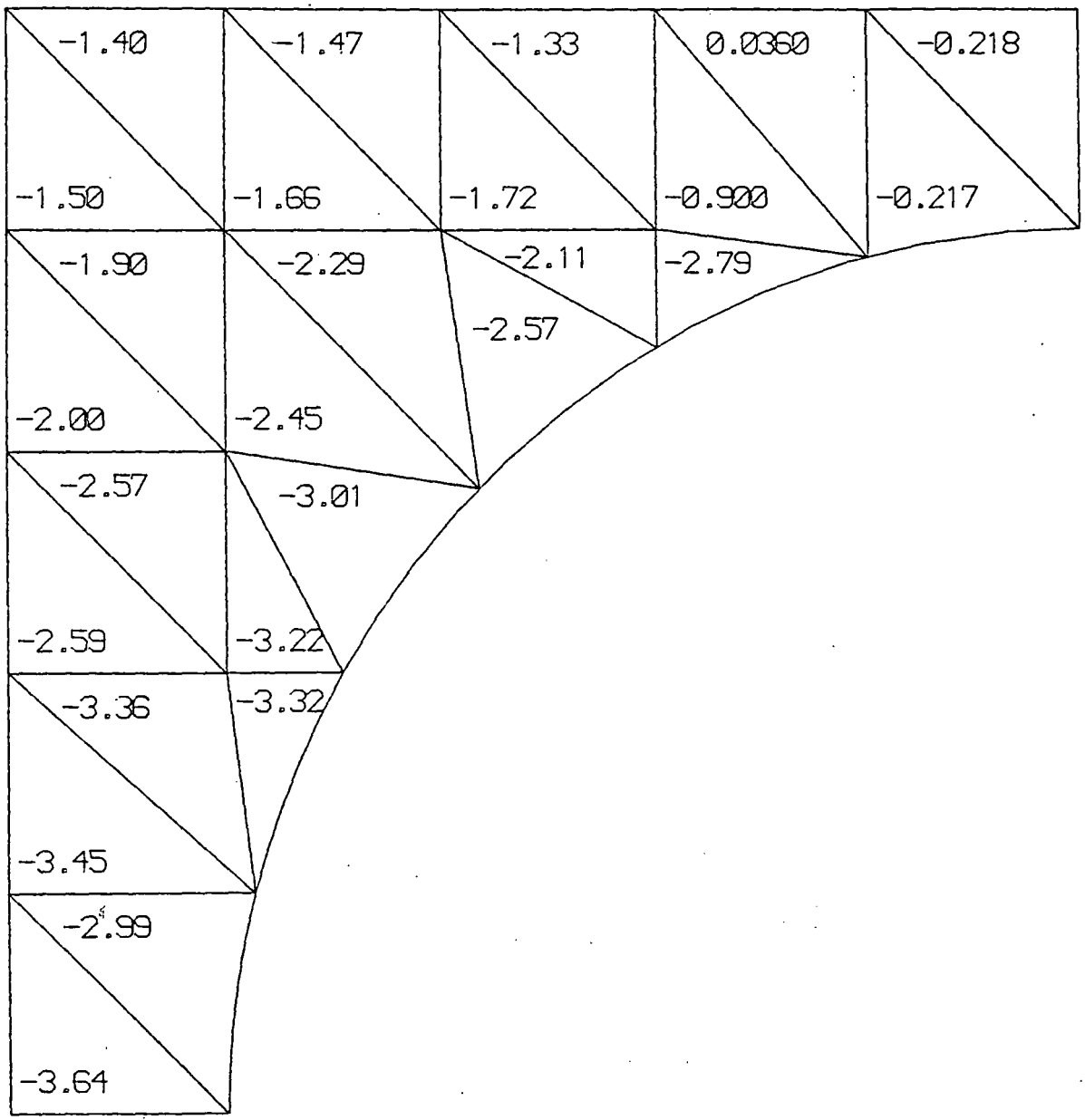

Figure 5.48 $\dot{\varepsilon}_v$ in a^{-1} for a compressible Glen rheology with χ = 1 alu²/bar.a and v_d = 10 alu/a (Case 29).

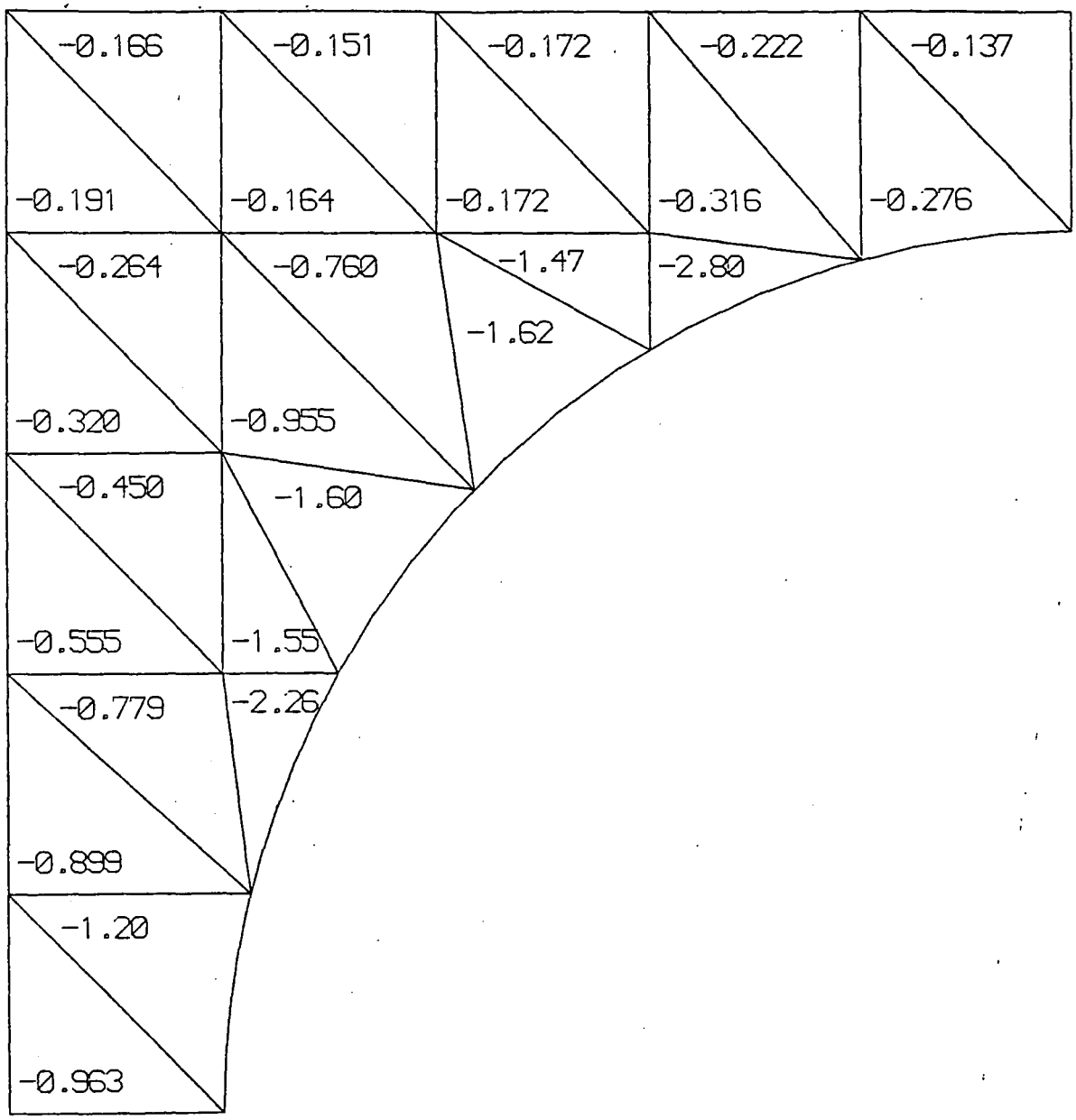

Figure 5.49 $\dot{\varepsilon}_v$ in a^{-1} for a compressible Glen rheology with χ = 1 alu²/bar.a and v_d = 400 alu/a (Case 33).

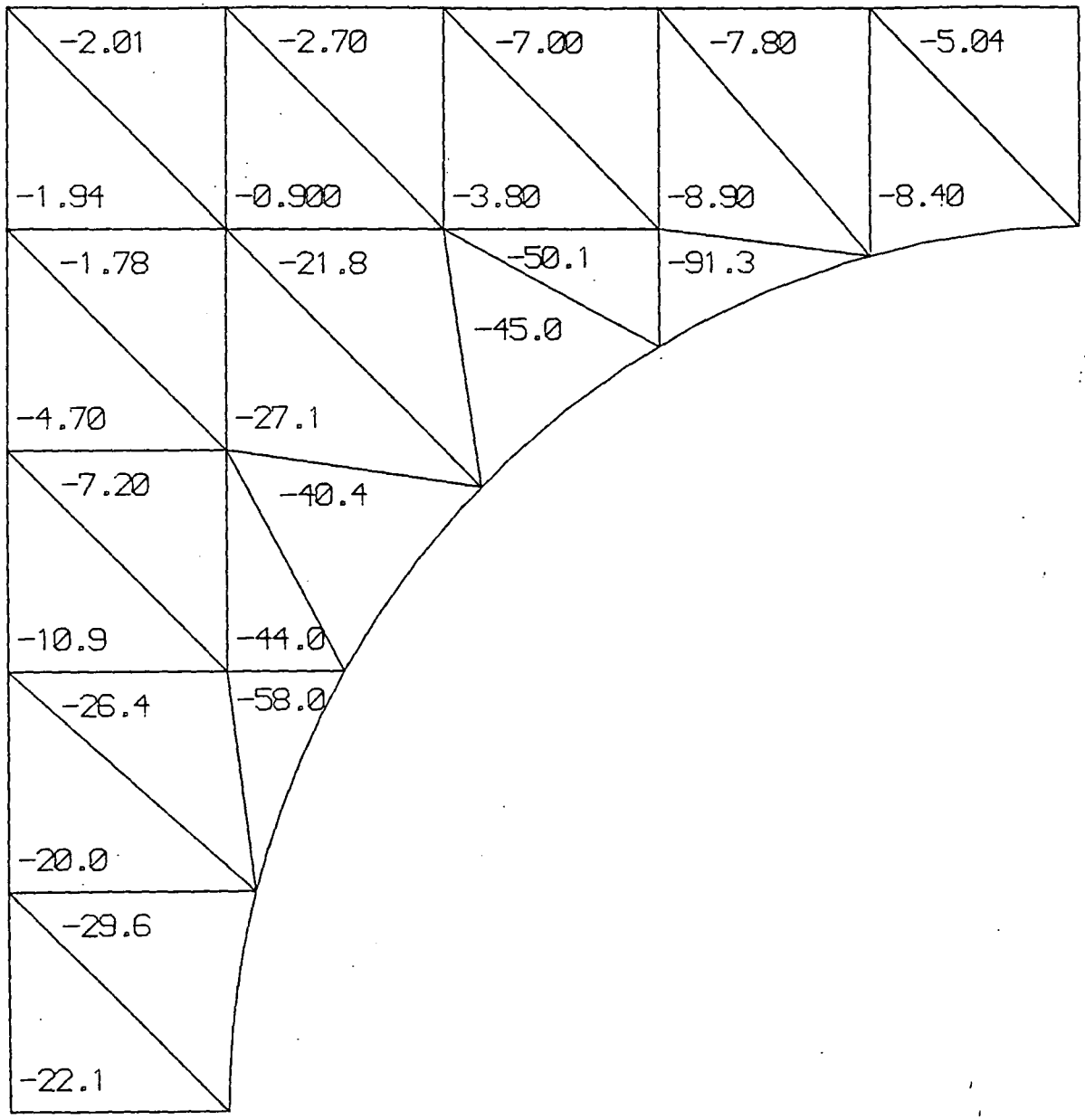

Figure 5.50 Regression exponent for $\dot{\epsilon}_v$ against v_d for a compressible Glen rheology with χ = 1 alu^2/bar.a (Cases 29 - 33).

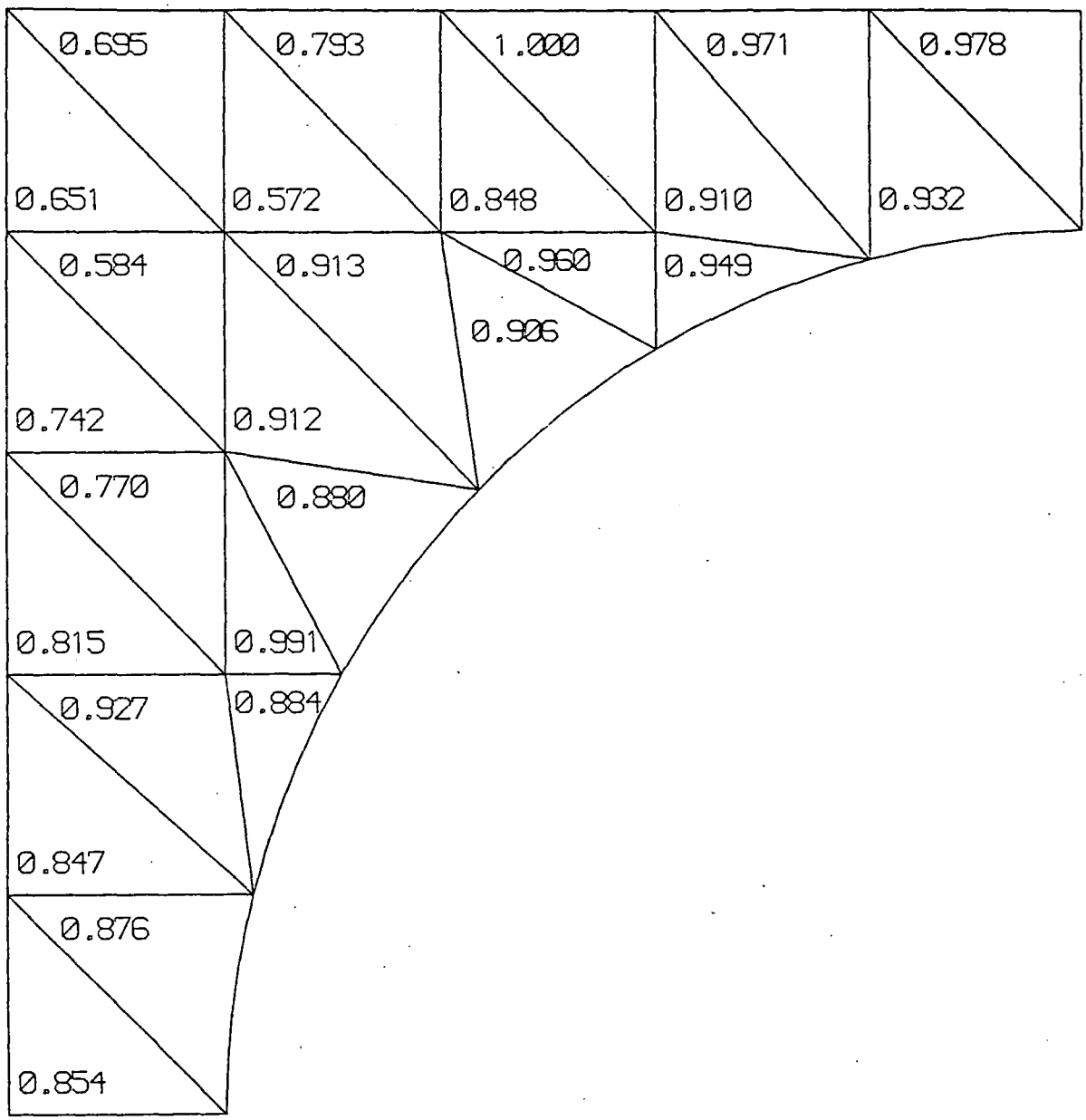

Figure 5.51 μ in bar.a for an incompressible Glen rheology with v_d = 10 alu/a (Case 23).

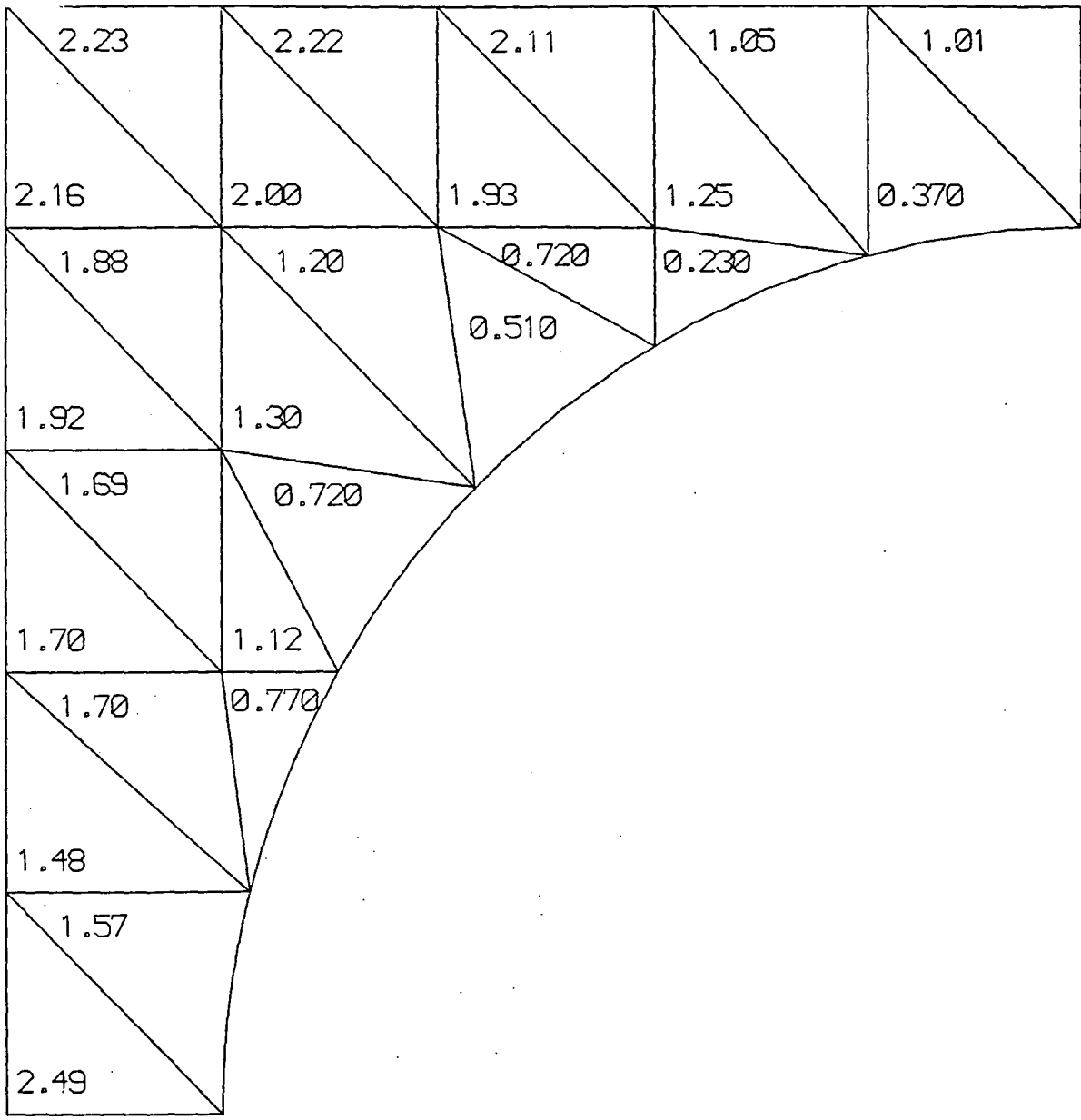

Figure 5.52 μ in bar.a for an incompressible Glen rheology with v_d = 400 alu/a (Case 26).

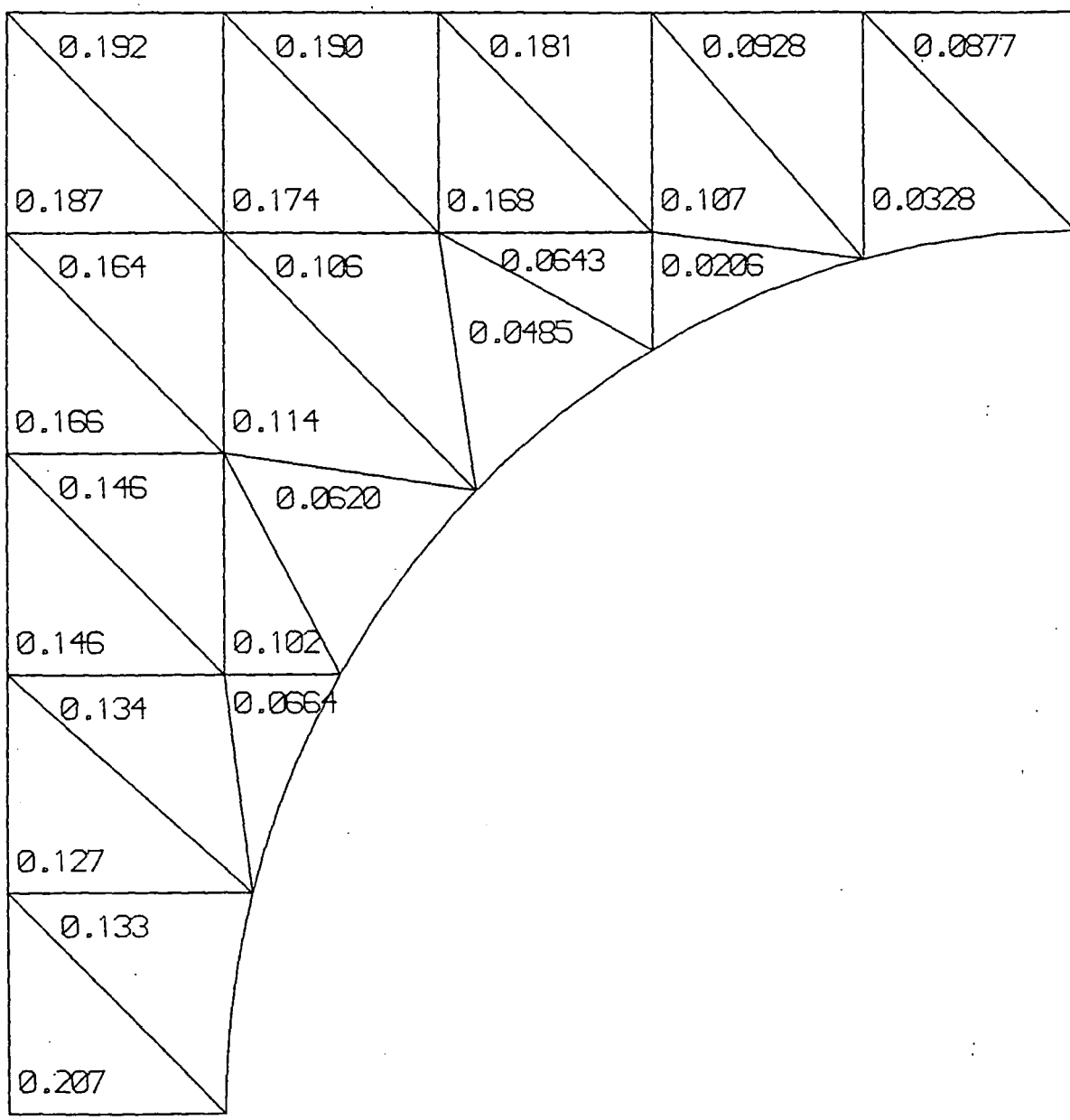

Figure 5.53 μ in bar.a for an incompressible Glen rheology with a cavity and v_d = 10 alu/a (Case 27).

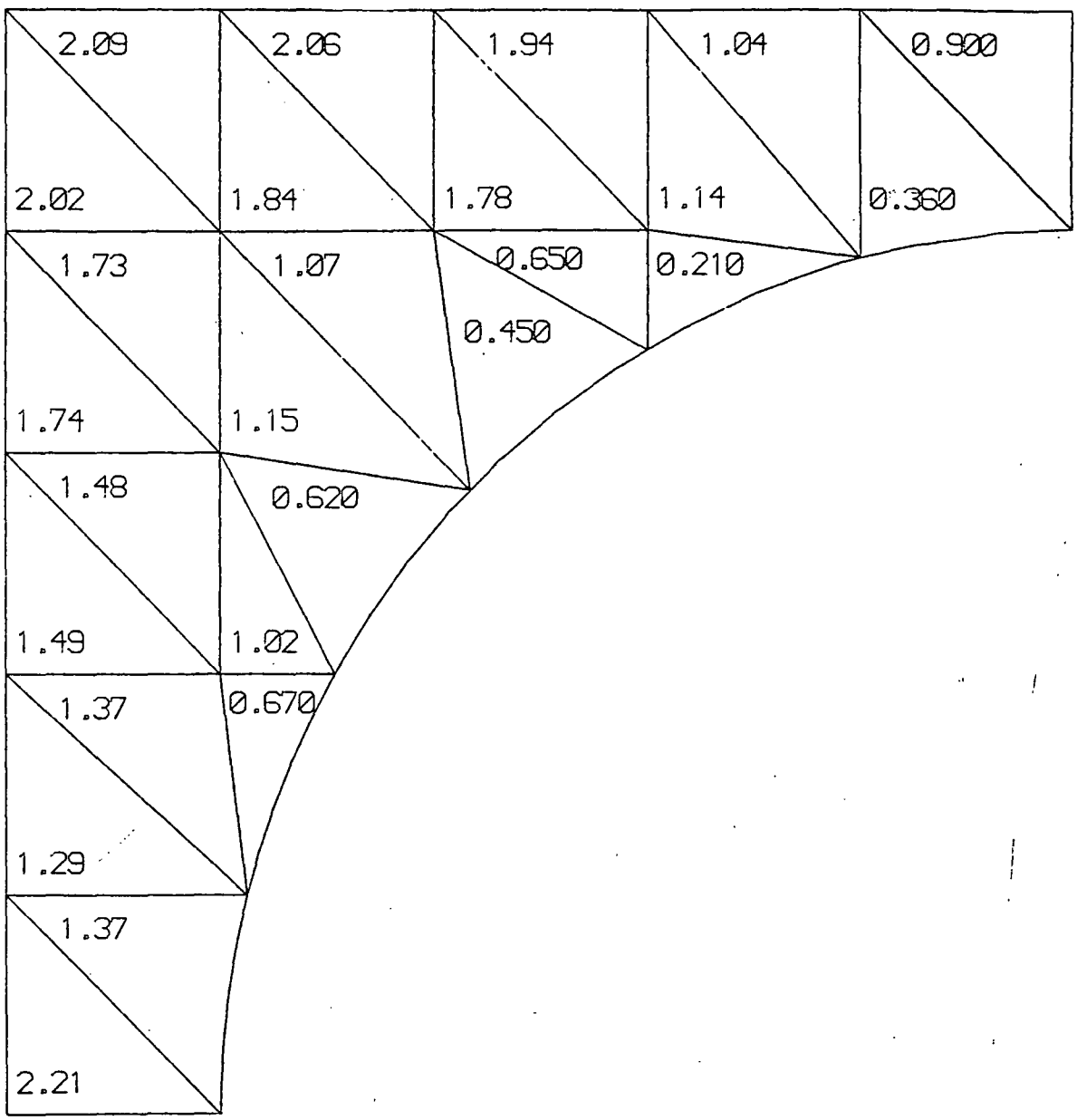

Figure 5.54 μ in bar.a for a compressible Glen rheology with χ = 1 alu^2/bar.a and v_d = 10 alu/a (Case 29).

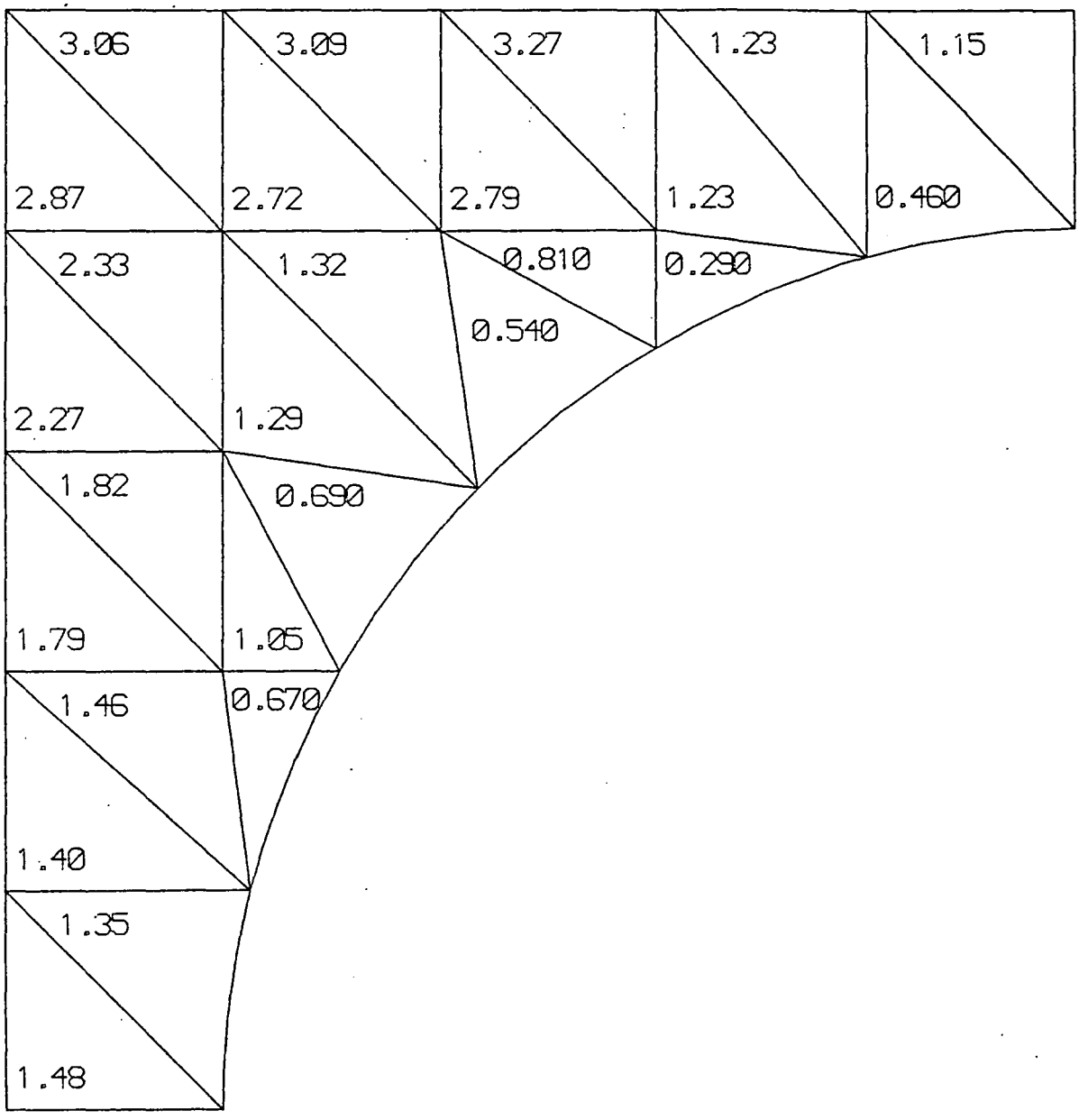

Figure 5.55 μ in bar.a for a compressible Glen rheology with $\chi = 1$ alu^2/bar.a with $v_d = 400$ alu/a (Case 33).

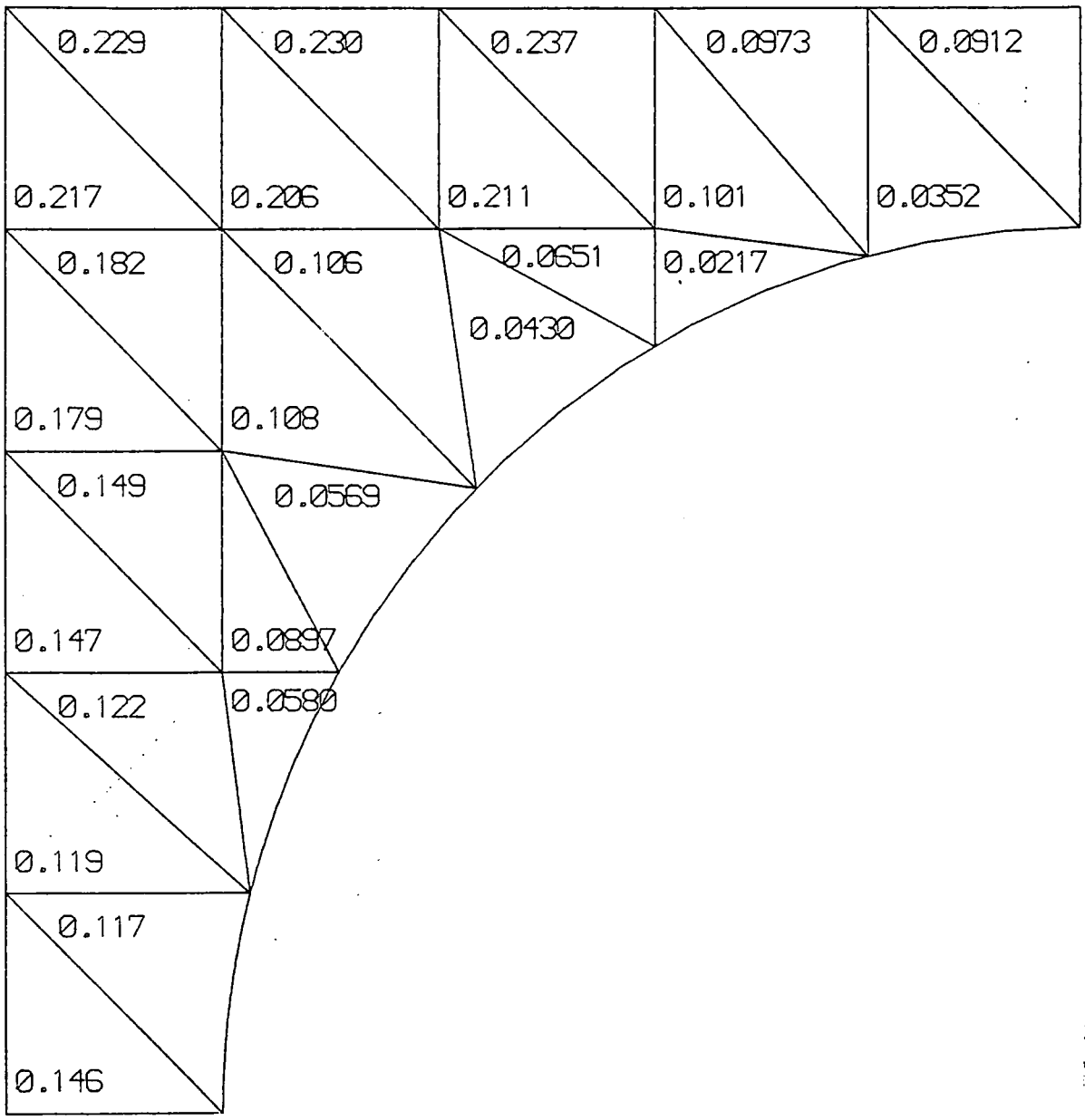

Figure 5.56 μ in bar.a for an incompressible Glen rheology with S = 10 alu/bar.a and v_d = 10 alu/a (Case 34).

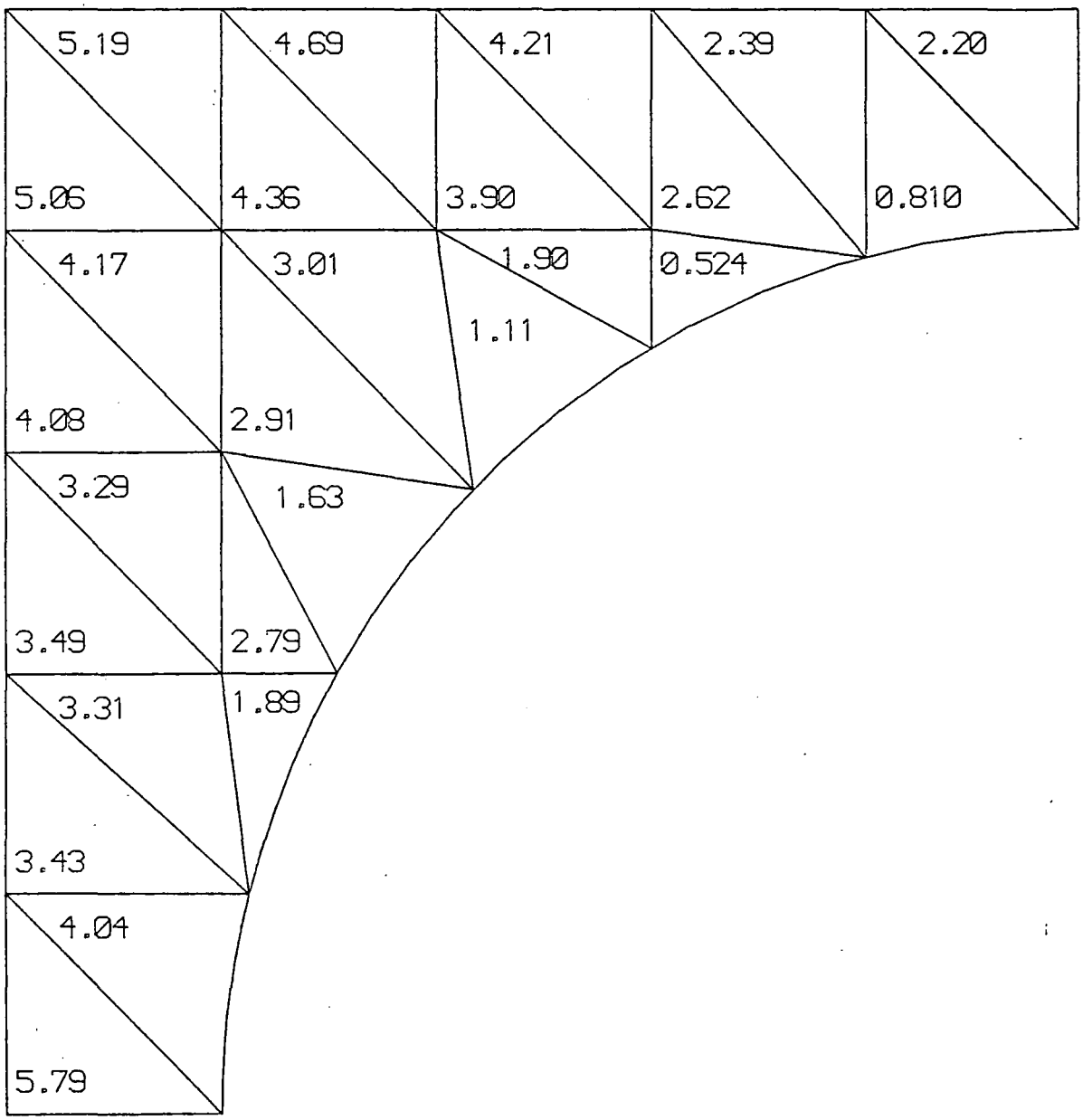

Figure 5.57 μ in bar.a for an incompressible Glen rheology with v_d = 10 alu/a for flow over a truncated sine ridge (Case 45).

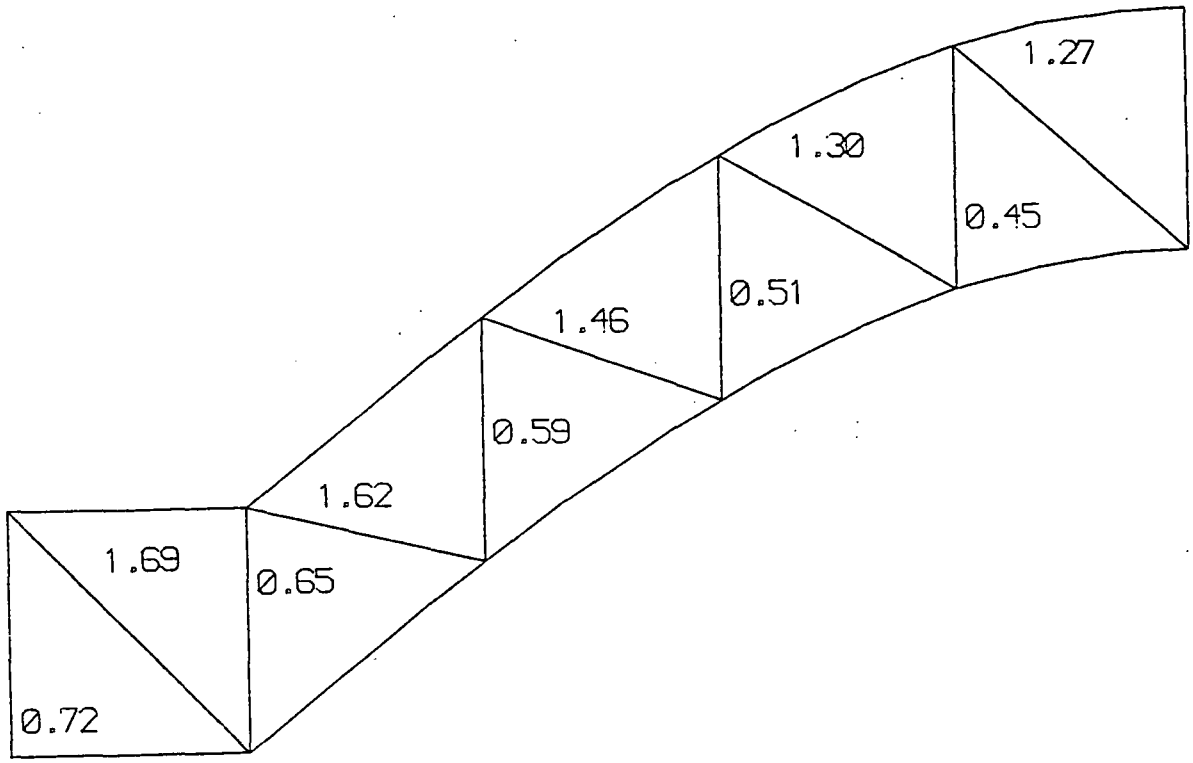

Figure 5.58 μ in bar.a for an incompressible Glen rheology with v_d = 400 alu/a for flow over a truncated sine ridge (Case 49).

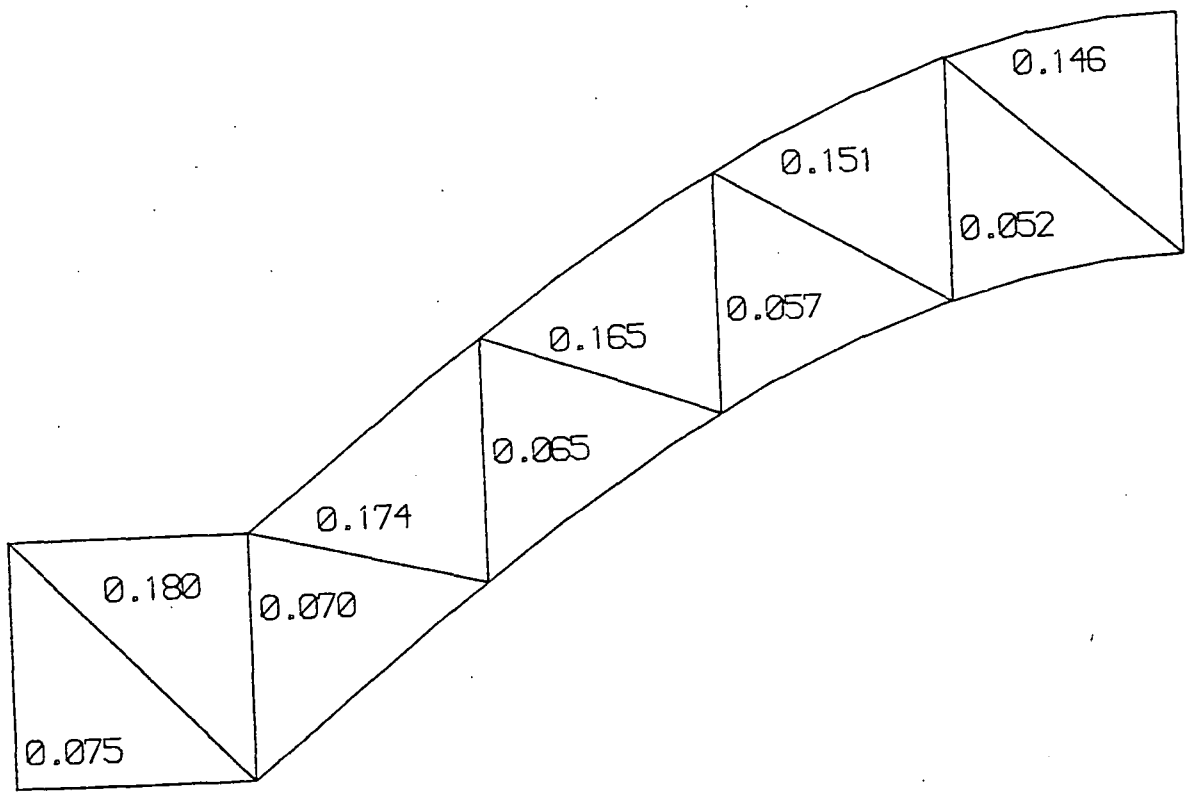

Figure 5.59 Regression exponent of μ against v_d for flow over a truncated sine ridge (Cases 45 - 49).

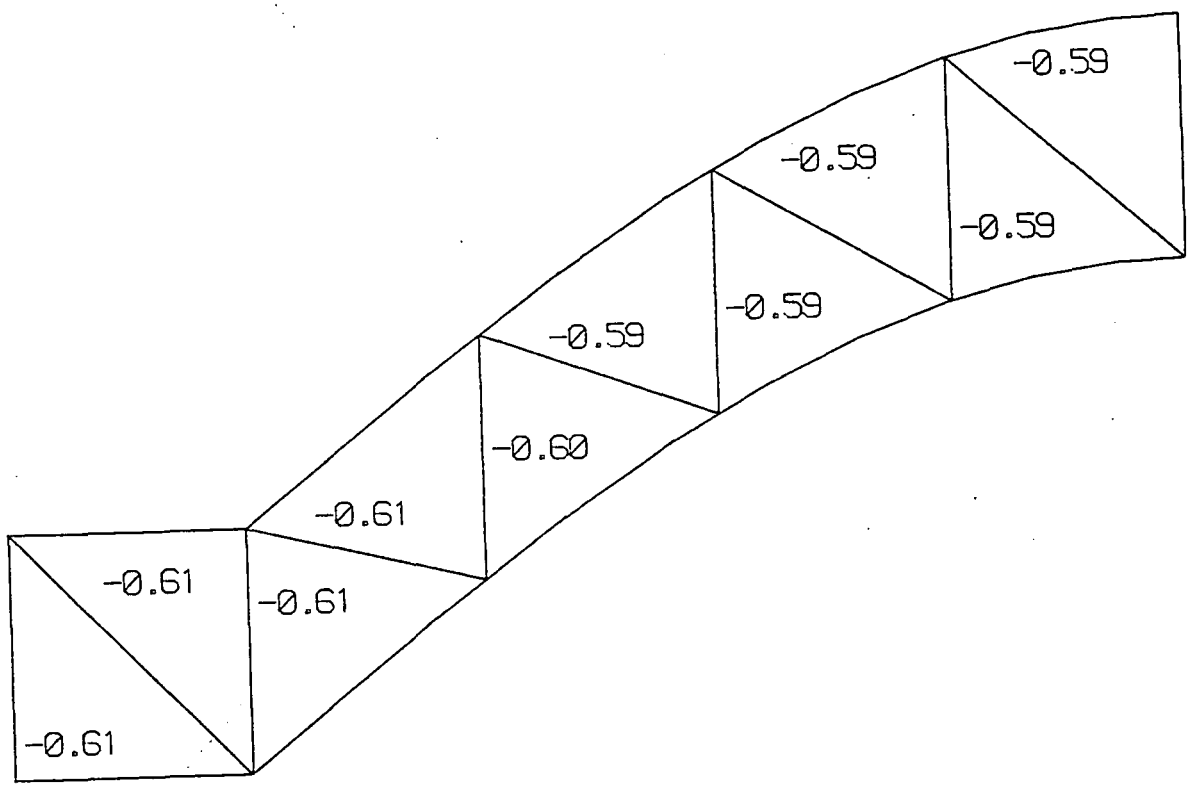

Figure 5.60 Semi-analytic interfacial stress for incompressible linear rheology with v_d = 10 alu/a.

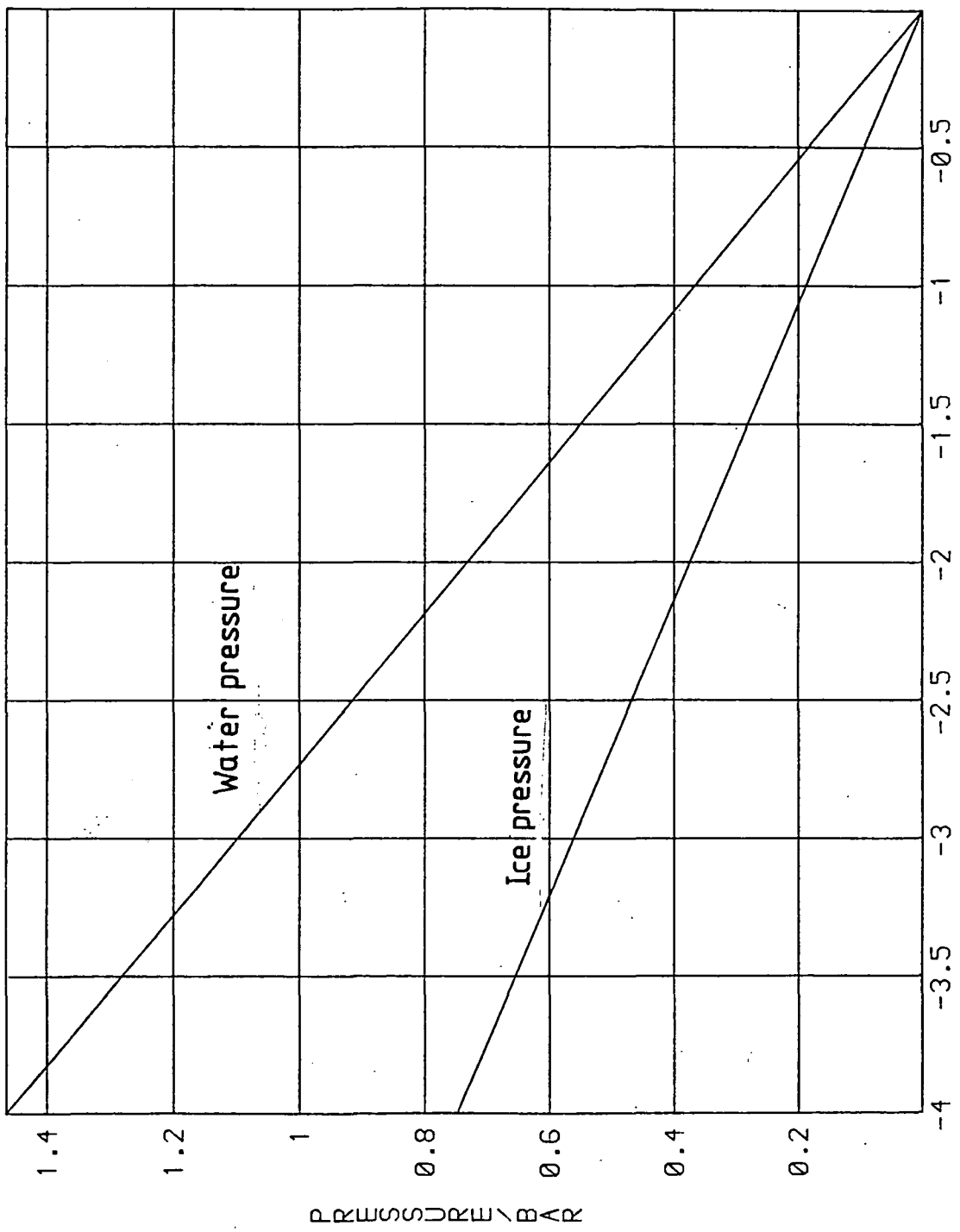

Figure 5.61 Semi-analytic interfacial stress for compressible linear rheology with χ = 1 alu²/bar.a and v_d = 10 alu/a.

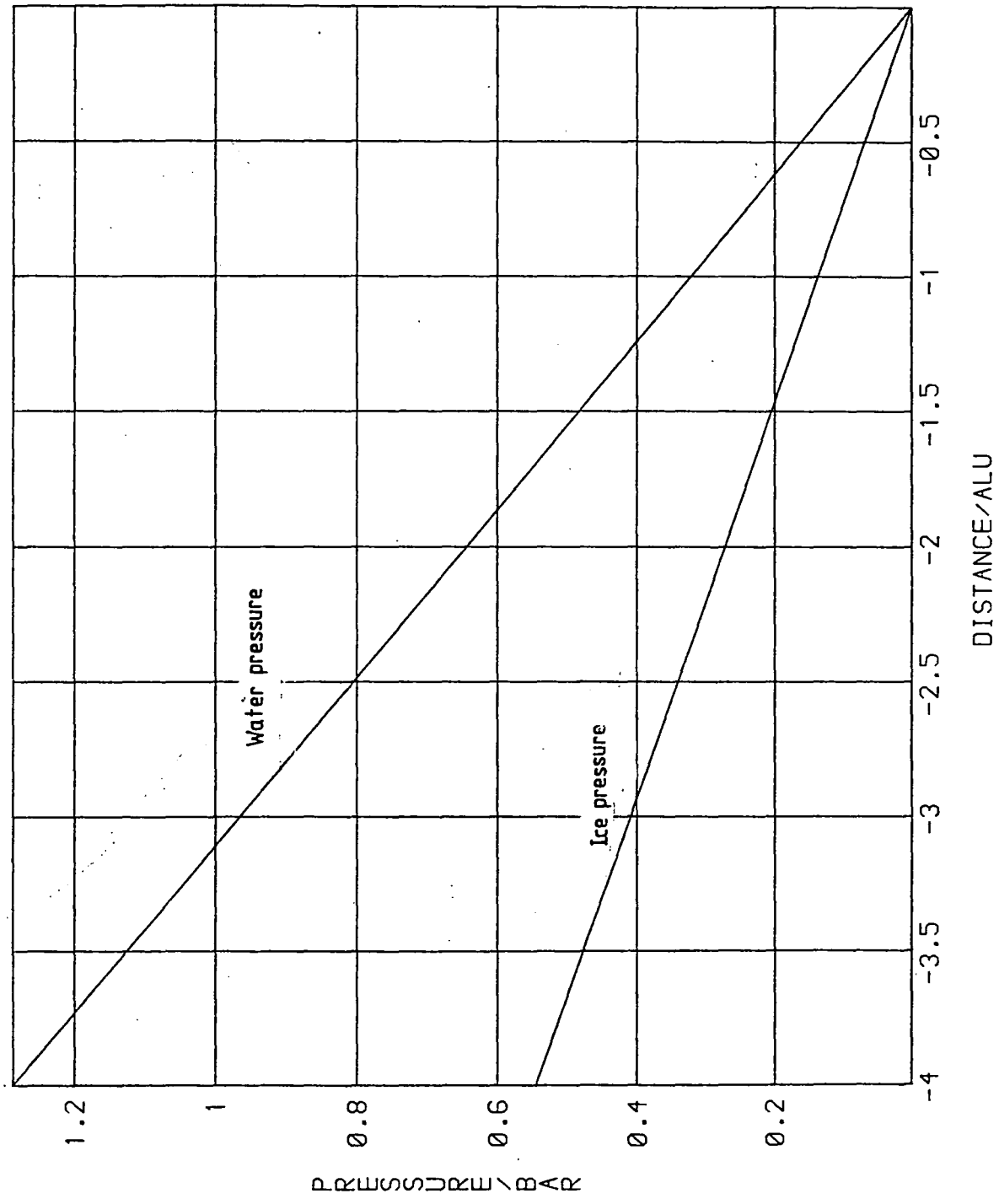

Figure 5.62 Semi-analytic interfacial stress for compressible linear rheology with χ = 10 alu^2/bar.a and v_d = 10 alu/a.

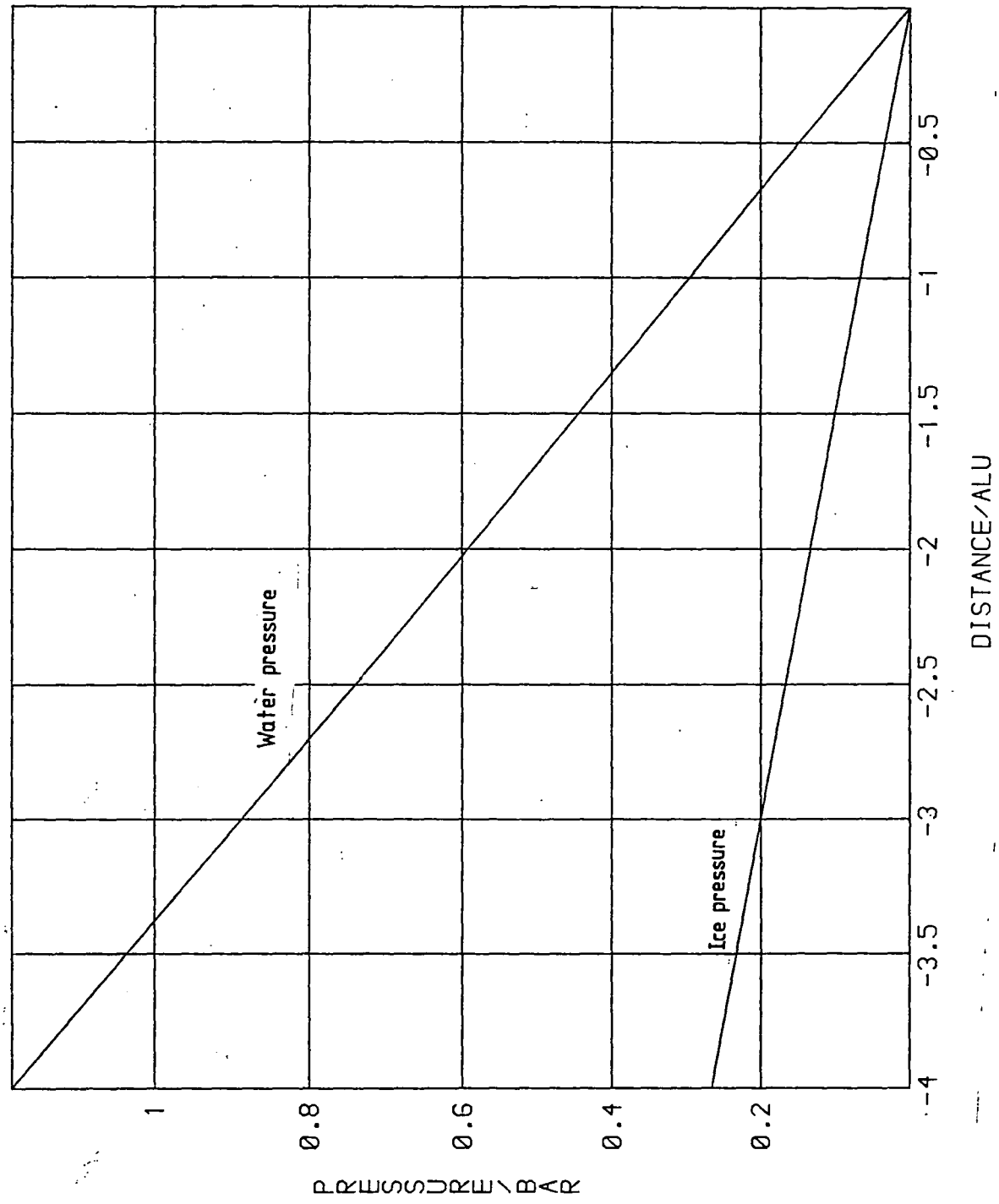

Figure 5.63 Semi-analytic interfacial stress for incompressible Glen rheology with v_d = 10 alu/a.

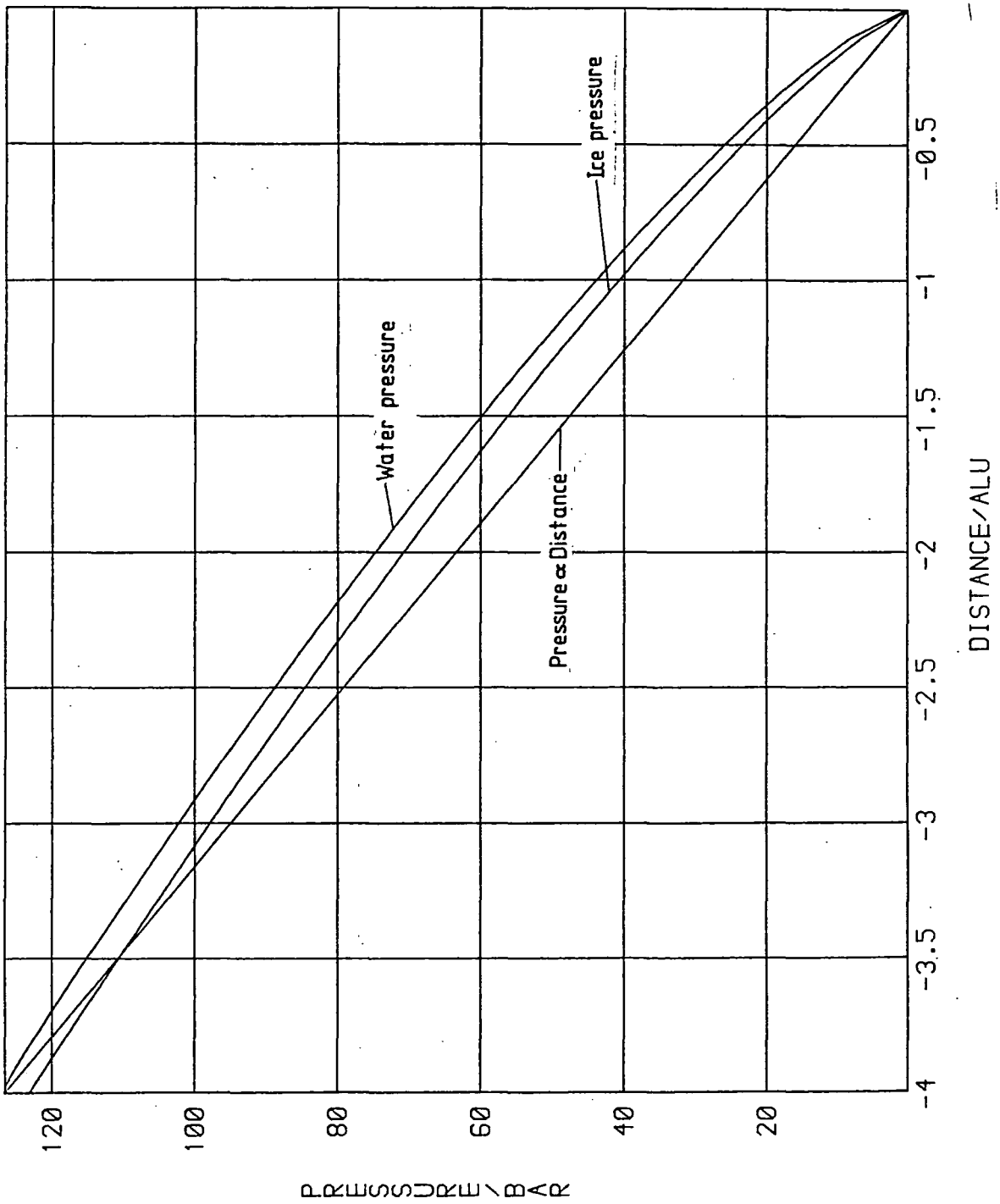

Figure 5.64 Semi-analytic interfacial stress for compressible Glen rheology with χ = 1 alu^2/bar.a and v_d = 10 alu/a.

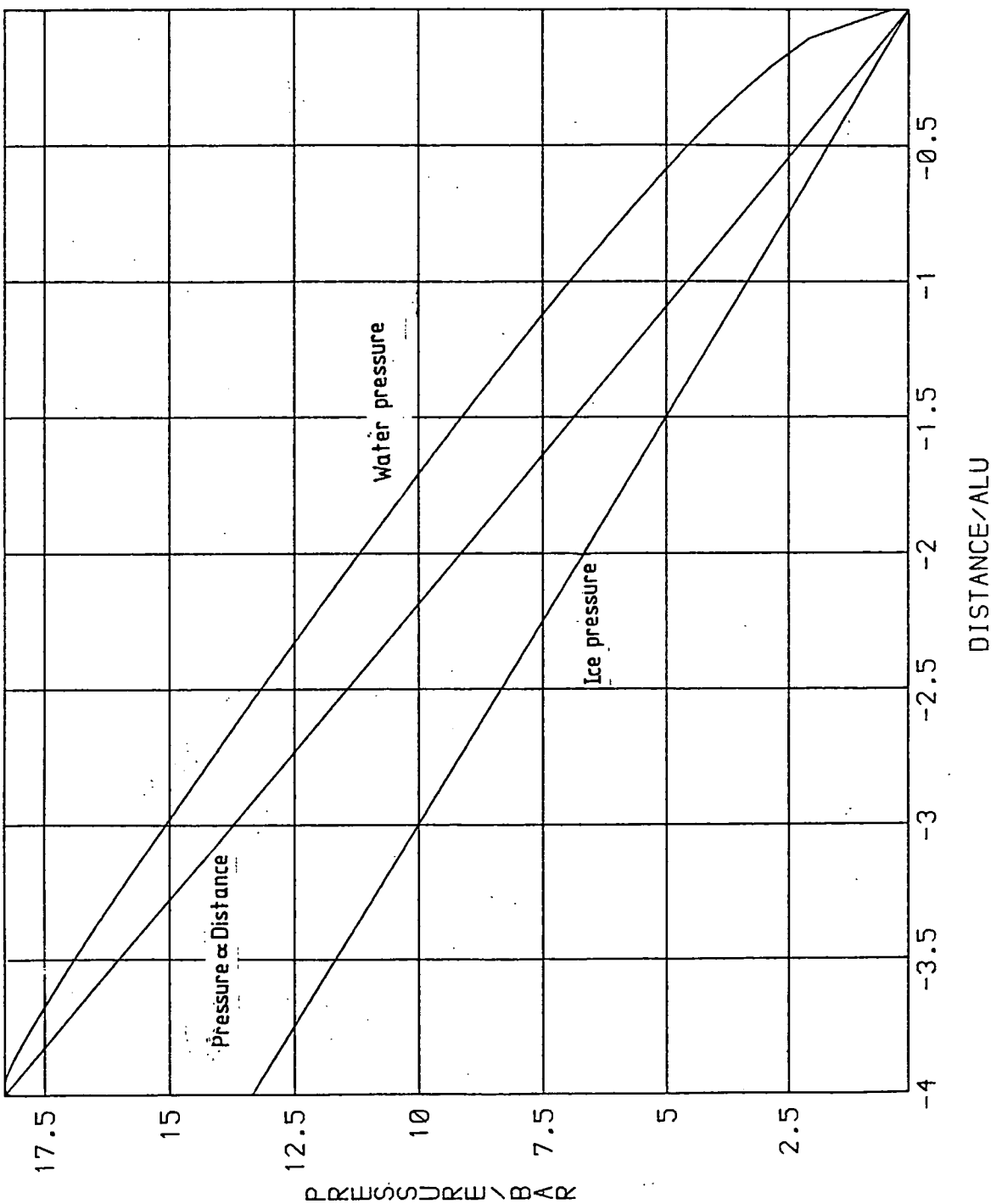

Figure 5.65 Finite element mesh for uni-axial flow modelling.

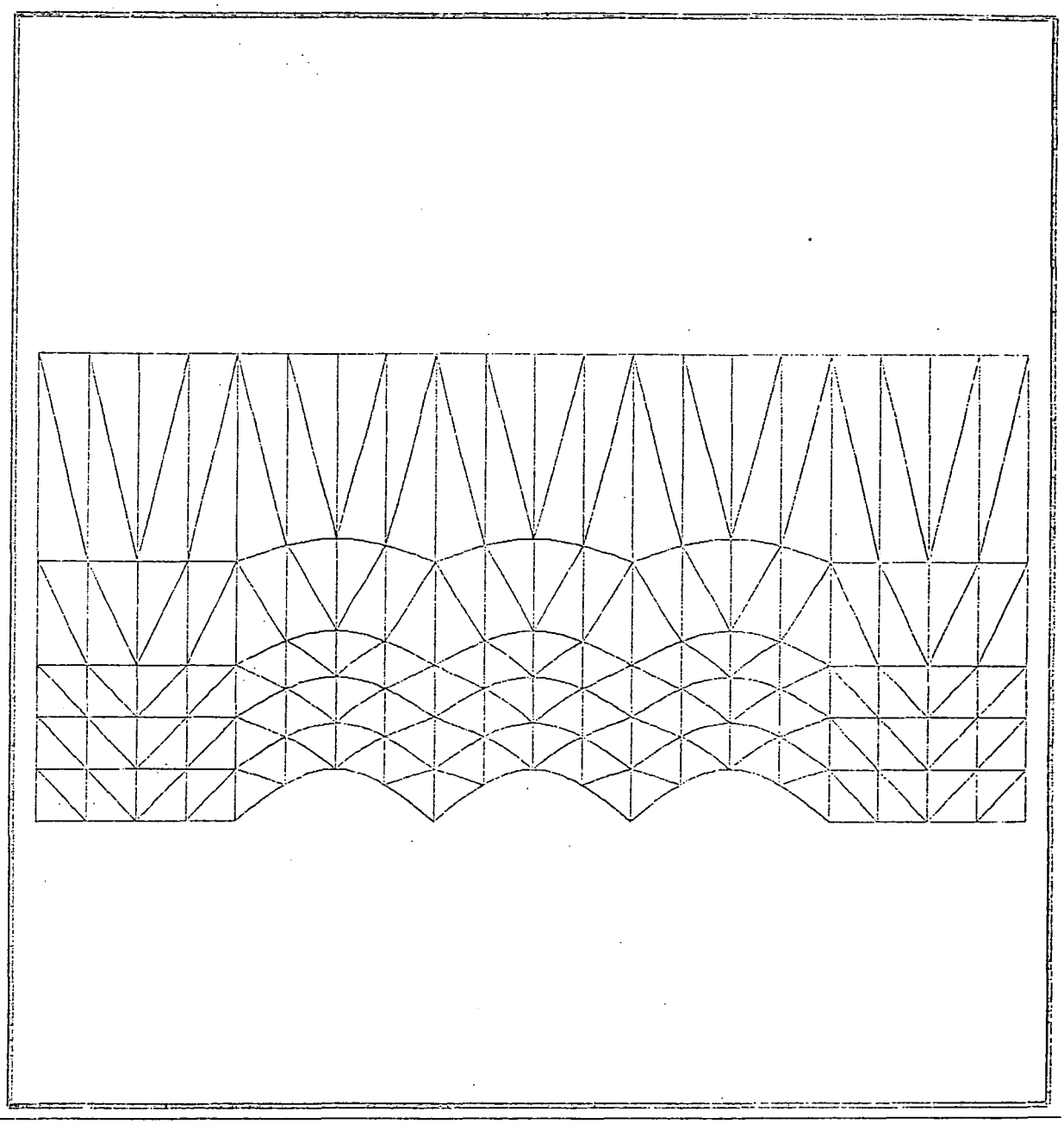

Figure 5.66 Velocity contours in alu/a for v_d = 10 alu/a and a bed of S = 0·002 alu/bar.a, wide-hummocked case.

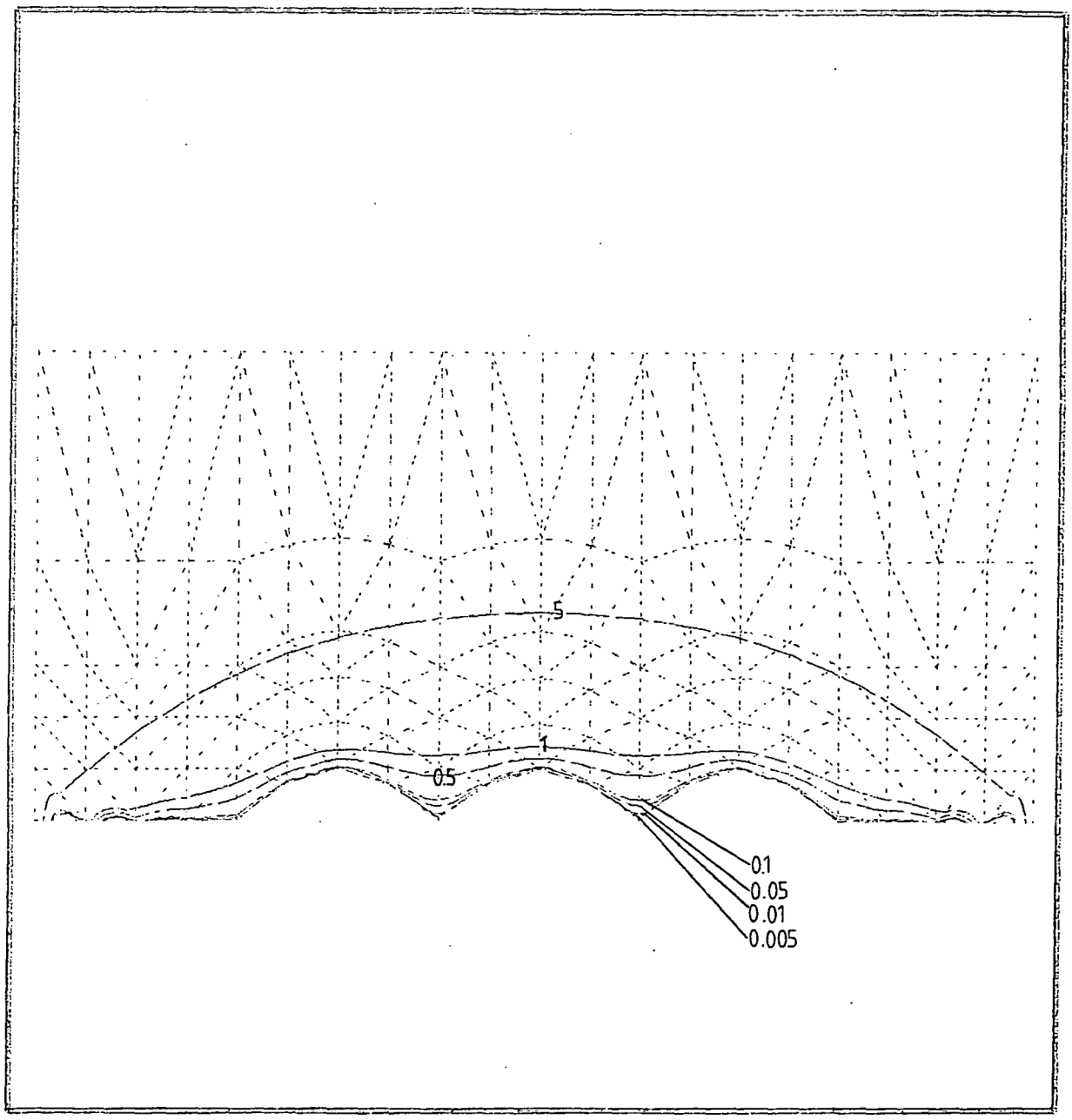

Figure 5.67 Velocity contours in alu/a for v_d = 10 alu/a and bed of S = 0·01 alu/bar.a, wide-hummocked case.

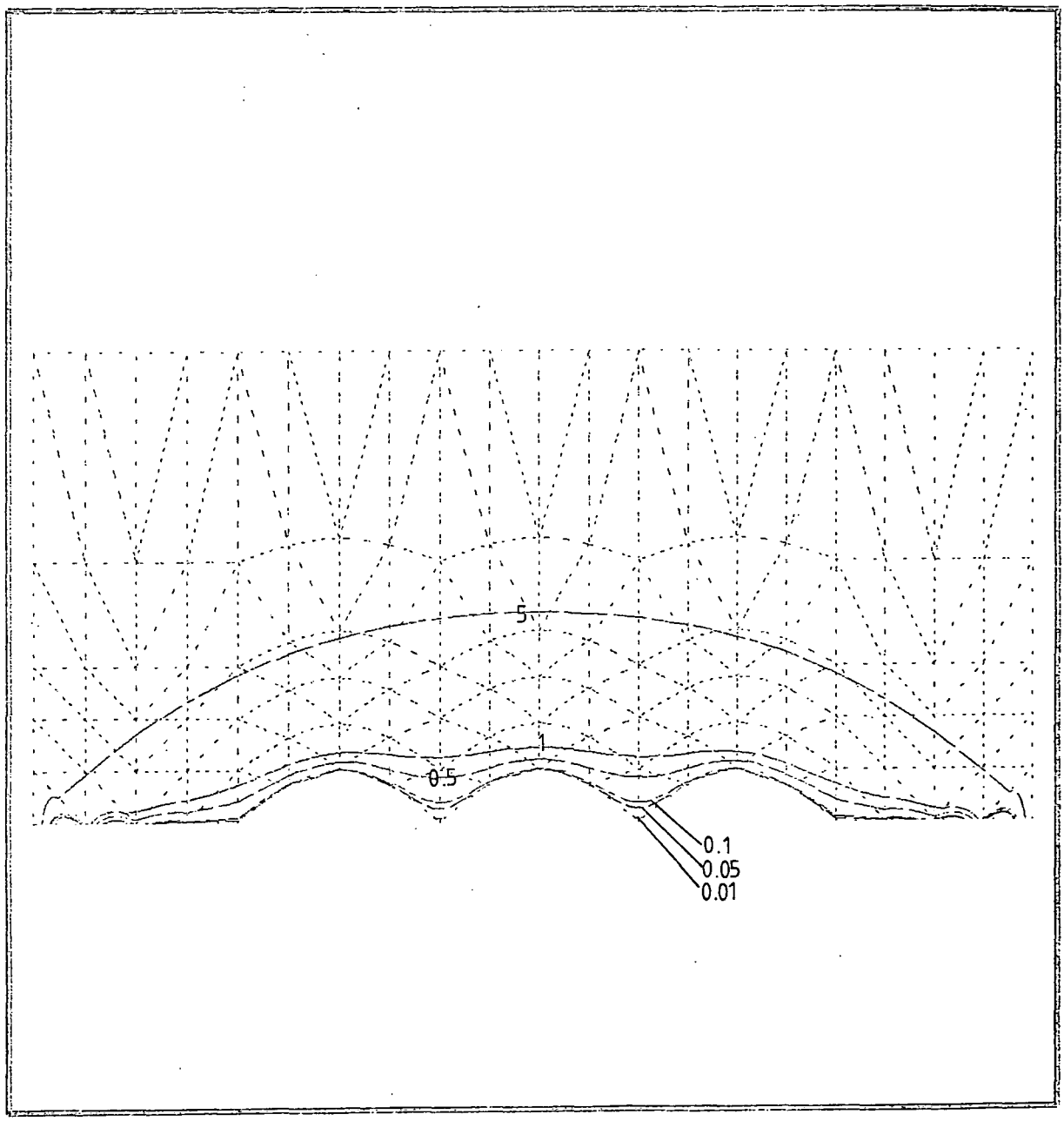

Figure 5.68 Velocity contours in alu/a for v_d = 10 alu/a and a bed of S = 0·02 alu/bar.a, wide-hummocked case.

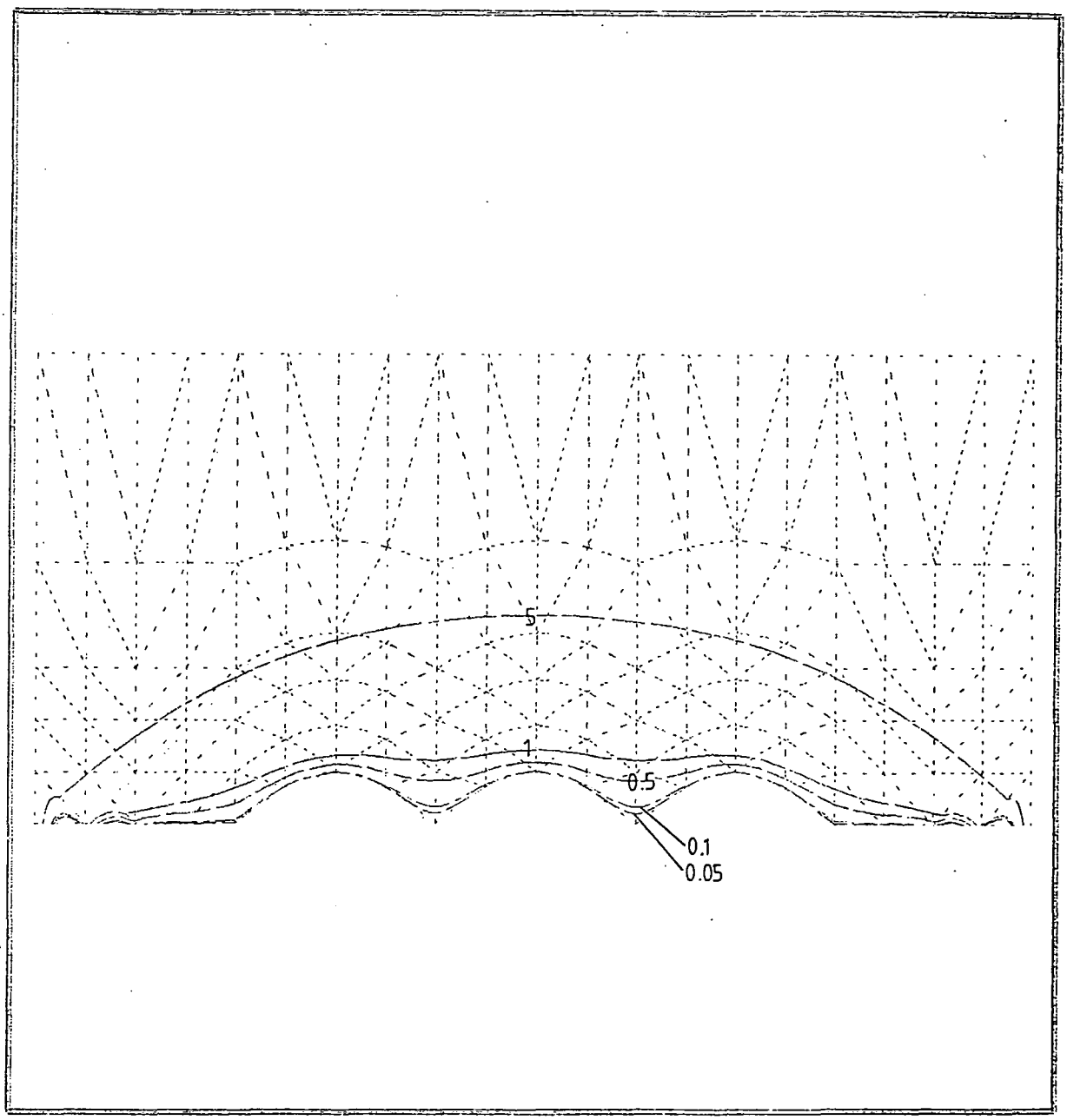

Figure 5.69 Velocity contours in alu/a for v_d = 10 alu/a and a bed of S = 0·1 alu/bar.a, wide-hummocked case.

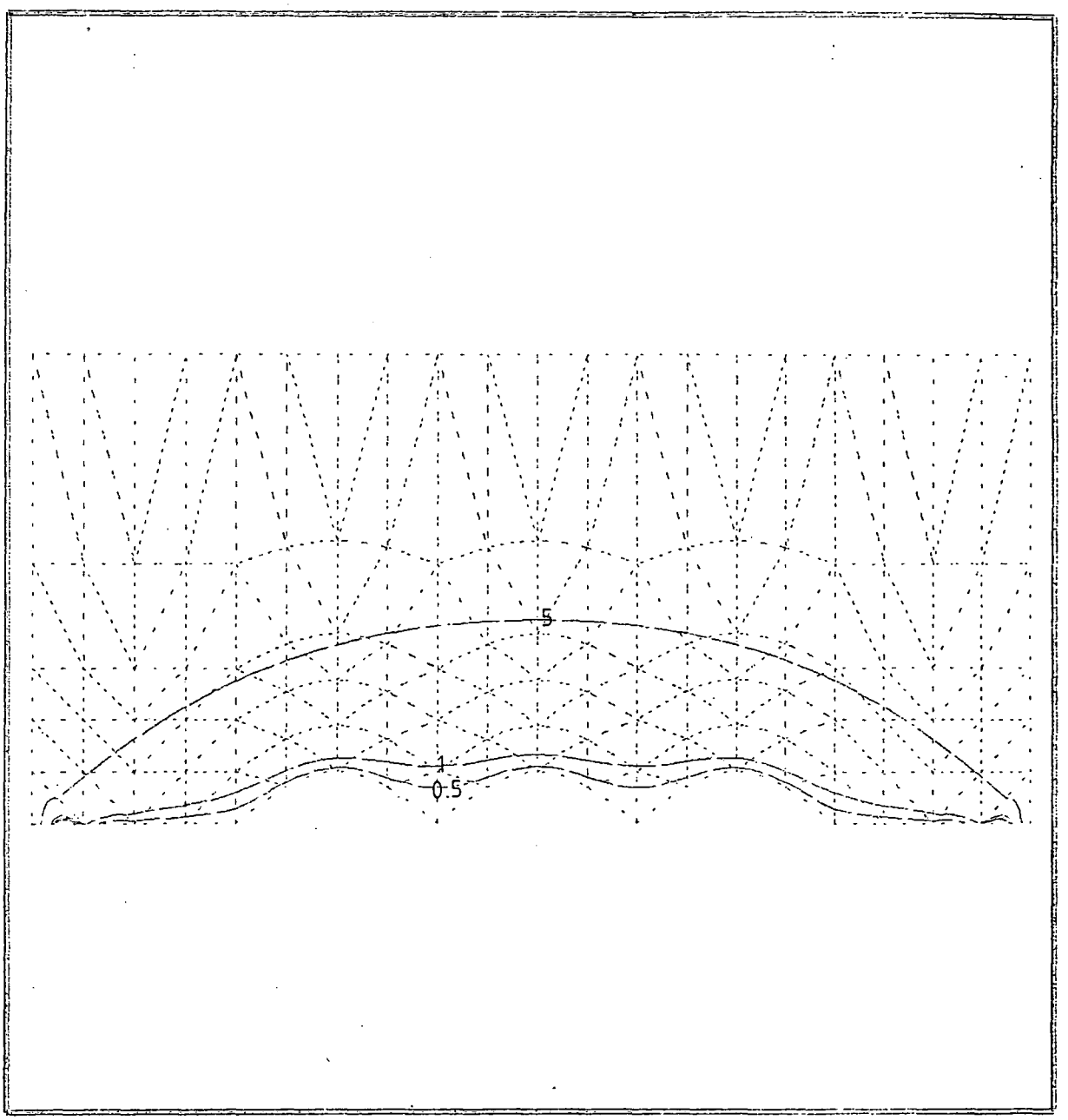

Figure 5.70 Velocity contours in alu/a for v_d = 10 alu/a and a bed of S = 0·2 alu/bar.a, wide-hummocked case.

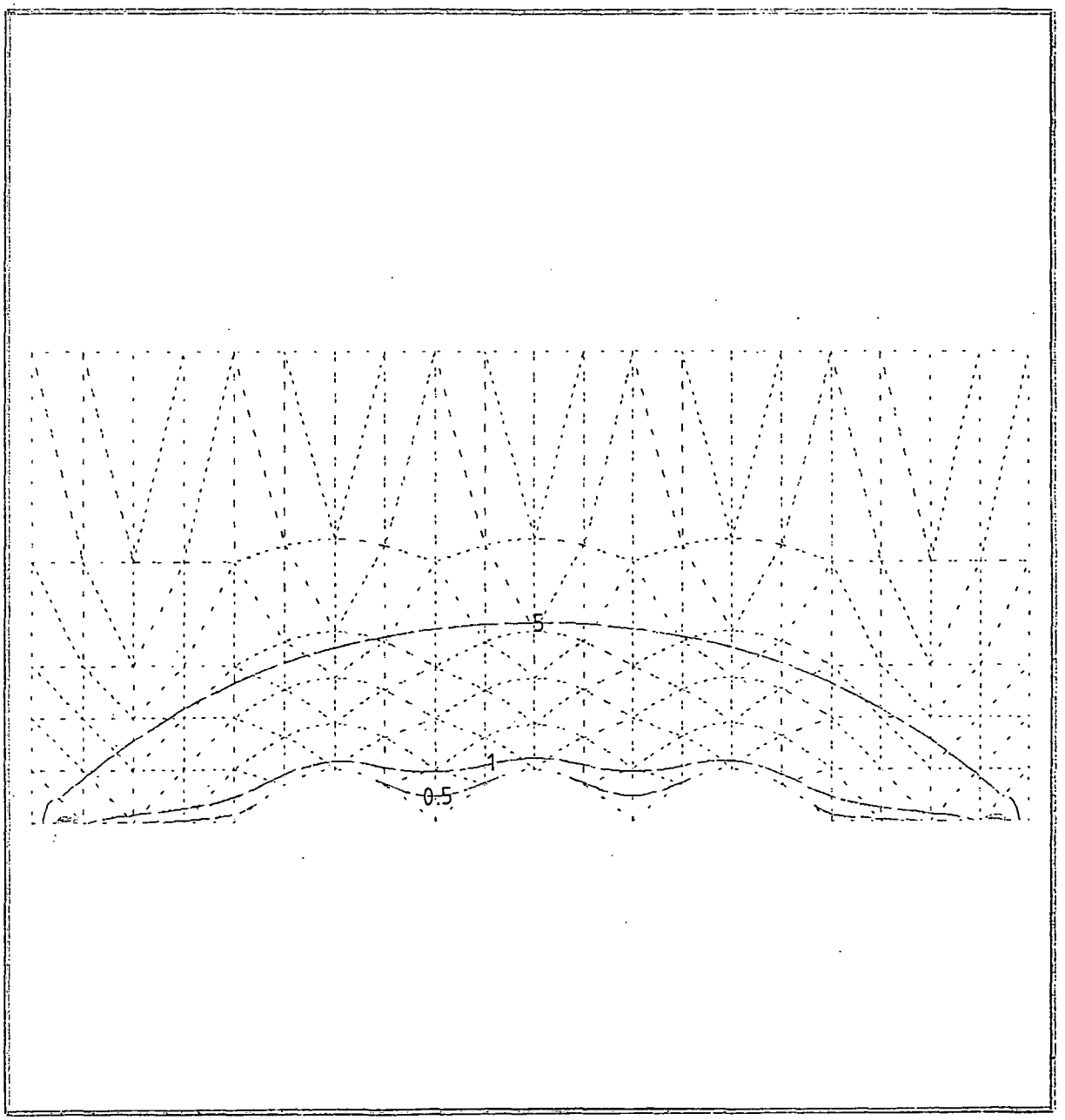

Figure 5.71 Velocity contours in alu/a for v_d = 10 alu/a, and a bed of S = 1 alu/bar.a, wide-hummocked case.

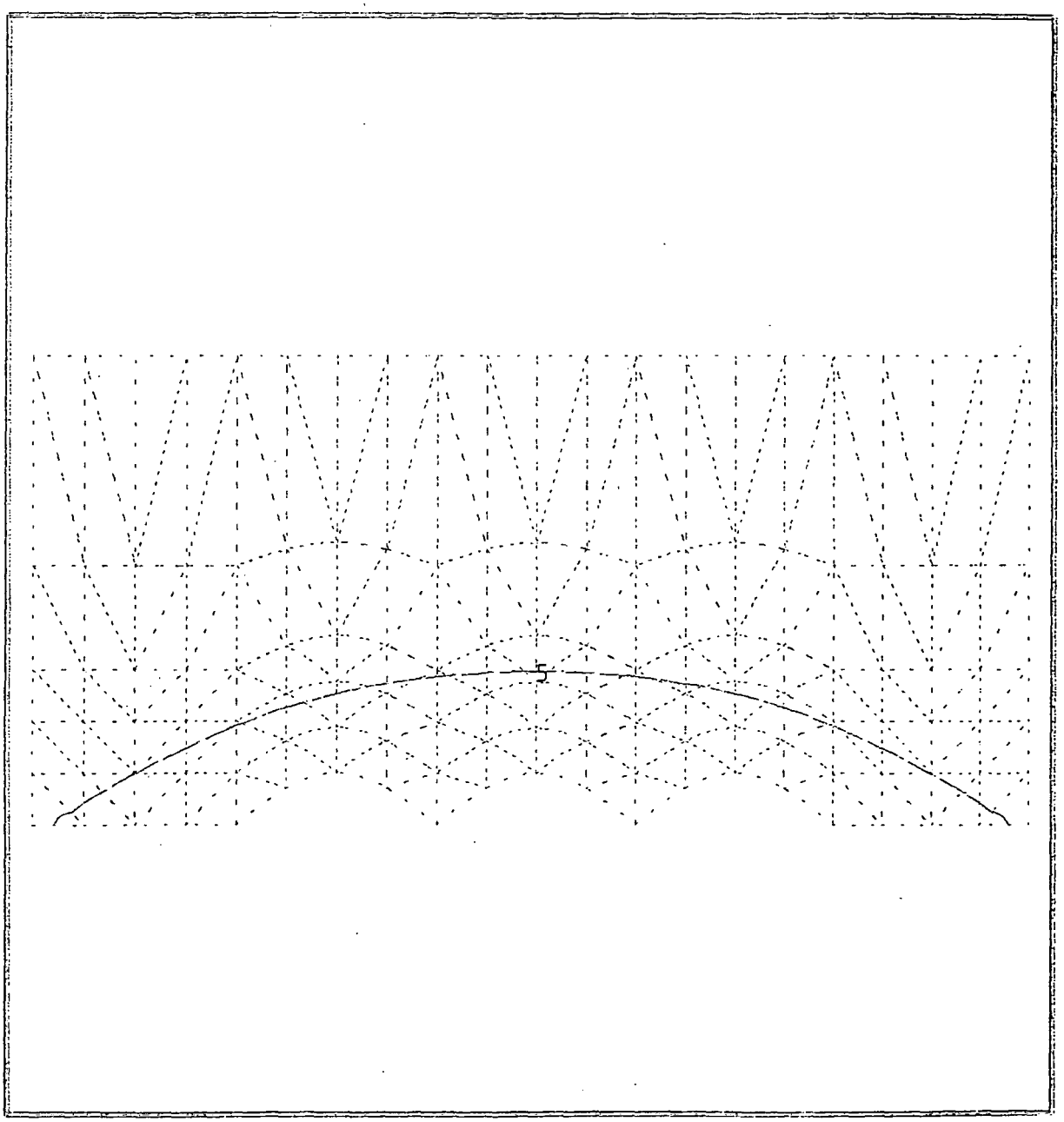

Figure 5.72 Velocity contours in alu/a for v_d = 10 alu/a and a bed of S = 2 alu/bar.a, wide-hummocked case.

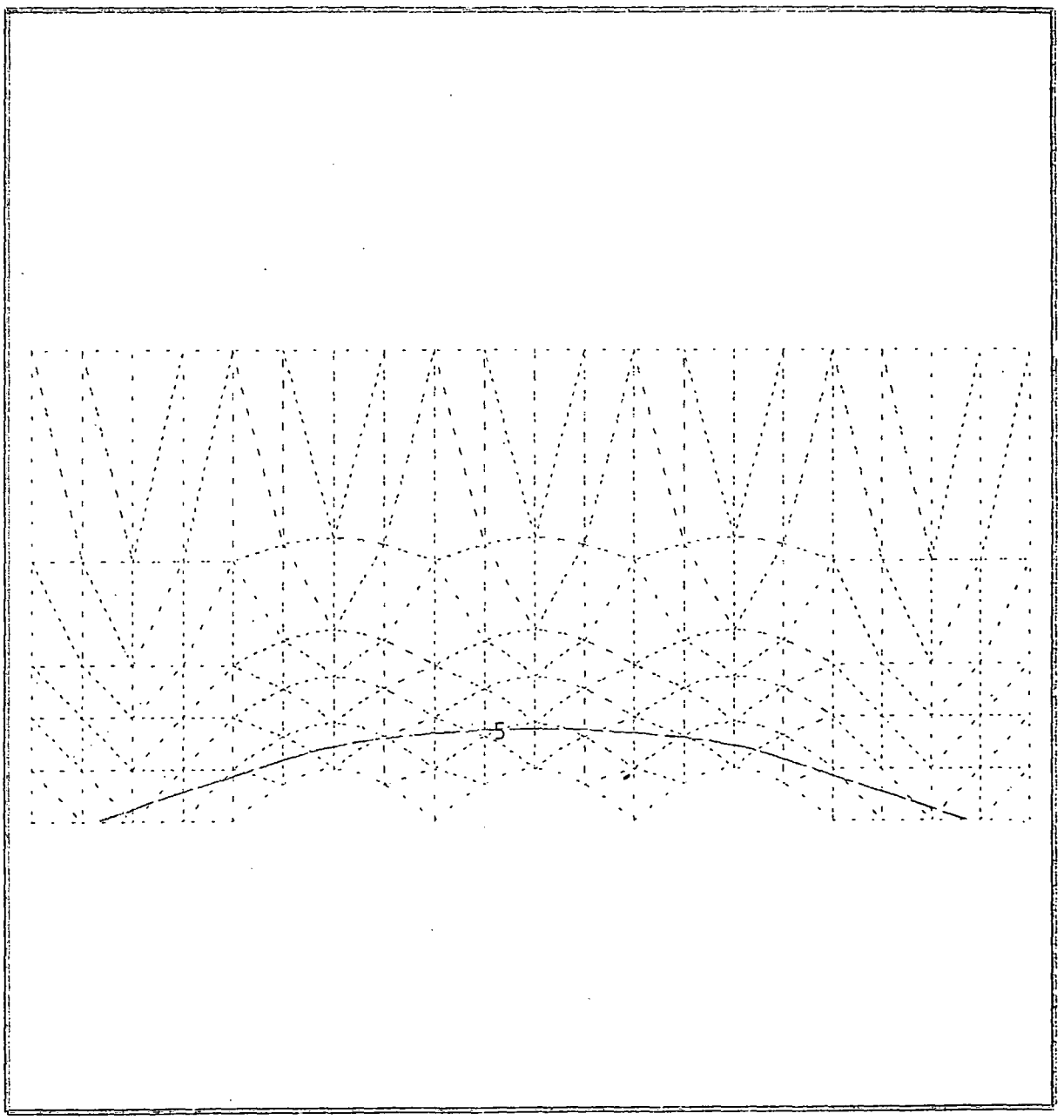

Figure 5.73 Velocity contours in alu/a for v_d = 50 alu/a and a bed of S = 0·01 alu/bar.a, wide-hummocked case.

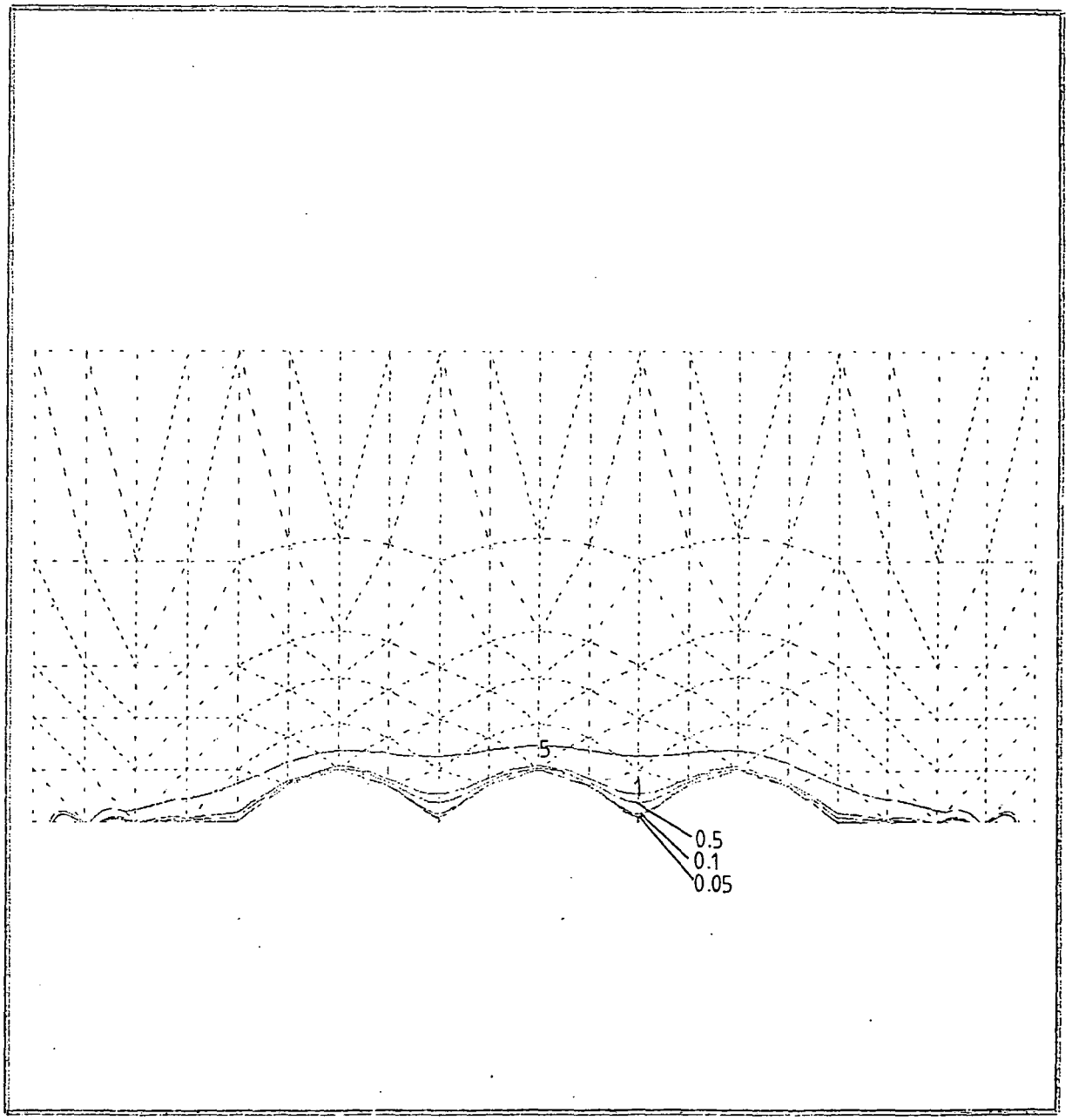

Figure 5.74 Velocity contours in alu/a for v_d = 100 alu/a and a bed of S = 0·01 alu/bar.a, wide-hummocked case.

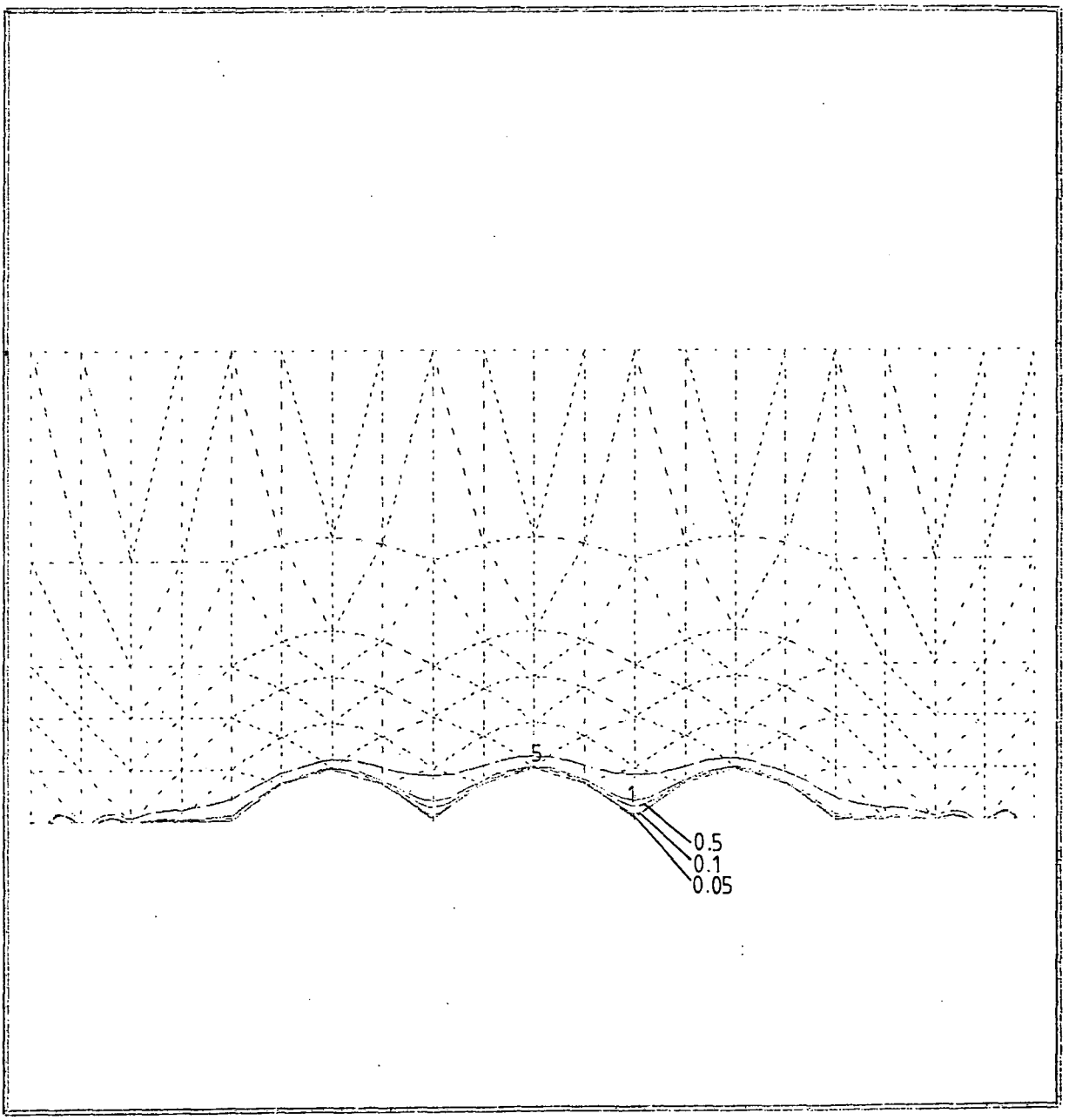

Figure 5.75 Velocity contours in alu/a for v_d = 200 alu/a and a bed of S = 0·01 alu/bar.a, wide-hummocked case.

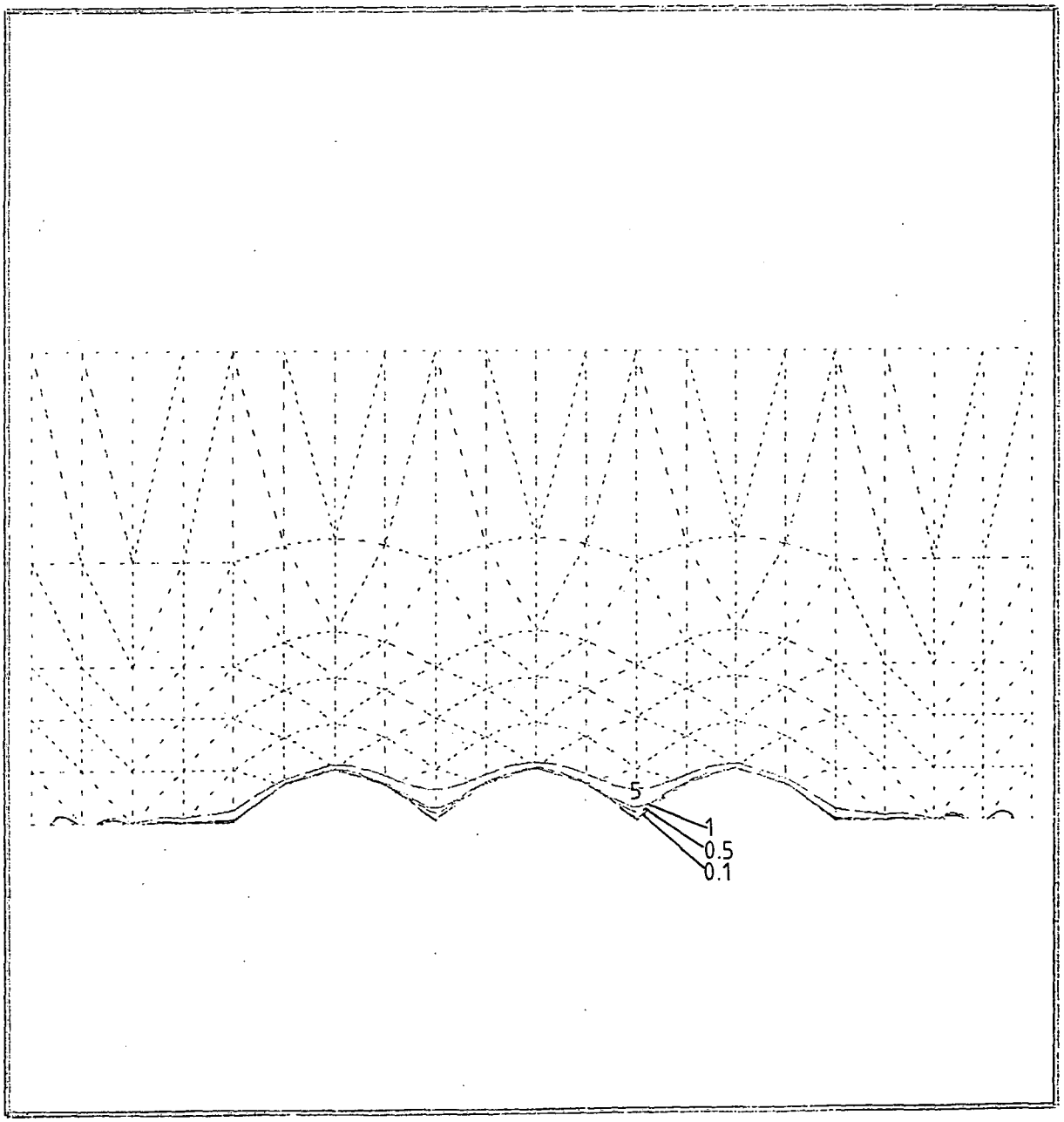

Figure 5.76 Velocity contours in alu/a for v_d = 10 alu/a and a bed of S = 0·02 alu/bar.a, narrow-hummocked case.

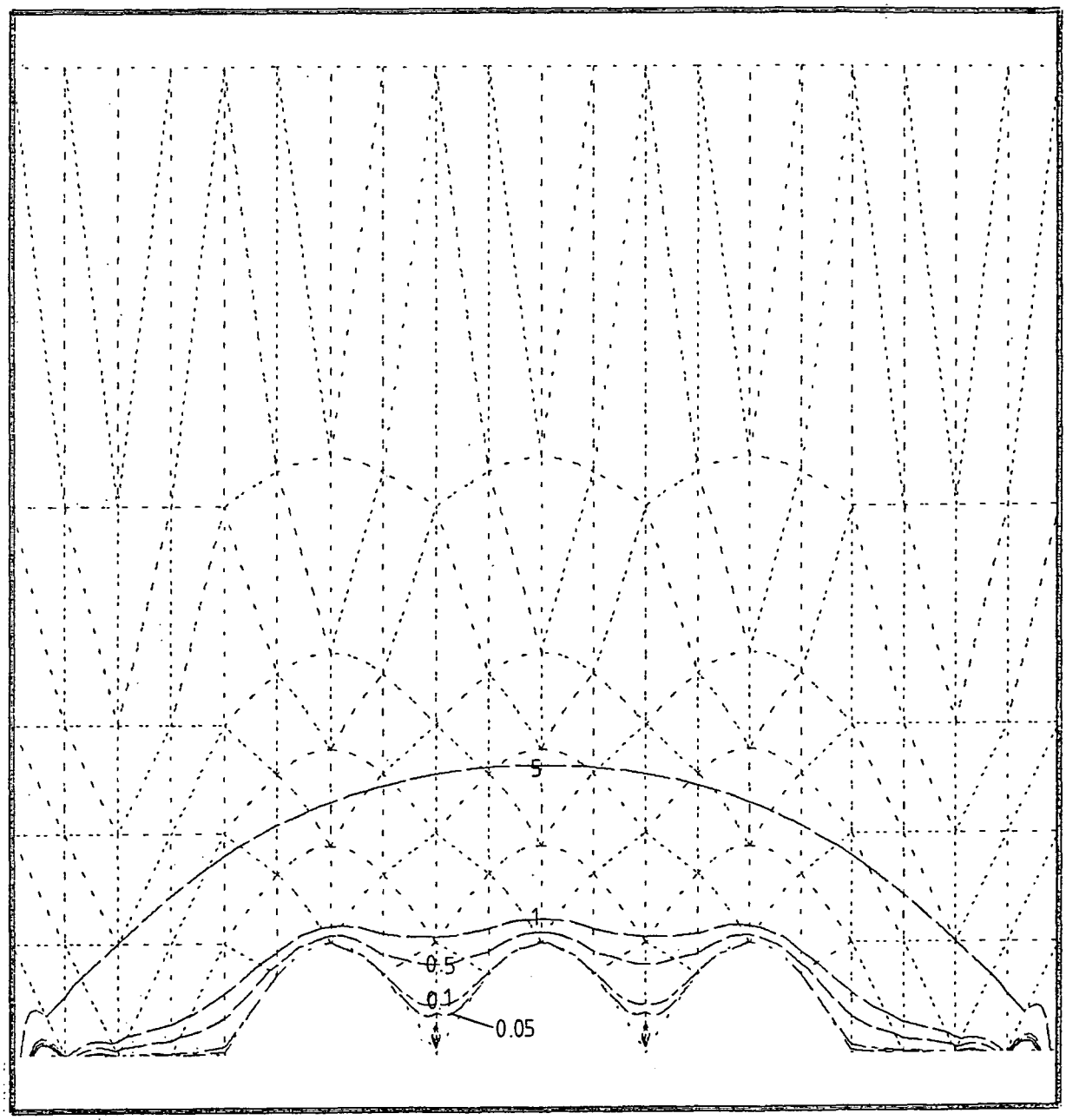

Figure 5.77 Velocity contours in alu/a for v_d = 10 alu/a, bed of S = 0·002 alu/bar.a, narrow-hummocked case.

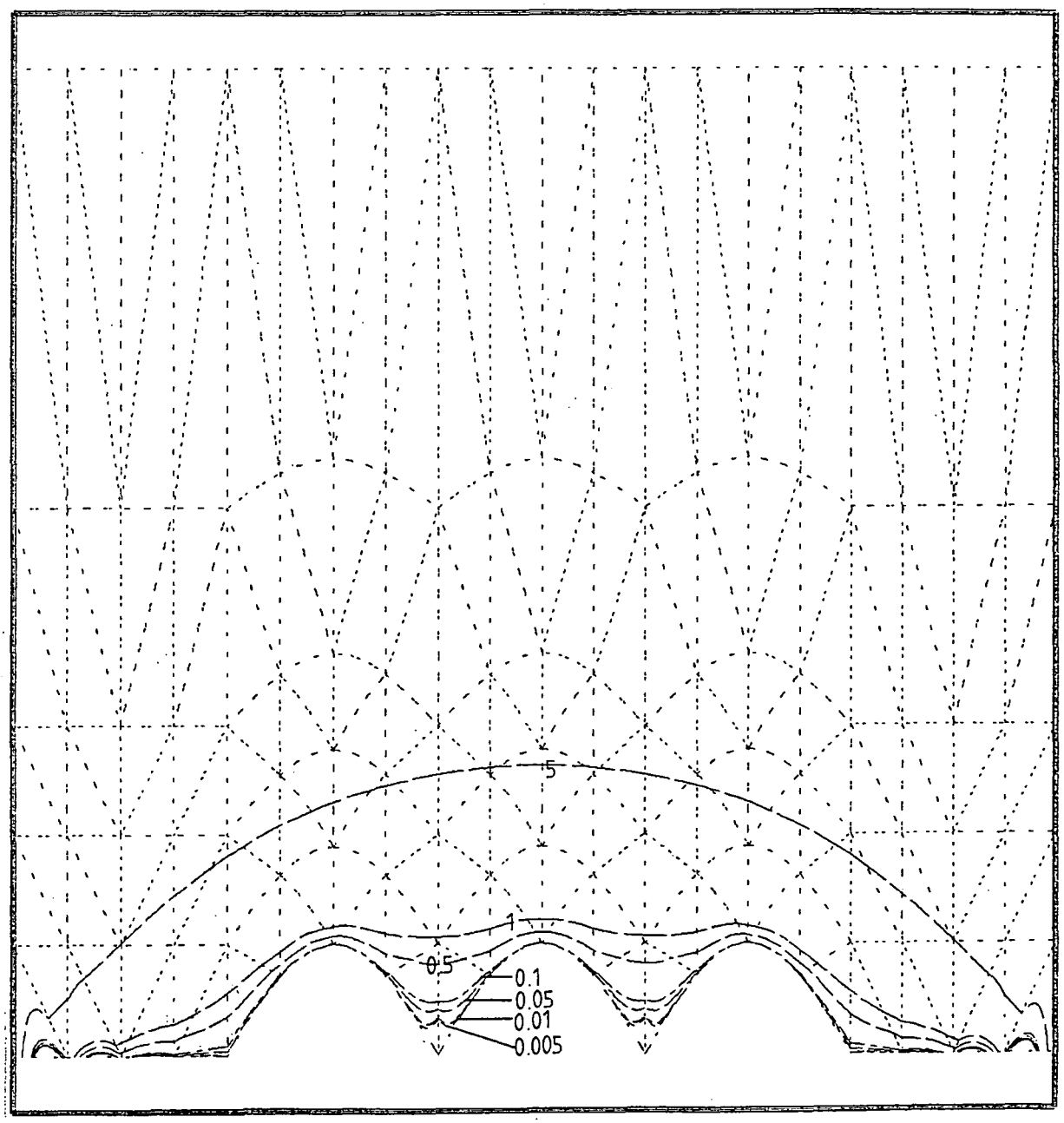

Figure 5.78 Velocity contours in alu/a for v_d = 400 alu/a, bed of S = 0·02 alu/bar.a, narrow-hummocked case.

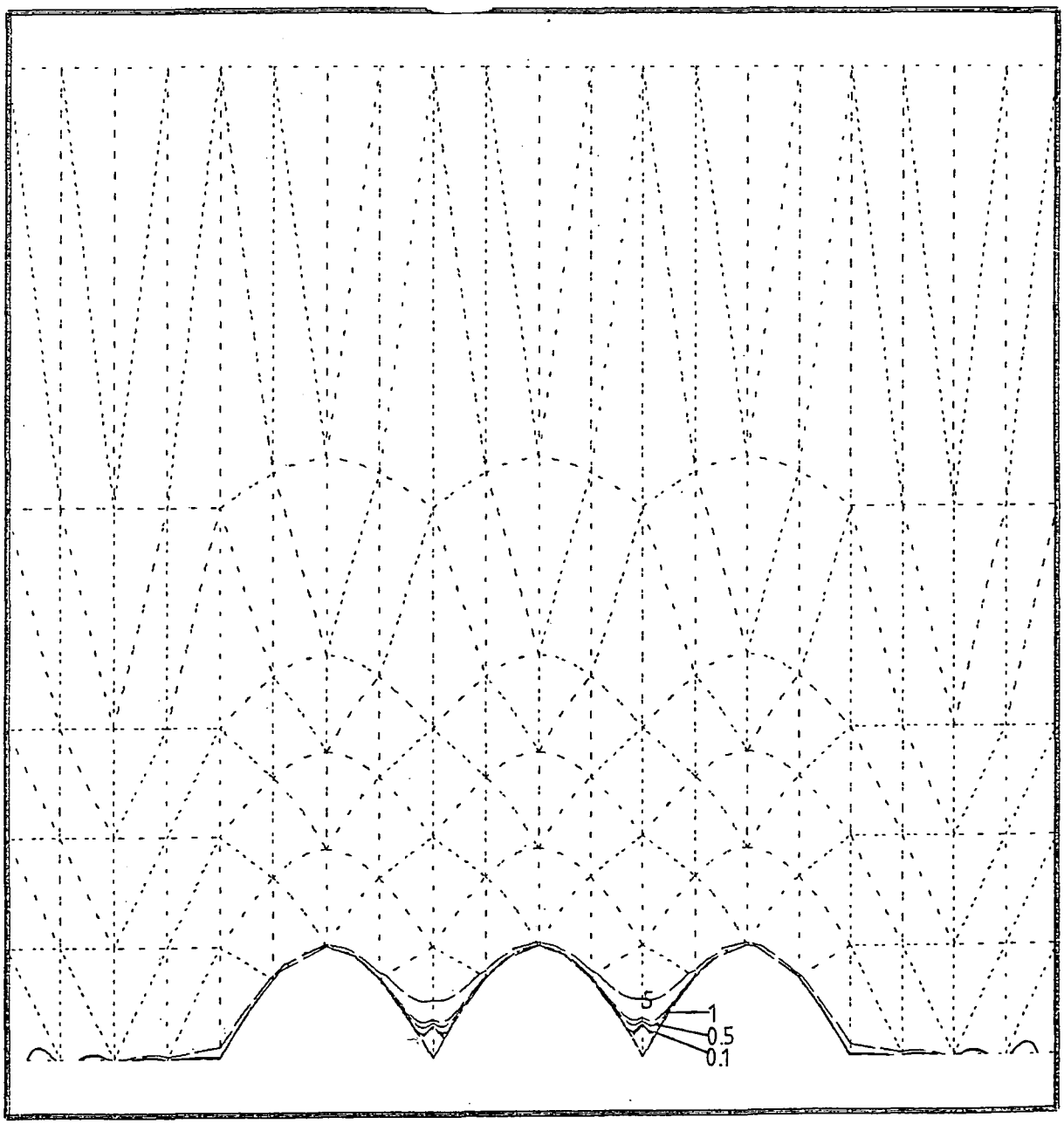

Figure 5.79 Velocity contours in alu/a for v_d = 10 alu/a, bed of maximum S = 0·02 alu/bar.a, smoothed-crested case.

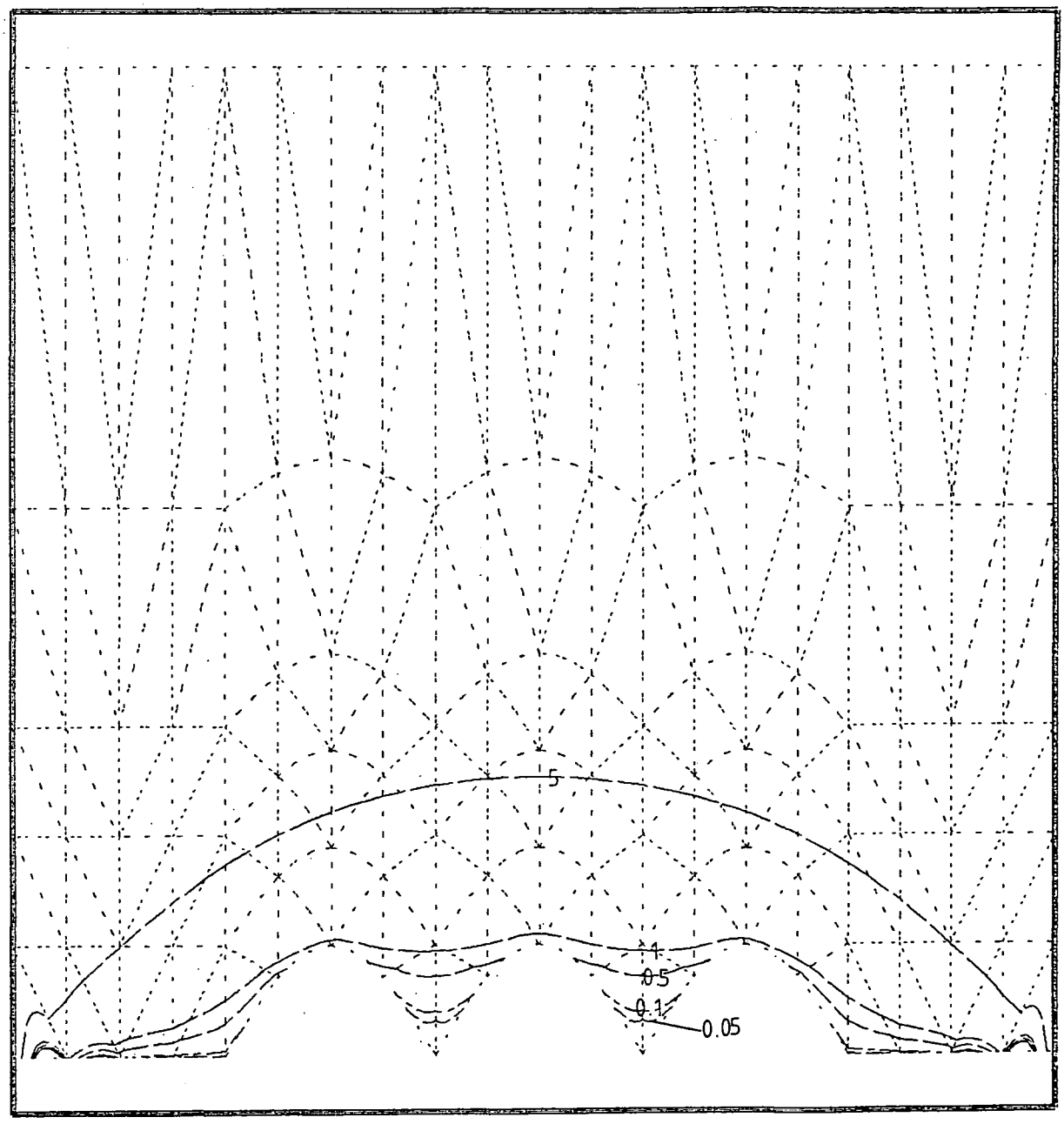

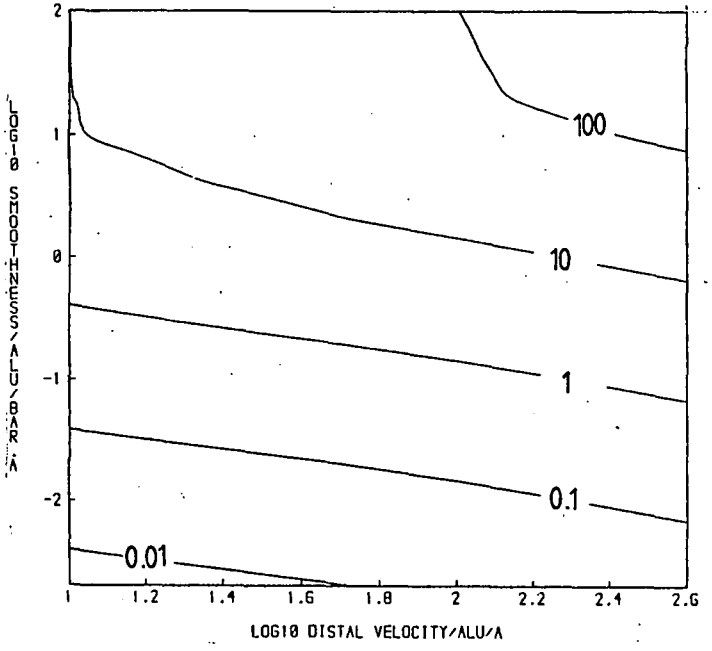

Figure 5.80 Crestal velocities in alu/a for the wide-hummocked case.

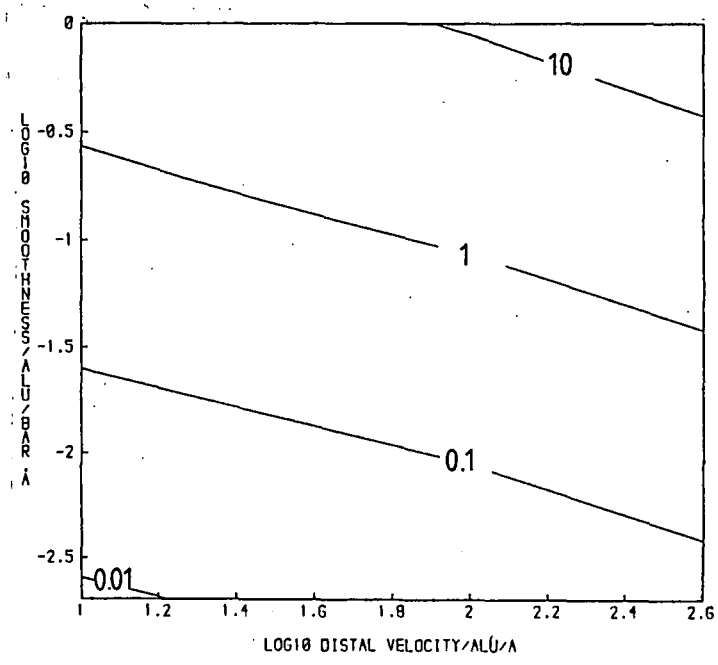

Figure 5.81 Crestal velocities in alu/a for the narrow-hummocked case.

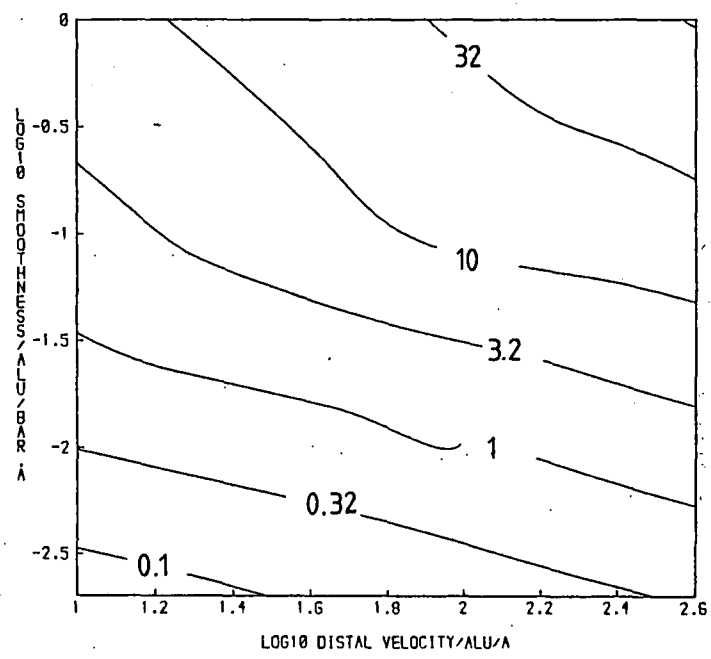

Figure 5.82 Crestal velocities in alu/a for the smooth-crested case.

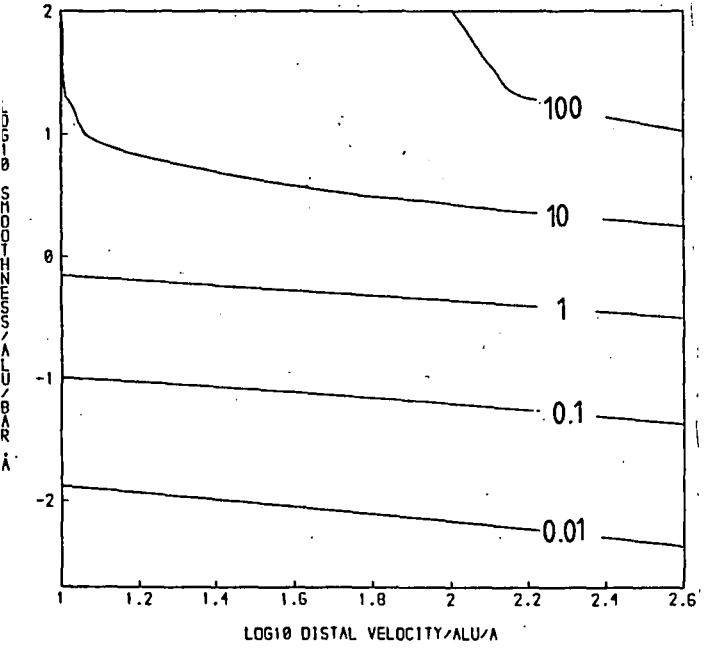

Figure 5.83 Trough velocities in alu/a wide-hummocked case.

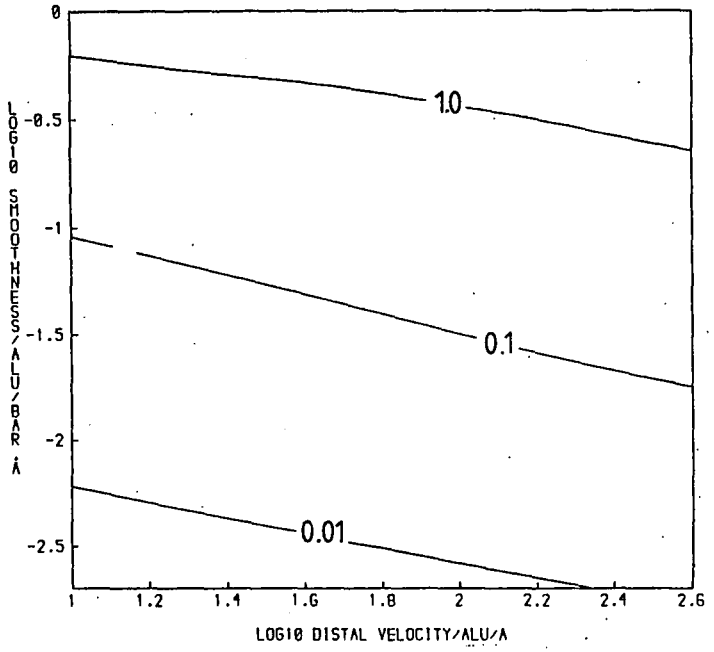

Figure 5.84 Trough velocities in alu/a for the narrow-hummocked case.

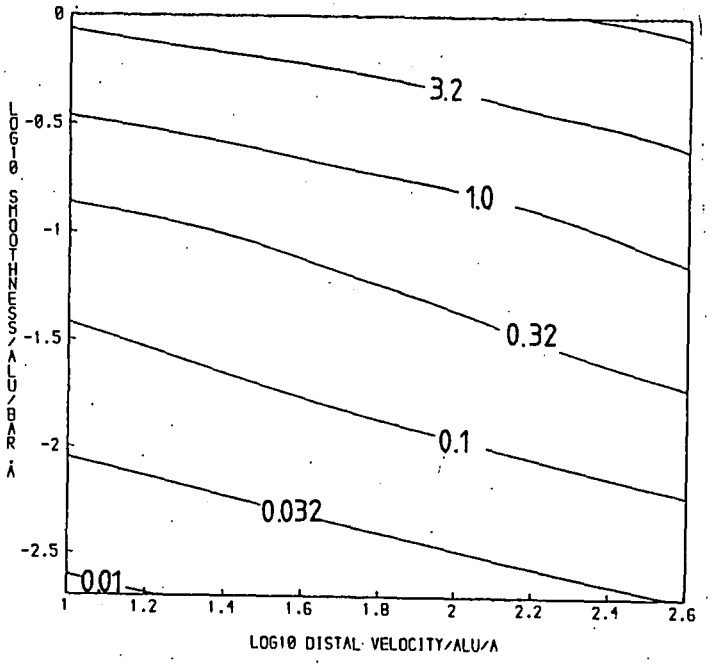

Figure 5.85 Trough velocities in alu/a for the smooth-crested case.

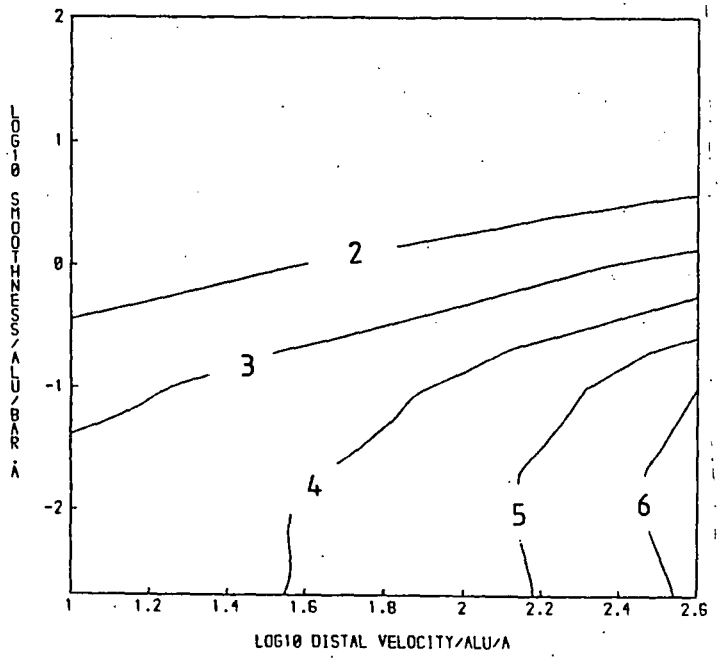

Figure 5.86 Crest/trough velocity ratios for the wide-hummocked case.

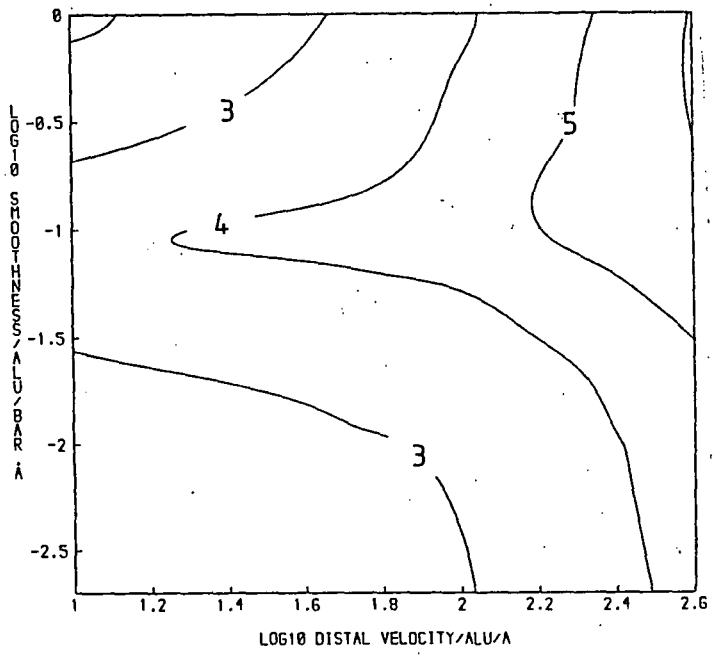

Figure 5.87 Crest/trough velocity ratios for the narrow-hummocked case.

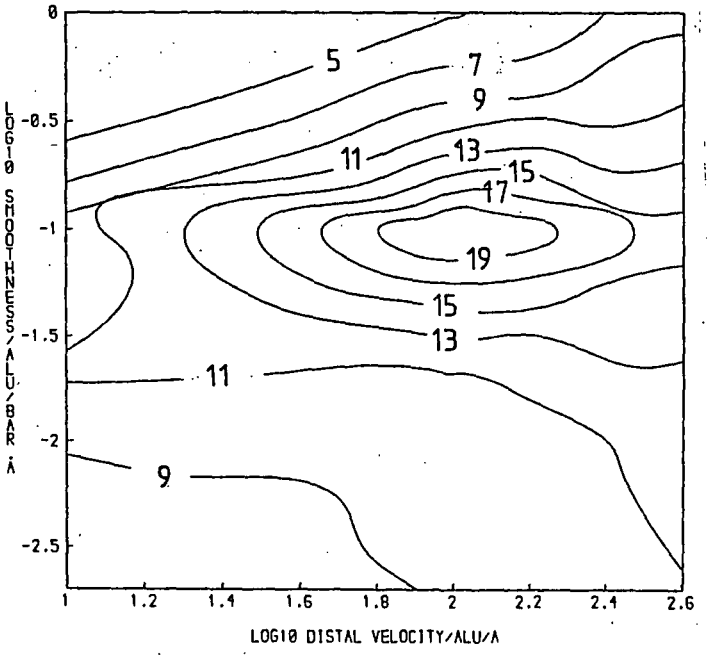

Figure 5.88 Crest/trough velocity ratios for the smooth-crested case.

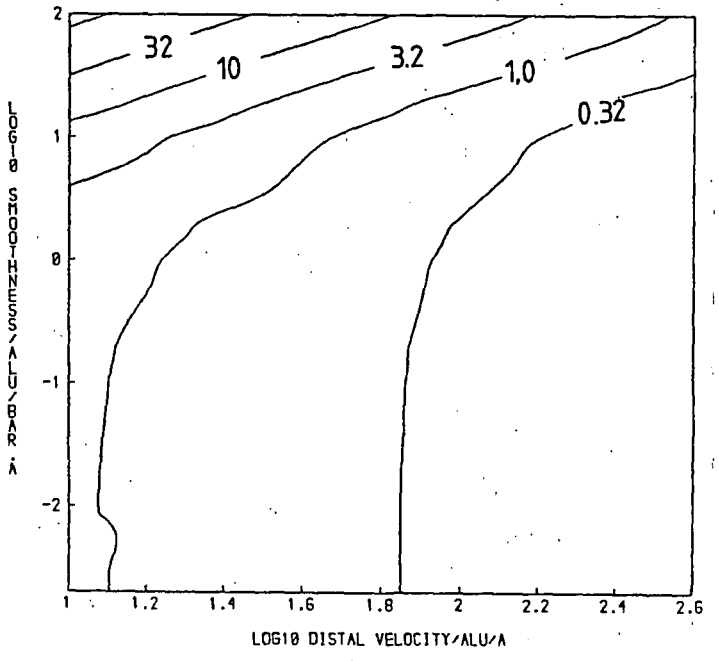

Figure 5.89 Crestal viscosity in bar.a for the wide-hummocked case.

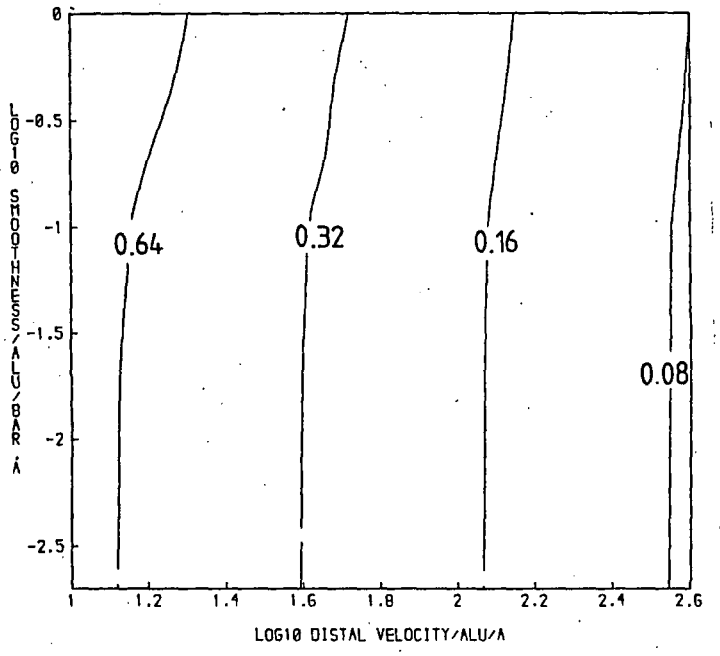

Figure 5.90 Crestal viscosities in bar.a for the narrow-hummocked case.

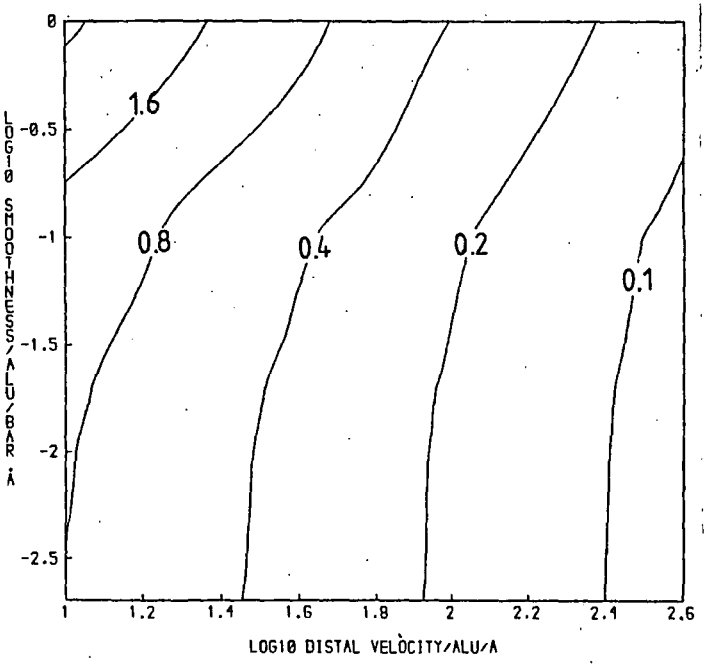

Figure 5.91 Crestal viscosities in bar.a for the smooth-crested case.

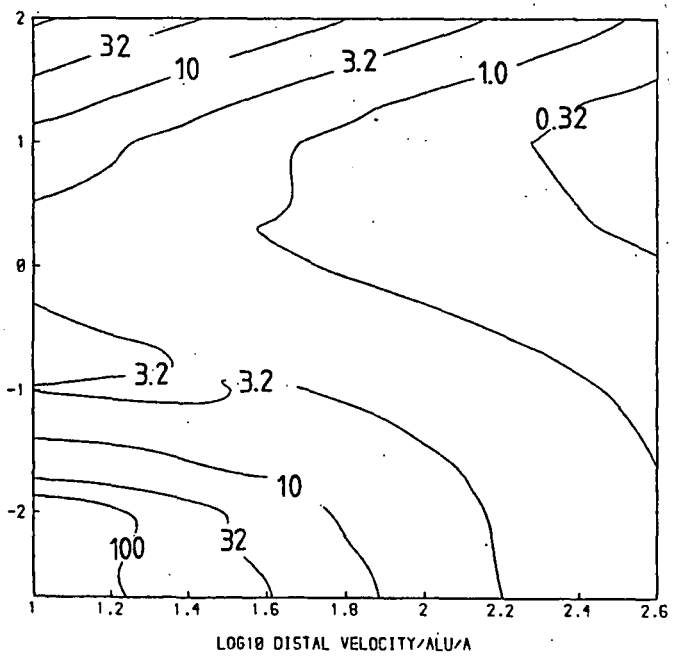

Figure 5.92 Trough viscosities in bar.a for the wide-hummocked case.

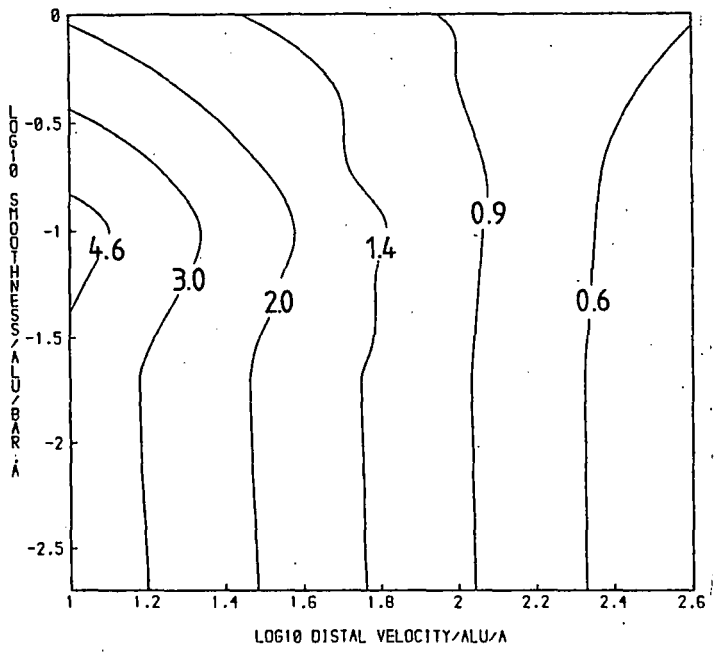

Figure 5.93 Trough viscosities in bar.a for the narrow-hummocked case.

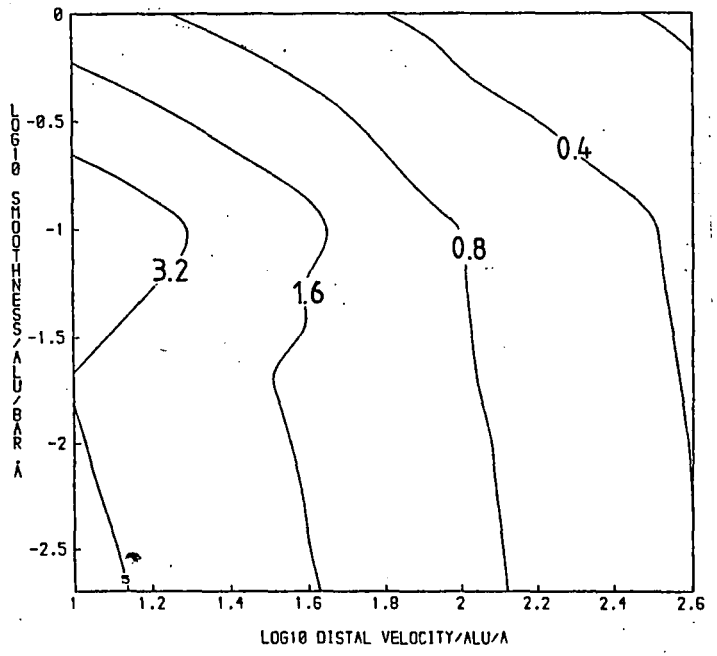

Figure 5.94 Trough viscosities in bar.a for the smooth-crested case.

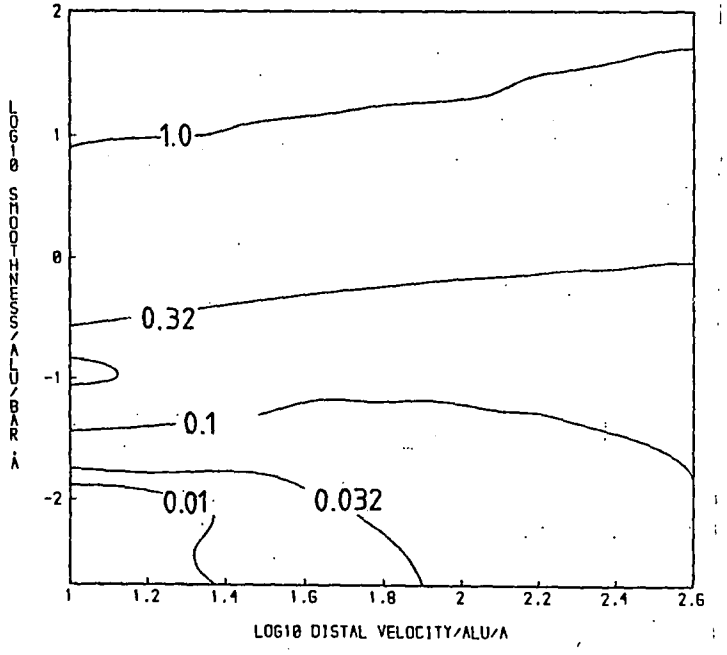

Figure 5.95 Crest/trough viscosity ratios for the wide-hummocked case.

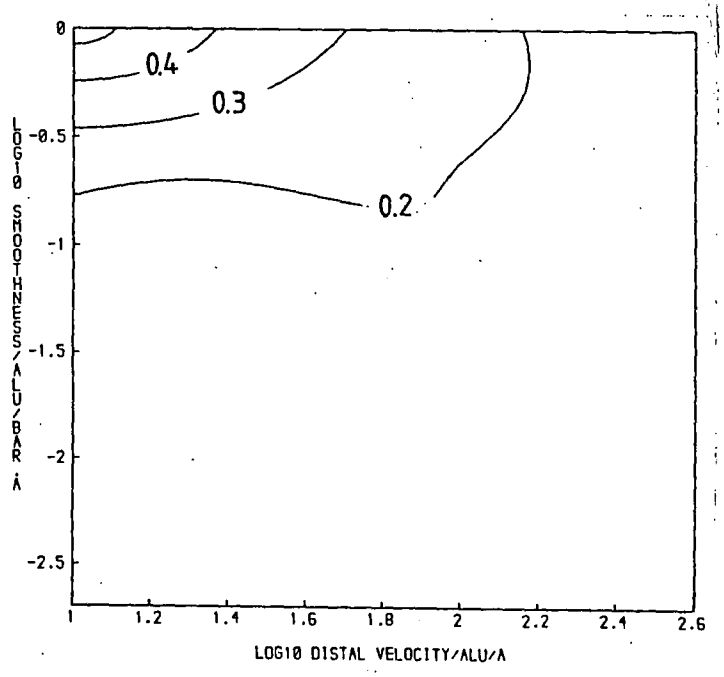

Figure 5.96 Crest/trough viscosity ratios for the narrow-hummocked case.

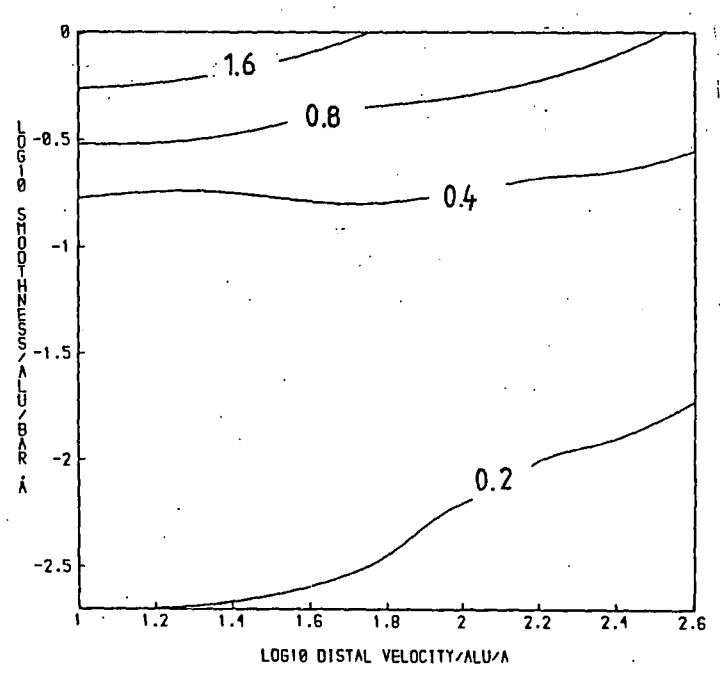

Figure 5.97 Crest/trough viscosity ratios for the smooth-crested case.

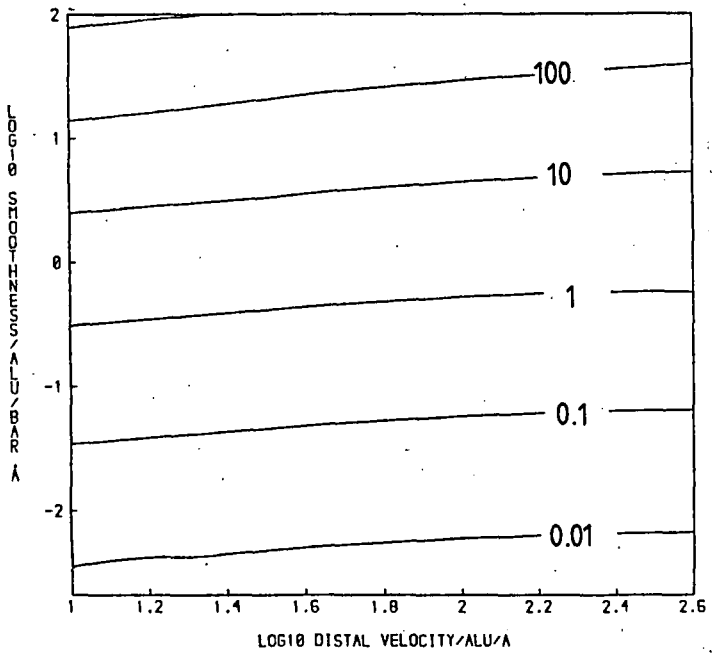

Figure 5.98 Crestal viscosity x velocity in bar.alu for the wide-hummocked case.

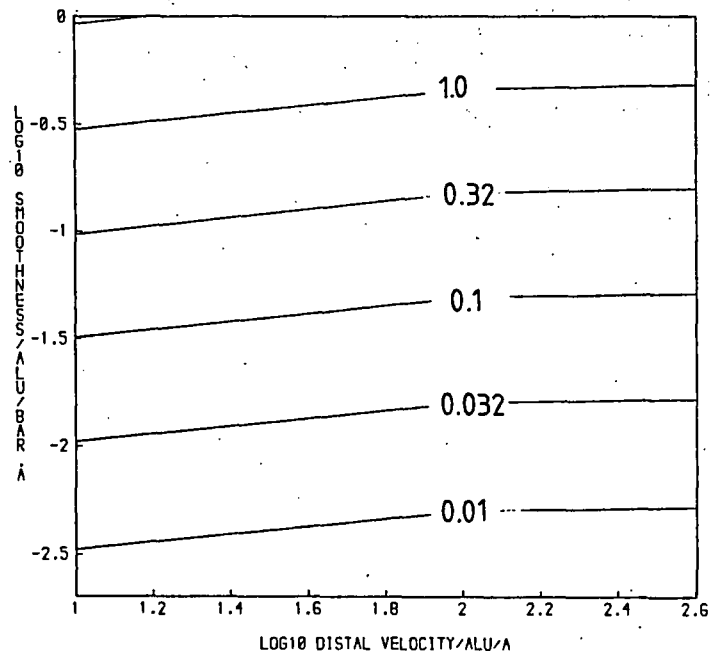

Figure 5.99 Crestal viscosity x velocity in bar.alu for the narrow-hummocked case.

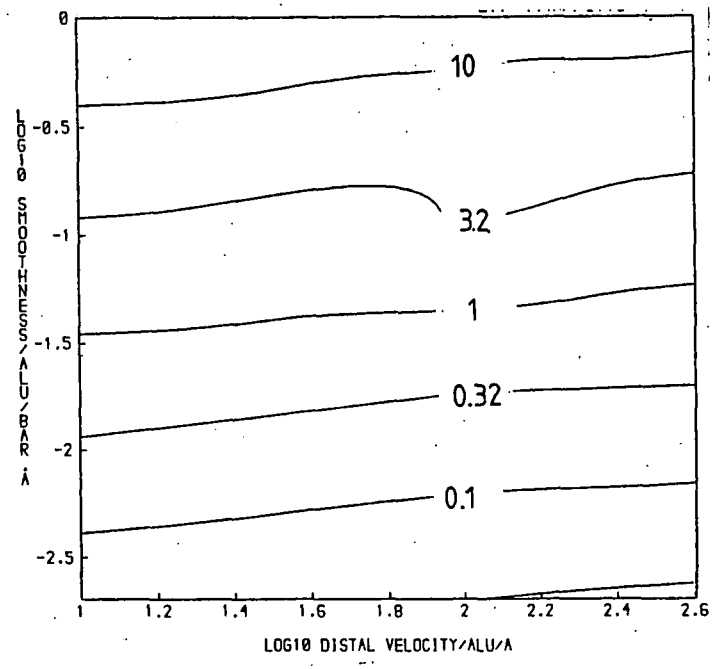

Figure 5.100 Crestal viscosity x velocity in bar.alu for the smooth-crested case.

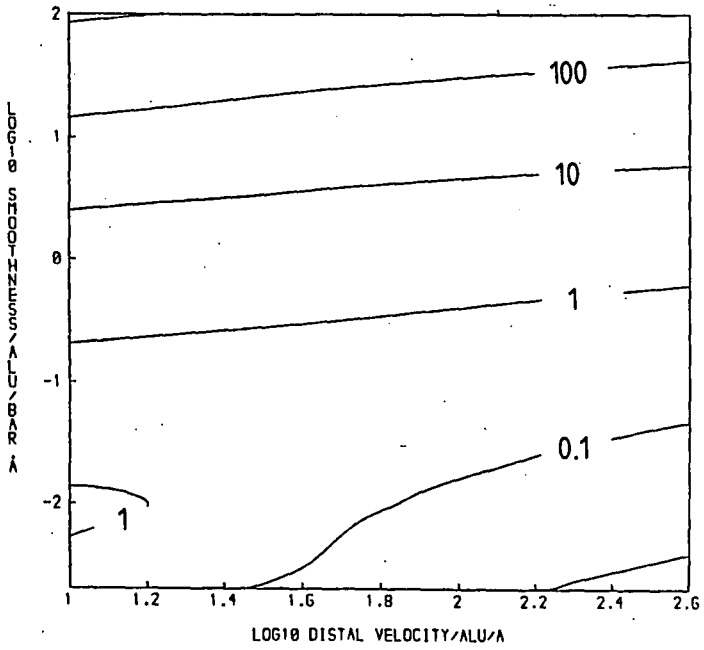

Figure 5.101 Trough viscosity x velocity in bar.alu for the wide-hummocked case.

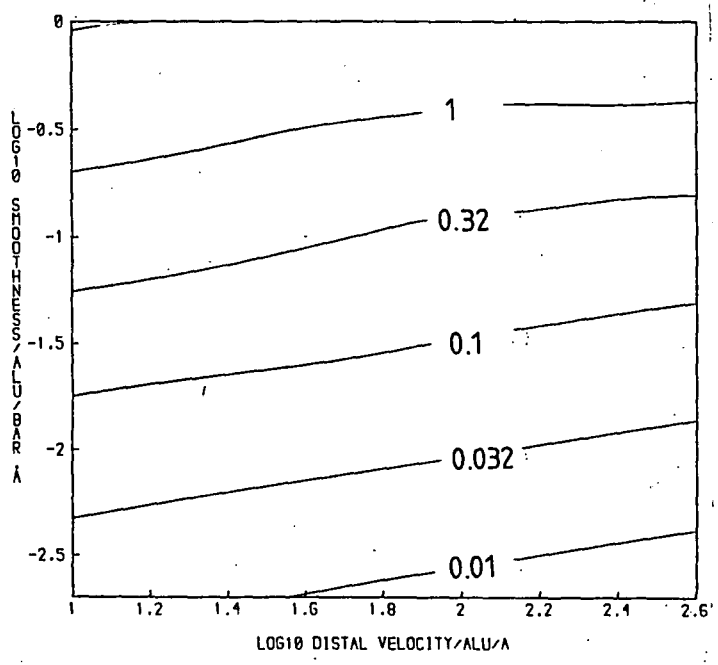

Figure 5.102 Trough viscosity x velocity in bar.alu for the narrow-hummocked case.

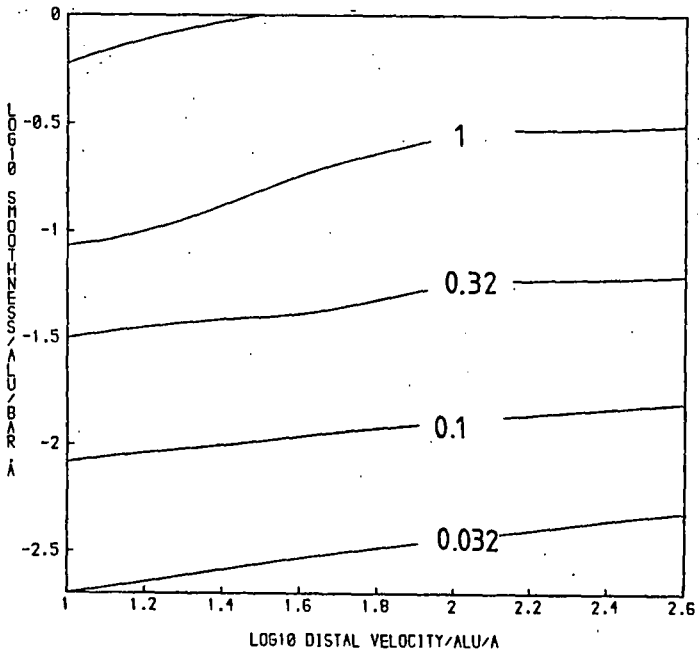

Figure 5.103 Trough viscosity x velocity in bar.alu for the smooth-crested case.

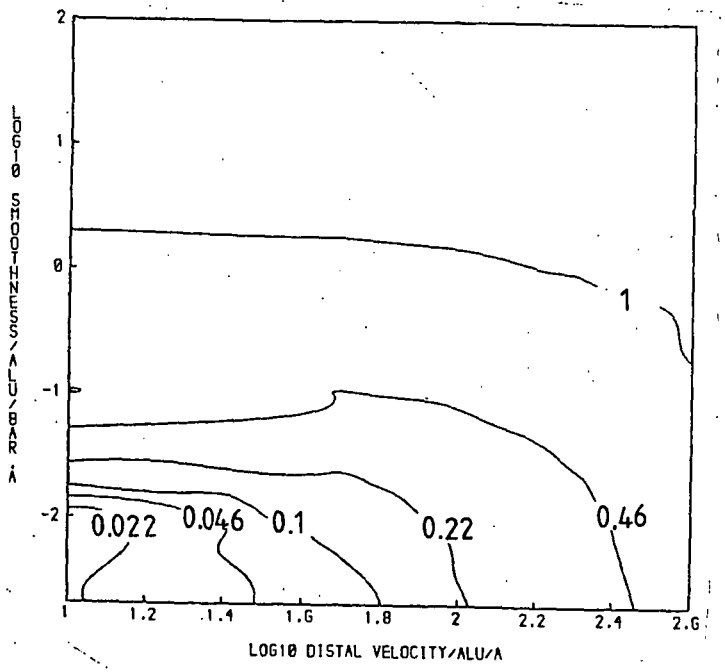

Figure 5.104 Crest/trough viscosity x velocity ratio for the wide-hummocked case.

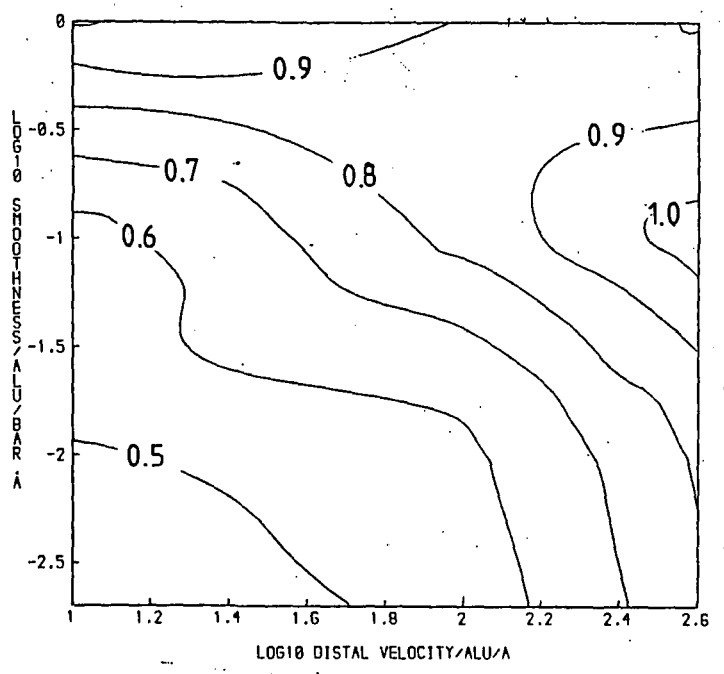

Figure 5.105 Crest/trough viscosity x velocity ratio for the narrow-hummocked case.

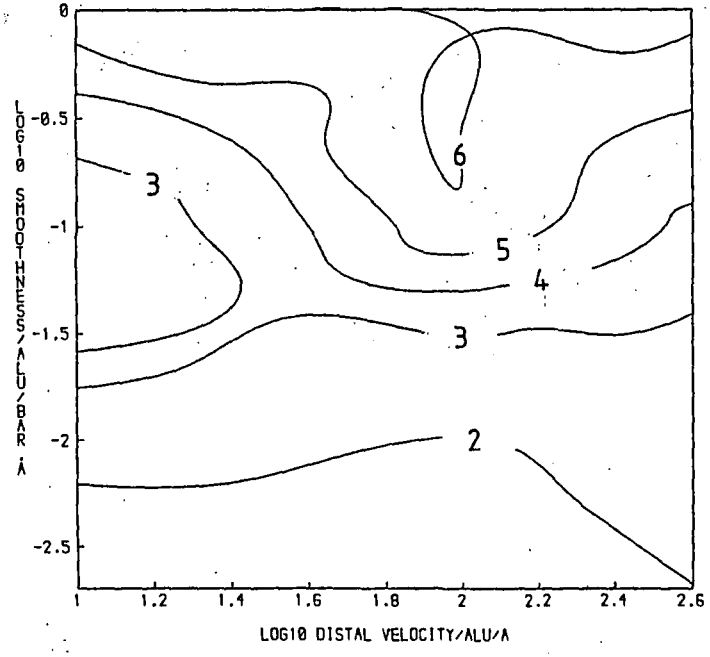

Figure 5.106 Crest/trough viscosity x velocity ratio for the smooth-crested case.

Figure 6.1

Clast at the base of a temperate glacier.

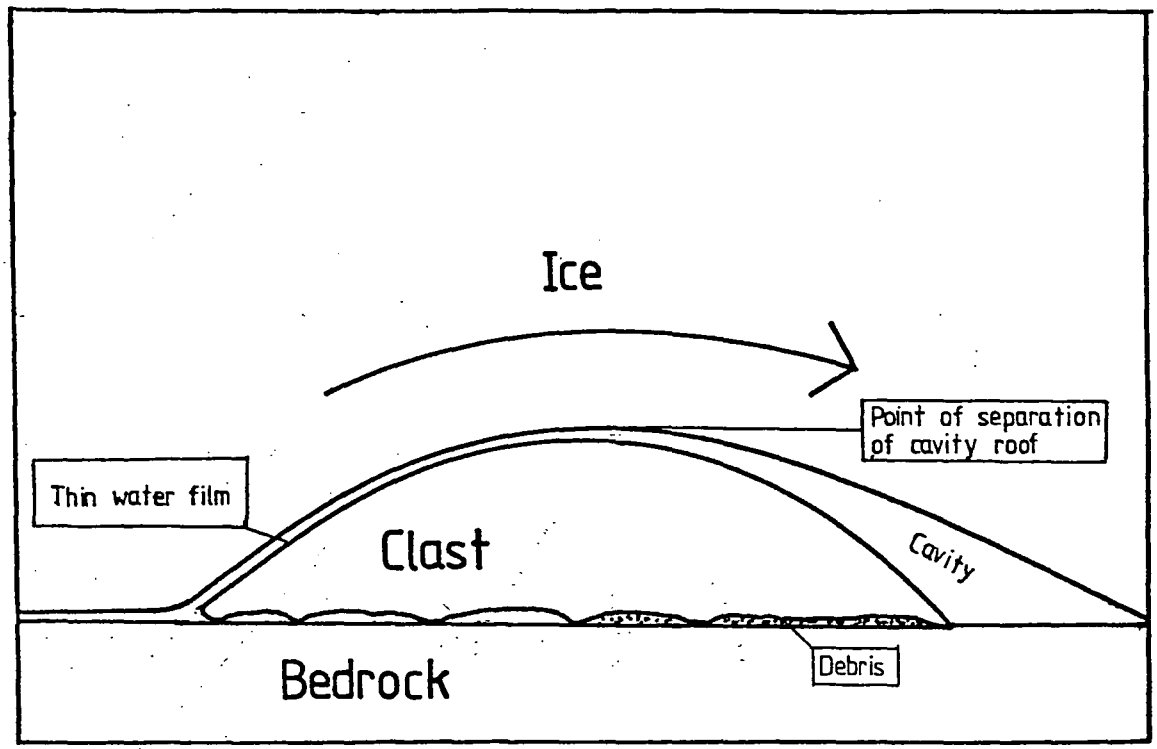

FIGURE 6.2 ICE-CLAST CONTACT GEOMETRIES

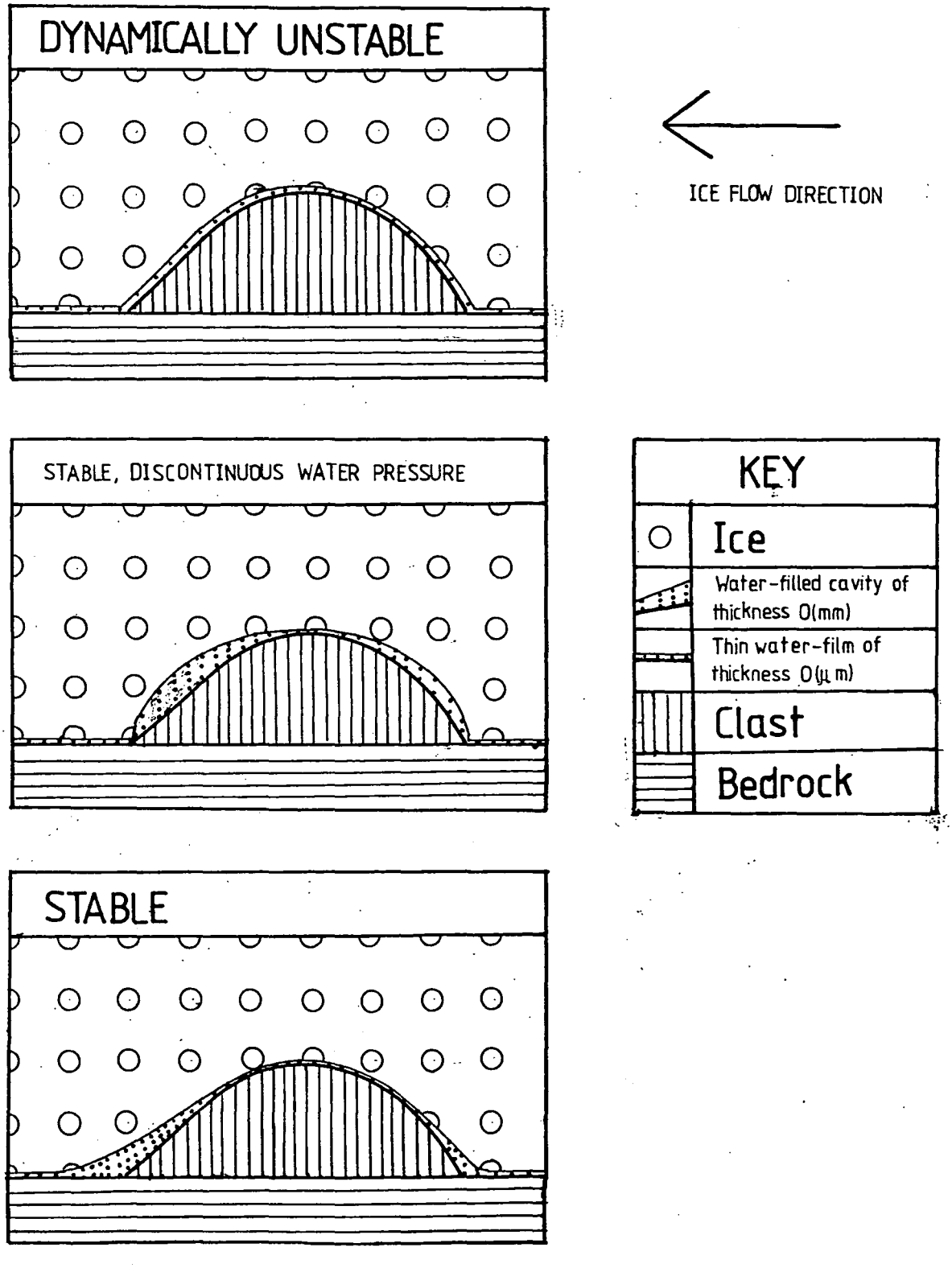

Figure 6.3 The effect of ice-clast contact geometries on the water pressure beneath the clast.

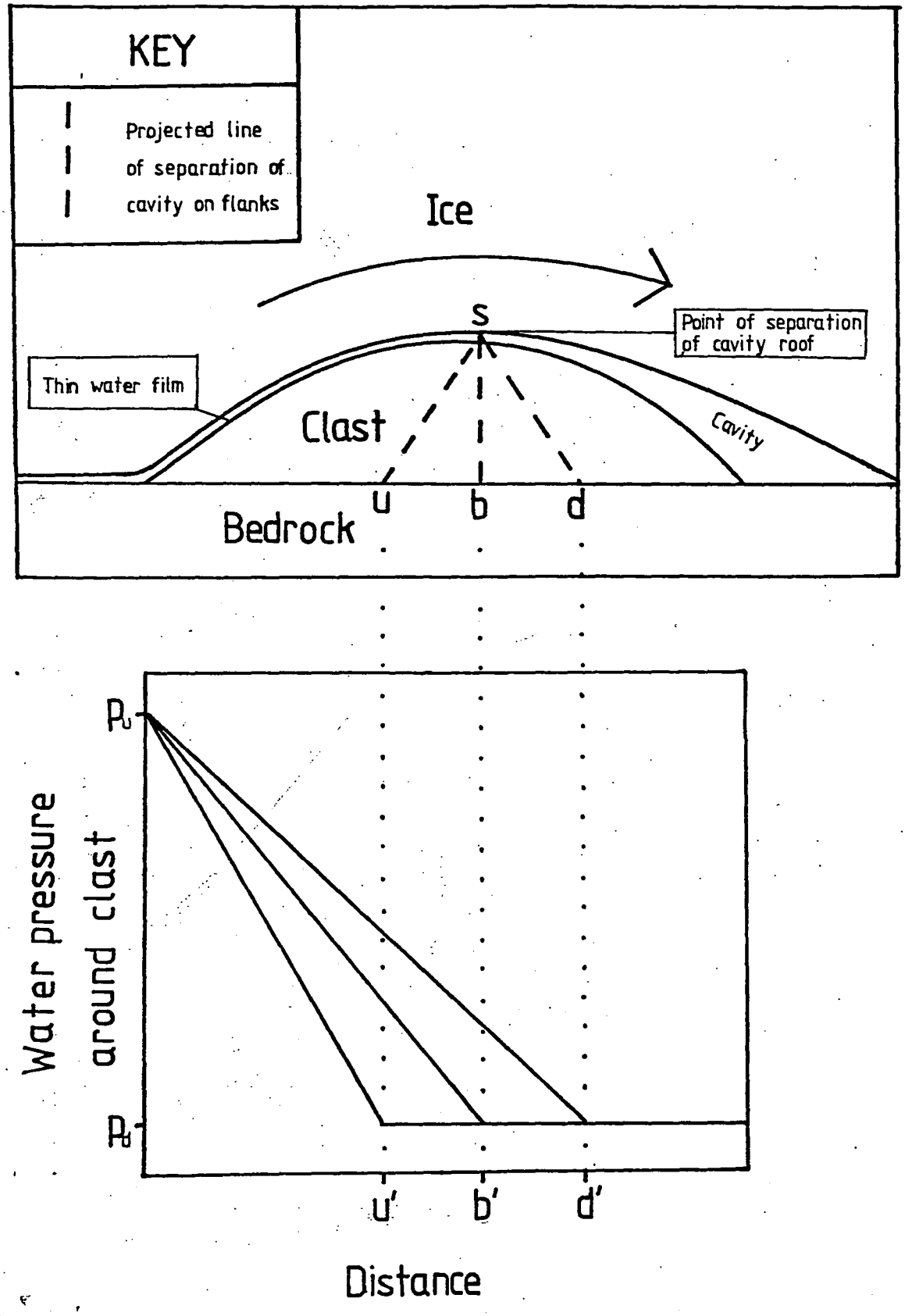

Figure 6.4 The effect of a generalised normal velocity on water pressure.

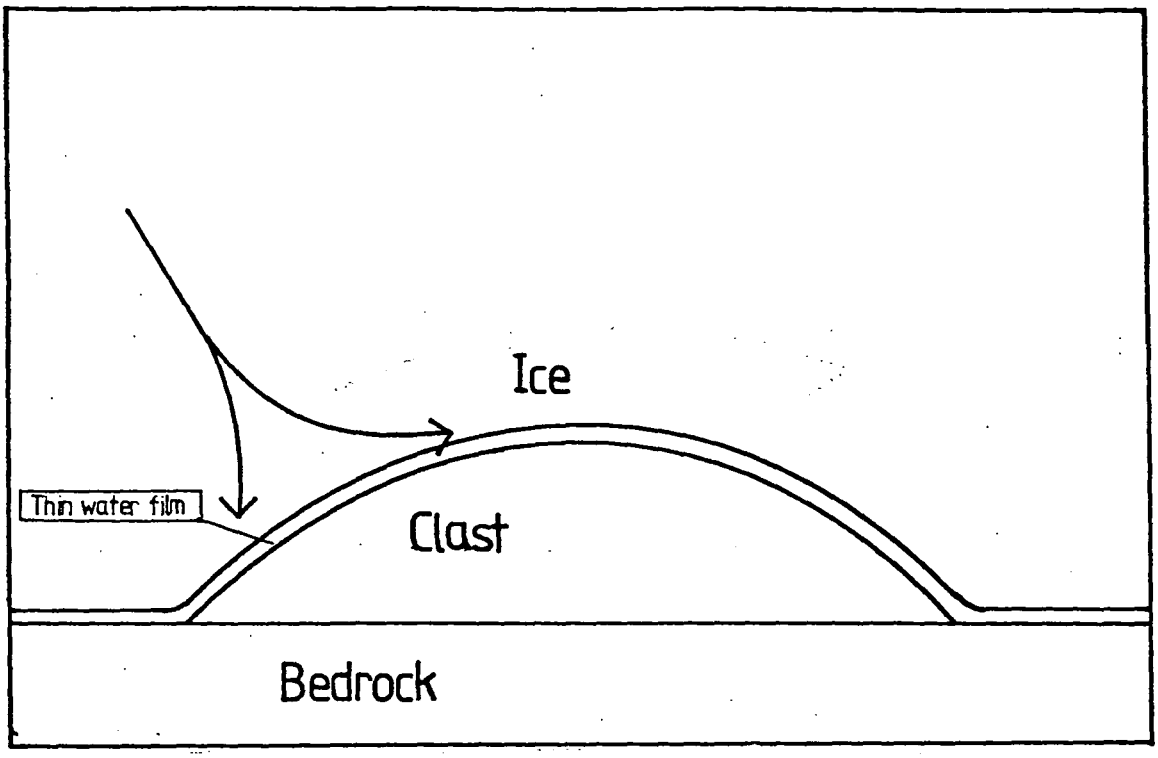

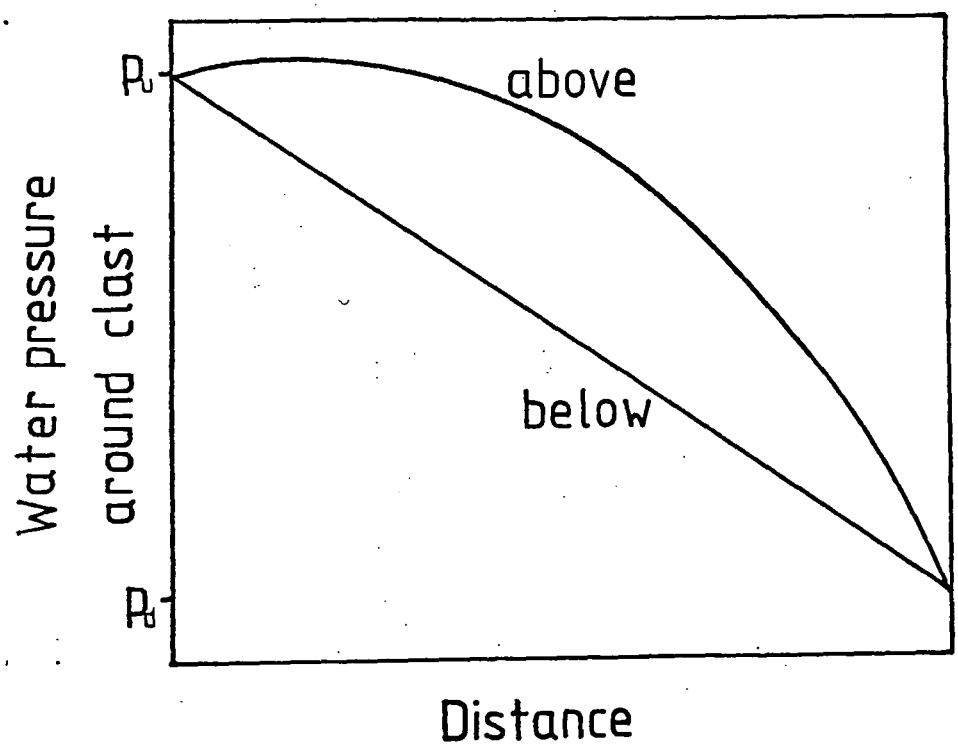

Figure 6.5 The effect of having pressure turning-points away from the clast edge.

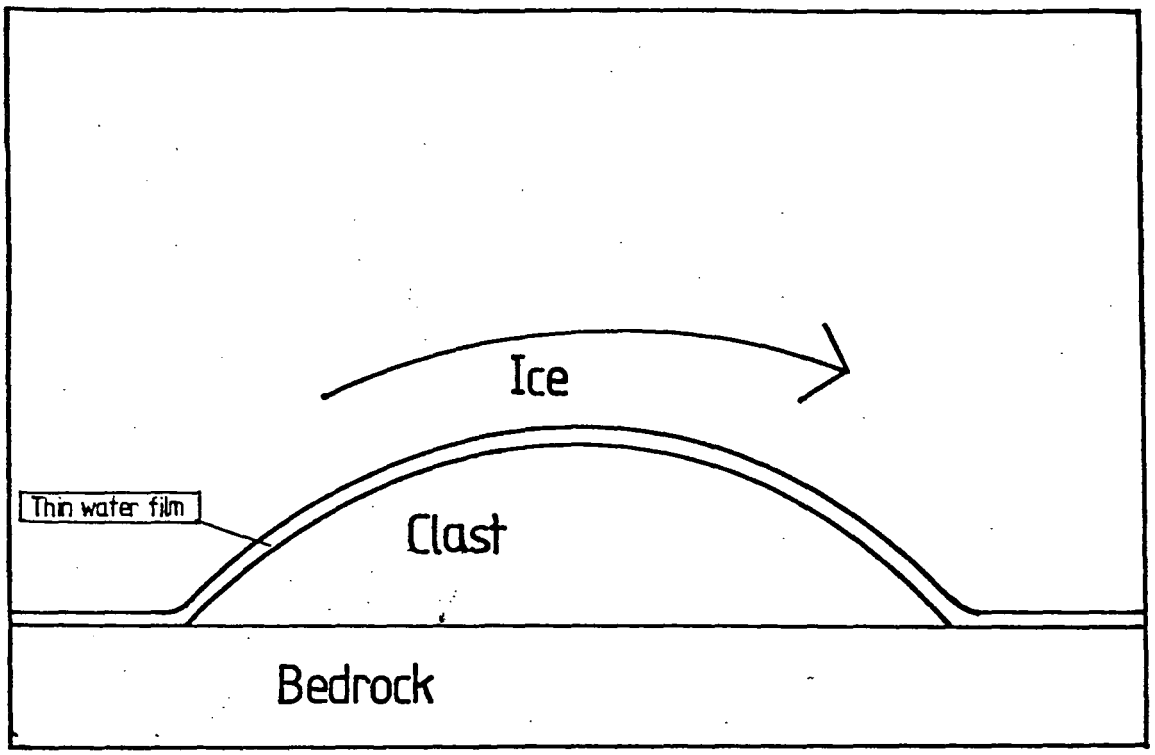

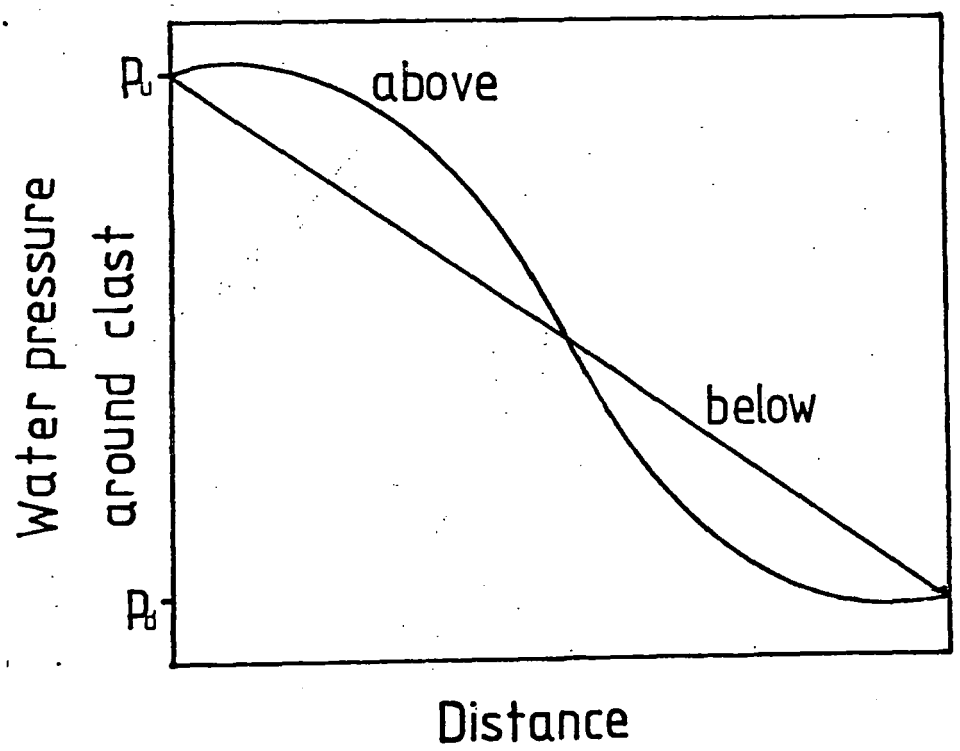

Figure 6.6 The effect of having a pressure turning point away from the clast-edge when a cavity exists.

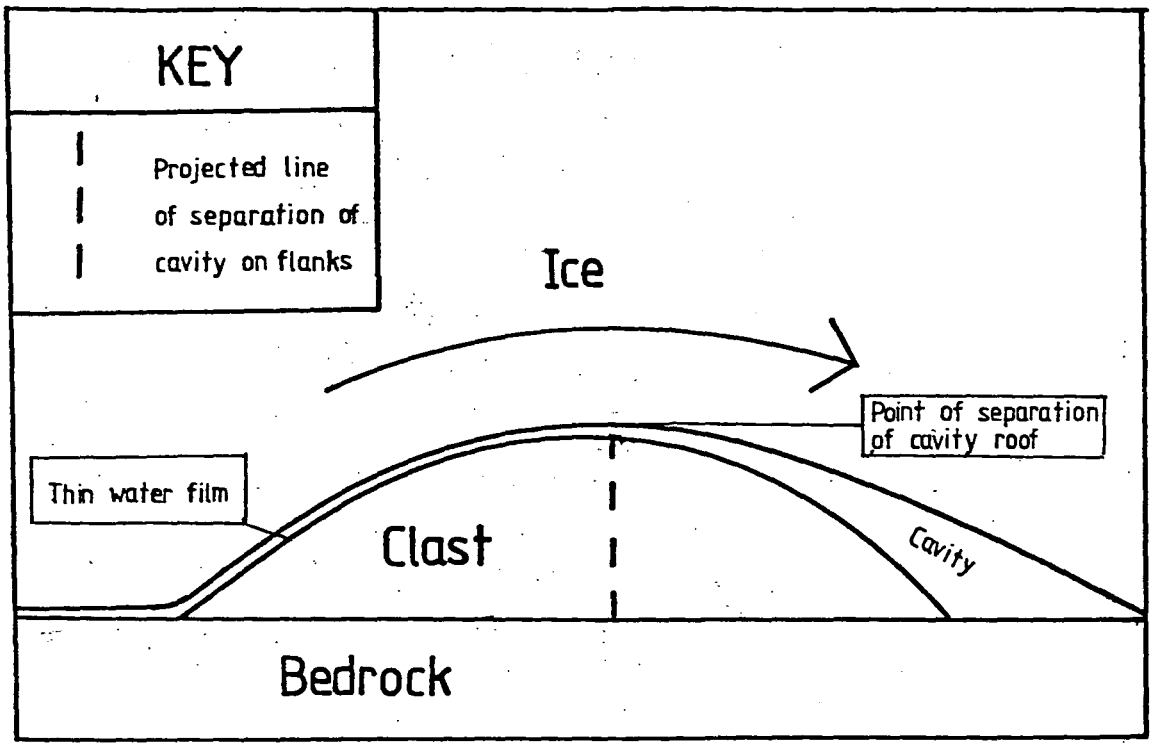

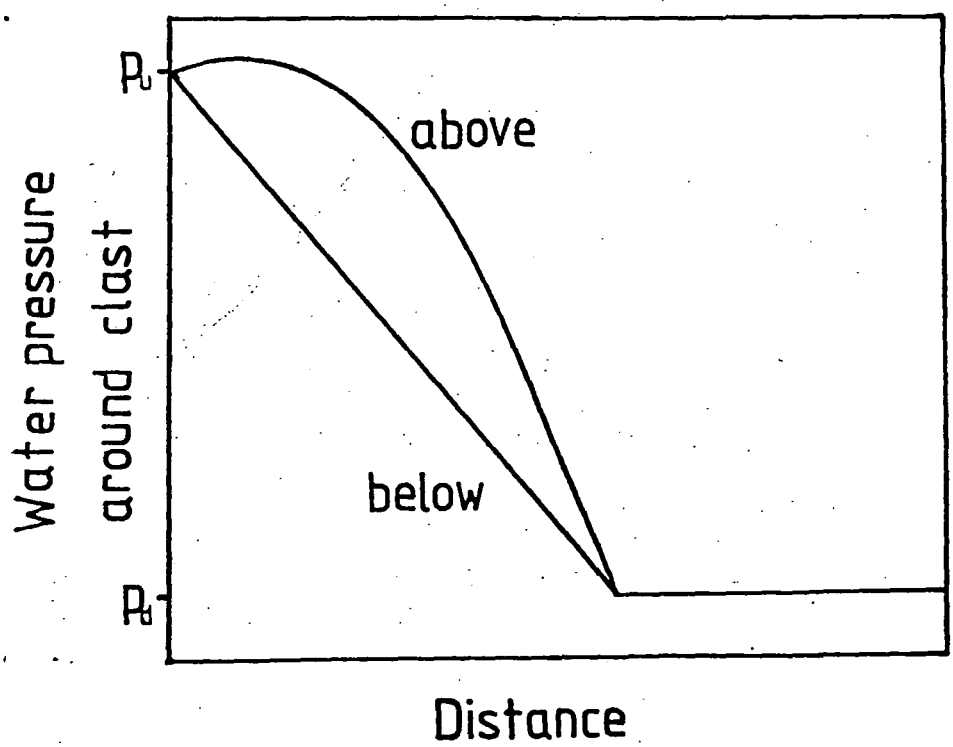

Figure 6.7 Sub-clast water pressures when the upstream end is less transmissible.

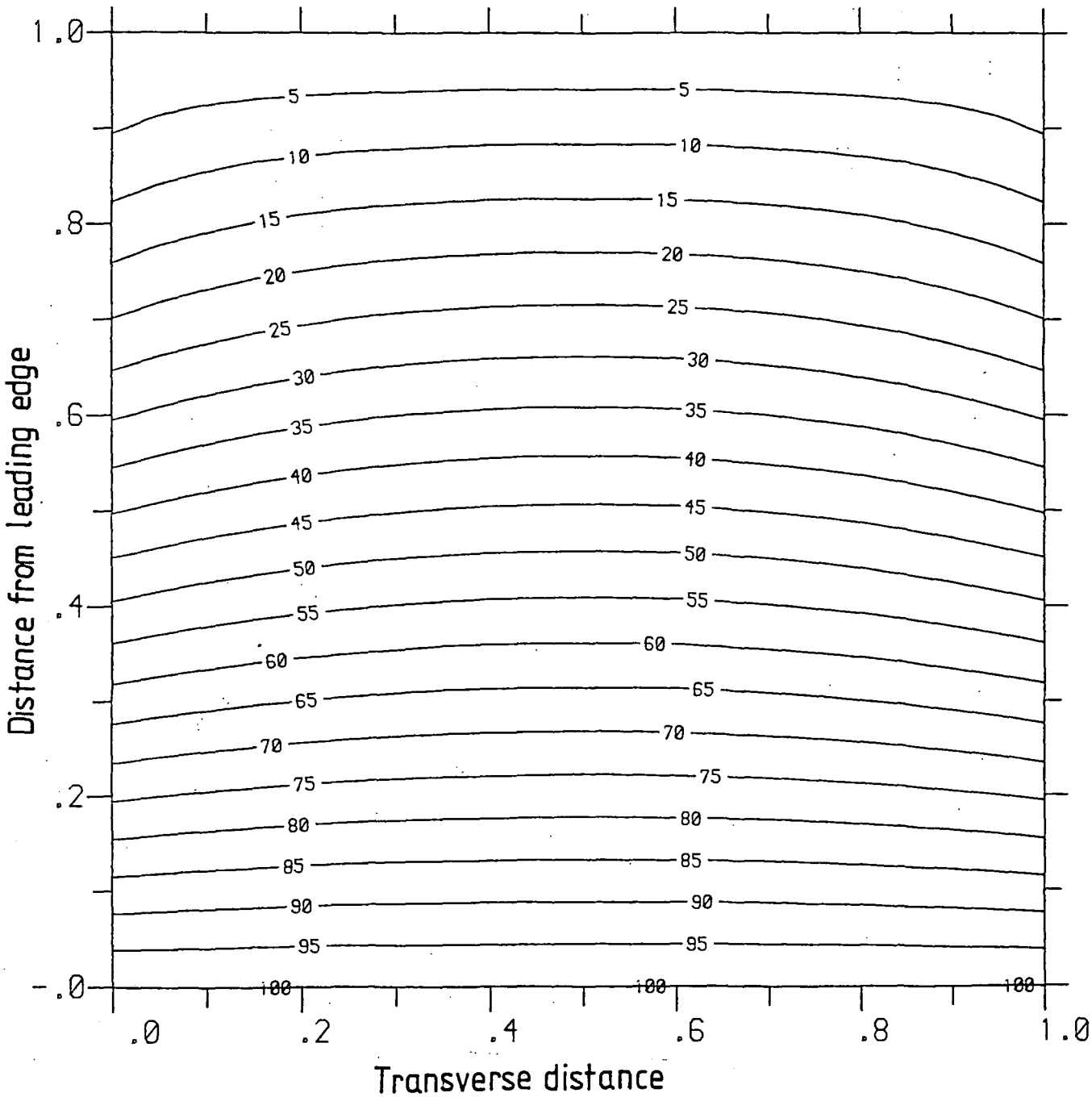

Figure 6.8 Sub-clast water pressures when the downstream end is less transmissible.

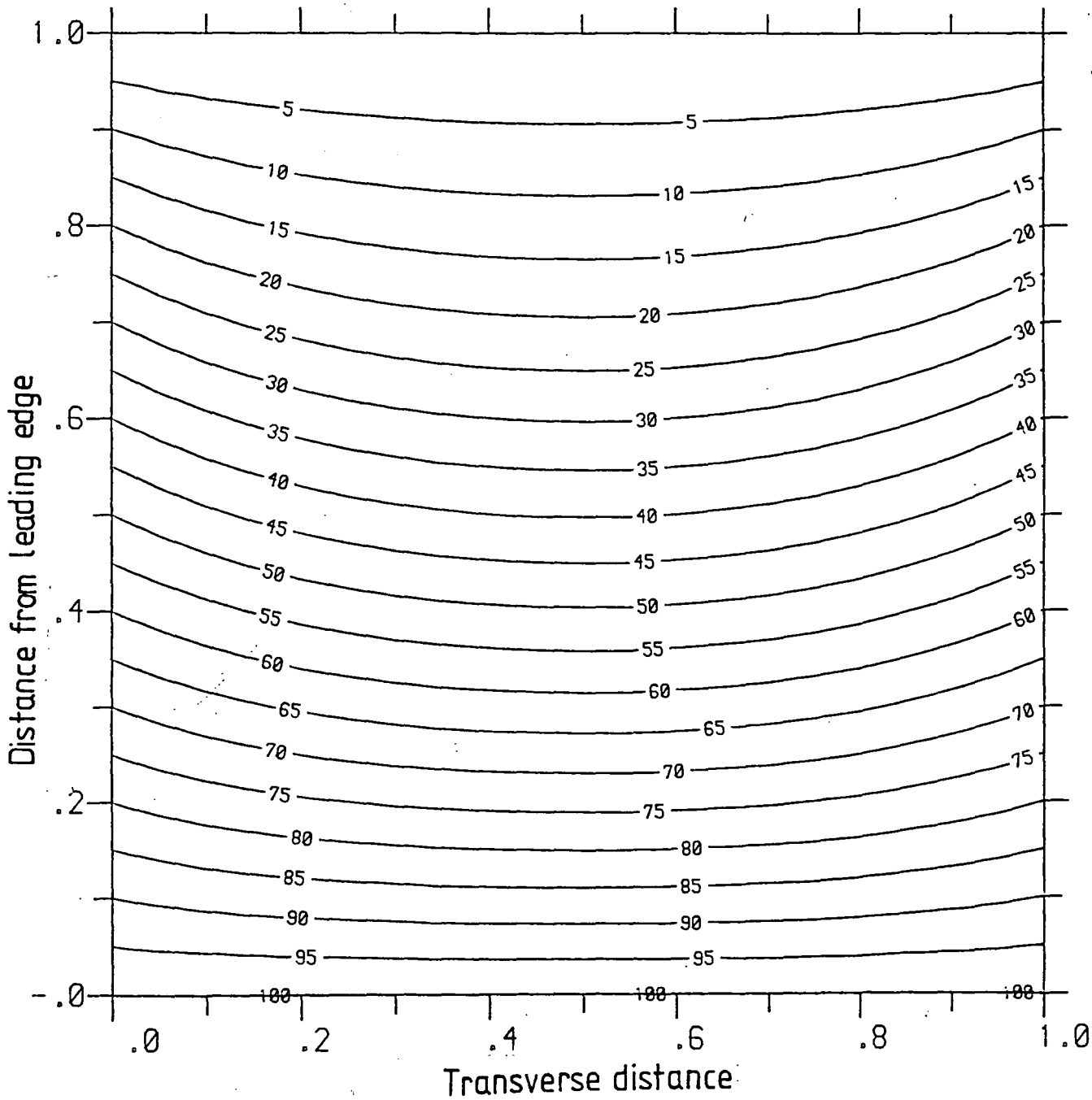

Figure 6.9 Sub-clast water pressures when the boundary pressure decline is slower than linear.

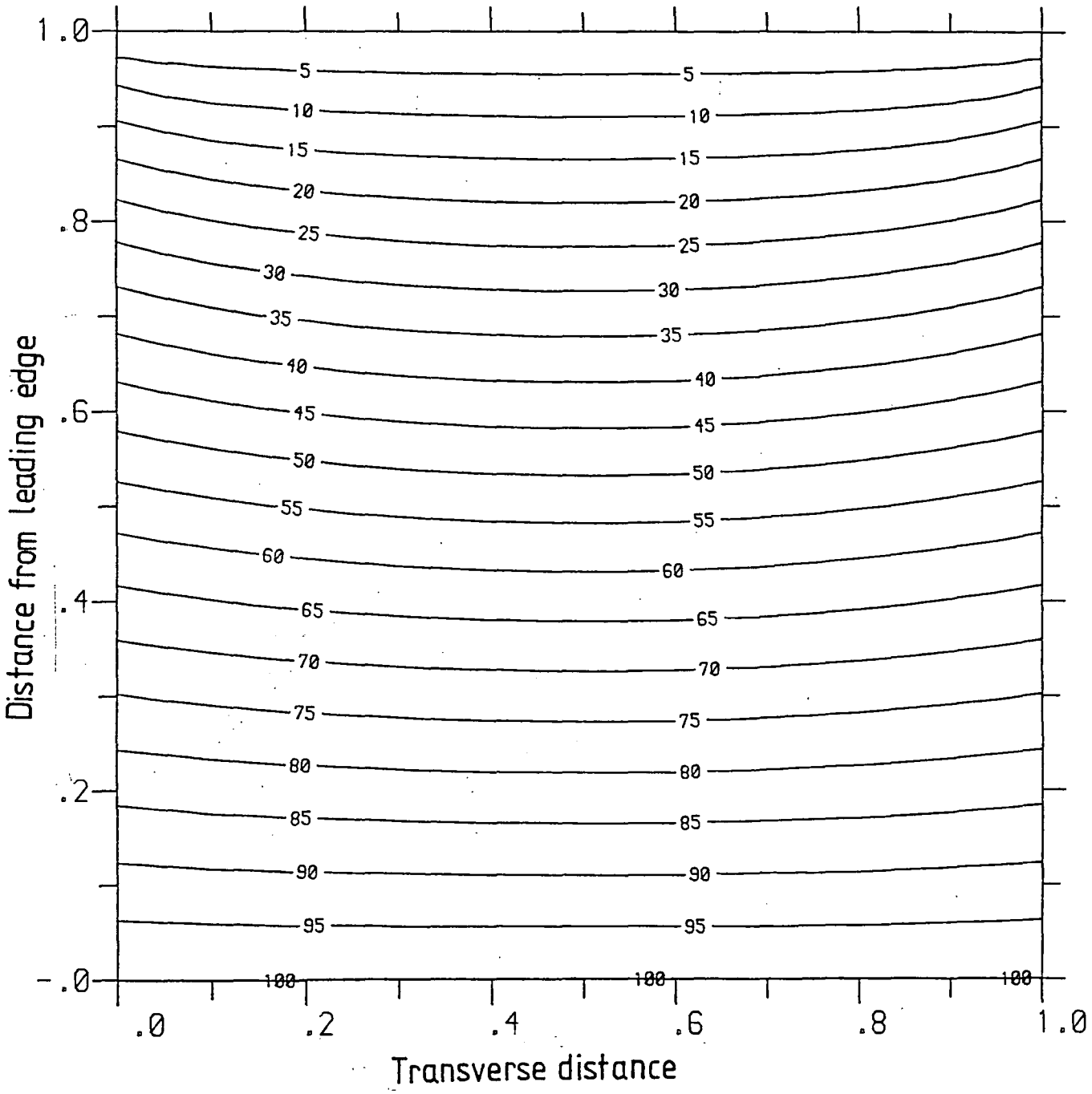

Figure 6.10 Sub-clast water pressures when the boundary pressure decline is faster than linear.

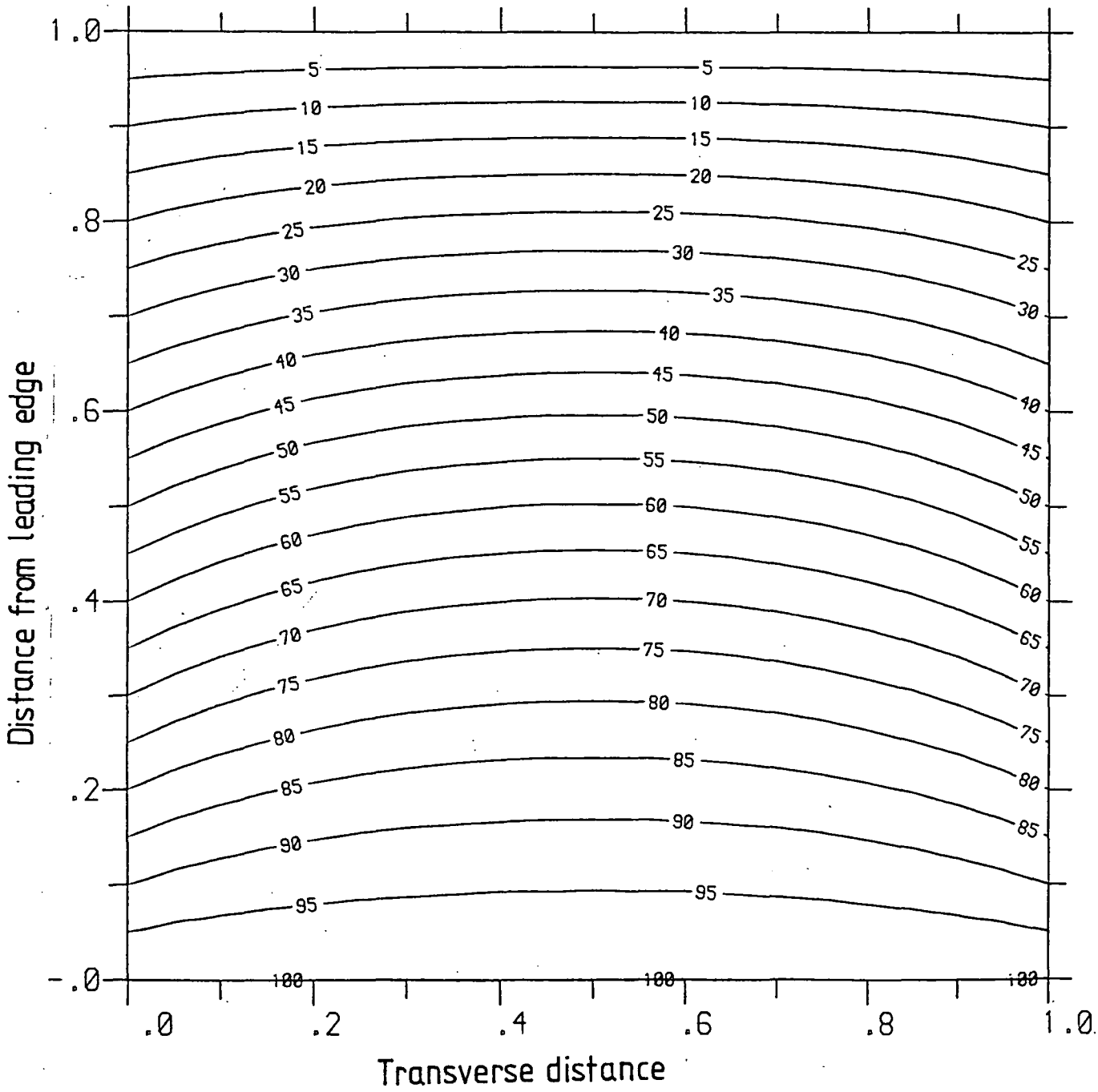

Figure 6.11 Dependence of abrasion rate on velocity and pressure.

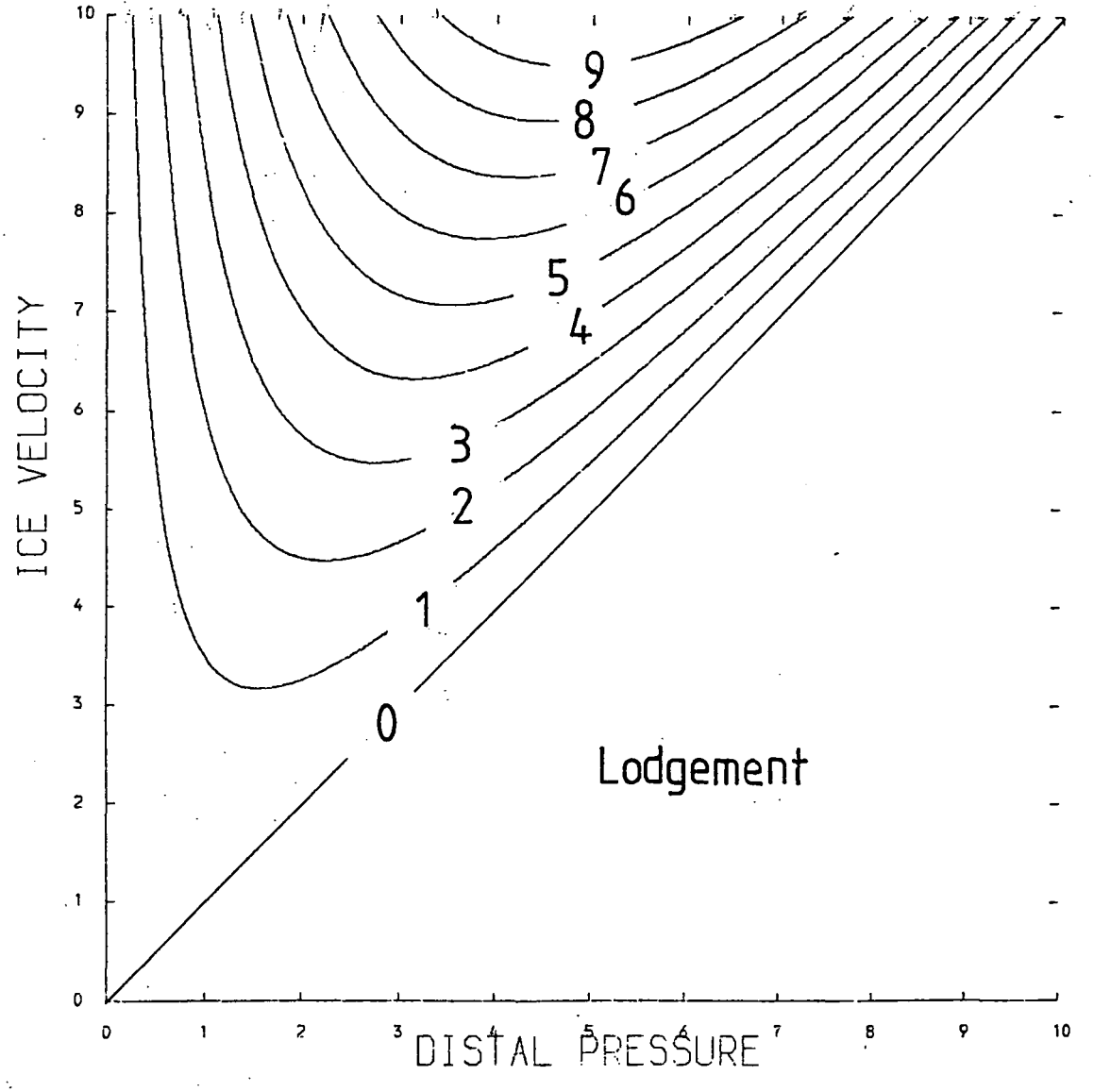

Figure 8.1 Three species mass-balance analysis

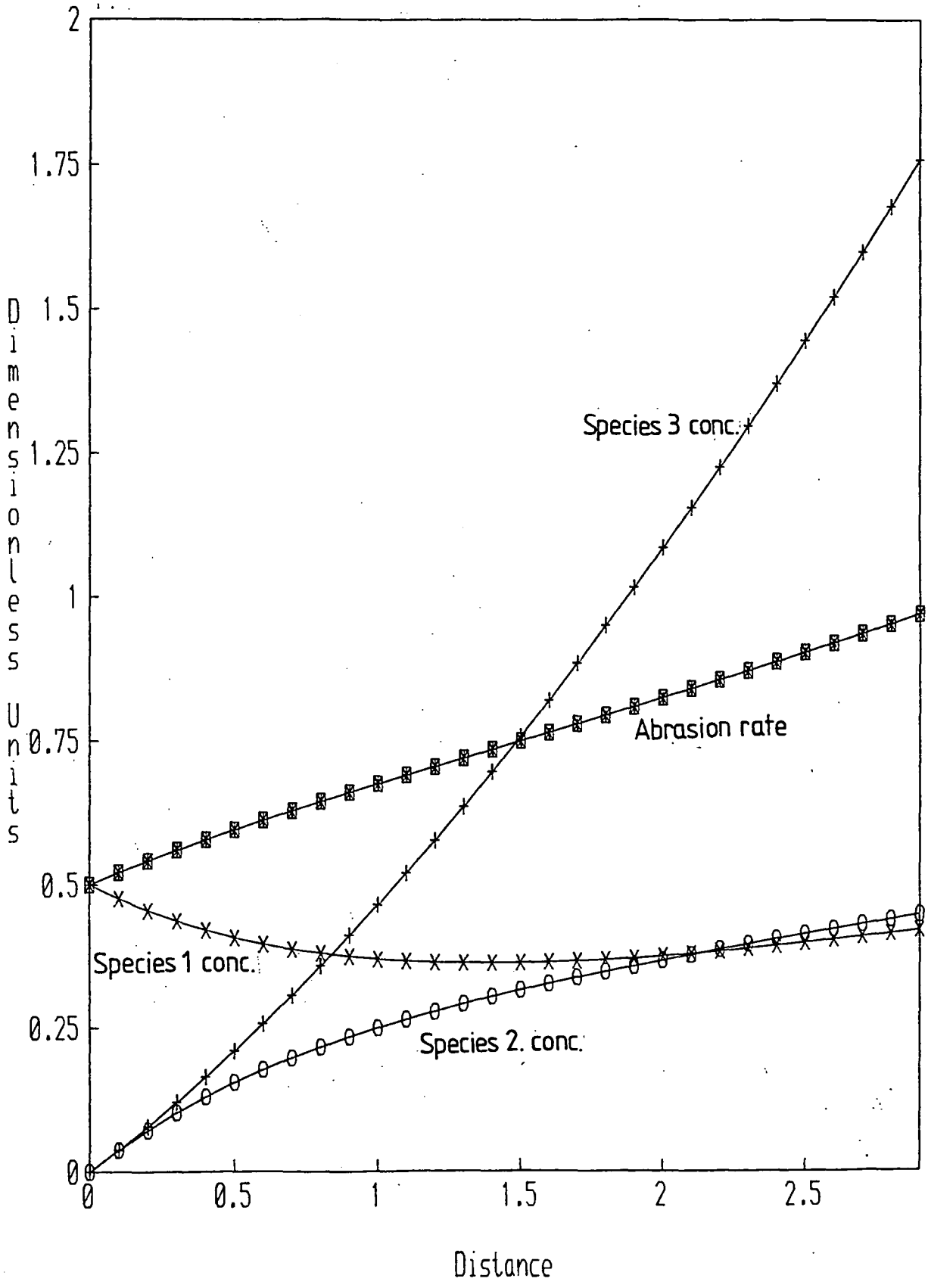

Figure 8.2 Four species mass-balance analysis.

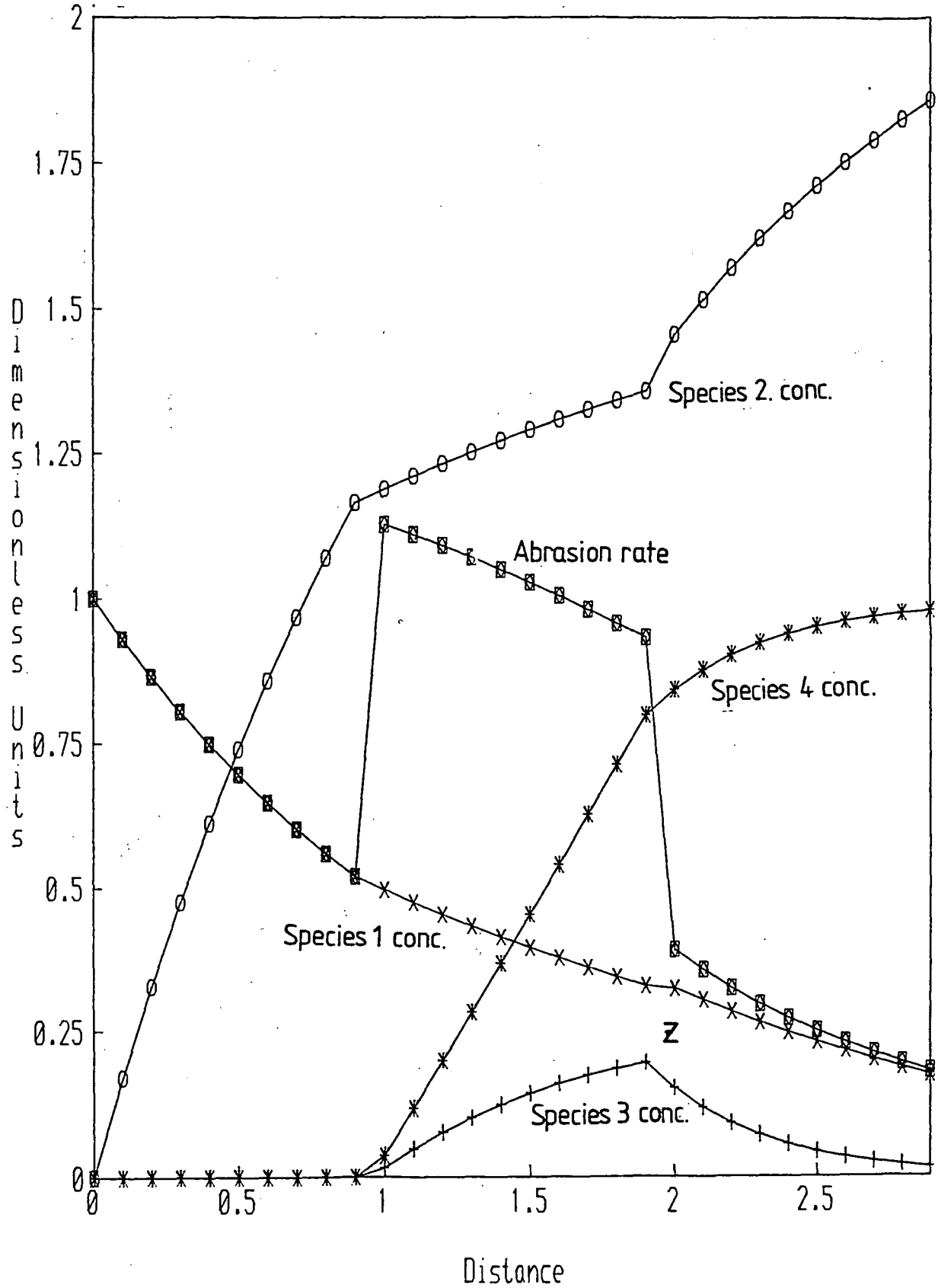

Figure 8.3 Four species mass-balance analysis with tool supply independent of abrasion rate.